ELECTRICAL CHARACTERISTICS OF N-INSB CRYSTALS USED FOR SUB-MM WAVE EMISSION AND DETECTION

Darrell I. Smith

A Thesis Submitted for the Degree of PhD
at the
University of St Andrews

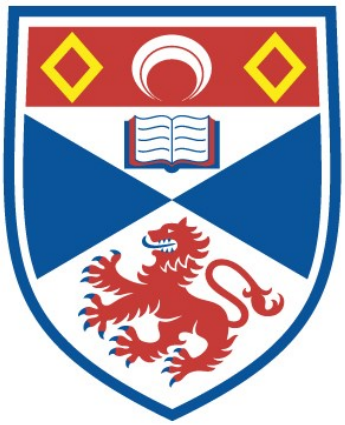

1993

Electrical Characteristics of n-InSb Crystals Used For Sub-mm Wave Emission and Detection

A thesis presented by
Darrell I. Smith BSc.
to The University of St Andrews
in Application for the degree of
Doctor of Philosophy.

September 1992

Declaration

I, Darrell I. Smith, hereby certify that this thesis has been composed by myself, that it is a record of my own work and that it has not been presented for any other degree or qualification.

This work was carried out in the J. F. Allen Physical Sciences Laboratory of St. Salvator's College, at the University of St.Andrews, under the supervision of Dr. J.C.G. Lesurf.

D.I.Smith

Certificate

I hereby certify that Darrell I. Smith has spent nine terms at research work in the J. F. Allen Physical Sciences Laboratory of St. Salvators College, at the University of St.Andrews, under my direction, that he has fulfilled the conditions of Ordinance No. 16 (St. Andrews) and that he is qualified to submit the following thesis in application for the degree of Doctor of Philosophy.

Dr. J.C.G.Lesurf
Research Supervisor

ACKNOWLEDGEMENTS

I would like to thank the University authorities for accepting me in the first place, My department for having faith in my abilities and all those in the department who have made my stay here so enjoyably memorable.

I would especially like to thank my colleagues Graham, Andy, Malcolm, Michael, Mike & Duncan for the conversations and discussions from which I learnt so much. In terms of learning I am greatly indebted to D.M.Finlayson, Prof.J.W.Allen & R.H.Mitchell for the interest they showed and the time and the advice they gave. Above all there is my superviser Jim Lesurf, from whom I have learnt so much. And who encouraged me and let me do it my way.

I would also like to thank all those who have let me use their equipment, especially Prof.J.W.Allen, J.G.M.Armitage, D.M.Finlayson & P.C.Riedi. Then there is the workshop without whom little would be done and none so cheerfully or well. I would also like to thank E.Puplett and G.J.White for their interest and support and their provision of two high purity n-InSb samples.

I would like to acknowledge the support of my friends outside the Physics Department who have helped to keep me sane (or should that be insane !!) and have been a source of inspiration as well as fun.

Then there is my family. I don't have the words to express what you mean to me. If I ever fly, it will be because you have given me the wings and the vision.

For

My Parents

and

the Glory of God

'Go ye and seek the truth,

For there will you will find beauty'

'The beauty of truth,

is its simplicity.'

ABSTRACT

A detailed study of the electrical characteristics of high purity n-InSb has been under taken. The main aim was to determine the effect of the electrical characteristics on the emission and detection properties of n-InSb. Several samples of high purity n-InSb, with different electrical properties, were used.

Calculations of the individual and combined effects of the relaxation and excitation mechanisms on the samples were made. Lattice temperatures of 1.5, 4.2 & 77 Kelvins were considered. The electrical properties predicted, agree well with previous results.

The variation of current density with electric field was measured at lattice temperatures of 1.5 & 4.2 K, from which the conductivity was calculated. The carrier concentrations of the crystals were measured and the mobilities were then calculated.

At an electric field of 0.25 Vcm^{-1}, a sharp rise in conductivity was observed in all samples and attributed to a transition between energy relaxation mechanisms.

At an electric field of 20 Vcm^{-1}, one sample showed a sharp rise in conductivity, which was shown (by Hall measurements) to be due to the ionisation of deep donors.

At an electric field of 80 Vcm^{-1}, a large increase in conductivity with an associated hysteresis was observed. Reasons for both are suggested. The hysteresis was also observed in the variation of the crystal resistance with lattice temperature.

The implications of this work on the possibilities for a tuneable sub-mm wave source or laser has been discussed.

CONTENTS

1 INTRODUCTION TO THE THESIS : ITS AIMS AND CONTENTS

1.1 Introduction

The origin of this work is in an attempt to use a cyclotron-resonance emission oscillator,(CREO), to produce a wide-band tuneable source in the near mm-wave region (λ=0.1 to 1.0 mm). The concept of a CREO is one of a plasma of electrons spiralling around magnetic field lines emitting radiation. In effect a mini aurora. The free space oscillator, known as a Gyrotron, requires large magnetic fields (10.72 Tesla for 300 GHz) and good containment of a powerful electron beam. The solid-state oscillator relies on the properties of the semiconductor crystal (such as the reduction of the effective electron mass) to reduce the magnetic field required (for Indium Antimonide,InSb, : 0.139 Tesla for 300 GHz) and remove containment problems. The advantages of a solid-state oscillator are tempered by the complexities of the electron plasma's properties as affected by the crystal. To understand the oscillator fully, one must understand the 'electronic' structure of the semiconductor crystal used. This describes the effect of the crystal on the electron plasma set up within it.

In order to appreciate the position of the CREO within the group of mm-wave sources a brief survey of available sources is undertaken in section 1.3. The uses of mm-wave radiation has been included in section 1.2 in order to give some justification for the development of mm-wave sources and to indicate the properties required of these sources. For the region of interest the only other source comparable with the CREO (in terms of frequency range of emission) is the Backward-Wave Oscillator(BWO), which is described in section 1.4.1. The reasons for not seeking to develop this source, at present, are given.

The initial approach and consequent aims for the work presented here are described in section 1.5. This section also explains the structure of this thesis in terms of approach and reasoning.

1.2 **MM/Sub-MM Wave Sources Applications**

Why make mm-wave sources? Well the usefulness of a source is determined by the usefulness of the radiation produced. So what are the applications of mm/sub-mm radiation?

The major uses for mm/sub-mm waves include :-

1) The Probing of Interstellar Molecular Clouds (IMC) : There are several resonances of diatomic Hydride molecules (e.g. HCN-0.337mm) and so detection of these frequencies can be used to detect the structure and composition of the IMC. The need here is for wide tuning range sources as local oscillators.

2) Radar/Guidance Systems and Topographical Imaging : MM-waves have several advantages over other frequencies for the above applications. The systems are smaller and have better resolution than microwave systems and there is less attenuation through fog and smoke relative to infrared. This has led to a great deal of interest in the development of mm-wave radar. The greater attenuation of sub-mm waves by the atmosphere has prevented its use in long range radar, but its superior resolution and reduced size has led to it being used for near-field radar, auto-guidance systems, topographical imaging and the modeling of mm-wave radar. There is the need here for high power sources (production of the radar beam) and moderately tuneable sources for the heterodyne receiver systems.

3) Spectroscopy : In determining the effectiveness of the radar systems and the reduction in intensity of the mm-waves detected by telescopes a measure of atmospheric absorption over the region for differing atmospheric conditions must be known. This spectroscopic absorption study of the atmosphere also gives information about atmospheric molecules. The mm/sub-mm wave equivalent-energy range (0.138meV to 13.8meV) is ideal for probing Band Structure in semi-conductors and other features causing resonances also found in other materials. A lot of work has been done in this area. Here wide-band coherent sources are ideal. High power is not required, but good resolution of the emitted wavelength is essential.

4) Communication : This is an expanding field in mm-waves as there is a large bandwidth available. In sub-mm waves,

communications are restrained by the high atmospheric absorption. They can be used for short-range communications, however, where it is preferable for detectors further away not to be able to detect the signals. This has various military applications. Here a medium-power coherent source is required.

The above uses define the output requirements of a source if it is to be useful.

1.3 Introduction to MM-Wave Sources

A brief overview of the history of mm-wave sources is given[1] in order that some of my approaches be explained. My interest is in the near-mm wave region and this produces the bias on the following.

The mm and sub-mm wave regions have long been neglected as the region is in the transition between optical and radio techniques. As can be seen in Fig. 1.1, the region lies, at one end, in the Extremely Far Infra-Red (optical term) and at the other in the

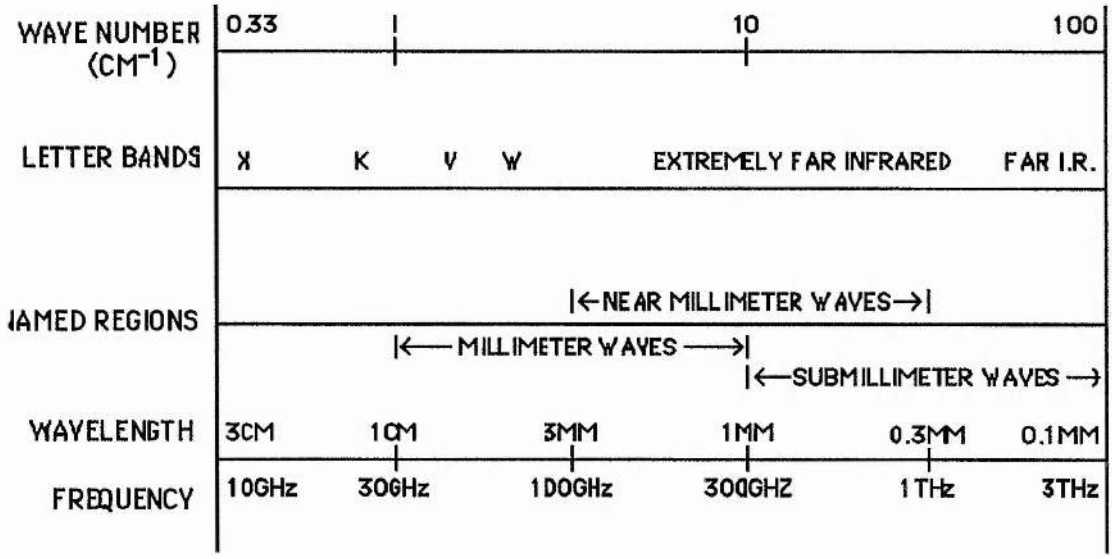

Figure 1.1 : Nomenclature for millimeter/submillimeter waves and other frequency ranges.

---

[1]Kantorowicz & Palluel, I.R.&MM Waves 1 , 185 (1979) (much of this section has been taken from this paper.

Extremely High Frequency or W Band (Radio terms). Two reasons for the neglect are, a lack of suitable sources and a debate as to whether optical or high frequency radio techniques should be used.

The first coherent sources were mainly vacuum electron devices developed originally for Radio/microwaves, but which were found to be suitable for higher frequencies[2]. 1936 saw a Magnetron emit at 47GHz. Soon after (1937) the first Klystron was built. This was followed by the cavity magnetron (1939). The travelling wave tube was developed late in World War II operating over a similar range. 1951 saw the first backward wave oscillator operating at 37GHz. The early 1960's saw the arrival of Lasers. Two gas discharge lasers operating at sub-millimeter frequencies: The HCN laser at 890 GHz and the Water Vapour Laser at 2.54THz. The Gunn diode(1962) and the Impatt diode(1964) provided the first solid state sources, though at frequencies of about 35GHz.

By the mid-1960's there were quite a few oscillators to choose from, though they were roughly grouped into three types: 1) Vacuum Tube Devices; 2) Solid-State Sources and 3) Masers. There were still no oscillators operating between 200GHz and 890GHz. The problem in trying to bridge this gap lay in the lack of tuneability of the lasers and the rapidly decreasing efficiency of the Vacuum Tube Devices with increasing frequency. Despite this, by 1969 B.W.O.'s had been built to operate at up to 1.1THz[3] and so the gap was bridged. Not very satisfactorily, however, as the output power was low and the tuneability reduced. The B.W.O. is still, however, the only source in general use that can produce coherent emission across the entire region.

Figure 1.2 shows the relative output power of most of the above sources across the region. Note the dip in available power for frequencies between 325 and 890 GHz which reaches as low as 10mW at 800 GHz. Not shown in the figure is the fact that tuneability at these frequencies is also very poor.

---

[2]Wiltse, IEEE.Trans.MM.Wave Th.&Tech.MTT.32, 9 , 1118 (1984)

[3]Golant et.al., Prib.i.Tekh.Éksp. 3 , 23 (1969)

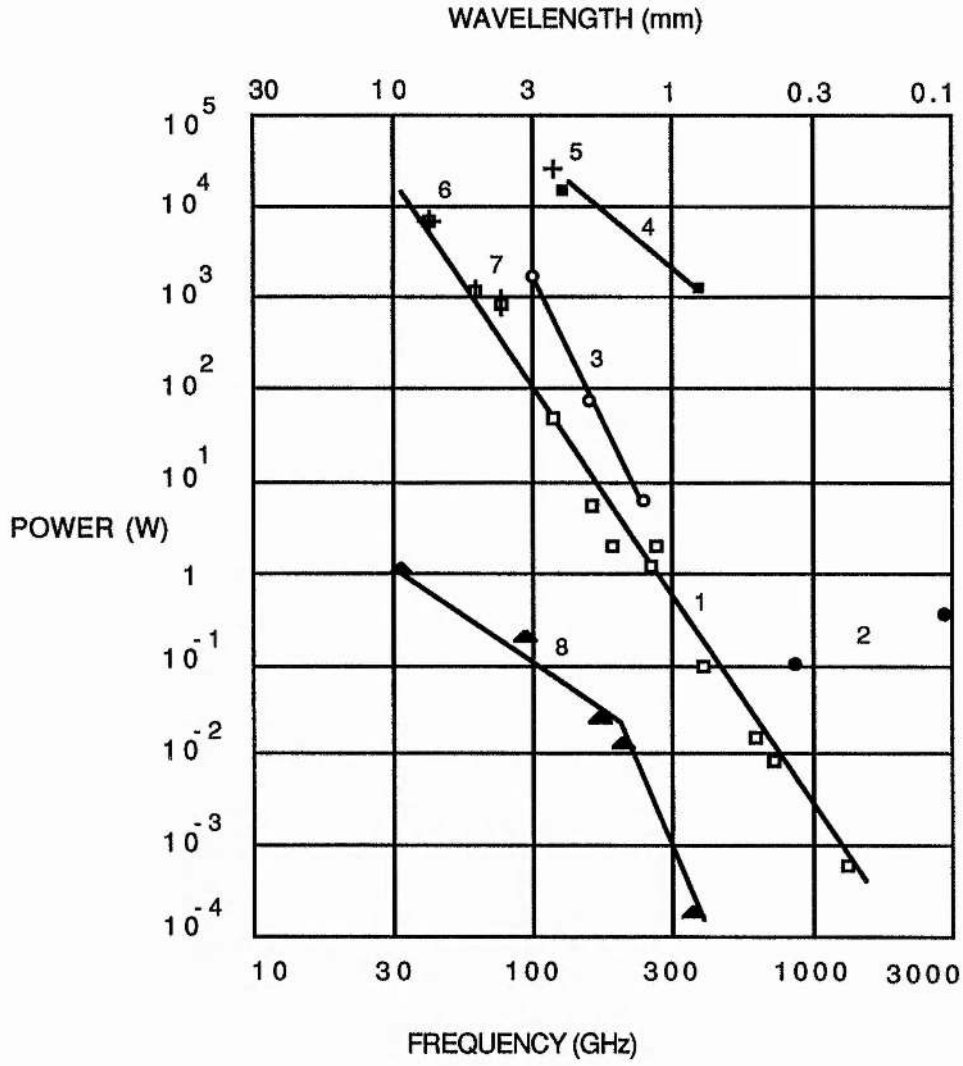

Figure 1.2 : Output powers of sources across the mm/sub-mm region : 1-Backward Wave Oscillator(continuous operation:c.w.); 2-Far Infra-Red Lasers(c.w.); 3-Extended Interaction Oscillator(pulsed); 4-Gyrotron(c.w.); 5-Magnetron(pulsed); 6-Klystron(c.w.); 7-Travelling Wave Tube(c.w.) and 8-IMPATT diodes.

To produce higher powers the Extended Interaction Oscillator (a development on the Magnetron) and the Gyrotron were developed in the early 1970's. The Gyrotron (which works on the concept of electron cyclotron emission) is important as it provides the greatest power output over the mm wave region (of the order of KW). The greatest limitation for all the Vacuum devices is the ability to produce and constrain very high energy electron beams.

In 1965[4,5,6] emission at microwave frequencies was reported from InSb under electric and magnetic Fields at Nitrogen temperatures. The processes involved were only vaguely understood and it was 1972 before anything similar was done. Then higher magnetic fields and lower temperatures were used and the first solid-state electron cyclotron emission oscillator was produced operating at 150-450GHz[7]. Powers of 10^{-8}W were obtained. Even more recent is the development of Quantum

Source	Bandwidth	Power	Frequency
Gyrotron	-	~5KW	325GHz
Magnetron	-	-	100GHz
EIO	<1%	10W	280GHz
BWO	30%	50mW	1.1THz
Klystron	10%	50μW	200GHz
Impatt	15%	5μW	330GHz
Gunn	10%	-	250GHz

Figure 1.3 : Comparison of mm-wave sources.
Bandwidth - range over which source can be tuned.
Power - maximum output power achievable at 200GHz
Frequency - maximum frequency obtained.
the above values are indications rather than fact as most of the sources are still being developed.

Well Devices whose place among mm-wave sources is still uncertain. Radiation at frequencies up to 500GHz has also been achieved by Gunn diode sources utilising high harmonics and frequency multiplying. The power output is low.

Fig 1.3 shows the tuning range of the sources and maximum power at 200GHz and maximum frequency obtainable.

---

[4]Phelan & Love, Phys.Rev. 133 , A1134 (1963)
[5]Eastman, Proc.IEEE. 53 , 761 (1965)
[6]Buchsbaum et.al., Appl.Phys.Letts. 6 , 67 (1965)
[7]Gornik, Phys.Rev.Letts. 29.9 , 595 (1972)

1.4 **Near-MM Wave Sources**

There are only two sources which emit over the entire near-mm wave region. These being the Backward Wave Oscillator (BWO) and the Cyclotron Resonance Emission Oscillator (CREO). The processes involved with the BWO have not been described fully in theoretical terms, but the technology required to construct them is known and they are produced commercially. The processes involved with the CREO have been described fully in theoretical terms, but the oscillator as useful source has not been developed. The advantages and disadvantages of the two sources are compared in the next two sections.

1.4.1 The Backward Wave Oscillator

The basic concept of a BWO is that a beam of electrons passing parallel and close to a periodic structure (of a conducting material) will set up electro-magnetic waves along the structure in the direction of the electron beam and also in the opposite direction. The electro-magnetic wave travelling in the opposite direction to the electron beam will interact with it causing electrons to bunch into groups at periodic intervals (the period being equal to the wavelength of the electro-magnetic wave). This enhances the ability of the beam to set up electro-magnetic waves and the greater the amount of electro-magnetic radiation the greater the bunching ecetera, ecetera. The frequency of the electro-magnetic wave emitted is that of the electro-magnetic wave travelling along the periodic structure. This frequency is determined by the period of the structure and the speed of the electrons in the beam.

To obtain higher frequencies the period of the periodic structure must be reduced and/or the speed of the electrons increased. This indicates the inherent difficulties of this source. The structure must have of period of about 100μm for frequencies of between 200-300GHz, whilst the electron beam must be of energy equivalent to 2.5-5KeV. This suggests that the construction of the periodic structure, production and confinement of the electron beam and heat dissipation will be problem areas. These problems can be overcome, however, and these sources are produced commercially.

The points raised restrict the power output and efficiency of the BWO at high frequencies. The increase in power supplied to the electron beam is in direct confrontation with need to focus the beam better in order to interact with the smaller periodic structure. This inevitably leads to the beam being insufficiently focussed, which causes the interaction to be less efficient. Also the reduction in size of the periodic structure causes a reduction in the maximum power it can transmit. With large energies concentrated into a small volume, heat dissipation also becomes a limiting factor.

The development of a more efficient quasi-optical BWO has been suggested[8], but its development is restrained by the problems involved in the production of a suitable electron beam (power supply, beam alignment and focussing) and the flexibility required for testing various types and sizes of periodic structures. Either separate electron beams are required (one for each structure) or a facility which allows structures to be interchanged. Neither option being available, research into BWO development is not dealt with further in this thesis.

1.4.2 The Cyclotron Resonance Emission Oscillator

A brief description of the conditions required for this source is given here. This is purely for comparison with the above as the rest of this thesis deals with the theory, conditions and technology involved in far greater detail. The concept is to utilise the low effective electron mass and the quantisation of the conduction band with the application of a magnetic field in InSb to produce in effect an aurora within a crystal. The magnetic field determines the frequency of emission: A field of 0.3 Tesla induces a frequency of 650GHz. In order to reduce thermal noise, helium temperatures are used (1.5 & 4.2°K). A bias field of between 5 and 20 Vcm^{-1} is applied[9,10].

The above requires the use of a cryostat, a fairly large variable magnet (though as helium temperatures are being used a superconducting coil can be used if available) and a pulsed voltage

---

[8]Private Discussion, Dr.G.M.Smith,Univ.St.Andrews (1990)
[9]Gornik, Optics & Laser Tech. 7 , 121 (1975)
[10]Gornik,Proc.Conf.ed.J.F.Ryan, 329(1978)

generator (pulsed to reduce crystal heating). In addition, in order to couple emission out of the cryostat a waveguide/optical cavity arrangement must be included. Most of the above technology has been developed as InSb has been used as detector/bolometer under almost identical conditions[11]. Indeed the cyclotron-resonance assisted detector/bolometer utilises the same principles as the source, but in reverse. The photons are absorbed causing an increase in conduction.

1.5 **Approach Taken in This Thesis**

The initial review of past development of the CREO and review of the theory involved (contained in Chapter 2) led to the conclusion that a knowledge of the electrical characteristics of InSb, in and around the region in which emission occurs, should be acquired. For the sake of completeness and out of a personal interest in investigating some peculiar and generally unexplained electrical characteristics reported in earlier studies of InSb, the aim of the following work was widened to a general investigation of the electrical properties of InSb. Initially characteristics for the temperature range 0 to 300°K and applied fields of 0 to 100Vcm^{-1} and 0 to 1 Tesla were obtained (see Chapter 6).

In order to understand and interpret the data obtained a review of solid-state theory was undertaken. This has been presented in two parts:
The first is a general and qualitative description of the relevant sections of solid-state theory. This is presented in Chapter 3; The second is the application of the solid-state theory to InSb in the conditions referred to above. This is presented in chapter 4.

The results of experimental work is presented and discussed in chapters 6 and 7. Unfortunately, the aim of a cyclotron emission oscillator was not fulfilled and this thesis is therefore dedicated, in the main, to the electrical characteristics involved in the regions where emission occurs. The prospects for sub-mm wave emission from n-InSb are discussed in chapter 7.

---

[11]Brown et.al., J.Appl.Phys. 58,5 , 2051 (1984)

2 HISTORICAL BACKGROUND FOR CYCLOTRON RESONANCE AND OTHER ELECTRICAL CHARACTERISTICS IN InSb

2.1 Introduction

As mentioned at the start of chapter 1, the initial purpose of this work was to develop a cyclotron resonance emission oscillator. To that end a review of the research papers involved with the theory and experimentation on cyclotron resonance in InSb was undertaken.

Due to the discovery of non-linear effects at low electric fields and hysterisis at high electric fields, the subject covered in this chapter (and the next two) was broadened to include the general electrical characteristics of high purity n-InSb.

The first section of this chapter involves a survey of the history of the development of semiconductor physics up to the start of semiconductor theory. The next section focuses on the development and application of that theory. The third section deals with the work done on emission from InSb. The next section deals with the development of knowledge on the electrical characteristics of InSb. A small section on the possibilities of tuneable lasers using the above knowledge is also included.

This chapter aims to provide a detailed, though by no means comprehensive, review of the work done in the areas of relevance to this thesis. It also provides a historical perspective to the work and to the approach taken. The references mentioned here provide the foundations for the work presented in the next two chapters.

2.2 **Conduction Theory**

2.2.1 The Development of Conduction Theory

To start from the very beginnings, the first concepts of electricity and magnetism were developed in the 18th century. Weber[1] in 1875 was the first to attempt to explain the passage of electricity through materials in response to the rapidly developing electrical technology. It was not until 1897, though, that the concept of an electron was introduced and given substance by Thomson[2] and Weichart[3]. At the turn of the century Drude[4] treated the problem of electrons within a metal as if they were particles in a gas and applied the dynamical theory of gases to the situation. By this method he was able to derive the empirical Wiedemann-Franz law (which states that the ratio of thermal to electrical conduction is a constant). The assumptions made by Drude give an indication of approach and are summarised as follows:-

1/ Certain electrons in metals act as if they are not constrained by the metal and are in effect 'free',
2/ 'Free' electrons are responsible for thermal and electrical conduction,
3/ The 'free' electrons form a gas where ordinary dynamical laws apply.

A more exact statistical approach was taken by Lorentz[5], whose theory also predicted the characteristics of the Wiedemann-Franz law.

The assumptions taken in this approach are as follows:-

1/ Atoms are rigid spheres so that collisions with electrons are elastic,
2/ Collisions between electrons are negligible,
3/ The concentration of 'free' electrons is dependent on the temperature of the metal,
4/ Atomic cores occupy only a small volume of the metal,

---

[1]Weber, Pogg. Ann. 156 , 1 (1875)
[2]J.J.Thomson, Phil.Mag.44 , 298 (1897)
[3]Weichart, Verhd.Phy.Ges.ZU.Konigsberg
[4]Drude, Ann.Physik 1 , 566 & 3 , 369 (1900)
[5]Lorentz, Proc.Amsterdam Acad. 7 , 438 & 586 (1905)

5/ Variations over a distance equal to the mean free path are small,

6/ Thermal excitation is far greater than electrical excitation

$$v_T = \sqrt{\frac{2kT}{m}} >> v_E = \sqrt{\frac{2eV}{m}} \quad .$$

Under these assumptions Lorentz was able to show that the Boltzmann transport equation could be used to describe the dynamics of the electron gas.

The above two models present the classical picture of electron dynamics and introduce the concept of an electron 'gas' of 'free' or 'quasi-free' particles. This concept is the fundamental precept of the quasi-classical approach to electron dynamics in semiconductors, which is utilised strongly in this thesis.

The next couple of decades saw the introduction of quantum mechanics and the derivation of the Schrödinger wave equation describing the electron motion in an electric potential. (The solution of the Schrödinger equation under certain conditions gives the electron transport equation under those conditions.) The introduction of quantum statistics theory led to a radical rethink of the definition of the electron. It could no longer be thought of as a discrete particle, but had to be thought of as a wave packet (or as a quasi-particle). Other effects of quantum theory included the Pauli exclusion principle allowing no two electrons to exist in the same energy and momentum state (these states were derived by quantum theory and defined by quantum numbers). The effect of the Pauli Exclusion principle to electrons in any system was calculated by Dirac[6] and its effect on a gas of ordinary atoms was calculated by Fermi[7]. The above two calculations were then combined and applied to "free" electrons in a metal[8]. They were also applied to metallic conduction[9].

---

[6]Dirac, Proc.Roy.Soc.A112 , 661 (1926)
[7]Fermi, Z.Physik. 36 , 902 (1926)
[8]Pauli, Z.Physik. 41 , 81 (1927)
[9]Sommerfeld, Z.Physik. 47 , 1 (1928)

2.2.2 Effect of a Magnetic Field on Conduction Theory

The initial appreciation of the effect of a magnetic field was empirical and qualitative. An example of this is Maxwell's 'corkscrew rule'[10]. The first quantitative descriptions were summarised in 'The Mathematical Theory of Electricity and Magnetism' by Jeans[11]. The fundamental equations being : $F = e(\mathbf{v} + \mathbf{E} \times \mathbf{B})$; $a = \frac{evB}{m}$; $r = \frac{mv}{eB}$. The first major step in including the effect of magnetic fields into quantum theory came when Landau derived the necessary modifications to Schrödingers wave equation[12]. He also showed that the electron diamagnetism (the field set up in opposition to an applied field) was equal to a third of the electron's spin magnetism.

2.3 **Development of Semiconductor Theory**

All the above calculations dealt with metals or insulators. The first theoretical appreciation of semiconductors was detailed in an essay based on the Thesis of Wilson[13]. This is generally thought of as the beginning of the semiconductor era. The essay showed how metals and semi-metals could be described with one theory.

Peierls[14] derived the theory of diamagnetism for conduction electrons and introduced the concept of an effective electron mass. This was expanded on by Blochinzev and Nordheim[15] who derived a theory for magnetic and thermo-electric effects in metals in which they define and use an effective mass tensor.

The next few years saw the introduction of some key textbooks by Wilson[16], Mott & Jones[17], and Seitz[18]. These provide a

---

[10]Hadley, 'Magnetism & Electricity' (1905)
[11]Jeans, 'The Mathematical Theory of Electricity and Magnetism' 2nd ed. (1911)
[12]Landau, Z.Physik 64 , 629 (1930)
[13]Wilson, Proc.Roy.Soc. A133 , 458 (1931)
[14]Peierls, Z.Physik. 80 , 763 (1932) & 81 , 186 (1933)
[15]Blochnizev & Nordheim, Z.Physik. 84 , 168 (1933)
[16]Wilson, 'The Theory of Metals' (1936)
[17]Mott & Jones, 'Properties of Metals & Alloys' (1936)
[18]Seitz, 'Modern Theory of Solids' (McGraw-Hill,N.Y.)(1940)

good review of the knowledge gained by 1940 and provide the basis for what was to follow.

2.3.1 The Quasi-Classical Approach

The above had led to the setting up of what will be described as the Quasi-Classical approach. (The validity of this approach, and the consequent model, is used as a basic assumption in this thesis.) The derivation of effective mass theory showed how, when solving Schrödingers equation for electrons in a crystal, a term related to the electron wave packet could be interpreted as the 'mass' of the wave packet and that if the term were taken as an effective mass the equations of motion could be reduced to the free electron case. This 'mass' term, in effect, includes within it the effect of the crystal on the electron. The ideal case is when the effect of the crystal on the electron is independent of the electron's energy or direction. This rarely occurs. So the effective mass may be different along the different crystal axes and may also be energy dependent. This complicates the situation, though the concept is the same. One can now treat the problem of conduction in a solid as that of free particles with an effective mass defined by the properties of that solid.

In this quasi-classical approach the electrons are treated as free particles in an effective electron-'gas'. This gas is then affected by a potential created by an applied electric field. As in an ordinary gas there will be collisions between the particles of the gas and as the application of an accelerating field will cause the 'gas' to heat up these collisions will ensure that the energy supplied to the gas is distributed in a fashion described by the Boltzmann distribution. The mean time between collisions for a particle is known as the lifetime of the particle.

2.3.2 Relaxation Mechanisms & Electron Lifetimes

The above presupposes the existence of some energy loss mechanism which will set up an equilibrium at some value of the average gas energy. In a real gas this energy loss is to its surroundings. In a solid this is also the case. The methods of

energy loss are split into two main sections: Phonon emission and photon emission. The phonon and photon are quasi-particles equivalent to a quanta of lattice structure excitations and a quanta of electromagnetic radiation respectively. The first is where there is an energy exchange between the electron 'gas' and the structure of the solid. This will result in the initiation of vibrations in the structure which can be observed as a change in the temperature of the solid. The second is where energy is emitted from the gas in the form of electromagnetic radiation. Energy can also be lost through a combined interaction with structural vibrations and electromagnetic radiation.

The development of electron lifetimes in semiconductors is as follows. Wilson introduced the concept of separate lifetimes for electrons under the influence of only one scattering process. These lifetimes could then be combined to provide the electron lifetime for a specific energy. Wilson[17] considered the lifetimes due to scattering by ionised impurities, acoustic phonons and optical phonons*. More exact calculations were then made of these lifetimes. Key papers on neutral and ionised scattering include those by Mott[19], Davydov & Schmuslkievich[20],Conwell & Weisskopf[21], Erginsoy[22], Brooks[23], Debye & Conwell[24] and Sclar[25]. Key papers on phonon scattering include those by Seitz[26], Bardeen & Shockley[27], Howarth & Sondheimer[28] and Radcliffe[29]. Key papers which deal with several of the scattering processes and their

---

* For definitions of these and other scattering processes see section 3.

[19]Mott, Proc.Camb.Phil.Soc. 32 , 281 (1936)

[20]Davydov & Schmushkievich, Usp.Fiz.Nauk 24 , 21 & J.Phys(Moscow), 3 , 359 (1940)

[21]Conwell & Weisskopf, Phys.Rev. 77 , 388 (1950)

[22]Erginsoy, Phys.Rev, 79 , 1013 (1950)

[23]Brooks, Phys.Rev. 83 , 879 (1951)

[24]Debye & Conwell, Phys.Rev. 93 , 693 (1954)

[25]Sclar, Phys.Rev. 104 , 1548 (1956)

[26]Seitz, Phys.Rev.B. 73 , 549 (1948)

[27]Bardeen & Shockley, Phys.Rev. 80 , 69 & 80 , 72 (1950)

[28]Howarth and Sondheimer, Proc.Roy.Soc. A219 , 53 (1953)

[29]Radcliffe, Proc.Phys.Soc. A68 , 675 (1953)

interaction, include those by Conwell[30], Barrie & Edmond[31], Barrie[32] and Greene[33].

2.3.3 Theory of Breakdown in Semiconductors

The above deals mainly with materials subjected to electric fields which will cause them to act as 'classical' semiconductors. (The definition of a 'classical' semiconductor, used here, being one where the conduction band is non-degenerate and Maxwell-Boltzmann statistics apply so that the electrons motion can be described by the Boltzmann transport equation. Conduction is by the extrinsic concentration.) If the impurity levels are close to or below the bottom of the conduction band then for low fields the material will be degenerate or partially degenerate. At high fields, when electrons are being ionised from the valence band creating an intrinsic concentration, the conduction band concentration can become large enough to cause the band to become degenerate again. This time it is completely degenerate and will conduct as a metal. The transition from non-degenerate to degenerate conduction band which is linked to the impact ionisation of electrons from the valence band is often linked with dielectric breakdown as the valence electrons are often the bonding electrons between atoms in the lattice. This means that for most semiconducting materials applying an electric field large enough to create breakdown has catastrophic results for the crystal. For this reason the region around dielectric breakdown is rarely studied.

A less catastrophic type of breakdown occurs when the dominant scattering process is unable to remove energy at a rate equal to that at which the electrons are obtaining it. The runaway situation will continue until a scattering process capable of removing the energy becomes dominant.

Von Hippel[34] in 1932 expounded a theory on breakdown in semiconductors. He proposed that breakdown in solids is a by-

---

[30]Conwell, Phys.Rev. 88 , 1379 (1952) & 90 , 769 (1953)
[31]Barrie & Edmond, J.Elect. 1 , 161 (1955)
[32]Barrie, Proc.Phys.Soc.(London) B69 , 553 & Phys.Rev. 103 , 1581 (1956)
[33]Greene, J.Elect.&Contr. 3 , 387 (1957)
[34]von.Hippel, Z.Physik 75 , 145 (1932)

product of the production of electron avalanches by electron impact. That electrons that are free within the solid are accelerated by an electric field and retarded by the 'friction' of lattice vibrations. He postulated that breakdown occurs when the average electron gains energy more rapidly from the field than it loses energy to the lattice for all velocities of motion less the value needed to produce ionisation by impact. He also proposed that electrons encounter the greatest 'friction' at energies equal to the longitudinal optical (LO) phonon energy.

Fröhlich[35], theorised that breakdown occurs when electrons are accelerated through the 'friction' barrier and reach energies greater than that required for ionisation. Also that the average electron energy can be lower than the ionisation energy, i.e. only a certain proportion are required to obtain energies in excess of the ionisation energy.

In 1949 Seitz[36] presented a paper on breakdown which concluded that the electrons which are most important in determining the initiation of breakdown are those which are accelerated from rest to energies in excess of the ionisation energy. Also that the average energy of the total concentration of electrons could be as low as 0.2 times the ionisation energy.

In 1950 Fröhlich and Seitz[37] combined to compare their theories and concluded that breakdown occurs due to some, as yet unspecified, factor, triggering an irreversible and unstoppable ionisation of the valence band. That the observed increase in electron concentration and conductivity before breakdown was due to an initial non-catastrophic breakdown.

In 1956, Fröhlich and Paranjape[38] described a temperature breakdown which was unrelated to an intrinsic breakdown. This breakdown being due to lattice vibrations being unable to impart their energy to the surroundings as fast as they receive energy by interaction with electrons.

---

[35]Fröhlich, Proc.Roy.Soc. 160 , 230;172 , 94 ; 178 , 493 ; 188 , 521&532 & Phys.Rev. 61 , 200

[36]Seitz, Phys.Rev. 76 , 1376 (1949)

[37]Fröhlich & Seitz, Phys.Rev. 79 , 526 (1950)

[38]Fröhlich & Paranjape, Proc.Phys.Soc. B69 , 21 (1956)

Frölich and Paranjape[39] also predicted that the current would become unstable in fields close to breakdown and the mobility can show two differing stable values.

Ehrenreich[40], in 1957, made the first calculations of the breakdown field for InSb and obtained values between 170 and 295 Vcm^{-1}.

Sodha[41] measured the variation of mobility with electric field for a non-degenerate semi-conductor. Prior[42],however, with InSb found his measurement of electron mobility to be constant for fields as high as 800 Vcm^{-1}.

Stratton[43] provides equations from which the breakdown field can be derived. The major review of the early work done on high field characteristics of semiconductors was carried out by Conwell[44] in 1967.

2.3.4 The Effect of a Magnetic Field on the Above and the Introduction of Cyclotron-Resonance (C.R.) Effects

Kapitza[45], in 1929, made the first observations of an increase in resistance with magnetic field in semiconductors. Landau derived the Schrödinger equation for the case of an applied magnetic field[46] and Seitz showed how the solution of the equation predicted a grouping of the energy levels in the conduction and valence bands into discrete energy levels separated by an energy ($\hbar\omega$)dependent on the magnetic field ($\omega = eB/m^*$)[47]. These levels are known as Landau levels. Titeica[48] studied the magneto-resistance in metals and included the effect of phonon scattering. Davydov & Pomeranchuk[49] then studied magneto-resistance in

---

[39]Fröhlich & Paranjape, Proc.Phys.Soc. B69 , 21 (1956)
[40]Ehrenreich, J.Phys.Chem.Sol. 2 , 584 (1957)
[41]Sodha, Phys.Rev. 108 , 1375 & 107 , 1266 (1957)
[42]Prior, J.Elec.& Cont. 4 , 165 (1958)
[43]Stratton, Proc.Roy.Soc. (London) A246 , 406 (1958)
[44]Conwell, 'High Field Transport in Semiconductors' (1967)
[45]Kapitza, Proc.Roy.Soc.(London) A123 , 292 (1929)
[46]Landau, Z.Physik. 47 , 1 (1930)
[47]Seitz, 'Modern Theory of Solids' (1940)
[48]Titeica, Ann.Physik. 22 , 129 (1935)
[49]Davydov & Pomeranchuk, J.Phys.(U.S.S.R.) 2 , 147 (1940)

semi-metals and included the effect of ionised impurity scattering. The above are some of the papers not included in an otherwise comprehensive review, on magneto-resistance in semiconductors, given by Johnson-Whitesell[50] in 1953.

The first note on CR effects in semiconductors was made by Dingle[51], in 1952, who showed that CR was as important as the skin effect in absorption of radiation. Dresselhaus, Kip & Kittel[52] developed the theory of CR for a carrier with an isotropic effective mass.

In 1956, Yafet, Keyes & Adams[53] used a model, where the impurity ions were treated as if they were hydrogen atoms, to determine the effect of a magnetic field on impurity levels. Continuing this work, Keyes & Sladek[54] were able to predict the occurrence of a magnetically induced 'freezing' out of the impurity levels*. Also that mobility would decrease with increasing magnetic field and that there is no saturation of magneto-resistance with magnetic field. This is in line with the predictions of Dresselhaus et.al..

Argyres & Adams[55] studied the effect of a magnetic field on the scattering of electrons in a semiconductor with spherical energy surfaces for which they believed that a saturation of magneto-resistance was possible, but that it would not affect the scattering processes. They were able to show how the scattering lifetimes would be affected for both lattice scattering and ionised impurity scattering.

In 1957, Wallis & Bowlden[56] discussed a theory for the photo-ionisation of impurities in the presence of a magnetic field (strong enough to cause impurity freeze-out).

---

[50]Johnson-Whitesell, Phys.Rev. 89 , 941 (1953)

[51]Dingle, PhD Thesis Camb.(1951) & Proc.Roy.Soc.(London) A212 , 38 (1952)

[52]Dresselhaus,Kip & Kittel, Phys.Rev. 98 , 368 (1955)

[53]Yafet,Keyes & Adams, J.Phys.Chem.Sol. 1 , 137 (1956)

[54]Keyes & Sladek, J.Phys.Chem.Sol. 1 , 143 (1956)

* The magnetic field induces a shift in the impurity level such that is isolated within the band gap.

[55]Argyres & Adams, Phys.Rev. 104 , 900 (1956)

[56]Wallis & Bowlden, J.Phys.Chem.Sol. 7 , 78 (1958)

A good text for the general theories of semiconductor characteristics up to this point in history is 'Semiconductors' by Smith[57].

2.3.5 The Band Structure of InSb

The major theoretical breakthrough for InSb was when Kane[58] calculated its band structure and introduced energy equations for electrons in these bands.

The calculation of the band structure of InSb, by Kane, proposed that the conduction band was non-parabolic in its energy profile which would imply that the effective electron mass would be energy dependent. This helped to reconcile different values obtained by experiments and theories as therein the mass had been assumed to be constant with energy. Also the triple degeneracy of the valence band coupled with the small band gap would imply strong interband interactions capable of causing the very small values of the effective electron mass and the high electron g value[59,*] .

The above was expanded on to provide the relation between the electron concentration at any specific energy in the crystal and the energy provided to the electrons[60,61]. This relation included generalised Fermi integrals whose properties and values were derived[62,63].

---

[57]Smith, 'Semiconductors' (C.U.P.,1959)

[58]Kane, J.Phys.Chem.Sol. 1 , 249 (1957)

[59]Bemski, Phys.Rev.Letts. 4 , 62 (1960)

* This is the value connected with the electron spin

[60]Zawadski, Phys.Letts. 4 , 191 & Phys.Stat.Sol. 3 , 1421 (1963)

[61]Zawadski & Kolodziejczak, Phys.Stat.Sol. 6 , 419 (1964)

[62]Kawalczyk et.al., Tables Pub. by Inst. of Phys.,Pol.Acad. of Science (Warsaw,1965)

[63]Zawadski,et.al., Phys.Stat.Sol. 10 , 513 (1965)

2.4 Experimental and Theoretical Advances in C.R. and Microwave Emission in n-InSb

The experimental study of the electrical characteristics of InSb with especial reference to C.R. began with the first observation of C.R. effects in InSb by Dresselhaus,Kip&Kittel[52]. They observed resonance by both electrons and holes. By illuminating an InSb crystal with radiation, of frequency equal to 24 GHz, whilst varying an applied magnetic field, resonance at specific values of the magnetic field were observed. These values implied an effective electron mass of 0.013 times the free electron mass. This value has been shown by later experiments to be quite accurate.

Evidence of C.R., in transmission experiments on InSb, was observed by Burstein,Picus&Gebbie[64](1956) at room temperature. Large magnetic fields were employed to ensure that the C.R. energy exceeded the thermal energy. This raised the C.R. frequency to about 8 THz. The value obtained for the effective electron mass was 0.015 times the free electron mass. Presented alongside the above by Blatt[65](1956), in conjunction with the above authors, was the practical evidence for the increase in the size of the intrinsic band gap energy with magnetic field as was predicted by Landau. Two papers by Keyes et.al.[66](1956) confirmed the results obtained by Burstein et.al..

The discovery that the effective mass in InSb is energy dependent helped to reconcile differences in the above results.

Haslett&Love[67](1959) presented the first study of the electrical and magneto-electrical characteristics of InSb. For a crystal with an excess donor concentration of 1.2×10^{16} cm^{-3} and dimensions 1x1x5 mm^3, it was found that for magnetic fields greater than 4 Tesla the variation in longitudinal resistance with magnetic field was constant at all temperatures. This was also found to be the case for all magnetic field values, provided the temperature was greater than 14 Kelvin. The above results were

---

[64]Burstein,Picus&Gebbie, Phys.Rev. 103 , 825 (1956)
[65]Burstein,Picus,Gebbie&Blatt, Phys.Rev. 103 , 826 (1956)
[66]Keyes et.al., Phys.Rev. 104, 1804 &1805 (1956)
[67]Haslett & Love, J.Phys.Chem.Sol. 8 , 518 (1959)

obtained under constant current conditions where the current density was 8.7Acm^{-2}. Electric field versus current density (E-J) characteristics were also obtained, for a crystal with an excess donor concentration 2.8x10^{14} cm^{-3}, at various magnetic field strengths up to 16.3 T at a temperature of 4 K. Various non-linearities and evidence for chaotic noise were reported and attributed to the impact ionisation of impurity levels which have been isolated below the conduction band by the effect of the applied magnetic field.

The non linearities were investigated further by Phelan&Love[68] (1963). They reported the observation of negative differential resistance in InSb at 1.1 K under constant current conditions with an applied magnetic field of at least 0.5 T. Typical excess donor concentrations, of the crystals used, being 9.5x10^{13} cm^{-3}. Again the non-linearities were attributed to the impact ionisation of the impurity levels. The threshold electric field for initiation of ionisation was shown to have a linear dependence on the magnetic field. Without an applied magnetic field it was noted that the crystal would react to an applied electric field within 10^{-6}s. The negative differential resistance was used to generate oscillations of frequency equal to 200 KHz.

Kogan[69] observed that irradiation of an InSb crystal would alter the current requirements of that crystal. This was developed further by Kinch & Rollin[70] who showed how energy absorbed, from radiation, by free carriers could be detected as a change in mobility or conductivity. They also suggested that the application of a magnetic field to the detector might cause photo-induced CR.

A large review paper on far-infrared photoconductivity was completed by Putley[71] in 1964. This paper also included a summary of some of the work mentioned above. Current-voltage characteristics, at temperatures of 1.38 K & 4 K, magnetic fields up to 0.7 T and under constant current conditions, were given. Negative differential resistance and an apparent hysteresis was

---

[68]Phelan & Love, Phys.Rev. 133 , A1134 (1963)
[69]Kogan, Sov.Phys.Sol.State 4 , 1386 (1963)
[70]Kinch & Rollin, Brit.J.Appl.Phys. 14 , 672 (1963)
[71]Putley, Phys.Stat.Sol. 6 , 599 (1964)

noted. These effects were attributed to the ionisation of electrons in the impurity level which have been trapped there by the combination of low temperature and high magnetic field. The effectiveness of InSb as a detector was discussed.

Emission of microwave radiation, connected with CR, from InSb was first reported by Buchsbaum et.al.[72] in 1965. A crystal of dimensions: 1x1x9 mm, with a carrier concentration of $2x10^{14}$ cm^{-3} whose mobility was $2x10^5$ $cm^2V^{-1}s^{-1}$ was subjected to an electric field of up to 300 Vcm^{-1} and a magnetic field of up to 0.4 T at a temperature of 77 K. The radiation emitted was of frequency equal to about 5 GHz. The current-voltage characteristics for the crystal, obtained under the above conditions, agree with those obtained by Glicksman & Steele[73] in 1959. The rapid increase in current was attributed to intrinsic breakdown (the point where the intrinsic concentration dominates over the uncompensated donor concentration as impact ionisation of valence band electrons occur).

Further microwave emission in InSb, under applied electric and magnetic fields was observed by Larrabee & Hicinbothem[74]. At a temperature of 77K with fields above those required for breakdown, the onset of emission almost coincides with the onset of lower frequency current oscillations. The current oscillations implied the presence of a current controlled negative differential region involved with or close to breakdown. The emission was observed to occur in conditions similar to those required for current oscillations, but continued for current values above those at which the current oscillations began to decrease. The onset conditions were given as being: An applied field of 300 Vcm^{-1}; An applied magnetic field of 0.6 T; And a temperature of 77 K. This was for a crystal of dimensions: 11x0.2x0.2 mm. A negative differential resistance oscillator was proposed. The possible output power was calculated theoretically to be 5 mW at 1 THz.

Edison and Kino[75] repeated Buchsbaums experiments with differing crystal sizes and observed in addition to noise, emitted

---

[72]Buchsbaum et.al., Appl.Phys.Letts. 6 , 67 (1965)
[73]Glicksman & Steele, Phys.Rev.Letts. 2 , 461 (1959)
[74]Larrabee & Hicinbothem, IEEE.Trans.Elec.Dev. 13(1) , 121 (1966)
[75]Edison & Kino, Appl.Phys.Letts. 8 , 183 (1966)

in the frequency range 30 MHz to 10 GHz, some narrow band microwave oscillations at lower electric fields. Crystal properties involved were an uncompensated donor concentration of $7x10^{13}$ cm^{-3} and an electron mobility of $5x10^5$ $cm^2V^{-1}s^{-1}$. The narrow band emission was electrically tuneable between 2.1 & 3.2 GHz, for an applied magnetic field of up to 0.225 T and an electric field of between 10.5 and 22.5 Vcm^{-1}. The oscillation was thought to connected with the crystal contacts.

Musha et. al.[76] discovered microwave radiation at even lower electric field values (> 3 Vcm-1) with magnetic fields of between 0.4 and 2 T. The frequency of the radiation was 2 to 4 GHz. The crystal's details were: an uncompensated donor concentration of $1x10^{15}$ cm^{-3} with an electron mobility of $1.3x10^5$ $cm^2V^{-1}s^{-1}$. At least two mechanisms are proposed as the cause of the emission. A noise background is obtained on which resonant spikes are observed. These occur periodically with magnetic field. The magnetic period of 0.0255 T is equivalent to a CR energy of 22.4 meV which is identical to the optical phonon energy for InSb.The possibility of phonon resonance was not discussed. Nor were any other explanations for the resonant spikes proposed. The above was repeated by Bekefi et.al.[77] at 77 & 4 K.

2.4.1 Experimental and Theoretical Work on CR and Microwave Emission for Fields Below Those Required for Breakdown.

The above work shows that microwave emission can occur at various electric fields. The first results were for fields which were able to cause breakdown. The results by Musha et.al. and Bekefi et.al. occur at fields where breakdown is not present. This section deals with the theory and experimentation involved with emission below the breakdown region.

In 1972 Gornik[78] reported emission from InSb at 2 & 4.2 K for electric fields above $100Vcm^{-1}$ and magnetic fields of up to 0.8 T. (Crystal characteristics : uncompensated donor concentration of $7x10^{13}$ cm^{-3}, electron mobility of $7x10^5$

---

[76]Musha,Lindvall & Hägglund, Appl.Phys.Letts. 8 , 157 (1966)
[77]Bekefi,Bers & Bruek, Phys.Rev.Letts. 19 , 24 (1967)
[78]Gornik, Phys.Rev.Letts. 29.9 , 595 (1972)

$cm^2V^{-1}s^{-1}$ and impurity concentration of $4.5x10^{14}$ cm^{-3}.) This was identified as emission from electrons relaxing from low conduction band landau levels to impurity levels. Maximum power levels measured were 10^{-8} W with an external power efficiency found to be 10^{-5}.

In 1973 Kobayashi et.al.[79] repeated and furthered the work done by Gornik, though with a pulsed electric field (400 μs,15 Hz, 0-20 V), and a perpendicular magnetic field (up to 2 T). They noted that the current-voltage characteristic did not change for any value of applied electric field (though they did not specify what it would have changed from). However, for the fields applied, it was expected that the current-voltage characteristics would be effectively linear. In connection with their experimental findings Kobayashi et.al.[80] went on to measure and calculate quantities like the electron concentration in Landau levels as a function of electric field; the electron temperature as a function of electric field; the dependence of transverse resistivity with electric field & lattice temperature; and the energies of the Landau levels as a function of magnetic field.

By 1975 Gornik[81] had progressed to the development of the CR emission into tuneable far-infrared sources. Three semiconducting materials were considered : InSb, GaAs & HgCdTe. The sources were used to measure Zeeman splitting of shallow donors in InP & GaAs to demonstrate their usefulness. The power output and wavelength dependences on magnetic field were calculated for InSb & GaAs for samples with geometries : 5x5x0.2 mm^3 and uncompensated donor concentrations of $1x10^{14}$ cm^{-3}. The electric field required was between 3 and 10 Vcm^{-1}, which corresponded to an effective electron temperature of 25 K.

Tyssen et.al.[82] analysed the Landau emissions in InSb by Fourier spectroscopy for frequencies below and above the optical phonon frequency and deduced that LO phonon-electron coupling was causing the cyclotron frequencies to increase for a given magnetic field and also induced an increase in the line width.

---

[79]Kobayashi et.al., Phys.Rev.Letts. 30.15 , 702 (1973)
[80]Kobayashi & Otsuka, J.Phys.Chem.Sol. 35 , 839 (1974)
[81]Gornik, Optics&Laser Tech. 7 , 121 (1975)
[82]Tyssen, Sol.State.Comm. 17 , 1459 (1975)

Gornik et.al.[83], in order to sharpen the linewidth, introduced a helium temperature Fabry-Perot interferometer. The emission from InSb was compared with that from a HCN laser. Due to the rapid decay in intensity in higher order harmonics for the CR emission it was concluded that the emission was too divergent. An improved optical system was suggested.

McCombe et.al.[84] undertook a systematic study of quantum limit cyclotron resonance linewidths in several InSb samples and concluded that, for fields where ionised impurity scattering is the dominant relaxation mechanism, the linewidths are proportional to the square root of the ionised impurity concentration; the linewidth exhibits a minimum in its relation with magnetic field and the linewidths and the position of their minimum value are independent of the free carrier concentration.

In 1976 the effect of background radiation on the electron population of Landau levels and the consequent effect on emission was investigated by Bauer et.al.[85]. This was followed up later on in more detail by Müller et.al.[86] who concluded that the effects of background radiation could account for the differences in the results obtained on emission so far.

In 1977 measurements leading to the evaluation of electronic lifetimes for electrons in the first Landau level and impurity levels were made by Gornik et.al.[87] They concluded that the electronic lifetimes were determined by inter-electron scattering in the first Landau level and by acoustic phonons in the impurity levels.

More work on the rise time and resolution of CR emission from InSb & GaAs was carried out by Müller et.al.[88]. This demonstrated that InSb has superior power dissipation, but GaAs has a narrower linewidth.

A summary of the work done in connection with CR emission was made by Gornik[89] in 1978. Included is the relation between

---

[83]Gornik et.al., IR.Phys. 16 , 109 (1976)
[84]McCombe et.al., Phys.Rev. B13 , 253 (1976)
[85]Bauer et.al., Phys.Stat.Sol. 75 , 543 (1976)
[86]Müller et.al., Phys.Stat.Sol. 86 , 205 (1978)
[87]Gornik et.al., Phys.Rev.Letts. 40 , 1151 (1978)
[88]Müller et.al., IR.Phys. 18 , 691 (1978)
[89]Gornik, Proc.Conf.ed.Ryan, 329 (1978)

electric field and effective electron temperature and the concentration of electrons in the Landau levels for several electric field values. The latter demonstrates the effect of optical phonon scattering in preventing emission by relaxation from levels above the optical phonon energy.

2.4.2 Experimental and Theoretical Work on CR and Microwave Emission at Fields Above Breakdown.

After the discovery of microwave emission associated with breakdown, this property was studied in order to probe the processes involved with breakdown. Initially work was done on determining the radiative recombination lifetime at breakdown[90,91,92]. Experimentation on the recombination radiation led to the conclusion that the orientation of an applied magnetic field had no effect on the emitted radiation, though it was observed to affect the threshold field for breakdown ($E_{th} \approx 40$ - 250 Vcm^{-1} for $B \approx 0.8$ - 1.0 T). It was noted that the electric field at the onset of radiation was always less than the threshold field[93]. The effect of optical phonon scattering on the non-linearity involved with breakdown was considered[94]. The possibilities of instabilities in the electron-hole plasma causing or being associated with the non-linearities was also investigated[95]. The diffusion length for the recombination radiation in this regime was found to be about 50 to 80 μm[96]. The effect of reabsorption is significant and was also dealt with by Müller et.al[97].

Spontaneous emissions at frequencies up to the sub-mm wavelength region were predicted for electric fields great enough to induce intense impact ionisation of the valence band (330 GHz

---

[90]Kadushkin, Sov.Phys.Semicon. 5 , 1549 (1972)
[91]Blaut-Blachev, Sov.Phys.Semicon. 9 , 247 (1975)
[92]Fossum et.al., Phys.Rev.B 8 , 2850 (1973)
[93]Grisheckina & Luchina, Sov.Phys.Semicon. 9 , 153 (1975)
[94]Gulyaev, Sov.Phys.Semicon. 9 , 599 (1975)
[95]Vladimirov, Sov.Phys.Semicon. 14 , 247 (1980)
[96]Malyutenko et.al., Sov.Phys.Semicon. 14 , 457 (1980)
[97]Müller et.al, Phys.Stat.Sol(b) 86 , 205 (1978)

at E ≈ 600 Vcm^{-1})[98]. Further work done on the breakdown region provided a calculated I-V characteristic for n-InSb at 77 K and more evidence of the magnetic dependence of the breakdown electric field[99]. The carrier concentration of the breakdown plasma has been measured. For a crystal with an uncompensated donor concentration of ≈ 1 x 10^{14} cm^{-3} the carrier concentration after breakdown was ≈ 7 x 10^{16} cm^{-3} (dependent on the threshold field and hence the magnetic field)[100].

2.5 **Experimental and Theoretical Work on The Electrical Characteristics of n-InSb**

Some of this work has already been included in earlier sections and will not be repeated. A good review of the subject is given by Conwell as mentioned in section 2.3.4. A rough summary of the concepts so far is given. This is then followed by more recent developments.

The view of the electrical characteristics in the late 1960's is as follows : - At extremely low electric fields and temperatures the main scattering processes are neutral impurity scattering and piezo-acoustic scattering. With a very slight increase in either temperature or field scattering by ionised-impurities will become more effective than scattering by neutral impurities. Throughout this region the scattering is efficient and the resistance of the crystal is high. On an increase of temperature or field the scattering processes will saturate and become ineffective. This allows a current runaway until scattering by deformation potential type phonons becomes effective. This transition can be seen as an s-type Negative Differential Conductivty (NDC) under constant current conditions. (An s-type NDC is where the negative gradient is caused by a decrease in voltage with increasing current. This can only be observed under constant current conditions.) Under constant voltage conditions it is seen as a sudden increase in current with electric field. On further increases in electric field the electron distribution can be heated such that it appears to be

---

[98]Vladimirov et.al., Sov.Phys.Semicon. 15 , 23 (1981)
[99]Abdurakhmanov et.al., Sov.Phys.Semicon. 19 , 236 (1985)
[100]Botte et.al., Sov.Phys.Semicon. 23 , 811 (1989)

at a greater temperature than the crystal. (The phonon distribution has a lower effective temperature. This is possible because the inter-electron collision lifetime is smaller than the electron lifetime for scattering by acoustic phonons.) This is known as the 'Hot-Electron' effect and leads to a smaller than expected rise in current with electric field (as the momentum scattering processes are more efficient at high electron energies). There is then a smooth transition to the region where electrons are most effectively scattered by optical phonons. Due to the high scattering efficiency of optical phonons the resistance of the crystal is once again high. On still further increasing the electric field the optical phonon scattering saturates and another current runaway occurs. This runaway may also be assisted by ionisation of the valence band.

The application of a magnetic field to the above increases the resistance at every point. At low electric fields and temperatures the application of a strong magnetic field can isolate the donor impurity levels below the conduction band. This increases the resistance greatly as conduction is only possible by impurity conduction (provided the impurity concentration is great enough to produce an impurity band) or by hopping conduction (provided the impurity concentration is great enough so that neighbouring impurity centres are close enough for the electrons to tunnel between them). Impact ionisation of the impurities then provides the right conditions for both NDC and chaotic oscillations. Increasing the electric field results in electrical conditions similar to those without a magnetic field until breakdown is reached. The threshold field was thought to be only slightly dependent on magnetic field[101].

Calculations were undertaken to obtain the average velocity of electrons accelerated by a finite electric field in the optical phonon scattering regime[102]. Also considered was the situation where the optical phonons would no longer be able to restrain the accelerating effect of the field. The lifetime of optical phonons was calculated for the situation when the optical phonon distribution is driven from equilibrium by energetic phonon

---

[101]Glicksmann & Steele, Phys.Rev.Letts. 2 , 461 (1959)
[102]Thornber & Feynman, Phys.Rev.B 1 , 4099 (1970)

emission by electrons, as could occur just prior to optical phonon scattering saturation[103]. A study of the electron conductivity and Hall effect in strongly compensated n-InSb for temperatures between 4.5 and 200 K was undertaken and the possibility and effect of hopping conduction was considered[104]. For pure n-InSb the electron concentrations in the Landau impurity levels and the first Landau level were determined with respect to the magnetic field and the temperature[105]. A calculation of the probabilities involved with the interaction between hot-electrons and acoustic phonons for temperatures of 77 and 300 K was made[106]. The transition between piezo-electric (acoustic phonon) and ionised impurity scattering was observed at low temperatures (1.68-2.47 K) and with an applied magnetic field (> 0.5 T)[107]. A theory dealing with the effect of optical phonon scattering on electrical characteristics was introduced[94]. Also included was further confirmation of an s-type NDC, under constant current conditions, on the transition from piezo-electric scattering to potential deformation phonon scattering. A study of the oscillatory behaviour of transverse magneto-resistance was made, which dealt with the transitions between piezo-electric (acoustic phonon), ionised impurity and optical phonon scattering[108].

A study of the threshold fields for impact ionisation of the valence band was undertaken[109]. From which it could be concluded that the minimum threshold field was $\approx$ 250 Vcm^{-1} and that for a carrier concentration of $\approx 8 \times 10^{13}$ cm^{-3} and a magnetic field less than $\approx$ 1 T no threshold field was obtainable at 77K.

Spontaneous oscillations were observed when an electric field triggered the breakdown of frozen out impurities[110].

Values of electron mobility versus electric field and temperature were obtained[111]. The results showed there to be a

---

[103]Ferry, Phys.Rev.B. 9 , 4277 (1973)
[104]Yaramenko, Sov.Phys.Semicon. 9 , 554 (1975)
[105]Gershenzon et.al., Sov.Phys.Semicon. 9 , 440 (1975)
[106]Akulinichev et. al., Sov.Phys.Semicon. 9 , 666 (1975)
[107]Kichigin et.al., Sov.Phys.Semicon. 9 , 640 (1975)
[108]Kadushkin, Sov.Phys.Semicon. 14 , 1195 (1980)
[109]Brazis et.al., Sov.Phys.Semicon. 14 , 842 (1980)
[110]Vladimirov et.al., Sov.Phys.Semicon. 15 , 894 (1981)
[111]Litvak-Gorskaya & Shapiro, Sov.Phys.Semicon. 17 , 1258 (1983)

maximum in the mobility of $5x10^5$ $cm^2 V^{-1}s^{-1}$ for a carrier concentration of 10^{14} cm^{-3}. This occurred at a lattice temperature of ≈ 80 K or on application of an electric field of ≈ 10 Vcm^{-1}. The energy and drift velocity of the electrons with an applied electric field for n-InSb at 77 K was also derived[112]. It was also shown that the carrier lifetime was dependent on the carrier concentration[113]. A handbook on semiconductors was introduced which included some useful reviews of specific approaches to areas of electrical characteristics in semiconductors[114]. Kane reviewed the approaches to energy band theory; Altarelli and Bassani dealt with the theoretical approaches to impurity states; Baranowski et.al. dealt with the practical approaches to impurity states; Roth revised the principals behind electron dynamics in a semiconductor with applied electric and magnetic fields; Conwell considered the validity of the Boltzmann transport equation; Ferry discussed the fundamental aspects of hot-electron phenomena and Zawadski summarised the knowledge on the CB structure of InSb and provides the complimentary equations for deducing the scattering lifetimes.

Further study of hopping conduction was made and a method which enabled its effect to be isolated was developed[115]. A theory which proposed the possibility of chaos during impact ionisation of impurities also proposed a possible NDC effect under the conditions of carrier cooling by an electric field (carrier cooling occurs when the electrons are accelerated into the optical phonon scattering regime and are scattered into the ionised impurity scattering regime)[116]. A special issue of Applied Physics A(solids and surfaces) was dedicated to 'Nonlinear and Chaotic Transport Phenomena in Semiconductors'. This dealt with the properties of semiconductors involved with impact ionisation of impurities. It includes a review paper on the theoretical approaches taken[117] and a paper on nonlinear oscillations and chaotic behaviour due to

---

[112]Brazis et.al., Sov.Phys.Semicon. 17 , 8 (1983)
[113]Spovskaya et.al., Sov.Phys.Semicon. 18 , 222 (1984)
[114]'Handbook on Semiconductors',Vol.1,Sections, 4A,5,6,8,10,11A & 12.
[115]Aronzon et.al., Sov.Phys.Semicon. 20 , 53 (1986)
[116]Mitin, Sov.Phys.Semicon. 21 , 142 (1987)
[117]Schöll, Appl.Phys.A 48 , 95 (1989)

impact ionisation of shallow donors in n-InSb[118]. The issue is biased towards the chaos effects, though other effects are mentioned.

2.6 Determination of Effective Electron Temperature

The determination and interpretation of the effective electron temperature in InSb began when Issacson & Bridges[119] first determined it experimentally in 1968. This was followed by Maneval et.al.[120], in 1969, who derived the electron temperature in InSb, in the absence of a magnetic, from the energy relaxation time measured using a pulse technique. Mijazawa[121] determined the electron temperature by resistivity and hall coefficient measurements. His results showed an initial suppression in the rise in the effective temperature with electric field, which could be due to impurity band effects. Once a temperature of 18 K is reached the rise in temperature is proportional to the energy (to the power of two sevenths) and hot electrons are predicted in the conduction band. For temperatures above 30 K the effective temperature concept is no longer valid. The results obtained by Stradling & Wood[122], confirmed those obtained by Sandercock[123], which implied a larger than expected power transfer to the lattice from the electrons for a temperature of between 10 and 20 K. A suggested explanation was the introduction of a two acoustic phonon process within the transfer from a single acoustic phonon process to a single optical phonon process.

Further derivations of the effective temperature and its relation to the electric field applied were made by Kobayashi & Otsuka[80] and Gornik[89].

---

[118]Song, Seiler & Lolee, Appl.Phys.A 48 , 137 (1989)
[119]Issacson & Bridges, Phys.Rev. 169 , 312 (1968)
[120]Maneval et.al., Phys.Rev.Letts. 23 , 848 (1969)
[121]Mijazawa, J.Phys.Soc.Japan 26 , 700 (1969)
[122]Stradling & Wood, J.Phys. C3 , 2425 (1970)
[123]Sandercock, Sol.Stat.Comm. 7 , 721 (1961)

2.7 Theoretical and Practical Results in the Extreme Quantum Limit

In 1962, Kazarinov et.al.[124] developed the first theory on electrical characteristics in InSb in the extreme quantum limit. This is where electrons can only occupy the first Landau level because the energy of the second level is greater than that of an optical phonon. Based on this theory several experimental results were obtained. Kotera[125] & Mijazawa[126] observed a peculiar warming process, Katayama[127] observed negative I-V characteristics and Askelrod[128] & Stradling[129] observed resonance phenomenon. These results were discussed and compared with a model set up by Yamada & Kurosawa. Distribution functions for the electrons in only one Landau level were derived[130]. The I-V characteristics and dynamic negative differential conductivity due to hot-electrons in this situation were predicted. A study of the heating of electrons in degenerate n-InSb under a quantising magnetic field led to values for the effective electron temperature with differing electric and magnetic fields[131].

2.8 Possibilities for a Magnetically-Tuned Laser in InSb

Phelan et. al.[132] developed the p-n junction InSb diode laser, operating at a frequency of around 5.8 THz. Due to the variation of the gap between the conduction and valence bands with magnetic field, the frequency of emission could be tuned. This facility caused this laser to be presented as the first magnetically-tuned laser.

---

[124]Kazarinov et.al., Zh.Ekspr.Teor.Fiz. 42 , 1047 (1962)
[125]Kotera et.al., J.Phys.Soc.Japan. 21(suppl.) , 411 (1966)
[126]Mijazawa et.al., J.Phys.Soc.Japan 23 , 290 (1967)
[127]Katayama, Appl.Phys.Letts. 23 , 31 (1972)
[128]Askelrod, Fiz.Tverd.Tela. 11 , 113 (1967)
[129]Stradling et.al., J.Phys. C3 , 2425 (1970)
[130]Andronov et.al., Sov.Phys.Semicon. 15 , 996 (1981)
[131]Kadushkin, Sov.Phys.Semicon., 17 , 699 (1983)
[132]Phelan et.al., Appl.Phys.Letts. 3 , 143 (1963)

A CR laser using a population inversion between the the spin levels of the first Landau level has been suggested[133]. The tuneability of such a laser is restricted by the necessity of the third Landau level being below the optical phonon scattering regime.

A laser that depended on the light amplification properties of crossed applied fields (**J** x **B**) has been demonstrated. The threshold conditions for lasing included a current density of ≈ 15 $KAcm^{-2}$ and a magnetic field of 2 T at a temperature of 80 K[134]. An Interband Laser which relies on the **J** x **B** force to excite the electrons and holes was then developed[135]. This, whilst increasing the magnetic field required to ≈ 7 T, reduced the current density required to ≈ 16 Acm^{-2} which is the lowest ever reported for a semiconductor laser.

2.9 **Conclusion**

This section summarizes the historical perspective into my perspective of the subject due to the work described here. Most of the papers provide detail to a concept which is founded on my own thoughts with the backing of some major papers. These major papers are necessarily few in number and can therefore be picked out and listed here.

For lattice temperatures of 1.5 and 4.2K and very low fields. A high purity n-InSb crystal will not have impurities within its band gap until a magnetic field of at least 0.5T has been applied. The scattering processes which dominate are ionised impurity scattering for the momentum relaxation and piezo-acoustic scattering for the energy relaxation. This holds only for very small fields as a small increase in field will cause the piezo-acoustic scattering process to become unable to remove enough energy. At this point a s-type NDC is possible, dependent on the degree of compensation in the crystal[136,137]. Beyond this deformation

---

[133]Dmitriev et.al., Sov.Phys.Semicon. 22 , 659 (1988)
[134]Morimoto & Chiba, Infrared Phys. 29 , 371 (1989)
[135]Morimoto & Chiba, J.Phys.Soc.Jpn. 60 , 2446 (1991)
[136]Conwell, 'High Field Transport in Semiconductors' (1967)
[137]Gulyaev, Sov.Phys.Semicon 9, 599 (1975)

potential scattering is the dominant process in energy relaxation and also is significant in momentum relaxation. Inter-electron interaction is dominant in momentum relaxation, though, and makes a hot-electron distribution possible. This causes a decrease in conductivity[138]. At still higher fields there is a transition from acoustic phonon and ionised impurity scattering to optical phonon scattering which is dominant for both momentum and energy relaxation. There is also a two acoustic phonon process involved in this transition which causes the conductivity to be reduced before the optical phonon scattering takes effect[139,140]. At high enough electric fields the optical phonon scattering process provides insufficient relaxation and a sharp increase in current occurs. A re-establishment of equilibrium is predicted by some, though a dominant scattering process which could achieve this is not suggested. The possibilities include photon emission (never likely to be the dominant process when the electric field is the only excitation process), a two optical-phonon emission process or some combination of scattering processes working together. Several papers have predicted and shown the possibilities for various types of negative differential conductivity and spontaneous emission at both the impact-ionisation of impurity bands (in the presence of a magnetic field) and the impact ionisation of the valence band (with and without the presence of a magnetic field). Their importance in the electrical characteristics is still to be defined.

To conclude, emission from high purity InSb can occur at the impact ionisation of impurity levels by low electric fields in the presence of a magnetic field. This emission occurs as microwave-noise. Emission can also occur under the conditions of acoustic phonon scattering in the presence of a magnetic field. This emission is cyclotron resonance emission, the frequency and resolution and the linewidth of which is determined by the strength of the magnetic field. Emission also occurs at, or near, the region where optical phonon scattering is saturated and a

---

[138]Smith, 'Semiconductors' (C.U.P.,1959)
[139]Sandercock, Sol.Stat.Comm. 7 , 721 (1961)
[140]Stradling & Wood, J.Phys. C3 , 2425 (1970)

current run-away is observed. This can also involve impact ionisation of the valence band. All three areas are studied here.

The main texts used in this area are by Smith[141] (basic semiconductor theory),Conwell[142] (high field transport in semiconductors), Elliott & Gibson[143] (solid state physics), Madelung[144] (solid state theory) and Blakemore[145] (semiconductor statistics). For more specific theory, volume 1 of the 'Handbook on Semiconductors'[146] was used extensively.

---

[141]Smith, 'Semiconductors' (C.U.P.,1959)
[142]Conwell, 'High Field Transport in Semiconductors' (1967)
[143]Elliott & Gibson, 'Solid State Physics' (Macmillan,1974)
[144]Madelung, 'Solid State Theory' (Springer-Verlag,1978)
[145]Blakemore, 'Semiconductor Statistics' (Dover,1987)
[146]'Handbook on Semiconductors',Vol.1,Sections, 1,3,4A,5,6,8,10,11A & 12.

3 INTRODUCTION TO SOLID STATE PHYSICS

3.1 Band Theory of Crystal Lattices

In an atom, the electrons surrounding a nucleus occupy distinct orbits equivalent to discrete energies (see figure 3.1). When two atoms approach each other they interact and the influence of individual nuclei on the electrons in their outermost orbits is decreased until these electrons are effectively shared between the two nuclei. Each nucleus having an equal effect on the electrons. These are valence electrons which are often involved in creating a bond between the two atoms.

If we are to consider a large group of atoms, separated such that they have no effect on their nearest neighbour, brought steadily closer till they have formed a lattice, then we see the effect of atoms on their neighbours as a spreading of the discrete energies, at which the electrons can exist, into energy bands (see figure 3.1). The structure of these bands determines the electrical characteristics of the lattice formed.

3.2 Effect of Band Structure on Electrical Conductivity

In a metal the band structure is such that there is no energy-gap and conduction can readily occur. In an insulator an energy-gap is formed. The bands on either side of this gap are known as the valence band (VB) and the conduction band (CB). The VB is occupied with electrons that are involved with the bonding of adjacent atoms and are restrained by those atoms. Electrons in the valence band are therefore not involved in conduction. The CB is occupied with electrons that are restrained only by the lattice structure as a whole. Electrons in the CB can thus be involved in conduction.

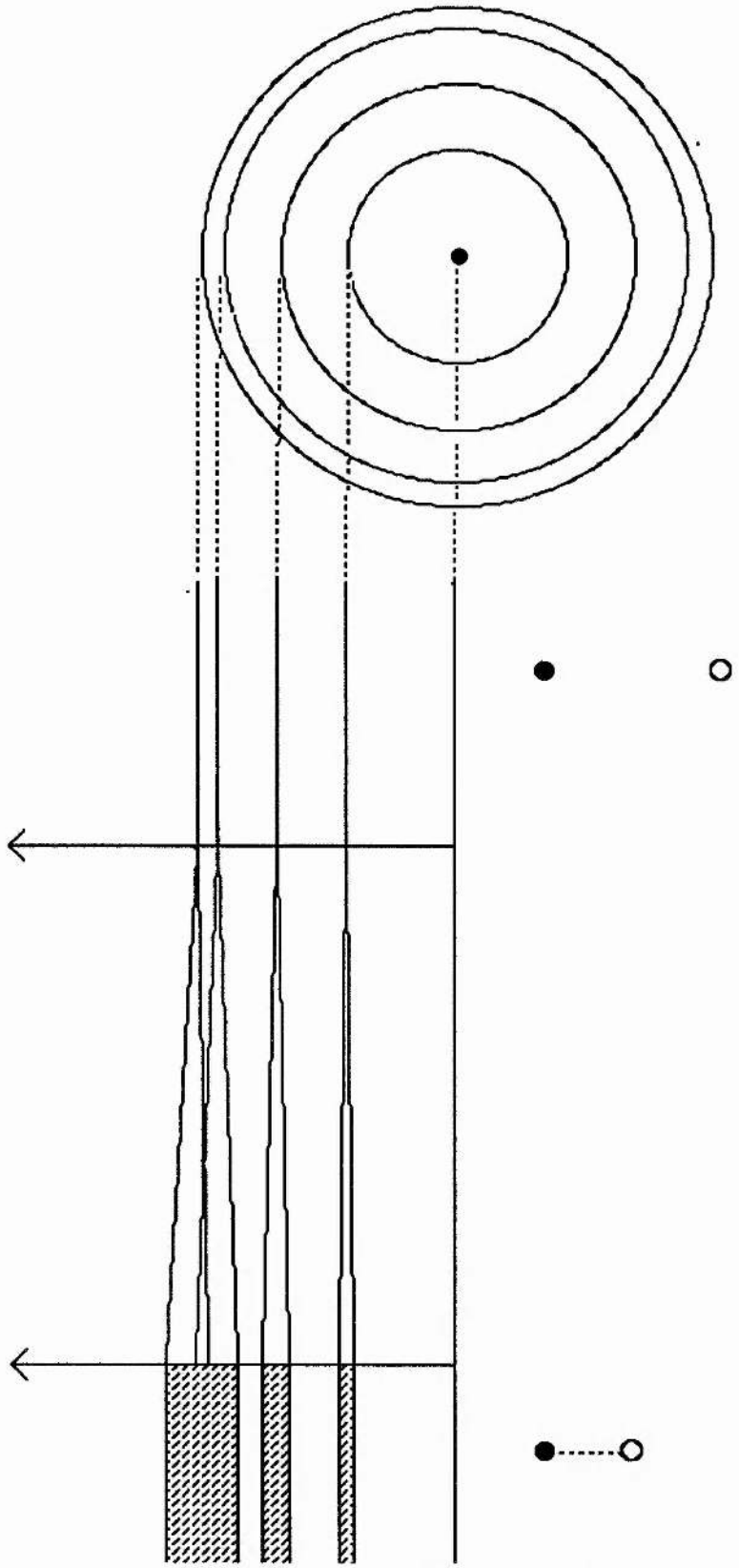

Figure 3.1 : Diagrammatical representation of the formation of energy bands.

In an insulator the CB is empty and the band-gap energy is large. Raising (ionising) electrons from the VB is not possible because this leads to a dielectric breakdown as the electrons involved with the inter-atomic bonds are affected. In a semi-conductor the energy-gap is not so great and the electrons are not so intimately involved with the bonding, so they can be raised (ionised) into the CB relatively easily.

The above is for intrinsic materials (no impurities) and leads to the simple conclusion that for conduction to occur with the application of a small electric field at low temperatures (such that the energy of the electrons is derived effectively only from the field), the band structure of the material's lattice must be such that there is a continuous distribution of states with energy (no energy-gaps). At higher temperatures the band gap must be small. For most materials the direct band-gap transition is too great to be overcome solely by the effect of heat and a greater applied electric field is required. On ionising electrons from the VB the effects of avalanche-impact ionisation and dielectric breakdown become important and restrict the possibilities of some semiconductors.

3.3 **Effect of Impurities on the Electrical Characteristics of Semi-Conductors**

The introduction of impurities and their energy levels can lead to electrons in the CB at low temperatures (providing conduction at low fields) despite the existence of a band gap. Also possible are impurities causing impurity energy levels for electrons within an energy-gap. The electrons in these impurity levels can then be ionised by a far smaller field than is required to ionise valence electrons. Whilst the electrons are in the impurity levels and the CB is empty no conduction* occurs. When the electrons are ionised into the CB conduction occurs. This ionisation can be caused thermally (heat the lattice) or optically (illuminate with a laser) as well as electrically (apply an electric field).

---

* Impurity/hopping conduction may occur in this situation. This possibility is discussed in section 4.4.

Dependent on the impurity atoms, the outermost electrons of the impurity atoms are either loosely bound (only one or two electrons in the outermost shell) and can be ionised to the CB or they are more tightly bound (the outermost shell is almost full and has only one or two holes) and electrons are more likely to be accepted from the VB creating holes there (this is often described as holes being ionised from the impurities into the VB). The first case is that of a donor causing electron conduction. The second case is that of an acceptor causing hole conduction (see figure 3.2).

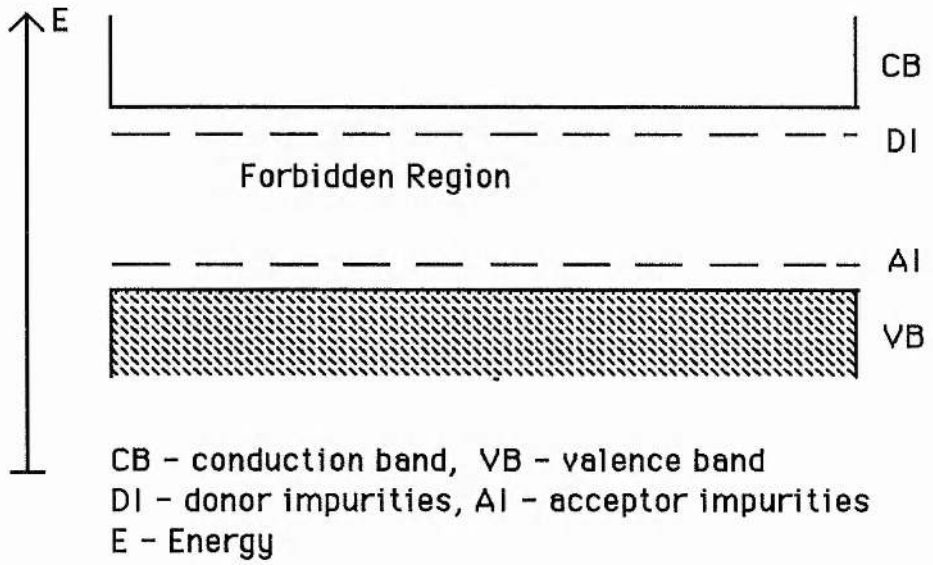

Figure 3.2 : Diagram of impurity levels in the forbidden region.

If there are equal numbers of donors and acceptors then they will counteract each others effect and the material will be unaffected in terms of current carriers. This interaction between impurities is known as compensation. All materials with impurities have some degree of compensation so that the carrier concentration is less than the impurity concentration.

If a material has more donors than acceptors, then the conduction is by electrons whose concentration is equal to the difference in donor and acceptor concentrations. This material is defined as being n-type. Conversely if a material has more acceptors than donors, then the conduction will be by holes whose concentration will be equal to the difference in acceptor and hole concentrations. This material is defined as being p-type.

For the following discussion an n-type material was considered. A similar argument, though, can be used for p-type materials.

3.4 Effect of the Conduction Band Structure on the Electrical Characteristics

Once electrons have been excited into the CB, their motion is governed by the properties of the CB (due to the lattice involved). In order to simplify the description of the electron motion, it is usual to consider the electrons as quasi-free. This involves deriving equations for their motion through the crystal and comparing the equations with the equations of motion for an electron in free space. For most materials this leads to a term known as the effective electron mass which takes the effects of the lattice medium into account. The free electron equations can then be used as if an electron with an effective mass were in motion in free space. This is the quasi-classical approach (c.f. section 2.3.1)

3.5 Electron Concentration and Distribution

To obtain the electrical characteristics one must consider the concentration of electrons involved. As only one electron can occupy any one state (Pauli's exclusion principle) the density of states must also be considered in order to obtain the distribution of electrons with energy. The number of electrons in the conduction band is described by the product of the probability of an electron existing with a specific energy and the energy dependent density of states, integrated over the energy interval zero to infinity (the CB minimum taken as the energy origin). When the Fermi-Dirac distribution is used to describe the possibility of an electron existing with a certain energy, the equation can be simplified into the product of a constant (known as the effective density of states) and an integral (known as the Fermi integral for which there are tables of solutions). For a quantitative description of this see Chapter 4, section 4.3.

3.6 The Fermi-Dirac Distribution

The Fermi-Dirac distribution is such that at zero Kelvin the probability of an electron existing with a certain energy is unity if that energy is less than the Fermi energy. This Fermi energy is thus defined at zero Kelvin by the total electron concentration and the density of states. At zero Kelvin all the electrons attempt to occupy the states with the least energy and so all the states are filled until all the electrons are accommodated. The energy of the outermost state then occupied is then equal to the Fermi level (see figure 3.3).

At non-zero kelvin, the Fermi level is defined as the energy at which the probability of occupation, for a level with that energy, is one half.

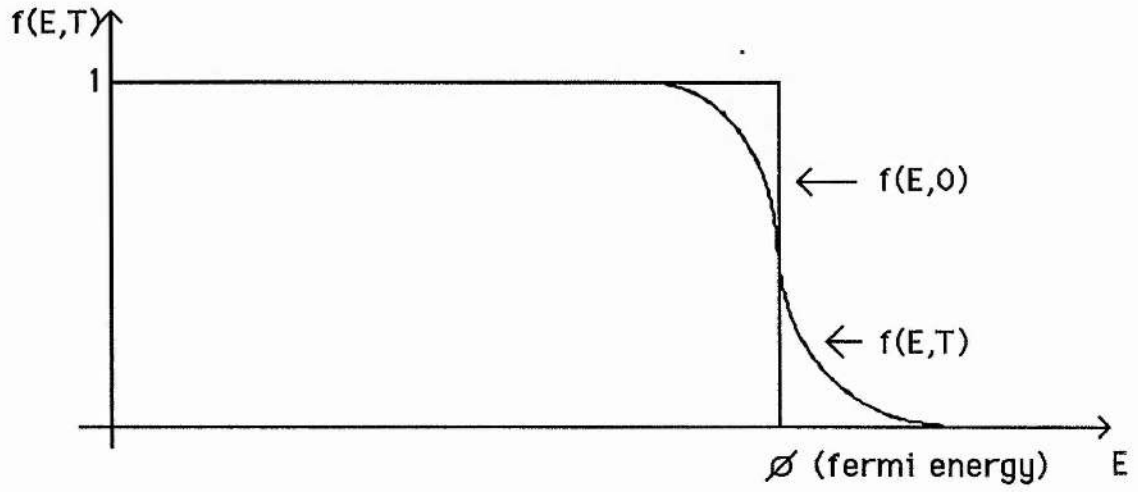

Figure 3.3 : Fermi-Dirac distribution

The system in this situation is described as being completely degenerate, since on application of a small electric field conduction will not occur as there are no free states at their energy which they can move to. Also on application of a greater electric field such that conduction can occur the probability function restricts the electron energy distribution to the region close to the Fermi-energy such that the average energy of the electrons involved with conduction has to be taken as equal to the Fermi-energy rather than the classical 3kT/2.

3.7 **Calculation of Fermi-level and implications for degeneracy**

To calculate the Fermi level we must know the value of the Fermi integral. This is equal to the fraction described by the electron concentration divided by the effective density of states. So values for these must either be known or calculated. The effective density of states can be calculated. The electron concentration at low temperatures is equal to the donor concentration minus the acceptor concentration. At higher temperatures the intrinsic electron concentration must be added to this.

Once this fraction has been evaluated, the table of solutions for the Fermi integrals can be used to obtain a value for the Fermi energy. The position of this energy relative to the CB determines whether the crystal is degenerate or non-degenerate. If the Fermi-energy is below the CB then at Zero Kelvin no conduction is possible, but when conduction is initiated the dynamics of the electrons can be described by classical mechanics and the crystal

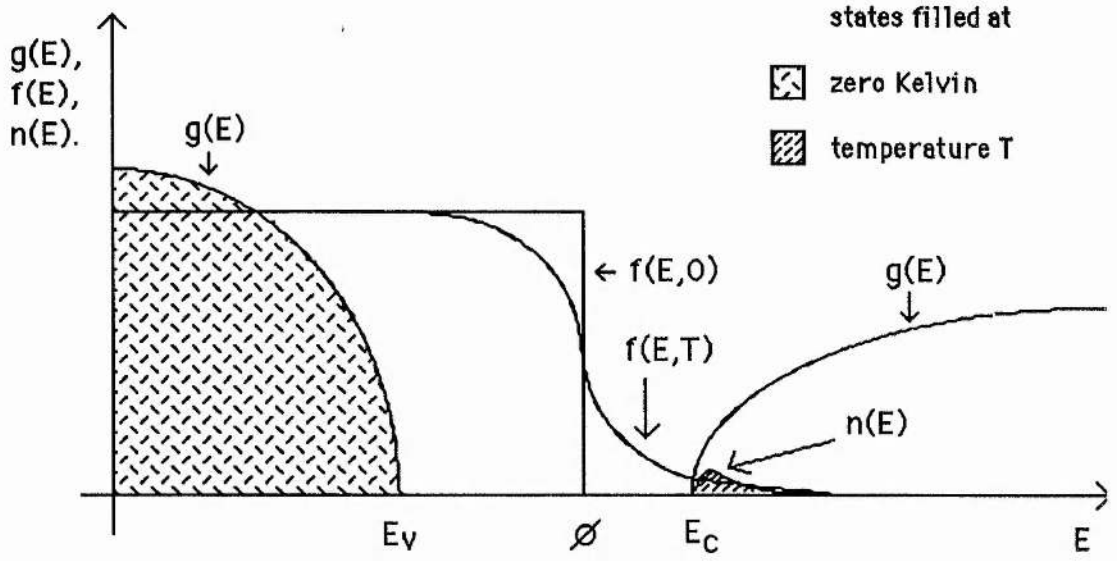

Figure 3.4 Electron distribution for Fermi energy below the CB
g(E) = density of states, n(E) = electron distribution

is non-degenerate since the concentration of electrons involved with conduction is far smaller than the density of available states (see figure 3.4).

If the Fermi energy is close to or within the CB then at zero Kelvin no conduction is possible and when conduction is initiated the dynamics of the electrons cannot be described classically as the electrons involved in the conduction are only those of energy close to the Fermi energy. So the crystal is degenerate (see figure 3.5).

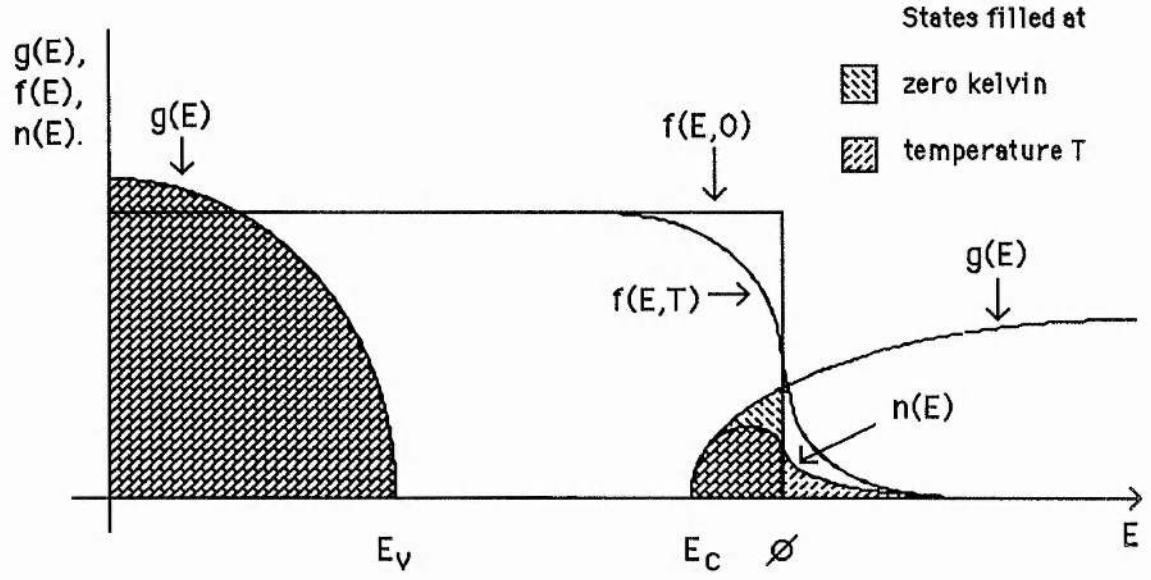

Figure 3.5 : Electron distribution when the Fermi energy lies within the CB. - g(E) = distribution of states, f(E) = Fermi distribution, n(E) = electron distribution.

3.8 **Electron Excitation Processes**

Upon establishing the concentration of electrons in the CB and the conditions under which the electrons effect transport, the next important considerations involved in determining the electrical properties are the processes which provide the electrons with their energy and momentum. There are several whose importance depends on external considerations

3.8.1 Phonon Absorption

Lattice structure excitations (induced either thermally or physically) are quantised. These quanta are known as phonons and can be considered as quasi-particles. When phonons are set up in a crystal they interact with the electrons. This interaction is generally considered as the interaction of two gases of quasi-particles. At low temperatures the phonon concentration will be low and the mean energy of the phonons will be low. The energy gained by electrons in this situation is low. At High Temperatures the energy gained can be high enough to cause electrons to be ionised from either impurity bands or the valence band. Phonon absorption is an energy excitation process as no preferential directionality is involved. In equilibrium and without an external exciting process there is no resultant energy flow either to or from the electrons as the absorption is equal to stimulated emission.

3.8.2 Photon Absorption

Electromagnetic radiation is quantised. These quanta are known as photons and can be considered as quasi-particles. When a beam of radiation is incident on the lattice, then interaction between the electrons within the lattice and the photons of the beam can occur. This can also be considered as interaction between two gases of quasi-particles. Due to the low efficiency of this interaction, it is only a dominant excitation process when a high intensity of light (e.g. a laser) is incident on the crystal. Under these conditions, electrons can be ionised into the conduction band. Similar to phonon absorption, this process imparts only energy to the electrons (it provides no directionality).

3.8.3 Application of an Electric Field

Applying an electric field is usually the most effective process for exciting electrons. The rate of energy to the electrons is proportional to the electric field. This process also induces momentum as the electric field is directional and the electrons are accelerated in the direction of the field.

3.8.4 Application of Perpendicular Electric and Magnetic Fields

According to the empirical equation (named after Lorentz) $F = e (\mathbf{v} + \mathbf{E} \times \mathbf{B})$, the application of perpendicular electric and magnetic fields will induce a force on moving electrons (and other charged particles, such as holes) in the direction perpendicular to both fields. For low magnetic fields this force is small in comparison with that induced by the electric field alone. For high magnetic fields this force will dominate. Note that the force due to the electric field alone is in a direction perpendicular to that due to this electro-magnetic force. Note also that the electro-magnetic force will act in the same direction for both electrons and holes.

3.9 **Electron Relaxation Processes**

If excitation processes were not balanced by relaxation processes (i.e. if the rate of energy from the electrons does not equal the rate of energy transferred to the electrons) electrons would gain energy continuously and a steady state would not be possible. In ohmic conditions a balance is set up with the average electron energy being equal to the classical value of 3kT/2. At medium to high electrical fields the balance may not be set up until a higher average energy is obtained. This will occur when at a specific energy the rate of energy to the electrons is greater than the rate of dissipation by the relaxation processes. In this condition the electrons will gain ever more energy and breakdown will occur, unless the relaxation processes involved become more efficient at higher energies or more efficient relaxation processes are initiated at higher energies. If an equilibrium is restored, this occurs for an electron distribution which is of greater energy than that expected

in an ohmic situation. The distribution may then appear similar to the Maxwell-Boltzmann distribution for a lattice of higher temperature. This temperature is then defined as the hot-electron or effective electron temperature.

The following scattering mechanisms produce relaxation in electrons. Some are more efficient at energy relaxation, whilst others are more efficient at momentum relaxation. Most induce both.

3.9.1 Energy and Momentum Scattering/Relaxation

The concept of differentiating between the energy and the momentum of electrons is necessary for understanding the effects of scattering on conductivity. Electrons have an energy due to the lattice energy which as discussed above is equal to 3kT/2 in the classical model. This energy has an equivalent velocity defined by the kinetic energy equation. The direction of this velocity is random as in a free gas. This velocity therefore is not directly involved in conductivity.

On applying an electric field the electrons are accelerated in the direction of the electric field and in equilibrium a drift velocity is set up. (The average momentum of the electrons being proportional to this velocity.) The electrons accelerate until they collide or interact. The average time between collisions depends on the average energy of the electrons and on the relaxation processes. On collision the energy and momentum of the electron are altered in a way dependent on the scattering process involved.

All scattering processes (except interelectron scattering) induce both energy and momentum relaxation. The efficiency of the processes in doing one or the other depends on the method of interaction. This allows the situation where the electrons interact more frequently with one scattering process and yet more strongly with another. An example of this is when electrons interact most frequently with ionised impurities. Ionised impurity scattering is inefficient at energy relaxation and so acoustic phonon emission is the main energy relaxation mechanism. Another way of looking at this is that acoustic phonons are an efficient energy scattering process. Ionised impurities are, however, for momentum scattering

of similar efficiency and as they interact more frequently they will be more effective.

So two details determine the effectiveness of a scattering process. The frequency with which it interacts with the electrons and the magnitude of the effect it has on interaction.

The efficiency of the most effective energy relaxation mechanism determines the energy distribution of the electrons (within the bounds set by the electron concentration and the available density of states : see section 3.7). A low efficiency in energy relaxation will allow an increase in the average energy of the electrons and, in general, the effect of inter-electron interaction will cause the distribution to remain similar to the Maxwell-Boltzmann distribution. (The Maxwell-Boltzmann distribution relies on the interaction between electrons being more efficient than the energy relaxation processes such that the energy applied to the electrons is redistributed uniformly.) A high efficiency in energy relaxation will cause a distortion in the 'classical' distribution.

3.9.2 Impurity scattering

Electrons interact with neutral and ionised impurities. For equal concentrations of neutral and ionised impurities, the ionised impurities will cause greater scattering due to the added coulomb (charge) interaction. This restricts the applicability of neutral impurity scattering to very low fields where few impurities have been ionised and to crystals with low compensation as the efficiency of this mechanism is proportional to the concentration of neutral impurities.

As a direct collision (one where the electron motion is directed towards the impurity as opposed to close to it) is unlikely, the majority of electron - impurity interactions will result in a change in the direction of the electrons motion rather than a change in speed or energy. Even in a direct collision the disparity in mass, between the electron and the impurity center, is such that the collision will be effectively elastic and energy loss will be minimal. This indicates that this form of scattering is more efficient at momentum relaxation than energy relaxation.

Another form of scattering involving impurities is that where neutral and ionised impurity atoms combine to form a quasi-hydrogen molecule with a positive charge. This process can become effective because of the increased volume of the positively charged scattering center. It is only significant when ionised impurity scattering is losing effectiveness due to increased electron energies. In this situation acoustic phonon scattering rapidly dominates and the quasi-hydrogen molecule scattering process becomes insignificant again.

3.9.3 Acoustic phonon scattering

The lattice vibrations where all the atoms in the lattice react identically to excitations regardless of their charge are known as acoustic phonons (due to their rate of propagation through a crystal being similar to the velocity of sound). Acoustic phonons can exist in both longitudinal and transverse modes though the longitudinal mode is dominant in the interaction with electrons.

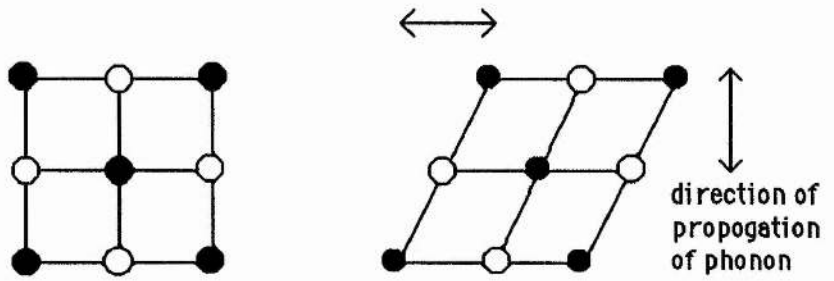

Undisturbed Lattice Lattice deformation by a transverse acoustic phonon

Figure 3.6 : Diagrammatic representation of the effect of a transverse acoustic phonon

The transverse mode creates a shear effect (see fig 3.6) which does not affect the interatomic spacing of the lattice significantly.

The longitudinal mode interacts with electrons in two ways: Deformation potential and piezo-electric scattering. The latter requires a polar piezo-electric crystal. The basis behind both

processes is the displacement of one atom relative to its nearest neighbour. (see fig 3.7) The exact mechanisms are discussed below.

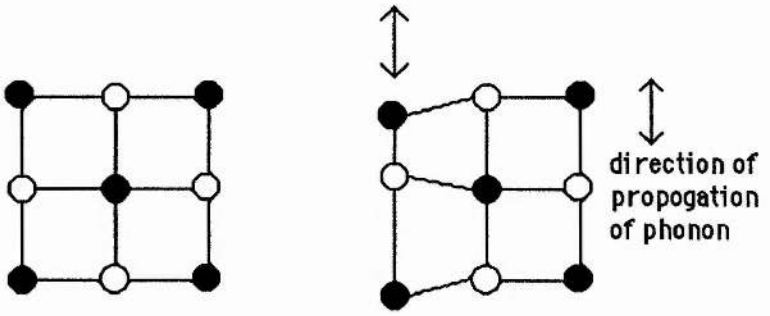

Undisturbed lattice Lattice deformation by longitudinal acoustic phonon

Figure 3.7 : Diagrammatic representation of the effect of a longitudinal optical phonon

Due to the periodic nature of the lattice one obtains a dispersion curve of Energy ($\hbar\omega$) against momentum vector, k[1]. This shows that for acoustic phonons there is a maximum energy. Electrons with an energy greater than this can relax by interaction with several phonons.

3.9.3.1 Deformation Potential Scattering

For an electron travelling through a perfect lattice on a trajectory where it is equidistant from the nearest atoms, it will effectively experience no interaction with the lattice. If one of the nearest atoms is displaced from its undisturbed position (due to phonon transport) then the electron will no longer experience a symmetry of influences and will be affected. This atomic motion will increase the collision cross-section (probability that an interaction will occur) as the interaction volume is increased by this motion. The deformation of the lattice by this motion affects the local conduction band structure and hence the motion of the electron. The shift in the conduction band minima is indicative of

[1]Landolt & Börnstein, "Num.Data.& Funct.Rel.in Sci.& Tech."Group III,17,a (1982) & Pain, "Phys. of Vibr. & Waves" 132 (1985)

the strength of this interaction. This energy shift is known as the Potential Deformation constant.

3.9.3.2 Piezo-electric Scattering

In a non-symmetrical lattice (in terms of charge) the application of pressure will produce a potential across the lattice. The action of a phonon in causing atoms to be displaced is identical to the affect of a localised pressure and will cause a localised potential. As this potential is directly related to the displacement of the atom, a high frequency phonon, where several periods of oscillation occur during the transit of the electron, will not affect the electron as the potential will be averaged to zero. For low frequency phonons the existence of a quasi-stable potential will enhance the phonon-electron interaction. For low frequency phonons the potential set up can be larger than the energy shift in the conduction band (caused by deformation) and have a proportionally greater affect.

3.9.4 Electron-Electron Scattering

This scattering if perfectly elastic will cause neither momentum nor energy relaxation. Thus it would affect only the scattering lifetime.

This process, though, may scatter electrons such that other scattering mechanisms become more efficient. This will affect the energy and momentum relaxation rates. If, as stated by Zawadski[2], the interelectron scattering is non-elastic, it will be a mechanism for both energy and momentum scattering in its own right. Its effect will be proportional to the concentration of 'free' electrons. In a highly degenerate situation the influence of interelectron interaction will decrease as the electrons are restricted to energies close to the Fermi level.

---

[2]Zawadski, Hdbk on Semicond. Ch12 (1982)

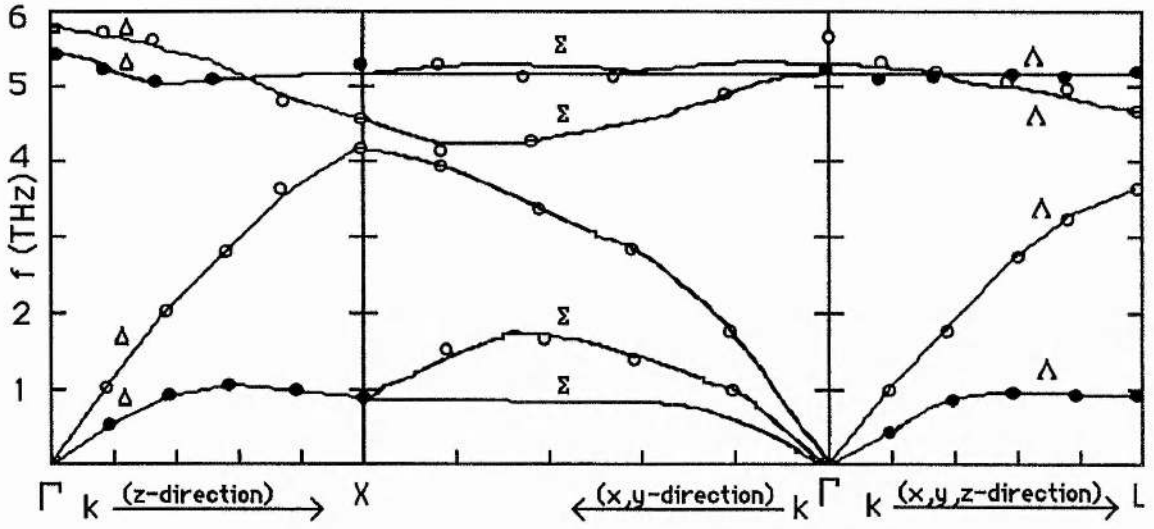

Figure 3.8a : The Phonon dispersion curves of InSb at room temperature (after Price et.al.[3]) which show the relations between crystal momentum and the energy of the phonons (depicted here in terms of frequency). The points which are marked with letters are points of symmetry in the lattice whose positions are shown in figure 3.8b

3.9.5 Optical Phonon Scattering

Vibrations of the lattice where adjacent atoms act in opposition are known as optical phonons. There are longitudinal and transverse optical phonons just as with acoustic phonons. Acoustic phonons have only a maximum frequency, whereas optical phonons have a minimum and maximum frequency (see figure 3.8). This implies that at low lattice energies and electron energies less than that implied by the minimum optical phonon frequency, there are no scattering processes involving optical phonons. It is convenient to split the optical phonon scattering into Polar and non-Polar situations.

---

[3]Price et.al., Phys.Rev.B 3 , 1268 (1971)

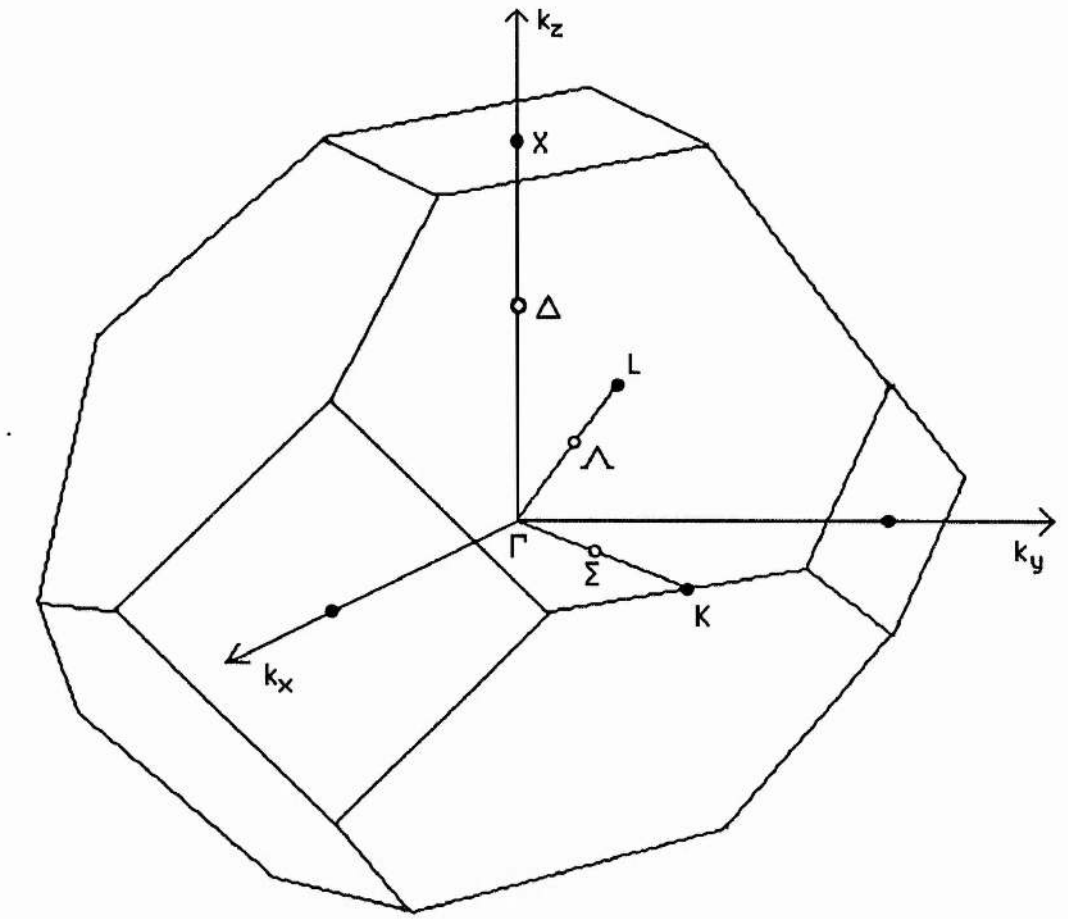

Figure 3.8b The First Brillouin Zone* for Face Centered Cubic Semiconductors showing the symmetry points and axes of the lattice as utilised in the dispersion curves depicted in figure 3.8a (after Jones[4] & Bouckaert et.al.[5]).

3.9.5.1 Polar Interaction

When the adjacent atoms have charges of differing sign the crystal is defined as being polar. The application of an electric field will cause adjacent atoms to move with or against the field dependent on their charge. If the field is varied periodically it will create a longitudinal optical phonon. The absorption of a periodically

---

* This is the unit cell of the lattice in reciprocal (k) space.

[4]Jones, 'The Theory of Brillouin Zones and Electronic States in Crystals'(North-Holland,Amsterdam).

[5]Bouckaert et.al., Phys.Rev. 50 , 58 (1936)

varying electro-magnetic field (e.g. from photons) will create transverse optical phonons. This is where the name for this type of lattice vibrations arises. It is somewhat misleading however as the application of optical radiation creates only one of the types of 'optical' phonons. The increase in the emphasis of the crystals polarity by an optical phonon provides the strongest interaction with electrons. The longitudinal modes are the most efficient due to reasons similar to those discussed with acoustic phonons.

3.9.5.2 Non - Polar Interaction

For crystals where there is no charge on the atoms, non-polar optical phonon scattering is the only optical phonon scattering process possible. (The mechanism involved is effectively the optical phonon equivalent to the deformation potential scattering.) Both longitudinal and transverse modes are possible. Again the longitudinal mode is dominant in electron interaction. In a polar crystal non-polar interaction occurs but is insignificant relative to the polar interaction.

3.9.6 Other Scattering Processes

There are other scattering processes which have not been included in the above. This is because they are either not relevant, have an insignificant effect in the conditions considered or cannot be calculated theoretically.

Lattice imperfections cause charge dislocations which can scatter electrons. The number of these dislocations is indeterminate and so their effect is indeterminate. The scattering by dislocations is usually considered as scattering by localised potential. The theoretical calculations on this type of scattering show the effect to be independent of electron energy as one would expect[6]. It is usually thought necessary to deform the crystal to attain enough dislocations to have a measurable effect.

Electron-hole scattering only comes into effect when the electron and hole concentrations are comparable. This occurs when breakdown across the gap has occurred. There are also two

---

[6]Zawadski, Hbk.Semicon. 1 , 750 (1982)

possibilities for photon emission. The first is where an electron relaxes within the CB emitting a photon, thus reducing its energy and momentum. This process is insignificant when compared with acoustic and optical phonon scattering processes. The second is where an electron relaxes into the VB, recombining with a hole, thus reducing the carrier concentration. Interaction between electrons and holes will also induce a drag effect on the minority carriers. In the situation considered here the minority carriers are the holes, so the effect on the electron mobility and energy is insignificant.

Another consideration is that of combined scattering processes like photon assisted phonon emission. A description of the various types of interaction which can lead to photon emission is given by Elliott & Gibson[7]. The concept of electron cooling by application of an increased electric field, mentioned in section 2.5, requires optical phonon and ionised impurity scattering to combine. The above processes are generally minority effects and except in specialised circumstances will not have a noticeable effect.

3.10 Calculation of the Total Energy Relaxation Rate and the Electron Mobility

For a specific electron energy it is possible to calculate both the energy relaxation rate and the momentum relaxation rate of the scattering processes available.

The energy relaxation rates can be compared in order to determine the dominant relaxation process, and can be added to obtain the total energy relaxation rate.

For the momentum relaxation rate it is more usual to calculate the momentum scattering lifetimes for each process. This lifetime is proportional to the mobility an electron would have if affected by only one scattering process. Comparing scattering lifetimes one can determine the dominant momentum relaxation process. To combine the effects of the scattering processes involved one then adds the inverse of the scattering lifetimes to obtain the inverse of the electron lifetime. This is then proportional to the electron mobility.

---

[7]Elliott & Gibson, 'Solid State Physics' p230 (Macmillan, 1974)

In determining the energy relaxation rate and the electrons mobility one has to consider the degeneracy of the electron gas. For complete degeneracy the electrons will be restricted to a specific energy (the Fermi level). This implies that the above method will be sufficient for calculating the energy relaxation rate and the electron mobility. If the electron gas is non-degenerate then for an average electron energy there is a distribution of electrons at other energies. In this situation one should obtain the energy dependent electron mobility. This is done by retaining the energy dependences of the individual scattering mobilities when combining to obtain the electron mobility. Then one must calculate the average over all the electron energies.

It is at this point that the processes, which distort the electron distribution without directly causing momentum relaxation, can be seen to have a considerable effect on the average electron mobility.

In a non-degenerate electron gas the energy relaxation rate must also be averaged over the range of electron energies.

(If the scattering processes are deemed to be non-elastic then the scattering transition probabilities should be added before calculating the conductivity[8].)

3.11 **Conclusion**

Once the energy equations for the conduction band have been obtained and solved the Fermi energy can be obtained. The level of degeneracy in the crystal can then be deduced and the correct equations of motion and energy distributions can be applied. Upon knowing the approximate average energy of the electrons, the valid relaxation processes can be investigated and the collision/scattering lifetimes obtained. This then allows the full picture of electron dynamics to be described.

---

[8]Zawadski, Hdbk.Semicon, 1 , 787 (1982)

CHAPTER 4 SOLID-STATE PHYSICS : A QUANTITATIVE LOOK AT n-INSB (APPLICATION OF CHAPTER 3 TO n-INSB)

4.1 Density of States and Energy Gap in n-InSb

The density of states of InSb have been calculated[1] and experimentally determined[2]. The distribution describing the density of states is found to possess bands, with a valence band (VB) and a conduction band (CB) separated by a small energy gap (see figure 4.1)[3].

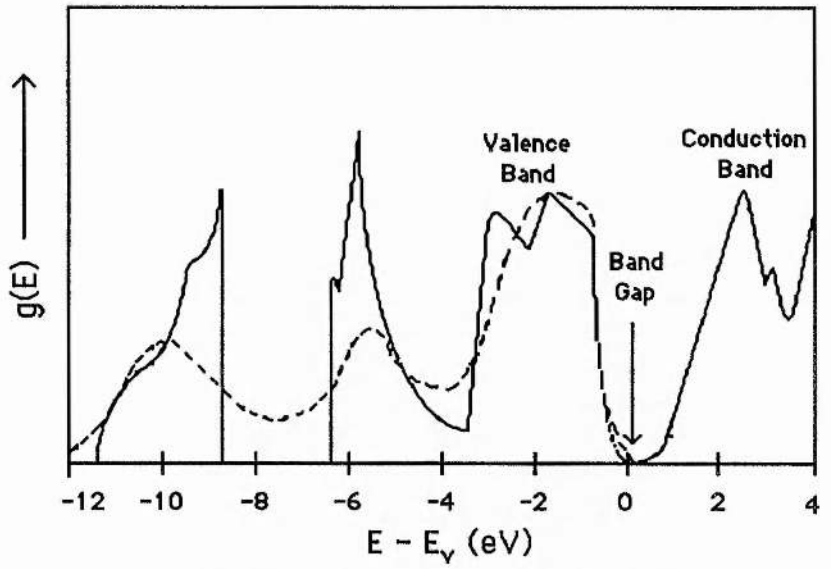

Figure 4.1 : Density of states in the conduction and valence bands as obtained theoretically (solid line[1]) and experimentally (dashed line[2]), showing the lack of states between the conduction and valence bands which creates the band gap.

1Lang et.al., Sov.Phys.Sol.St. 16 , 54 (1974)
2Chelikowsky & Cowen, Phys.Rev. B14 , 556 (1976)
3Landolt & Börnstein, Num.Data&Funct.Rel.in Sci.&Tech.Group III,vol.17,subvol.group IV&III-V comp.

The value of this band gap can be described by equation 4.1.[4]

$$E_G(T) = E_G(0) + aT \quad \text{(in eV)} \qquad \text{.....4.1}$$

where, T=Temperature

a= 0.00027

$E_G(0)$= 0.26 eV - this a theoretical extrapolation and is not equal to the band gap energy at zero degrees Kelvin

For the full relationship between band gap and temperature see figure 4.2. Note that equation 4.1 does not hold for low temperatures (T< 80K). At very low temperatures (T< 1.5K) the gap is observed to increase with decreasing temperature. As the very low temperature regime is not considered in the following work this anomaly is ignored.

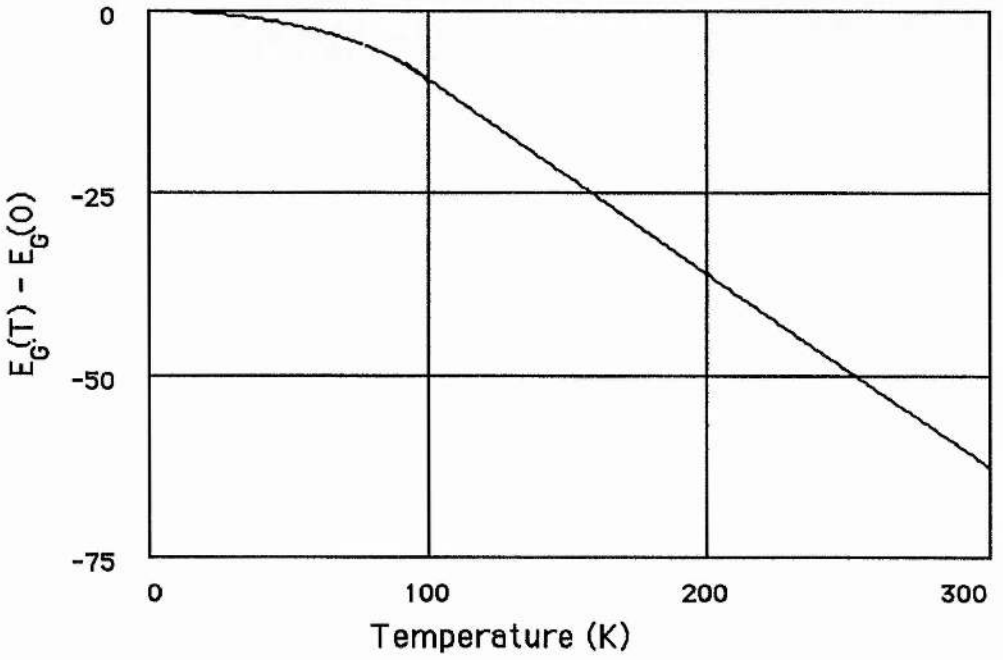

Figure 4.2 : Variation of the band gap with temperature

[4]Blakemore, 'Semiconductor Statistics' (Dover,1987) p107

The density of states in the conduction band, as derived by Smith[5], is given by

$$N_c = 2\left(\frac{2\pi m^* k_B T_L}{h^2}\right)^{3/2} \quad \text{..... 4.2}$$

where, h = Planck's constant,
$m^* \approx 0.014 m_o$: m_o=free electron mass,
k_B = Boltzmann's constant
T_L = lattice temperature (in Kelvin)

4.2 **Conduction Band Structure**

The band structure of InSb was calculated by Kane[6] in 1957. Included in the calculations was the triple structure of the V.B. (see figure 4.3) and its effect on the C.B.. The small band gap allows for strong interband interaction. It has been suggested that this interaction is the cause of the strong spin degeneracy ($g \approx 50$: c.f. usual value of $g = 2$) and the small effective electron mass in the C.B. ($m^* \approx 0.014 m_o$: m_o=free electron mass)[7].

---

[5]Smith 'Semiconductors' p78 (C.U.P.,1959)
[6]Kane, J.Phys.Chem.Sol. 1 , 249 (1957)
[7]Roth, Hdbk,Semicond.Vol.1,Ch.8, 474 (1982)

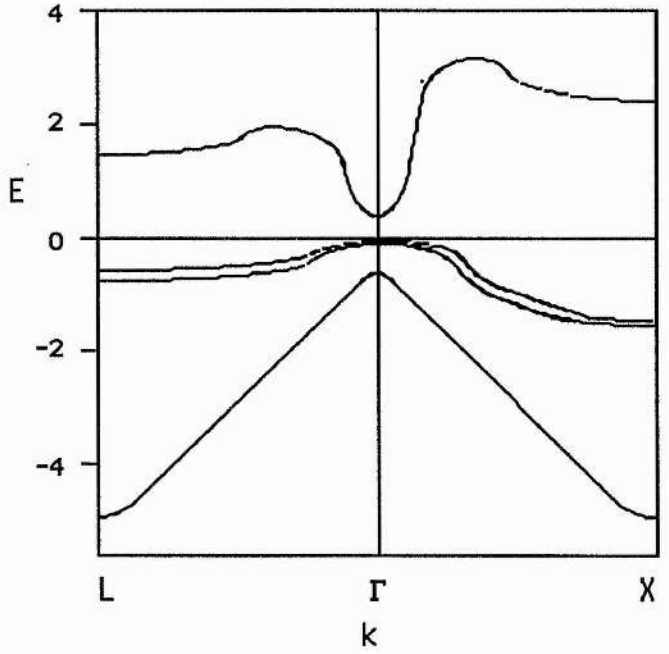

Figure 4.3 : Diagramatic representation of the band structure of InSb as obtained from Kane's equations

The expression describing the C.B. structure for InSb, as derived by Kane is given in equation 4.3

$$E = \frac{\hbar^2 k^2}{2m} + \frac{E_G + \left(E_G^2 + \frac{8P^2k^2}{3}\right)^{1/2}}{2} \qquad \text{.....4.3}$$

where, P = interband interaction parameter
E = electron energy
k = wave no. ($2\pi/\lambda$)
m = electron mass
$\hbar$ = Planck's constant / 2π

The first term on the right in equation 4.3 is the free electron kinetic energy, the second term is the effect of the band gap and interband interaction on an electron in the C.B.. This equation can be simplified by the following:-

1/ Putting $\frac{1}{m_o^*} = \frac{4P^2}{3\,\hbar^2 E_G}$,

where m_o^* is tentatively defined as the effective electron mass at the C.B. minimum (see equation 4.8 for confirmation of this)

2/ Noting that as $m_o^* << m$,

then $\frac{\hbar^2 k^2}{2m} << \frac{\hbar^2 k^2}{2m_o^*}$

and the $\frac{\hbar^2 k^2}{2m}$ term may be neglected.

3/ Taking the C.B. minimum to be the energy origin.

The above (as done by Zawadski[8]) gives

$$E = -\frac{E_G}{2} + \left[\left(\frac{E_G}{2}\right)^2 + E_G\frac{\hbar^2 k^2}{2m_o^*}\right]^{1/2} \qquad \text{.....4.4}$$

This can be rearranged as

$$\left(E + \frac{E_G}{2}\right)^2 = \left(\frac{E_G}{2}\right)^2 + E_G\frac{\hbar^2 k^2}{2m_o^*}$$

$$E^2 + EE_G + \left(\frac{E_G}{2}\right)^2 = \left(\frac{E_G}{2}\right)^2 + E_G\frac{\hbar^2 k^2}{2m_o^*}$$

$$\frac{E(E + E_G)}{E_G} = \frac{\hbar^2 k^2}{2m_o^*}$$

$$E\left(1 + \frac{E}{E_G}\right) = \frac{\hbar^2 k^2}{2m_o^*} \qquad \text{.....4.5}$$

---

[8]Zawadski, Hdbk,Semicond.Vol.1,Ch.12, 713 (1982)

To describe the motion of the electrons in the C.B. as if they were free particles in an electron gas, an effective electron mass for the electrons in the C.B. is defined by,

$$\frac{dE}{dk} = \frac{\hbar^2 k}{m^*} \qquad \text{.....4.6}$$

From equation 4.5 one obtains

$$\frac{dk}{dE} = \frac{m_o^*}{\hbar^2 k}\left(1 + \frac{2E}{E_G}\right) \qquad \text{.....4.7}$$

Combining equations 4.6 and 4.7 by putting $\frac{dE}{dk} = \left(\frac{dk}{dE}\right)^{-1}$ one obtains

$$m^* = m_o^*\left(1 + \frac{2E}{E_G}\right) \qquad \text{.....4.8}$$

This confirms the definition of m_o^* as the effective electron mass at the C.B. minimum.

4.3 **Electron Concentration and Distribution in the C.B.**

The energy distribution of electrons in a crystal is, in the first approximation, determined by the concentration of electrons in the C.B. and the density of states there.(The first approximation being that the electron excitation and relaxation processes will not distort the electron distribution.) Since by Pauli's exclusion principle no two electrons may exist in (occupy) the same state we require more states than there are electrons for conduction to be possible.

So the concentration of electrons and the density of states in the C.B. must be calculated. These two values are connected by the expression given in equation 4.9.

$$n = \int_0^{\infty} f(E)g(E)dE \qquad \text{.....4.9}$$

where, n = electron concentration in C.B.

$g(E)$ = density of states

$f(E)$ = probability of an electron having energy E

$f(E)$ is usually described by Fermi-Dirac statistics which gives the electron occupation of states as (see also figure 3.3.)

$$f(E) = \frac{1}{1 + \exp\left(\frac{E - \phi}{k_B T_L}\right)}$$

where, k_B = Boltzmann's constant

T_L = temperature (in Kelvin)

which implies that at zero Kelvin all the states are occupied up to an energy,ϕ, known as the Fermi energy. As all the states are occupied no conduction is possible until energy is introduced to the system by means of heat or an applied electric field. This will affect the distribution of electrons as shown in figure 3.5. As can be seen the electrons able to be involved in conduction on application of a small field or amount of heat are those with energy close to ϕ. They will also have an average energy of ϕ and not $3k_BT_L/2$ as electrons in a free gas would. This situation is described as degenerate and classical dynamics are not accurate. The position of the Fermi energy is important in determining whether a crystal is degenerate or not.

This is shown in diagrams 3.4 and 3.5, and explained in section section 3.7. Equation 4.9 describes the situation and it can be used to determine the Fermi energy. Equation 4.9 is usually rearranged to the form shown in equation 4.10.

The concentration of electrons in the conduction band is given by

$$n = N_C F_{1/2}\left(\frac{\phi}{k_B T}\right) \quad \text{.....4.10}$$

where, $N_c = 2\left(\frac{2\pi m^* k_B T}{\hbar^2}\right)^{3/2}$ = effective density of states (eqn4.2)

$F_n\left(\frac{\phi}{k_B T_L}\right)$ = Fermi integral

k_B = Boltzmann's constant

n is usually measured (by the Hall effect : see section 6.4), the density of states can be calculated from the above expression and the ratio of n to N_c determines the value of the Fermi integral which determines the value of ϕ.

The above holds for semiconductors with a parabolic conduction band structure (where the effective electron mass is energy independent). For semiconductors, like InSb, which have spherical conduction band structures (where the effective electron mass is energy dependent), an equation equivalent to equation 4.10 can be derived. This was done by Kolodziejczak[9] and the equation is shown as equation 4.11.

$$n = N_c^{*0} L_0^{3/2} \quad \text{.....4.11}$$

with $$N_c^* = \frac{1}{3\pi^2}\left(\frac{2 m_o^* k_B T_L}{\hbar^2}\right)^{3/2} \quad \text{.....4.12}$$

= generalised effective density of states

and $$^{n}L_k^{m}(\eta,b) = \int_0^{\infty}\left(\frac{-df(E)}{dz}\right) z^n \left(z + bz^2\right)^m \left(1 + 2bz\right)^k dz \quad \text{.....4.13}$$

= generalised Fermi integrals

where $z = \frac{E}{k_B T_L}$; $\eta = \frac{\phi}{k_B T_L}$; $b = \frac{k_B T_L}{E_G}$

---

[9]Kolodziejczak, Acta.Phys.Polon. 20 , 289 (1961)

Exact solutions to these integrals do not exist, but numerical approximations for various values of η and b do. So upon knowing the electron concentration, the generalised effective density of states and the energy of the crystal lattice (necessary for determining b and N_c^*), the Fermi energy can be determined. The major difficulty involves determining the electron concentration. This can either be measured or calculated for intrinsic materials. For extrinsic materials (crystals with impurities) the uncompensated impurity concentration will dominate at low temperatures so this concentration must be determined.

4.4 The Effect of Impurities on the Electron Concentration and Band Structure

Impurity atoms facilitate conduction at electric fields and temperatures too low for substantial intrinsic conduction. This is due to the energies of the outermost electrons of these atoms (hereafter referred to as impurity levels) being in, or close to the C.B.(for n-type InSb : The donor impurity atom concentration is greater than the acceptor impurity atom concentration). If the impurity level is within the C.B. then conduction is possible and the impurity atoms cannot restrain their outermost electrons. If the impurity level is found to be below the C.B. by less than $k_B T_L$ then conduction can occur as the outermost electrons will be thermally ionised.

For impurity levels more than $k_B T_L$ below the conduction the phenomena of impurity conduction is possible. For a very large impurity concentration with low compensation the impurity level will be broadened into a band whose density of states is greater than the electron concentration. In this situation conduction occurs in a similar way to conduction in the C.B.. This phenomena, in InSb, is rarely possible because the broadening of the impurity level to this extent usually causes it to overlap the C.B. and so combine with it.

The above is for situations where the impurity concentration is great enough for impurity atoms to interact with their neighbours. This has been taken to be where the Coulomb spheres overlap. This has been shown to be inaccurate as interaction can still occur when

there is no overlap. Conduction involving interaction without overlapping Coulomb spheres is known as hopping conduction.

The definitions and conclusions of the above are summarized in figure 1 of chapter 10 in 'Hopping Transport in Solids'[10]. For the impurity concentrations, temperatures and electric fields considered here, hopping conduction is not thought to be influential.

4.4.1 Evaluation of Hydrogenic Model for Impurity Ionisation

The calculation to determine the concentration at which the radius of the Coulomb sphere (the Bohr radius in Hydrogen) is equal to the half of the interatomic separation of the impurities involves treating the impurity atoms as being hydrogen-like and applying Coulomb's law. Putley quotes the result of this approach[11]. The full method has been included here as, though it is simplistic and inaccurate, it provides some useful insight into the situation.

From the Schrödinger wave equation for a hydrogen atom one obtains energy eigenvalues,

$$E_n = -R^*/n^2 \quad \text{.....4.14}$$

For impurity centres in a semiconductor, R^* is the effective Rydberg constant and is related to the Rydberg constant by,

$$R^* = \frac{m^* e^4}{2\hbar^2 \kappa_0^2} = \left(\frac{m^*}{m_o}\right)\left(\frac{1}{\kappa_o}\right)^2 R_h \quad \text{in c.g.s units .....4.15}$$

$$= \frac{m^* e^4}{2\hbar^2 \kappa_0^2}\left(\frac{1}{4\pi\varepsilon_o}\right)^2 \quad \text{in S.I. units}$$

where, R_h is the Rydberg constant($=1.1\times10^7 m^{-1}$);
m^* = effective electron mass ($=1.27\times10^{-32}$Kg);
κ_o = dielectric constant of InSb (=16.8-18)
and ε_o = dielectric constant of free space($=8.854\times10^{-12} CV^{-1}m^{-1}$).

This implies that in a semiconductor there will be an effective

---

[10]Mansfield,'Hopping Transport in Solids' ch.10,p349(unpubl)
[11]Putley, Phys.Stat.Sol. 6 , 571 (1964)

Bohr radius given by,

$$a_b = \frac{\hbar^2 \varepsilon_o}{m^* e^2} = \left(\frac{m_o}{m^*}\right)\varepsilon_o a_h \quad \text{in c.g.s units} \qquad \text{.....4.16}$$

$$= 4\pi\varepsilon_o \frac{\hbar^2 \varepsilon_o}{m^* e^2} \quad \text{in S.I. units}$$

where a_h is the Bohr radius for hydrogen(= $5.29\text{x}10^{-11}$m).

The above gives the following values,

$$R^* = 5.46\text{x}10^{2}\text{m}^{-1}$$
$$a_b = 6.348\text{x}10^{-8}\text{m}$$

From the effective Bohr radius one can calculate the volume occupied by an impurity atom to be

$$V = \frac{4\pi(a_b)^3}{3}$$

Taking the simplistic view that neighbouring atoms do not interact unless the interatomic separation is less than $2a_b$, then one can obtain a minimum impurity concentration for which conduction can occur.

$$n_{min} = 1/V$$
$$= 9.33\text{x}10^{14}\text{cm}^{-3}.$$

This is in agreement with the results obtained by Putley. Putley mentions that this minimum value is merely a first order approximation and concludes that from practical evidence conduction will occur at any temperature for concentrations greater than 10^{13}cm^{-3}.

By looking at the ratio of minimum concentration to actual impurity concentration a first order estimate of the energy required to cause interaction between impurity atoms can be determined.

We have

$$n_{min}V_{min} = n_iV_i = V = \text{unit volume}$$

where, V_{min} & V_i are the volumes available to each impurity atom.
n_{min} & n_i are the minimum and actual impurity concentrations.

So

$$\frac{V_{min}}{V_i} = \frac{(4/3)\pi(r_{min})^3}{(4/3)\pi(r_i)^3}$$

and $\quad 1/r_{min} = ((4/3)\pi n_{min})^{1/3}$
and $\quad 1/r_i = ((4/3)\pi n_i)^{1/3}$

Then using Coulombs law we find that the energy required to raise an electron from its impurity potential to the potential between impurities (so making conduction feasible), is given by

$$P_i = \left(\frac{e^2}{4\pi\varepsilon_o}\right)\left(\frac{4\pi}{3}\right)^{1/3}\left(n_{min} - n_i\right)^{1/3} \quad \text{.....4.17}$$

This has been evaluated for different impurity concentrations. These results have been used to obtain the graph of impurity concentration against 'ionisation' energy shown in figure 4.4.

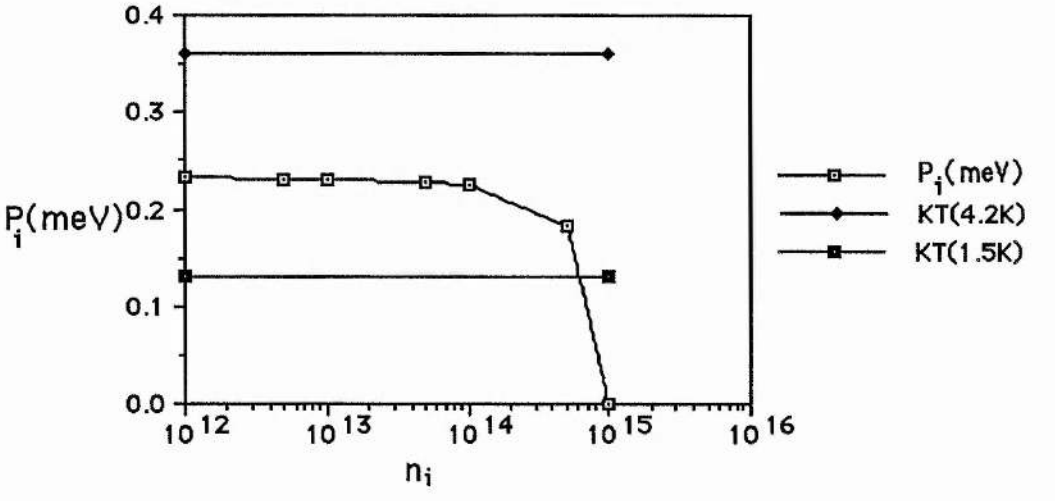

Figure 4.4 : Graph of Impurity Ionisation energy against Impurity Concentration, Showing the values for Thermal Noise at 1.5 and 4.2K.

This simplistic approach implies that at 4.2K extrinsic conduction is possible through thermal 'ionisation' of impurities. At 1.5K no conduction is predicted (unless by hopping conduction) until the electrons are ionised by an applied electric field. Also that the ionisation potential is roughly constant for concentrations less than 10^{13} cm^{-3}.

4.5 **Calculation of Electron Concentration in C.B.**

From the above we can can assume that for temperatures above 1K the uncompensated donor impurity atoms are ionised into the C.B. and the concentration of electrons in the C.B. is equal to the uncompensated donor impurity atom concentration plus the intrinsic electron concentration. The latter is negligible for low temperatures.

In a spherical C.B. we have equation 4.11

$$n = N_c^{*0}L_0^{3/2}$$

where $$N_c^* = \frac{1}{3\pi^2}\left(\frac{2m_0^* k_B T_L}{\hbar^2}\right)^{3/2}$$

= generalised effective density of states

and $$^0L_0^{3/2}(\eta,b) = \int_0^\infty \left(\frac{-df(E)}{dz}\right)\left(z + bz^2\right)^{3/2} dz$$

= generalised Fermi integrals

where, $z = \frac{E}{k_B T_L}$; $\eta = \frac{\phi}{k_B T_L}$; $b = \frac{k_B T_L}{E_G}$

with $\hbar$ = Planck's constant / 2π

m_o^* = the effective electron mass at the C.B. minimum

k_B = Boltzmann's constant

T_L = lattice temperature (in Kelvin)

n = electron concentration in C.B.

E = electron energy

E_G = band gap energy

ϕ = Fermi energy

so $$ {}^{0}L_{0}^{3/2} = \int_{0}^{\infty} \left(\frac{-df(E)}{dE}\right)\left\{\frac{E}{k_BT}\left(1 + \left(\frac{E}{k_BT}\right)\left(\frac{k_BT}{E_G}\right)\right)\right\}^{3/2} dE \quad \text{.....4.18} $$

Now

$$ f(E) = \left[\exp\left(\frac{E-\phi}{k_BT_L}\right) + 1\right]^{-1} $$

so putting $x = \left(\frac{E-\phi}{k_BT_L}\right) \rightarrow \frac{dx}{dE} = \frac{1}{k_BT_L}$

and $y = \exp(x) + 1 \rightarrow \frac{dy}{dx} = \exp(x)$

$$ f(E) = \frac{1}{y} \rightarrow \frac{df(E)}{dy} = -y^{-2} $$

$$ \frac{df(E)}{dE} = \frac{dx}{dE} \cdot \frac{dy}{dx} \cdot \frac{df(E)}{dy} $$

$$ = \frac{-1}{k_BT_L}\exp\left(\frac{E-\phi}{k_BT_L}\right)\left(\exp\left(\frac{E-\phi}{k_BT_L}\right) + 1\right)^{-2} $$

Substituting this into equation 4.18 one obtains

$$ {}^{0}L_{0}^{3/2} = \int_{0}^{\infty} \frac{\exp\left(\frac{E-\phi}{k_BT_L}\right)}{\left(\exp\left(\frac{E-\phi}{k_BT_L}\right) + 1\right)^{2}} \left(\frac{E}{k_BT_L}\right)^{3/2}\left(1+\frac{E}{E_G}\right)^{3/2}\frac{dE}{k_BT_L} $$

.....4.19

This can be simplified under the assumptions that $\frac{E-\phi}{k_BT_L} >> 1$ and $E << E_G$ to

$$ {}^{0}L_{0}^{3/2} = \exp\left(\frac{\phi}{k_BT_L}\right)\int_{0}^{\infty}\left(\frac{E}{k_BT_L}\right)^{3/2}\exp\left(\frac{-E}{k_BT_L}\right)\frac{dE}{k_BT_L} \quad \text{.....4.20} $$

$$ = \exp\left(\frac{\phi}{k_BT_L}\right)\int_{0}^{\infty} z^{3/2}\exp(-z)\,dz \qquad \text{where } z = \frac{E}{k_BT_L} $$

This integral can be solved by integrating by parts to give

$$= \exp\left(\frac{\phi}{k_B T_L}\right)\left[\left(-z^{3/2}e^{-z}\right)_0^{\infty} + \frac{3}{2}\int_0^{\infty} z^{1/2}e^{-z}dz\right]$$

the first term in the brackets is equal to zero. The second term is a standard integral which is equal to $\frac{3}{4}\frac{\pi^{1/2}}{2}$. This implies that equation 4.18 under the assumptions mentioned can be written as,

$$n = N_c^* \frac{3\pi^{1/2}}{4}\exp\left(\frac{\phi}{k_B}\right) \quad \text{.....4.21}$$

Now Smith[12] has shown that $\frac{\phi}{k_B T_L}$ can be described by

$$\frac{\phi}{k_B T_L} = -\frac{E_G}{2k_B T_L} + \frac{3}{4}\ln\left(\frac{m_p}{m_e}\right) + \frac{ae}{2k_B} \quad \text{.....4.22}$$

where, m_p = effective mass of carriers in the V.B.
m_e = effective mass of carriers in the C.B.

From the known data of InSb[3] we have the values of $m_p = 0.1$ and $m_e = 0.014$ (in units of electron mass) which gives $\ln(m_p/m_e) \approx 3.5$.

The value for a has been determined as ≈ 0.00027 (for $T > 200$ K) (see section 4.1 and equation 4.1), giving the value 1.56 for the third term (which takes account of the variance of the band gap with temperature).

Now substituting equation 4.22 into equation 4.21 one obtains,

$$n = \frac{3\pi^{1/2}}{4}N_c^*\exp\left(\frac{3}{4}\ln\left(\frac{m_p}{m_e}\right) + \frac{ae}{2k_B}\right)\exp\left(-\frac{E_G}{2k_B T_L}\right) \quad \text{.....4.23}$$

---

[12]Smith, 'Semiconductors' p78(C.U.P.,1959)

On evaluating the terms not involving T_L one obtains the relation between the intrinsic electron concentration in the C.B., n, and the Temperature of the crystal lattice, T_L.

$$n = 4.69 \times 10^{14} T_L^{3/2} \exp\left(\frac{-1326.3}{T_L}\right) \quad \text{.....4.24}$$

The above compares well with the expression derived by Howarth et.al.[13] for InSb which is given as

$$n^2 = 1.8 \times 10^{32} \left(\frac{T_L}{290}\right)^3 \exp\left[- \frac{0.253}{k_B}\left(\frac{1}{T_L} - \frac{1}{290}\right)\right]$$

which can be rearranged to give

$$n^2 = 7.38 \times 10^{14}\ T_L^3 \exp\left[- \frac{2933}{T_L} + 10.11\right]$$

and

$$n = 4.27 \times 10^{14}\ T_L^{3/2} \exp\left[- \frac{1467}{T_L}\right]$$

So for temperatures above one Kelvin we have the electron concentration in the C.B. of InSb, n_t, being

$$n_t = n + n_i$$

where n_i is the uncompensated donor concentration.

Figure 4.5 shows plots of n_i,n & n_t against temperature.

---

[13]Howarth et.al., Proc.Phys.Soc. B70 , 124 (1957)

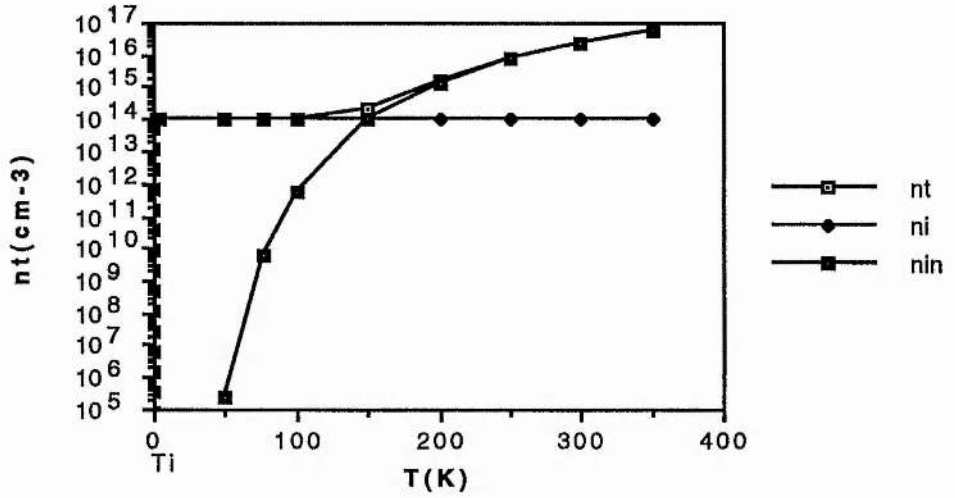

Figure 4.5 : Plot of the variations in electron concentration in the C.B., due to impurity ionisation (n_i) and ionisation of electrons from the V.B. (n_{in}) and their combination (n_t), with temperature

Due to the assumptions taken in obtaining equation 4.24 it is only valid for temperatures greater than 200 degrees Kelvin, but since the intrinsic concentration does not effect the total electron concentration till the temperature is about 200 degrees Kelvin the expression for the total electron concentration in the conduction band is accurate for all temperatures (provided the uncompensated donor concentration is greater than 10^{13} cm^{-3})

4.6 **Calculation of the Energy of the Fermi Level and the Implications for Degeneracy.**

Returning to equation 4.11 which gives.

$$n = N_c^{*0} L_0^{3/2}(\eta, b)$$

Values for the ratio n/N_c^* can now be obtained from the last section, so values of η can be acquired from tables of numerical approximations to the solutions of the generalised Fermi integrals as derived by Kowalczyk et.al[14]. The other variable b ($= \frac{k_B T_L}{E_G}$) equals

[14]Kowalczyk et.al.,'Generalised Fermi Dirac Integrals' (Warsaw,1965)

unity for a temperature of 2724.6K. As most of the experimentation dealt with here involves helium temperatures (1.5 & 4.2K), b can generally be taken to be zero. The only case where this is not valid is where the effective electron temperature is high (≈250K) at which point b must be determined and involved in the determination of η. The variation of η with lattice temperature has been obtained for various uncompensated donor concentrations and is presented in figure 4.6. Numerical values are given in appendix 4.1.

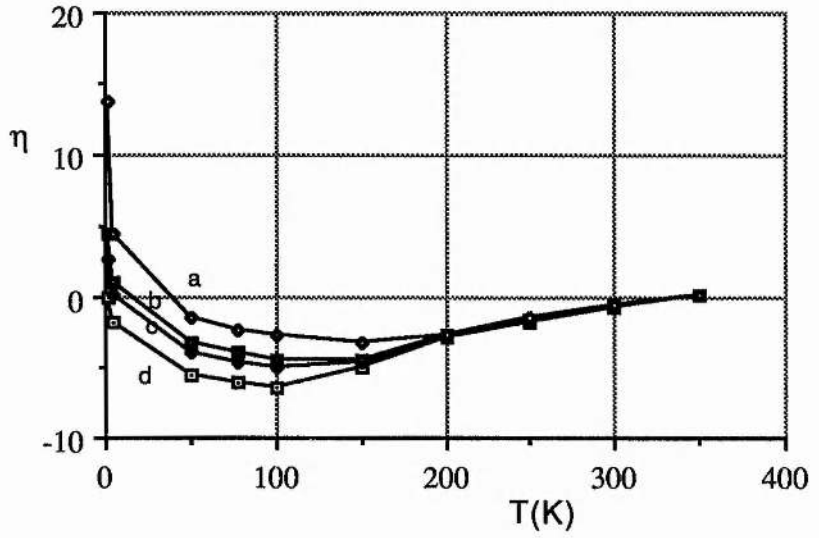

Figure 4.6 : Variation in the Fermi level (in eV with respect to the C.B.) with temperature and carrier concentration (a = 10^{13} cm^{-3}, b = 5 x 10^{13} cm^{-3}, c = 10^{14} cm^{-3} & d = 5 x 10^{14} cm^{-3}).

4.7 **The Calculation of the Effect of the Various Excitatior and Relaxation Processes**

Having obtained the electron concentration and distribution in the conduction band, the next task is to determine the effect of the various excitation and relaxation mechanisms on the distribution and hence the conductivity.

To do this one must derive the Boltzmann transport equation (which describes the electrons motion and probability of

interaction) for the situation one wishes to investigate*. For most cases the Boltzmann equation may be rearranged into a linear form. This form is an integral equation, known as the Bloch equation. In general, a solution to this equation in its closed form cannot be obtained. Two analytic methods are used to obtain solutions. The most accurate and involved method is that using the variational procedure[15]. This method is essential for obtaining accurate solutions in situations involving non-elastic scattering processes. For situations where the scattering processes involved are elastic, a more direct method, known as the relaxation time approximation (RTA) method, can be used. This produces momentum scattering lifetimes, for each scattering process, which are dependent on the electrons' energies. The inverse of these scattering lifetimes can be summed to obtain the total relaxation time and the total mobility (see section 4.8.8). The details of the above methods have not been included here as they have been covered comprehensively elsewhere (variational proceedure15,[16,17] ; RTA[18,19,20]). Note that the rate of momentum scattering is incorporated into the scattering lifetimes. The rate of energy scattering is dealt with seperately (see section 4.9).

---

* This involves combining the band structure equations with the transition probabilities involved with interaction.

[15]Kohler, Ann.Physik.40 , 601 (1942)

[16]Fletcher&Butcher, J.Phys.C. 5 , 212 (1972)

[17]Pfeffer&Zawadski, Phys.Stat.Sol.(b), 80 , 247 (1978)

[18]Boguslawski, Phys.Stat.Sol.(b), 70 , 53 (1975)

[19]Zawadski, Hdbk,Semicond.Vol.1,Ch.12, 713 (1982)

[20]Conwell, Sol.Stat.Phys.,suppl.9 , Ch3. (1967)

4.8 Evaluation of Scattering Lifetimes

The following equations have, mostly, been taken from Zawadski[19] With comparisons made to those presented by Conwell[20] and Fletcher & Butcher[16] showing them to be equivalent. For most of the scattering processes the interaction is affected by the screening effect of other carriers. A term, known as the screening wavelength, which is characteristic of this screening effect is used in the RTA derived equations to include the effect of screening.

4.8.1 Evaluation of Screening Wavelength

Zawadski & Szymanska[21] and Kolodziejczak[22] have shown that for a non-parabolic band (as described by equations 4.4 & 4.5) the screening wavelength is given (in c.g.s. units) by

$$\frac{1}{\lambda^2} = \frac{2}{\pi}\frac{e^2}{\kappa_o k_B T_L}\left(\frac{2 m_o^* k_B T_L}{\hbar^2}\right)^{3/2} {}^{0}L_1^{1/2}(\eta,b)\ \text{cm}^{-2} \qquad \text{.....4.25a}$$

where ${}^{0}L_1^{1/2}(\eta,b)$ is defined as in equation 4.13,

$e = 4.8 \times 10^{-10}$ e.s.u. - electronic charge,

$\kappa_o = 17.5$ [23],

$k_B = 1.38 \times 10^{-16}$ ergs/deg - Boltzmann's constant,

T_L = Lattice Temperature (in Kelvin),

$m_o^* \approx 0.013 \times 9.1 \times 10^{-28}$ grams - effective electron mass,

$\hbar = \frac{h}{2\pi} = 1.0546 \times 10^{-27}$ ergs.secs. - $\frac{1}{2\pi}$ x Planck's constant.

---

[21] Zawadski&Szymanska, Phys.Stat.Sol.(b), 45 , 415 (1971)

[22] Kolodziejczak, Acta.Phys.Polon. 20 , 289 (1961)

[23] Landolt&Börnstein, Num.Data&Funct.Rel.in Sci.&Tech.Group III,vol.17,subvol.group IV&III-V comp.

or (in S.I. units),

$$\frac{1}{\lambda^2} = \frac{2}{\pi}\frac{e^2}{4\pi e_o \kappa_o k_B T_L}\left(\frac{2 m_o^* k_B T_L}{\hbar^2}\right)^{3/2} {}^0L_1^{1/2}(\eta,b)\ cm^{-2} \quad .....4.25b$$

where, $e = 1.6 \times 10^{-19}$ - electronic charge,

$\kappa_o = 17.5$ - dielectric constant for zero frequency radiation,

$e_o = 8.85 \times 10^{-12}$ - dielectric constant of free space,

$k_B = 1.38 \times 10^{-23}$ J/deg - Boltzmann's constant,

T_L = Lattice Temperature (in Kelvin),

$m_o^* \approx 0.013 \times 9.1 \times 10^{-31}$ Kg-effective electron mass,

$\hbar = \frac{h}{2\pi} = 1.0546 \times 10^{-34}$ J.s. $= \frac{1}{2\pi} \times$ Planck's constant.

such that,

$$\frac{1}{\lambda^2} = 9.65 \times 10^{13} T_L^{1/2}\, {}^0L_1^{1/2}(\eta,b) \quad m^{-2} \quad .....4.26$$

the evaluation of the screening wavelength with respect to temperature and electron concentration is given in figure 4.7. Numerical values are given in appendix 4.2.

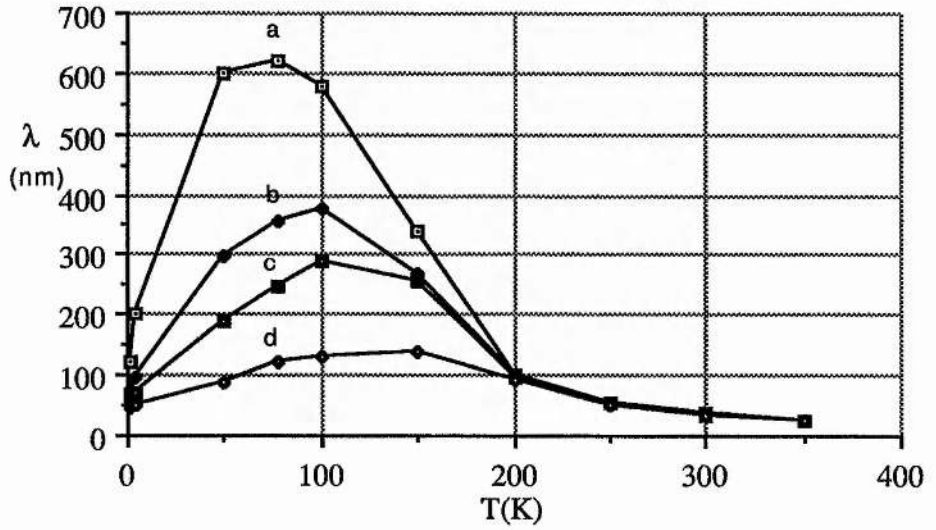

Figure 4.7 : Variation of the screening wavelength with temperature and carrier concentration (a = 10^{13} cm^{-3}, b = 5×10^{13} cm^{-3}, c = 10^{14} cm^{-3} & d = 5×10^{14} cm^{-3}).

4.8.2 Evaluation of Electron Lifetime for Neutral Impurity Scattering

The first treatment of neutral impurity scattering by Erginsoy[24] led to an expression for the relaxation time which was independent of the electron energy. It can be written as,

$$\frac{1}{\tau_n} = \frac{20\kappa_o \hbar^3}{e^2 (m_o^*)^2} n_n \qquad \text{.....4.27}$$

$$= \frac{20 a_b}{m_o^*} n_n \qquad \text{where } a_b = \text{effective Bohr radius}$$

It was found that for low electron energies (at which this process is effective[20]) the above equations are inaccurate. Blagosklonskaya et.al.[25] using a more exact theory were able to account for the discrepancies at low energies. At high energies there results agree with those of Erginsoy. The energy dependent relaxation time obtained is,

$$\frac{1}{t_n(E)} = \frac{\sqrt{2}\pi a_b n_n}{\sqrt{m_o^*}} \left[\frac{1}{(E/E_i) + 0.0275} + 10 \right] E^{1/2} \qquad \text{.....4.28}$$

In order to obtain values for the neutral impurity concentration, n_n, expressions have been used that were presented by Smith[26]. Smith gives the concentration of impurity electrons ionised into the conduction band as,

$$n_{ie} = \frac{1}{\sqrt{2}} (n_d N_c^*)^{1/2} \exp\left(\frac{-E_i}{2k_B T}\right)$$

with, $n_d = \dfrac{n_e + n_i}{2}$ = the donor impurity concentration

n_e = uncompensated donor concentration

n_i = impurity concentration

N_c^* = generalised effective density of states in the CB as defined in equation 4.12

---

[24]Erginsoy, Phys.Rev. 79 , 1013 (1950)

[25]Blagosklonskaya et.al., Sov.Phys.Sol.State 11 , 2402 (1970)

[26]Smith, 'Semiconductors' 90 (1959)

E_i = uncompensated donor impurity ionisation energy

Then the concentration of neutral impurities is given by,

$$n_n = n_e + n_{ie}.$$

As no detailed study of the ionisation energy of shallow donors in high purity n-InSb, at low temperatures, has been undertaken, it is impossible to use an accurate value for E_i. Landolt & Börnstein[3] suggest a value of ≈ 0.7 meV for impurity concentrations of at least 10^{13} cm^{-3}. As none of the crystals used in this investigation have an impurity concentration close to 10^{13} cm^{-3} (the lowest concentration being ≈ 8×10^{14} cm^{-3}), the value for the ionisation energy is clearly not valid. If one compares the value with those obtained by the hydrogenic model impurity calculation (see figure 4.3 in section 4.4), it is possible to conclude that the impurity concentrations in figure 4.3 are incorrect by a factor of 10^2 as was suggested by Putley[27]. If this is true then for impurity concentrations greater than 10^{14} cm^{-3}, all uncompensated donors will be ionised thermally at lattice temperatures greater than one degree Kelvin. The neutral impurity concentration is then zero and neutral impurity scattering will not occur.

4.8.3 Evaluation of the Ionised Impurity Scattering Lifetime

The expression for the relaxation lifetime for ionised impurity scattering in a non-parabolic band, including the effect of screening, as presented (with reservations) by Zawadski[28] is given (in c.g.s. units) as,

$$\tau_{ii}(E) = \frac{1}{2\pi}\frac{\kappa_o^2\,\hbar}{e^4 n_{ii}}\frac{1}{F_{ii}}\left(\frac{dE}{dk}\right)k^2 \qquad \text{.....4.29}$$

where, n_{ii} = concentration of ionised impurities
$= n_i - n_n \approx n_i$ (see section 4.8.2)

---

[27]Putley, Phys.Stat.Sol. 6 , 571 (1964)
[28]Zawadski, Hdbk,Semicond.Vol.1,Ch.12, 716,725 (1982)

$$\frac{dE}{dk} = \frac{\hbar^2 k}{m^*} \quad \text{(equation 4.6)}$$

$$k = \frac{\sqrt{2m^* k_B T}}{\hbar} \quad \text{(from equation 4.6)}$$

and $$F_{ii}(\xi,L) = \ln(\xi + 1) - \frac{\xi}{\xi + 1} - L(3-L)f_1 + \frac{3}{2} L^2 f_2 \quad \text{.....4.30}$$

where, $$f_1 = 1 + \frac{1}{\xi + 1} - \frac{2}{\xi} \ln(\xi + 1)$$

$$f_2 = 1 - \frac{4}{\xi} - \frac{2}{\xi(\xi + 1)} + \frac{6}{\xi^2} \ln(\xi + 1)$$

and $\xi = (2k\lambda)^2$

where λ = screening wavelength (see section 4.8.1)

k = wave number (defined above and in equation 4.6)

also $$L = \frac{E}{E_G + 2E}$$

where E_G = Band gap energy (see section 4.1)

For the region in which ionised impurity scattering is effective (T<150K : from comparison of results by Fletcher & Butcher[29] with data presented in Landolt & Börnstein's tables[3]), L is small (= 5.49 x 10^{-2} at 150K). So with only a small loss in accuracy one can take L = 0 which simplifies equation 4.30 to,

$$F_{ii}(\xi) = \ln(\xi + 1) - \frac{\xi}{\xi + 1}$$

Equation 4.29 was evaluated by substituting for dE/dk to obtain,

$$\tau_{ii}(E) = \frac{1}{2\pi} \frac{\kappa_o^2 \hbar^3}{e^4 m_o^*} \frac{1}{n_{ii}} \frac{1}{F_{ii}} k^3$$

$$= 9.1 \times 10^{-14} \frac{1}{n_{ii}} \frac{1}{F_{ii}} k^3$$

$$= 9.1 \times 10^{-29} \frac{k^3}{F_{ii}} \quad \text{(for } n_{ii} = 10^{15} \text{ cm}^{-3}\text{)}$$

Now $$k^3 = \left(\frac{\sqrt{2m^* k_B T}}{\hbar}\right)^3 = 1.59 \times 10^{14}\ T^{3/2}$$

---

[29] Fletcher & Butcher, J.Phys.C. 5 , 212 (1972)

with T = temperature equivalent to electrons' energy

so $$\tau_{ii}(E) = 1.45 \times 10^{-14} \frac{T^{3/2}}{F_{ii}} \quad \text{.....4.31}$$

Values for F_{ii} were obtained and the variation of τ_{ii} with temperature was evaluated. In order to compare the results more readily with experimental data, the variation of the electron mobility with temperature was obtained using the relation

$$\mu_{ii}(T) = \frac{e\tau(T)}{m^*(T)} \quad \text{.....4.32}$$

The results of this calculation are shown in figure 4.8 and compared and combined with the results for the other scattering processes in figure 4.13 , Numerical values for the lifetime and mobility at various temperatures are given in appendix 4.3.

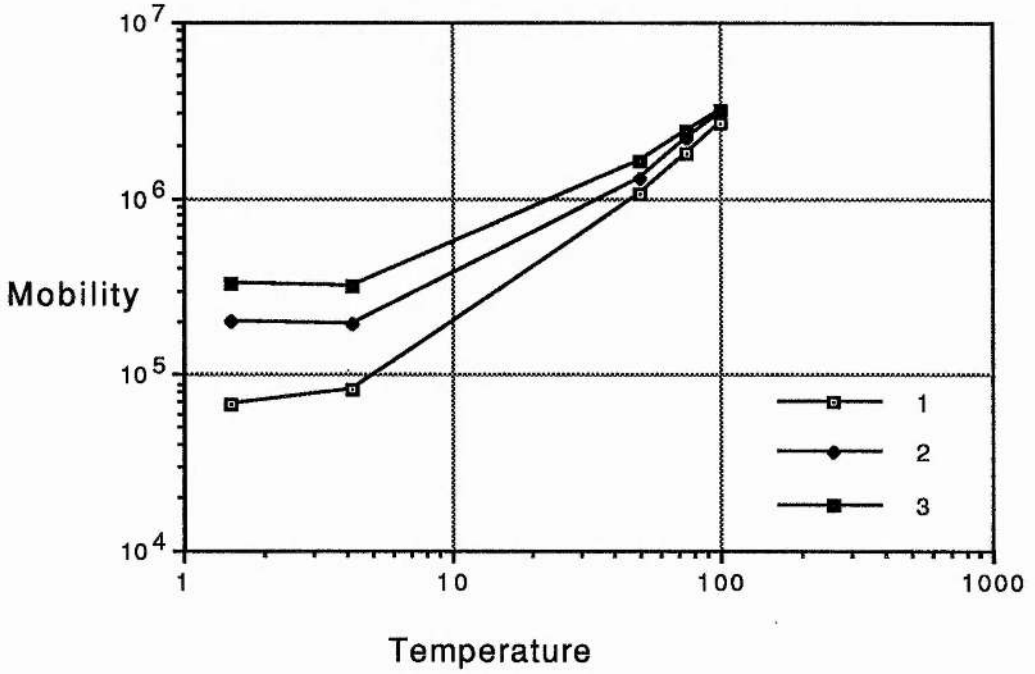

Figure 4.8 : Variation of mobility with electron temperature and carrier concentration (1 : $n_c = 10^{13}$ cm^{-3}; 2 : $n_c = 5 \times 10^{13}$ cm^{-3} & 3 : $n_c = 10^{14}$ cm^{-3}) under ionised impurity scattering. The total impurity concentration = 10^{15} cm^{-3}.

4.8.4 Evaluation of The Piezoelectric Acoustic Phonon Scattering Lifetime

The following expression was derived by Zawadski & Szymanska[30] for the piezoelectric acoustic phonon scattering lifetime in small band gap materials. It is equivalent to the expression presented by Conwell[31] for this type of scattering, though it is more specific and more accurate. The expression derived by Zawadski & Szymanska can be written (in c.g.s. units) as,

$$\frac{1}{\tau_{pe}} = \frac{8\pi P^2 e^2 k_B T_L}{\kappa_o^2 \hbar}\left(\frac{K_\upsilon}{c}\right)_{av}\frac{dk}{dE}F_{pe} \qquad \text{.....4.33}$$

By comparison with results obtained by Fletcher and Butcher[32] the following expressions may be written,

$$P^2 = 4e_{14}^2$$

where e_{14} = non-zero component of the piezoelectric tensor
$= 7.17 \times 10^{-6}$ cm^{-1} $= 2.151 \times 10^4$ e.s.u. cm^{-1}

and $$\left(\frac{K_\upsilon}{c'}\right)_{av} = \left(\frac{16}{35c_t} + \frac{12}{35c_l}\right)$$

where c_t, c_l = average of elastic constants transverse and parallel to the phonon direction.

where $$c_t = c_{44} - \frac{1}{5}(c_{12} + 2c_{44} - c_{11})$$
$$= 2.5 \times 10^{11} \text{ dyne.cm}^{-2}$$
$$c_l = +\frac{2}{5}(c_{12} + 2c_{44} - c_{11})$$
$$= 5.644 \times 10^{11} \text{ dyne.cm}^{-2}$$

as $c_{11} = 6.65 \times 10^{11}$ dyne.cm^{-2}
$c_{12} = 3.78 \times 10^{11}$ dyne.cm^{-2}
$c_{44} = 3.13 \times 10^{11}$ dyne.cm^{-2}

---

[30]Zawadski & Szymanska, Phys.Stat.Sol.(b), 45 , 415 (1971)
[31]Conwell, Sol.Stat.Phys.,suppl.9 , Ch3. (1967)
[32]Fletcher and Butcher, J.Phys.C. 5 , 212 (1972)

so equation 4.33 (by substituting in $\frac{dk}{dE} = \frac{m^*}{\hbar^2 k}$) can be rewritten as,

$$\frac{1}{\tau_{pe}} = \frac{8\pi(2e_{14})^2 e^2 k_B T_L}{\sqrt{2}\kappa_o^2 \hbar^3}\left(\frac{16}{35c_t} + \frac{12}{35c_l}\right) k^{-1} F_{pe}$$

then substituting in $k = \frac{\sqrt{2m^* k_B T_L}}{\hbar}$ gives,

$$\frac{1}{\tau_{pe}} = \frac{8\pi(2e_{14})^2 e^2 (k_B m^*)^{1/2}}{\sqrt{2}\kappa_o^2 \hbar^2}\left(\frac{16}{35c_t} + \frac{12}{35c_l}\right) F_{pe}\, T_L\, T_e^{-1/2}$$

$$= 3.52 \times 10^7\, F_{pe}\, T_L\, T_e^{-1/2} \qquad \text{.....4.34}$$

where $F_{pe} = A - \frac{1}{2} L(4 - L)\, B + L^2 C$

with $A = 1 - \frac{2}{\xi}\ln(\xi + 1) + \frac{1}{\xi + 1}$

$$B = 1 - \frac{4}{\xi} + \frac{6}{\xi^2}\ln(\xi + 1) - \frac{2}{\xi(\xi + 1)}$$

$$C = 1 - \frac{3}{\xi} + \frac{9}{\xi^2} - \frac{12}{\xi^3}\ln(\xi + 1) + \frac{3}{\xi^2(\xi + 1)}$$

with $\xi = (2k\lambda)^2$

$$L = \frac{E}{E_G + 2E}$$

For the region where piezoelectric scattering is thought to have the greatest effect on the electron mobility ($T < 50$ K[33]), the value for F_{pe} is between 0.893 & 1 and is often taken as unity. In evaluating the lifetimes from equation 4.34 the exact value for F_{pe} was taken here. For low electron energies L can be approximated to zero as was done in section 4.8.3. This leads to a simplified expression for F_{pe}.

$$F_{pe} = A = 1 - \frac{2}{\xi}\ln(\xi + 1) + \frac{1}{\xi + 1}$$

---

[33]Conwell, Sol.Stat.Phys.,suppl.9 , Ch2. (1967)

Again the mobility was also calculated and it is the variation of mobility with electron temperature which is displayed in figure 4.9. The mobilities and lifetimes were obtained for different lattice temperatures so that when comparing with experimental data it might be possible to identify where either the electron distribution alone or both the electron and phonon distributions are being heated. Numerical values for the mobilities and lifetimes are given in appendix 4.4.

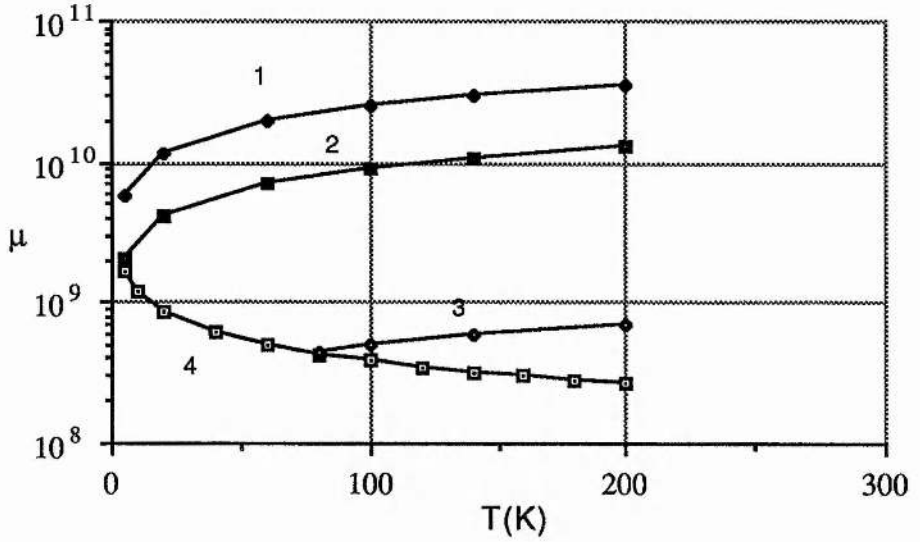

Figure 4.9 : Variation of mobility (units = $cm^2\ V^{-1}\ s^{-1}$) with electron temperature (equivalent to energy) at various lattice temperatures (1: T_L = 1.5K; 2: T_L = 4.2K; 3: T_L = 77K & 4: $T_L = T_e$) under piezoelectric acoustic phonon scattering.

4.8.5 Evaluation of the Potential Deformation Acoustic Phonon Scattering Lifetime

For potential deformation acoustic phonon scattering the equation derived by Zawadski & Szymanska[34] was for mobility,

$$\mu_{pd} = \frac{\pi e \rho}{\hbar\, k_B T_L} \frac{v^2}{F_{pd}} \left(\frac{dE}{dk}\right)^2 k^{-3} \qquad \text{.....4.35}$$

This can be rearranged, using equation 4.32, to obtain :

[34]Zawadski & Szymanska, Phys.Stat.Sol.(b), 45 , 415 (1971)

$$\frac{1}{\tau_{pd}} = \frac{\hbar k_B T_L}{m^* \pi \rho} \frac{F_{pd}}{v^2} \left(\frac{dk}{dE}\right)^2 k^3$$

This is equivalent to the equation derived by Conwell[35].

Substituting for $\frac{dk}{dE}$ and k (using the equations derived from equation 4.6) one obtains,

$$\frac{1}{\tau_{pd}} = \frac{\sqrt{2}(k_B m^*)^{3/2}}{\pi \hbar^4 \rho} \frac{F_{pd}}{v^2} T_L T_e^{1/2} \quad \text{.....4.36}$$

where $\frac{F_{pd}}{v^2} = \frac{F_{pd}^{||}}{(v^{||})^2} + \frac{F_{pd}^{\perp}}{(v^{\perp})^2}$

$v^{||}$, $v^{\perp}$ = average sound velocities for longitudinal and transverse modes

ρ = density of the crystal

$F_{pd}^{||}$ & $F_{pd}^{\perp}$ are given by some lengthy expressions. In most cases, however, $F_{pd}^{||}$ & $F_{pd}^{\perp}$ can be approximated by,

$$F_{pd}^{||} = P_D^2 (1 - \frac{3}{10} L)^2$$

$$F_{pd}^{\perp} = \frac{1}{8} P_D^2 L^2$$

Now, as mentioned in section 4.8.3, for temperatures below 150K, L can be approximated to zero and so

$$\frac{F_{pd}}{v^2} = \frac{F_{pd}^{||}}{(v^{||})^2} = \frac{P_D^2}{(v^{||})^2}$$

substituting this into equation 4.36 gives,

$$\frac{1}{\tau_{pd}} = \frac{\sqrt{2}(k_B m^*)}{\pi \hbar^4} \frac{P_D^2}{\rho (v^{||})^2} T_L T_e^{1/2}$$

---

[35]Conwell,Sol.Stat.Phys.,suppl.9 , Ch3. (1967)

which is equivalent to the equation obtained by Fletcher & Butcher[36]. Evaluating the constants gives,

$$\frac{1}{\tau_{pd}} = 1.14 \times 10^8 \, T_L T_e^{1/2} \quad \text{.....4.37}$$

with $\rho(v^{||})^2 = c_l = 8.156$ dyne cm^{-2}

and $P_D = 30$ eV*

From the above equations, the variation of the lifetime and the mobility with lattice temperature and electron energy (equivalent temperature) was obtained. The results are depicted in figure 4.10. Numerical values are given in appendix 4.5.

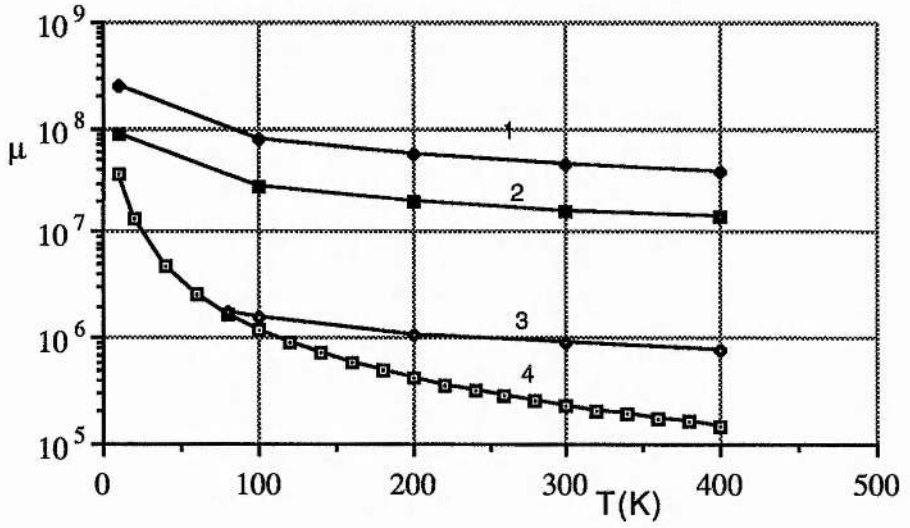

Figure 10 : Variation of mobility (units = cm^2 V^{-1} s^{-1}) with electron temperature (equivalent to energy) for various lattice temperatures (1: T_L = 1.5K; 2: T_L = 4.2K; 3: T_L = 77K & 4: $T_L = T_e$) under potential deformation acoustic phonon scattering

---

[36]Fletcher & Butcher, J.Phys.C. 5 , 212 (1972)

* This value is not known accurately

4.8.6 Evaluation of the Polar Optical Phonon Scattering Lifetime

The importance of this scattering process in polar crystals was first shown by Ehrenreich[37]. Ehrenreich calculated the electron transport coefficients in pure InSb using the variational procedure (generalising on the work done by Howarth & Sondheimer[38]) and the formulas derived for the non-parabolic band of InSb by Kane[39]. The equation, derived from Ehrenreich's work, presented by Conwell[40] is given as,

$$\frac{1}{\tau_{po}} = \frac{2eE_o}{(2mE)^{1/2}}\left[N_q \sinh^{-1}\left(\frac{E}{\hbar\omega_l}\right)^{1/2} + (N_q + 1)\sinh^{-1}\left(\frac{E - \hbar\omega_l}{\hbar\omega_l}\right)^{1/2}\right] \quad \text{.....4.38}$$

where,
$$eE_o = \frac{m^* e^2 \hbar\omega_l}{\hbar^2}\left(\frac{1}{\kappa_\infty} - \frac{1}{\kappa_o}\right)$$

$$N_q = \left[\exp\left(\frac{\hbar\omega_l}{k_B T_L}\right) - 1\right]^{-1}$$

= number of phonons with wave vector **q** such that their energy is $\hbar\mathbf{q}$.

The second term in the brackets in equation 4.38 corresponds to phonon emission. This term is only valid for electron energies greater than that of an optical phonon.

At higher electron energies ($E >> \hbar\omega_l$) Conwell concludes from the above that

$$\tau_{po} = \frac{(2mE)^{1/2}}{eE_o(2N_q + 1)}$$

which implies that at high energies the electron mobility will increase.

---

[37]Ehrenreich, J.Phys.Chem.Sol. 2 , 131 (1957)
[38]Howarth & Sondheimer, Proc.Roy.Soc. A219 , 53 (1953)
[39]Kane, J.Phys.Chem.Sol. 1, 249 (1957)
[40]Conwell,Sol.Stat.Phys.,suppl.9 , Ch3. (1967)

Zawadski & Szymanska[41] following work done by Kolodziejczak[42] derived a more exact equation for the polar optical phonon scattering lifetime in a non-parabolic band, taking into account the effect of screening. This expression is given (in c.g.s. units) as

$$\frac{1}{\tau_{po}} = \frac{8\pi(e e^*)^2 k_B T_L}{\Omega M \hbar \omega_l^2} F_{po} \frac{dk}{dE} \qquad \text{.....4.39}$$

where $$(e^*)^2 = \frac{\Omega M \omega_l^2}{4\pi}\left(\frac{1}{\kappa_\infty} - \frac{1}{\kappa_o}\right)$$

e^* = effective ionic charge
Ω = Volume of unit cell
M = reduced mass of the ions
ω_l = angular frequency of the optical phonons
κ_o, κ_∞ = dielectric constants

substituting for e* and dk/dE in equation 4.39 one obtains

$$\frac{1}{\tau_{po}} = \frac{2m^* e^2 k_B T_L}{\hbar^3}\left(\frac{1}{\kappa_\infty} - \frac{1}{\kappa_o}\right) F_{po}\, k^{-1}$$

where the similarity to equation 4.38 is apparent. Substituting for k one obtains

$$\frac{1}{\tau_{po}} = \frac{2(m^* k_B)^{1/2} e^2}{\hbar^2}\left(\frac{1}{\kappa_\infty} - \frac{1}{\kappa_o}\right) F_{po}\, T_L T_e^{-1/2}$$

$$= 7.85 \times 10^{10} F_{po}\, T_L\, T_e^{-1/2} \qquad \text{.....4.40}$$

where F_{po}, the screening factor, is equal to F_{pe}, the screening factor in the piezoelectric scattering regime. Values for the lifetime and mobility and their variation with lattice temperature and electron

---

[41] Zawadski & Szymanska, Phys.Stat.Sol.(b) 45 , 415 (1971)
[42] Kolodziejczak, Acta.Phys.Polon. 20 , 379 (1961)

temperature have been obtained using equation 4.40, and are presented in figure 4.11. Numerical values are given in appendix 4.6.

The above expression has been derived using the relaxation time approximation and is only accurate at very high electron energies ($E >> \hbar\omega_l$) where the interaction is elastic. For electron energies close to and below the optical phonon energy. the assumption of elastic interaction becomes inaccurate and the variational procedure must be used. The need for this was shown quite conclusively by Pfeffer & Zawadski[43], who obtained working analytical expressions for the electrical conductivity using the variational procedure and were able to compare their results with those obtained by the relaxation time approximation method. Fletcher & Butcher[44] solved the transport difference equation numerically and were able to show that for electron energies up to eight times that of the optical phonon energy, the concept of a relaxation time is flawed. Due to the perturbing effect of the optical phonon interaction on the electron distribution and the quantised nature of the optical phonons, the variation of the relaxation time with energy shows discontinuities at multiples of the phonon energy. At high energies these discontinuities become less distinct and the variation of the relaxation time with energy tends towards the $E^{1/2}$ predicted by Conwell[45] These perturbations are not included in the variation procedure treatment carried out by Pfeffer & Zawadski, though Zawadski[46] points out that that, as the variational procedure is insensitive to the quality of the trial distribution function used, the results obtained have an accuracy of better than 20%.

Simplified expressions for the electron mobility at low and high temperatures, derived using the variational procedure, are presented by Blatt[47]. These state that,

$$\mu_{po} = \frac{3\pi^{1/2}\hbar^2}{2^{5/2}e(m^*)^{3/2}} \frac{1}{\left(\frac{1}{\kappa_\infty} - \frac{1}{\kappa_o}\right)} (k_B T_L)^{-1/2} \text{ for } T > \Theta_o \quad \text{....4.41a}$$

---

[43]Pfeffer & Zawadski,Phys.Stat.Sol.(b) 88 , 247 (1978)
[44]Fletcher & Butcher, J.Phys.C. 5 , 212 (1972)
[45]Conwell,Sol.Stat.Phys.,suppl.9 , Ch3. (1967)
[46]Zawadski, Hdbk,Semicond.Vol.1,Ch.12, 764,5 (1982)
[47]Blatt, 'Phys of Elec.Cond.in Solids' (McGraw-Hill),1968)

and

$$\mu_{po} = \frac{\hbar^2}{\left(2e^2(m^*)^3 k_B \Theta_o\right)^{1/2}} \left(e^{\Theta o/T} - 1\right) \quad \text{for } T < \Theta_o \text{ .....4.41b}$$

where $\Theta_o \approx 280$ K = Einstein Temperature

These are known to be inaccurate in quantity but fairly accurate in character, so once a comparison with practical data has been done a correcting factor should be included. Values obtained using the above equations have been given in figure 4.11. Numerical values can be found in appendix 4.6.

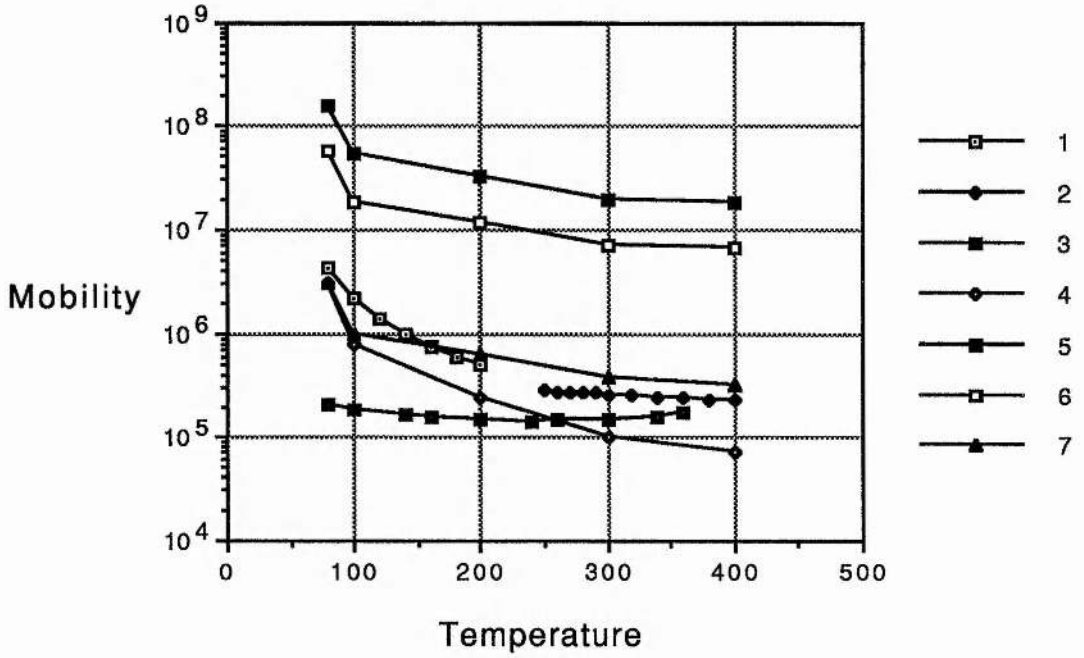

Figure 4.11 : Variation of mobility (units = $cm^2\ V^{-1}\ s^{-1}$) with electron temperature (units = K), equivalent to the electron energy, under polar optical scattering. Lines 1&2 are after Blatt; Line 3 is after Zawadski & Szymanska; Lines 4,5,6,&7 are after Ehrenreich[48] and Trifonov & Yaramenko[49] with the lattice temperature , $T_L = T_e$ for lines 1 - 4, T_L = 1.5K for line 5, T_L = 4.2K for line 6, T_L = 77K for line 7.

---

[48]Ehrenreich, J.Phys.Chem.Sol. 2 , 131 (1957)

[49]Trifonov & Yaramenko, Sov.Phys.Semicond. 5 , 839 (1971)

4.8.7 Evaluation of the Non-Polar Optical Phonon Scattering Lifetime

Non-polar optical scattering is the optical equivalent of potential deformation acoustic phonon scattering and a potential deformation theory was set up by Bir & Pikus[50] to investigate the effects of this scattering mechanism. The validity of this method was subsequently investigated by Lawaetz[51]. Boguslawski[52] applied the potential deformation theory to the situation where the band structure could be described by Kane's three level band model of InSb[53] with a general formulation of electron-phonon interactions. The equation derived by Boguslawski is given (in c.g.s. units) by,

$$\frac{1}{\tau_{npo}} = \frac{k_B T_L \, m^*}{\pi a_b^2 \, \rho \, \hbar^3} \left(\frac{F_{npo}}{\omega^2}\right) k \qquad \text{.....4.42}$$

substituting for m* (using equation 4.8) one obtains

$$\frac{1}{\tau_{npo}} = \frac{k_B T_L \, m_o^* \left(1 + 2E/E_G\right)}{\pi a_b^2 \, \rho \, \hbar^3} \left(\frac{F_{npo}}{\omega^2}\right) k$$

now substituting for k gives

$$\frac{1}{\tau_{npo}} = \frac{\sqrt{2}\left(k_B m_o^* \left(1 + 2E/E_G\right)\right)^{3/2}}{\pi a_b^2 \, \rho \, \hbar^4} \left(\frac{F_{npo}}{\omega^2}\right) T_L T_e^{1/2}$$

---

[50] Bir & Pikus, Fiz.Tverd.Tela 2 , 2287 (1960)
[51] Lawaetz, Phys.Rev. 183 , 730 (1969)
[52] Boguslawski, Phys.Stat.Sol(b) 70 , 54 (1975)
[53] Kane, J.Phys.Chem.Sol. 1 , 249(1957)

then evaluating the constants gives

$$\frac{1}{\tau_{npo}} = 3.227 \times 10^{50} \left(1 + 2E/E_G\right)^{3/2} \left(\frac{F_{npo}}{\omega^2}\right) T_L T_e^{1/2} \quad \text{.....4.43}$$

where $$\frac{F_{npo}}{\omega^2} = \frac{F^L_{npo}}{\omega_L^2} + \frac{F^T_{npo}}{\omega_T^2}$$

ω_L^2, ω_T^2 = angular frequency of longitudinal and transverse optical phonons

$\omega_L^2 = 3.71 \times 10^{13}$, $\omega_T^2 = 3.481 \times 10^{13}$

$$F^L_{npo} = \frac{3}{2} b^4 d_o^2 + 6a^2 b^2 d_1^2$$

$$F^T_{npo} = 3b^4 d_o^2 + \frac{2}{3} a^2 b^2 d_1^2$$

d_o, d_1 = potential deformation constants

d_o = 34.8 eV = 5.568×10^{-11} ergs

$d_1 \approx$ 5eV = 8×10^{-12} ergs

(the values for the deformation potential constants are taken from Zawadski[54])

$$a = (1 - L)^{1/2}$$

$$b = \left(\frac{L\beta^2}{3}\right)^{1/2}$$

$$L = \frac{E}{E_G + 2E}$$

$$\beta^2 = \frac{\Delta^2}{(\Delta + E_G)(\Delta + (3/2)E_G)}$$

The above is derived under the assumption that the band gap is much smaller than the spin-orbit interaction energy ($E_G << \Delta$). This assumption holds for most temperatures in InSb. Using the above equations, the variation of the lifetime with lattice temperature and electron temperature was obtained. For comparison purposes, the variation of the electron mobility with lattice and electron temperature was calculated and it is this which is depicted in figure 4.12. Numerical values of the variation in electron lifetime and

---

[54]Zawadski, Hdbk,Semicond.Vol.1,Ch.12, 772,5 (1982)

mobility with electron and lattice temperature are presented in appendix 4.7.

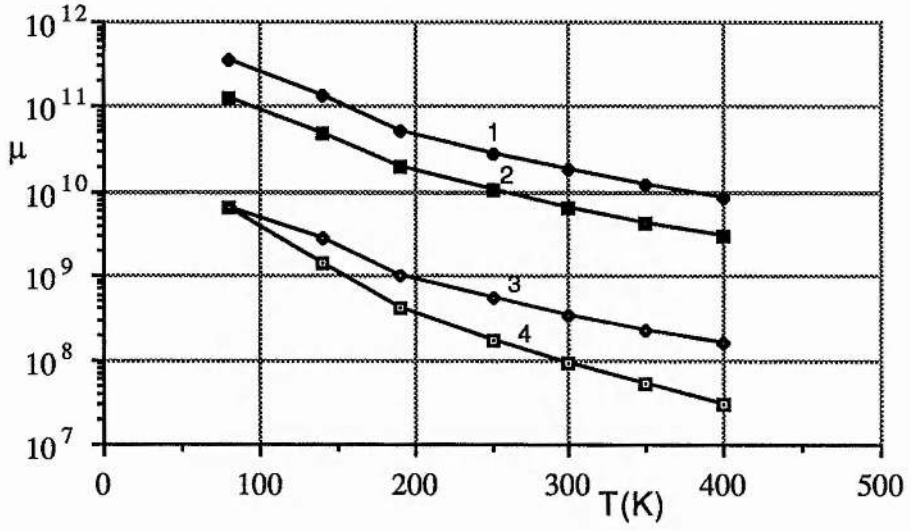

Figure 4.12 : Variation of mobility (units = $cm^2\ V^{-1}\ s^{-1}$) with electron temperature (equivalent to energy) at various lattice temperatures (1: T_L = 1.5K; 2: T_L = 4.2K; 3: T_L = 77K & 4: $T_L = T_e$) under non-polar optical phonon scattering

4.8.8 Evaluation of Total Mobility When There are Several Scattering Processes in Operation

All the equations derived and evaluated in sections 4.8.2 - 4.8.7 are valid when that particular scattering process is the only scattering process in operation or is highly dominant. In most situations there are several scattering processes in operation and their combined effect will determine the mobility. For the non-degenerate case where the electrons possess a distribution of energies the following method must be employed for calculating the total mobility: The inverse mobilities (as functions of the electron energy) must be summed to obtain a total mobility as a function of energy. Then the average over the electron energies should be calculated to obtain the mean mobility which will determine the conductivity. In the degenerate case, where all the electrons possess an energy close to the Fermi energy, the above is simplified. The

need for averaging over the electron energies is removed. Zawadski[55] has summarized the above into the following equation,

$$\frac{1}{\mu_T(E)} = \frac{m^*(E)}{e\tau_T(E)} = \sum_s \frac{1}{\mu_s(E)} \qquad \text{.....4.44}$$

This equation has been used to obtain the total mobility as shown in figure 4.13. The mobilities for the individual scattering processes have been included so that the relationship between the individual and total mobilities can be seen.

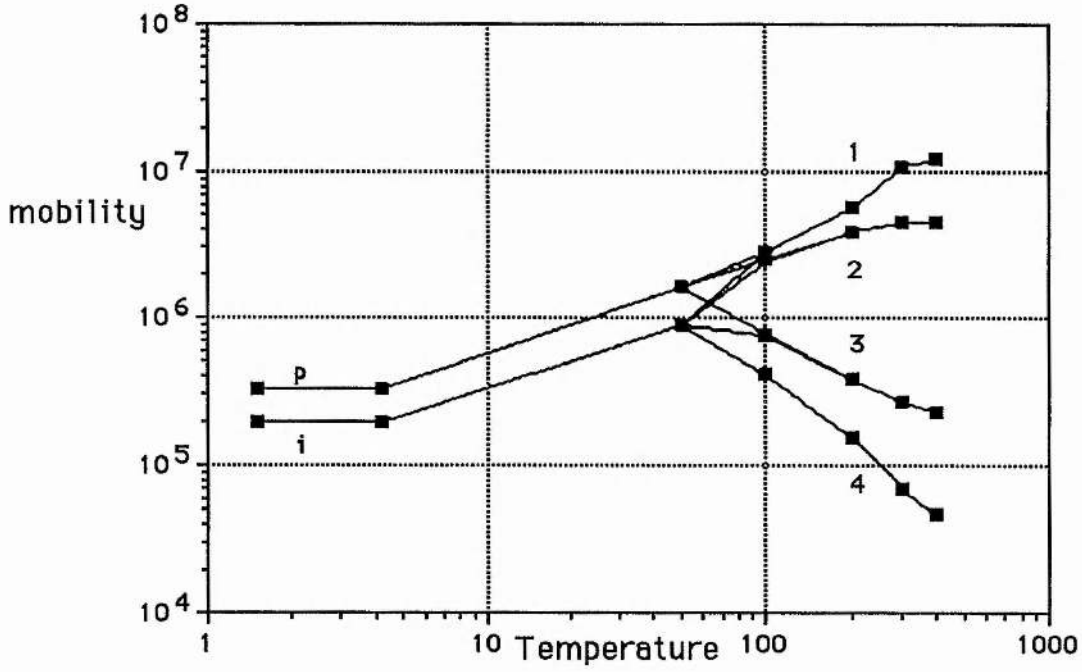

Figure 4.13 : Variation of the total mobility with electron temperature (equivalent to energy) for various lattice temperatures (1 : T_L = 1.5K ; 2 : T_L = 4.2K ; 3 : T_L = 77K ; 4 : T_L = T_e) and various carrier concentrations (i : n_c = 5 x 10^{13} cm $^{-3}$; p : n_c =10^{14} cm^{-3}).The impurity concentration = 10^{15} cm^{-3}.

One further restriction must be made when considering the combined mobility. Equation 4.44 is not accurate for inelastic scattering mechanisms as the individual lifetimes are not valid.

---

[55]Zawadski, Hdbk,Semicond.Vol.1,Ch.12, 787 (1982)

This applies mainly to the region where optical phonon scattering is dominant ($T_e > \Theta_D$). This region has to be dealt with in more detail. The situation was considered in section 4.8.6.

4.9 **Electron Energy Excitation and Relaxation Rates**

The above has only dealt with one part of the picture. It was also, in the main, derived under the assumption that the electron energy distribution can be described by the Maxwell-Boltzmann distribution. To check on the validity of this assumption one must calculate the rate of energy to and from the electrons at all possible electron energies.

4.9.1 Rate of Energy to an Electron on Application of an Electric Potential/Field

The rate of energy supplied to the electrons by an electric field is given by,

$$\left(\frac{dE}{dt}\right)_E = e\mu E^2 \qquad \text{.....4.45}$$

E = electric field (Vcm^{-2})
e = electron charge
μ = mobility ($cm^2V^{-1}s^{-1}$)

Now the mobility is determined by the electron temperature which is determined by the electric field so that it is awkward to determine the rate of energy gain for a particular electric field. For most situations the energy loss is due to electron scattering by acoustic and optical phonons, so that in a steady state situation the energy gained from the electric field equals the energy lost due to electron scattering by phonons.

So

$$\left(\frac{dE}{dt}\right)_E = e\mu E^2 = \left(\frac{dE}{dt}\right)_{ap} + \left(\frac{dE}{dt}\right)_{op}$$

Now, $\left(\frac{dE}{dt}\right)_{ap}$ and $\left(\frac{dE}{dt}\right)_{op}$ are functions of the average electron temperature so that if one writes

$$E^2 = \frac{1}{e\mu(T_{ea})}\left(\frac{dE}{dt}\right)_{ap}(T_{ea}) + \frac{1}{e\mu(T_{ea})}\left(\frac{dE}{dt}\right)_{op}(T_{ea}) \quad \text{.....4.46}$$

then, for the range of electron temperatures expected, the electric field required to obtain those temperatures can be obtained. To do this though, the rates of energy loss due to phonon scattering must be obtained. This is done in sections 4.9.2 & 4.9.3 and evaluation of equation 4.46 is shown in figure 4.17. Note that in the evaluation of 4.46 the electron temperature does not equal that used in sections 4.8.2 to 4.8.8, but equals the average electron energy of the electron energy distribution. This causes another complication, since the variations of mobility with temperature obtained so far (see figure 4.13) are with reference to the electron temperature (equivalent to energy) or the lattice temperature. To obtain the variation of the mobility with the average electron temperature one must combine the mobility equations as described in section 4.8.8 and then derive the mobility for the average electron energy of the distribution present by means of a weighted sum. This involves a knowledge of the energy distribution which is determined by the energy excitation and relaxation mechanisms, at which point the interdependency of the variables to be determined restrains the possibility of a direct solution. In general a trial electron distribution is used and the results obtained compared with those expected from practical results, whereupon the distribution is refined and more exact results obtained.

4.9.2 Rate of Energy Loss to Acoustic Phonons

For acoustic phonon interaction to be an energy loss mechanism the electron and phonon distributions must be of different average energies. When the electron and phonon distributions have no energy differential, the energy loss due to phonon emission is equal to the energy gain through phonon absorption. For low rates of energy loss, the excitation of the electron distribution from its equilibrium state will be small and the distribution can still be described by the Maxwell-Boltzmann distribution. The usual approach taken to this situation is to describe the excited distribution by the Maxwell-Boltzmann distribution for a higher average energy. This is equivalent to an equilibrium distribution at a higher lattice temperature. This temperature is defined as the electron's effective temperature and provides an indication of the 'heating' of the electron distribution relative to the phonon distribution.

Based on the assumption that the concept of an electron temperature will hold for the electron energies considered the following expression was derived by Conwell[56] for the rate of energy loss through acoustic phonon scattering,

$$\left(\frac{dE}{dt}\right)_{ap} = \frac{8(2)^{1/2}}{\pi^{3/2}} \cdot \frac{E_1^2 m^{3/2}}{\hbar^4 \rho} \left(k_B T_{ea}\right)^{3/2} \left(1 - \frac{T_L}{T_{ea}^{1/2}}\right)$$

and evaluating the constants gives,

$$= 2.03 \times 10^{-9}\, T_{ea}^{3/2} \left(1 - \frac{T_L}{T_{ea}}\right) \qquad \text{.....4.47.}$$

The variation in the rate of energy loss with effective electron temperature for various lattice temperatures was calculated. The results of that calculation are given in figure 4.14 with numerical values given in appendix 4.8.

---

[56]Conwell,Sol.Stat.Phys.,suppl.9 , Ch3. (1967)

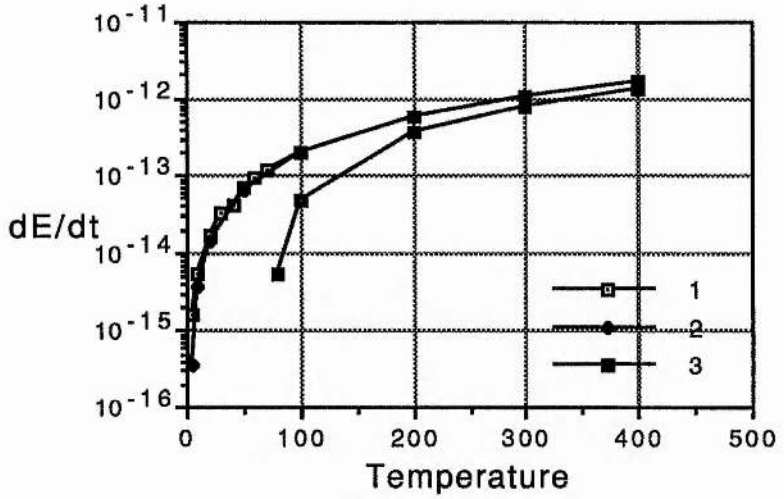

Figure 4.14 : Variation in rate of energy loss (W) by accoustic phonons with electron temperature (K) at various lattice temperatures (1 : T_L = 1.5K ; 2 : T_L = 4.2K ; 3 : T_L = 77K.)

4.9.3 Rate of Energy Loss to Optical Phonons

For energy loss due to optical phonon emission Conwell[57] derived the following equation

$$\left(\frac{dE}{dt}\right)_{op} = -\left(\frac{2k_B\Theta_D}{\pi m}\right)^{1/2} eE_o \left(\frac{e^{(x_o - x_e)} - 1}{e^{x_o} - 1}\right) x_e\, e^{x_e/2} K_o\left(\frac{x_e}{2}\right) \qquad \text{.....4.48}$$

where, $$eE_o = \frac{me^2\,\hbar\,\omega_l}{\hbar^2}\left(\frac{1}{\kappa_\infty} - \frac{1}{\kappa_o}\right)$$

$$x_o = \frac{\hbar\,\omega_l}{k_B T_L}$$

$$x_e = \frac{\hbar\,\omega_l}{k_B T_{ea}}$$

and $K_o(x)$ = Bessel function

[57]Conwell,Sol.Stat.Phys.,suppl.9 , Ch3. (1967)

Evaluating the constants one obtains

$$\left(\frac{dE}{dt}\right)_{op} = 0.02533\left(\frac{e^{(x_o - x_e)} - 1}{e^{x_o} - 1}\right) x_e\, e^{x_e/2} K_o\left(\frac{x_e}{2}\right) \quad \text{.....4.49}$$

from where the variation of the rate of energy loss with effective electron temperature at various lattice temperatures can be calculated. The results of this calculation are presented in figure 4.15. Numerical values are given in appendix 4.9.

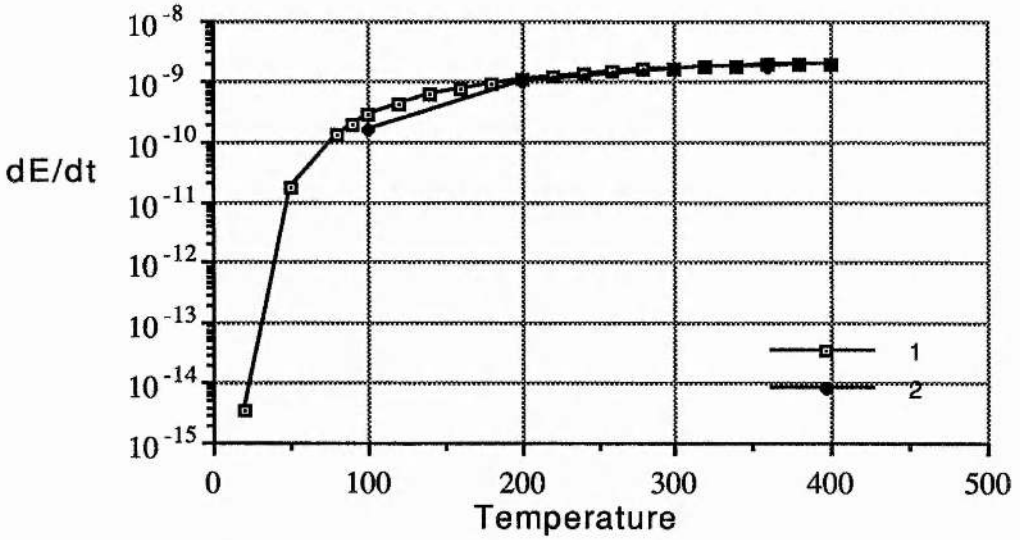

Figure 4.15 : Variation in energy loss (in Watts) by optical phonons with electron temperature (in Kelvin, equivalent to energy) at lattice temperatures of 4.2K (line 1) and 77K (line 2).

4.9.4 Balancing of Energy Excitation and Relaxation Rates

As mentioned in section 3.9, for a steady state to occur the energy excitation and relaxation rates must balance. As a steady state does occur one can write,

$$\left(\frac{dE}{dt}\right)_E = \left(\frac{dE}{dt}\right)_{ap} + \left(\frac{dE}{dt}\right)_{op} \quad \text{.....4.50}$$

in the region where energy loss is due to electron scattering by acoustic and optical phonons. This implies that the energy supplied by the electric field can be derived by adding the rates of energy

loss calculated in sections 4.9.2 and 4.9.3. The results of this summation are presented in figure 4.16.

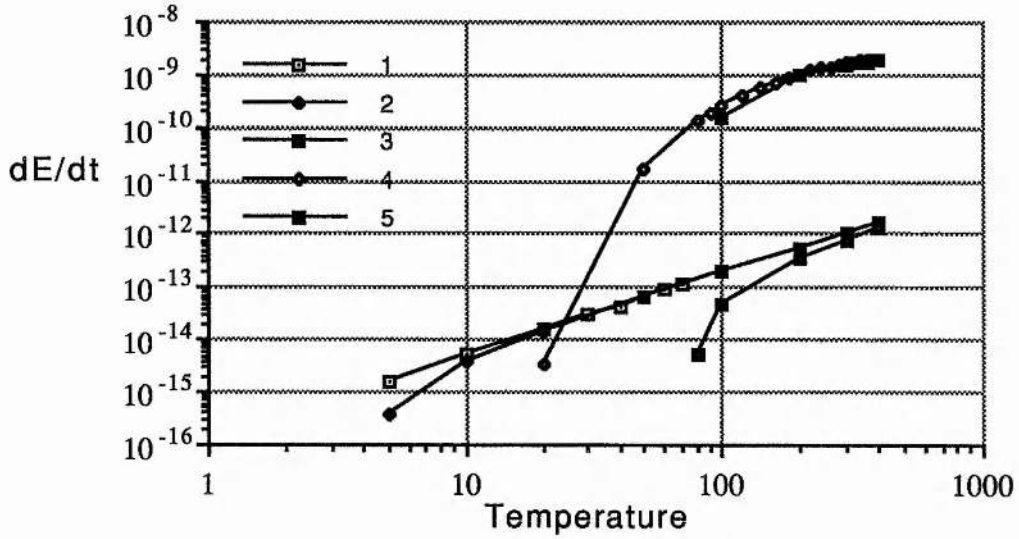

Figure 4.16 : Variation of energy loss (W), due to phonon scattering, with average electron temperature (K) for different lattice temperatures, showing the components due to acoustic (lines 1 (T_L = 1.5K), 2 (T_L = 4.2K) & 3 (T_L = 77K) and optical (lines 4 (T_L = 4.2K) & 5 (T_L = 77K) phonons.

The above agrees well with the result deduced by Sandercock[58] from a study of the current-density variation with electric field for high purity InSb, except that there is a slight variation at the transition where the energy loss due to the different phonons is approximately equal. The variation is explained by Stradling & Wood[59] as being due to a two-acoustic phonon scattering process. Sandercock also derived theoretical curves to fit his data. For optical phonons the theoretical curve obtained was given as

$$\left(\frac{dE}{dt}\right)_{op} \alpha\ e^{(-282/T)}$$

[58]Sandercock, PhD Thesis, Oxford Univ. (1968)
[59]Stradling & Wood, J.Phys.C 3 , 2425 (1970)

Now from equation 4.48 (from Conwell[60]) it can be seen that the only factor with a strong dependence on T is the factor enclosed in the brackets (see appendix 4.8), so one can write

$$\left(\frac{dE}{dt}\right)_{op} \alpha \left(\frac{e^{(x_o - x_e)} - 1}{e^{x_o} - 1}\right)$$

where, $x_o = \frac{\hbar \omega_l}{k_B T_L}$

and $x_e = \frac{\hbar \omega_l}{k_B T_{ea}}$

now $e^{(x_o - x_e)} >> 1$ and $e^{x_o} >> 1$ for $T_L = 4.2K$,

so $\left(\frac{dE}{dt}\right)_{op} \alpha \left(\frac{e^{(x_o - x_e)}}{e^{x_o}}\right) = e^{-x_e}$

and as $\hbar \omega_l = k_B \Theta$ one can write

$$\left(\frac{dE}{dt}\right)_{op} \alpha \ e^{-\Theta/T}$$

which is equivalent to that obtained by Sandercock as $\Theta \approx 283K$.

In an attempt to obtain a variation of mobility with average electron temperature the following calculation was done. Under the assumption that all energy loss is due to phonon emission the scattering lifetime can be obtained using,

$$\frac{1}{\tau_{po}} = \left(\frac{dE}{dt}\right)_{op} \times \frac{1}{\hbar \omega_l} \qquad \text{.....4.51}$$

which can be derived from Conwell's equations for optical phonon scattering. This provides the scattering lifetime for the electrons whose energies are greater than that of an optical phonon and are involved in phonon emission. This concept is valid because electrons which attain an energy greater than that for an optical phonon are rapidly scattered emitting an optical phonon whose energy is

---

[60]Conwell,Sol.Stat.Phys.,suppl.9 , Ch3. (1967)

accurately known. Due to the high efficiency of energy relaxation it is also the main momentum relaxation process, so the lifetime is also the momentum scattering lifetime. For a lattice temperature of 4.2K, the lifetime and corresponding mobility, for electrons whose energy is greater than the phonon energy, obtained using equation 4.51 is less than the mobility as calculated using equation 4.44 for the total mobility. This implies that the lattice temperature has been heated and is no longer at 4.2K, which implies that the rate of energy loss calculated for a lattice temperature of 4.2K is inaccurate as a constant lattice temperature was assumed. This leads to another cyclic method for approximating the correct values.

A lattice temperature is assumed and the energy loss calculated; the mobility of the high energy electrons is calculated and compared to the expected mobility for electrons of that energy at that lattice temperature. A new and more accurate lattice temperature is obtained and the cycle is repeated. This has provided a method for calculating the heating of the lattice by the electric field, but does not, as hoped for, provide a method for calculating the variation of the electron mobility with average electron energy.

However, if the lattice temperature can be calculated accurately for all average electron energy values then the energy loss due to phonon emission can be calculated accurately for all values of average electron energy. This is then equal to the rate of energy obtained from the electric field which is what was required from the balancing of the energy excitation and relaxation rates.

4.10 **Electron - Electron Scattering**

Interelectron scattering, as mentioned in section 3.9.4, is neither a direct momentum or energy scattering process. It acts, rather, as a redistribution process reducing the probability of electrons existing with energy or momentum greatly different from the average electron energy and momentum. In this fashion it plays an important role in determination of the energy distribution.

If the rate of energy distribution is far greater than the rate of energy loss, then the energy distribution is found to be as a Maxwell-Boltzmann distribution. If the rates of energy gain and loss are such as to require the energy of the average electron to be

noticeably larger than the lattice temperature then the distribution will appear as the Maxwell-Boltzmann distribution for a higher lattice temperature. This is the principal behind the effective electron temperature and shows why the effective electron temperature is only valid when the inter-electron redistribution is more effective than the energy loss scattering process. In this situation the interelectron scattering also has a great influence on the electron mobility and rate of energy loss. This is due to the efficiency of the scattering processes in this region (acoustic phonon scattering is the energy scattering mechanism and ionised impurity scattering is the momentum scattering mechanism) having a large electron energy dependence.

If the rate of energy redistribution is less than or approximately equal to the rate of energy loss then the electron energy distribution will be distorted away from the Maxwell-Boltzmann distribution and becomes more difficult to approximate.

The rate of energy redistribution by interelectron interaction is given (in c.g.s. units) by,

$$\left(\frac{dE}{dt}\right)_{ee} = \frac{4\pi n (e^*)^4}{p} \log \nu \qquad \text{.....4.52}$$

as presented by Frölich & Paranjape[61] and Stratton[62] and credited to Pines[63]. The variables and constants in equation 4.52 are defined as,

e^* = the effective ionic charge as defined in section 4.8.6.

= 0.146e where e = the electron charge = 4.8×10^{-10}e.s.u.

p = electron momentum = $\hbar k = \sqrt{2 m_o^* k_B T_e}$

log ν = a slowly varying term ≈ 1

n = electron concentration (cm^{-3})

now using the above definitions one can write,

---

[61] Frölich & Paranjape, Proc.Phys.Soc.B 69 , 21 (1956)

[62] Stratton, Proc.Roy.Soc (London) A246 , 406 (1958)

[63] Pines, Phys.Rev(1953) - this is the reference quoted by Frölich & Paranjape for equation 4.52, but the paper has no equation of the form presented. Stratton implies that the equation was in a paper published in 1955, but omits to give the full details.

$$\left(\frac{dE}{dt}\right)_{ee} = \frac{4\pi n (e^*)^4}{(2 m_o^* k_B T_e)^{1/2}} = 5.26 \times 10^{-18} n T_e^{-1/2}$$

which by evaluating the constants gives

$$\left(\frac{dE}{dt}\right)_{ee} = 2.63 \times 10^{-11} T_e^{-1/2} \text{ Joules per second} \quad \text{.....4.53a}$$

for $n = 5 \times 10^{13}$ cm^{-3}

and $$\left(\frac{dE}{dt}\right)_{ee} = 5.26 \times 10^{-11} T_e^{-1/2} \text{ Js}^{-1} \quad \text{.....4.53b}$$

for $n = 1 \times 10^{14}$ cm^{-3}.

Equations 4.53a & 4.53b have been evaluated to obtain the variation of the rate of energy redistribution with electron temperature. The result is depicted in figure 4.17 alongside the variations in rate of energy loss due to phonon scattering.

The effect of interelectron scattering on the mobility of the electrons has been calculated for several different regions. Appel[64], using the variational procedure and describing the interaction by means of a Coulomb potential, calculated that when ionised impurity scattering is the main momentum scattering process the mobility is reduced by a factor of 0.57 due to interelectron interaction. When acoustic phonon scattering is the main momentum scattering process then the mobility was found to be almost unaffected. Stratton[65] calculated the effect on the mobility when optical phonon scattering is the main scattering process and found the mobility to be decreased, though only by a small amount. All the above effects are dependent on the electron concentration and for high-purity and highly compensated crystals the effect is decreased.

---

[64]Appel, Phys.Rev. 122 , 1760 (1961)

[65]Stratton, Proc.Roy.Soc (London) A246 , 406 (1958)

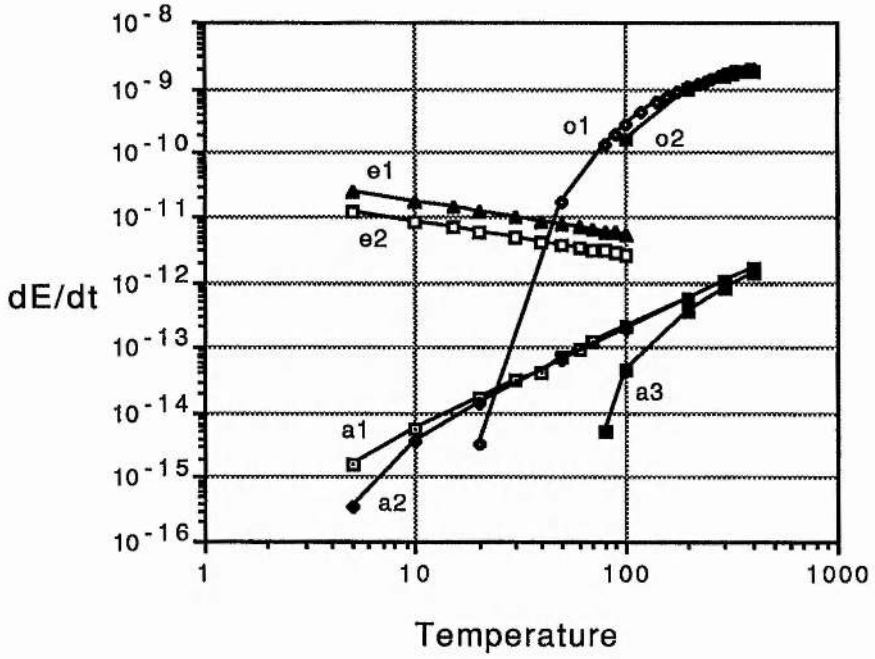

Figure 4.17 : Variation of rate of energy redistribution (Js^{-1}) by interelectron scattering with electron temperature (K)(equivalent to energy) for a carrier concentrations of 5 x 10^{13} cm^{-3} (line e2) and 10^{14} cm^{-3} (line e1). Also shown are the variations with average electron temperature of the rates of energy loss due to phonon emission at various lattice temperatures (acoustic phonons : a1 - T_L = 1.5K, a2 - T_L = 4.2K, a3 - T_L = 77K; optical phonons : o1 - T_L = 4.2K, o2 - T_L = 77K)

4.11 **Conclusion**

This chapter has brought together all the major theoretical work dealing with the basic electrical characteristics of InSb. It has shown both the potential and success of this work as well as its limitations.

The expressions obtained under the relaxation time approximation for the scattering processes, are seen to be in good agreement with practical results. The proviso to this statement being, that, for optical phonon scattering at an average electron energy below the energy of the optical phonon, the relaxation time approximation does not hold. Results obtained using the variational procedure are more accurate, but the most insightful results are

obtained using the method employed by Fletcher & Butcher[66] where they calculated a quasi relaxation time. The energy loss equations presented by Conwell[67] also agree well with practical results.

The major weakness of the theory presented is the inability to obtain the variation of electron mobility with average electron temperature and hence the variation of effective electron temperature with applied electric field. This problem is due to the uncertainty relating to the electron energy distribution. As can be seen from figure 4.17, for temperatures where acoustic phonon scattering is the main energy scattering process, the interelectron scattering will determine the energy distribution and a Maxwell-Boltzmann distribution can be taken. When optical phonon emission becomes the main energy scattering process then the energy distribution becomes far more difficult to determine. When the average electron energy is close to that of the phonon energy, the electron distribution will become degenerate, with a degeneracy temperature proportional to the phonon energy. This occurs because electrons with greater energy are rapidly scattered and electrons with less energy are rapidly accelerated by the field to the phonon energy. When the average electron energy is less than the optical phonon energy then the distribution becomes like a truncated Maxwell-Boltzmann. This occurs as electrons which attain energies greater than the optical phonon energy are rapidly scattered creating in effect an energy maximum for the distribution.

The conclusions in terms of electrical characteristics for high-purity InSb at low lattice temperatures are as follows :

1/ At very low lattice temperatures ($T < 5K$) and low electric fields ($E < 0.5\ Vcm^{-1}$), ionised impurity scattering is the main momentum scattering process and piezo-electric scattering is the main energy scattering process. Piezo-electric scattering is very similar to polar optical phonon scattering in that at high electron energies (relative to the low lattice energy) the rate of energy loss due to piezo-electric scattering decreases with increasing electron energy. This causes a breakdown in stability until the energy gained by the

---

[66]Fletcher & Butcher, J.Phys.C. 5 , 212 (1972)
[67]Conwell,Sol.Stat.Phys.,suppl.9 , Ch3. (1967)

electric field is balanced by the energy lost through potential deformation acoustic phonon scattering. The above creates a non-linear electrical characteristic under constant voltage conditions and negative differential resistivity under constant current conditions.

2/ On increasing the electric field till the potential deformation acoustic phonon scattering is the main energy scattering process and the ionised impurity scattering is the main momentum scattering process, the main effect on the electrical characteristics is that caused due to the heating of the electron distribution. The increase in the average energy of the electrons induces greater energy loss and momentum scattering and so decreases the conductivity of the crystal. This effect is known as the hot-electron effect.

3/ On further increasing the electric field, the polar optical phonon scattering process becomes the main momentum and energy scattering process. This decreases the conductivity very markedly, since the efficiency of the scattering is high. Also contributing to the decrease in conductivity is the distortion and compression of the electron energy distribution into a smaller energy interval.

4/ Eventually, the optical phonon scattering process will saturate as, for electrons with energies several times that of the optical phonon, the rate of energy loss is decreasing with increasing electron energy. A current instability similar to that obtained for piezo-electric acoustic phonon scattering occurs. This is exacerbated by the increase in electron concentration due to the intrinsic concentration now becoming substantial. The energy balance is only restored when another scattering process becomes sufficiently effective. Possible scattering processes include potential deformation acoustic phonon scattering and electron-hole scattering. The latter has been considered by Ehrenreich[68]. Conwell[69] suggests that impact ionisation of lattice atoms occurs before the

---

[68]Ehrenreich, J.Phys.Chem.Sol. 2 , 131 (1957)
[69]Conwell,Sol.Stat.Phys.,suppl.9 , Ch4. (1967)

optical phonon scattering saturates thus preventing the current instability from occuring. This is the interpretation on the findings of Glicksmann & Steele[70] which show a large increase in carrier concentration just before a large increase in current.

[70]Glicksmann & Steele, Phys.Rev.Letts. 2 , 461 (1959)

5 EQUIPMENT AND EXPERIMENTAL DETAILS

5.1 Introduction

In order to observe the effects predicted by the solid state theory of chapters 3 & 4, various physical conditions must be met. As stated in chapter 3 sections 2, 3 & 7, low temperatures of less than one Kelvin are required to observe some of the effects. With the application of a magnetic field the lowest temperature deemed necessary is raised to the order of several Kelvin (dependent on the field strengths).

Temperatures down to one and a half Kelvin are readily achievable with most Helium cryostats. Temperatures much below this are more difficult to achieve requiring more specialised cryostats and reducing the flexibility in approach (changing samples and other experimental parameters take four times as long). For the study reported here 1.5 Kelvin was taken to be the lower temperature limit. A detailed description and appraisal of the cryostats used is given in section 5.2.

The magnetic field required in order to achieve quantum behaviour in the conduction band electron transitions ($\hbar\omega_c >> kT$) is of the order of 0.5 Tesla at 1.5 Kelvin[1]. A Bitter magnet, with a range of 0-1 Tesla, was made available for this study. An iron core magnet, with a range of 0-0.7 Tesla, was also used. These are described in section 5.3.

To obtain the electrical properties of the crystal it was necessary to apply electrical potentials across the crystal. This required electrical contacts to be made. The process for creating electrical contacts is recorded in section 5.5

The electric field requirements were uncertain as the electrical properties were the subject of this study. Thus the crystal bias circuits were modified as more became known of the characteristics. The evolution and details of the bias circuits are described in section 5.4.

---

[1]Gornik, Optics & Laser Tech. 7 , 121 (1975)

Bias circuitry and amplification and evaluation electronics were also developed for a crystal which was used as a detector at liquid helium temperatures. These are also dealt with in section 5.4.

5.2 **The Cryostats Used**

5.2.1 Introduction and General Operating Procedure

Due to the uncertainty of approach inherent to this study (until a rough picture of the electrical characteristics is known*), a purpose built cryostat would have been of limited value. The result was that several different cryostats were employed for different measurements.

The basic principles behind the operation of the cryostats used is the same: They have a radiation shield which is cooled by a liquid nitrogen reservoir within which there is (liquid)helium can. The different sections of the cryostat are separated by a vacuum as is the radiation shield from the exterior of the cryostat (see figure 5.1).

The procedure for cooling the cryostat begins with checking that the vacuum in the evacuated sections is good and that leaks into these sections are acceptably low. Then the helium can is evacuated and filled with helium gas. This can be done at St.Andrews University by connecting the helium section to the helium return line in the department (this is possible because the department has its own liquid helium manufacturing and recycling facility). The nitrogen reservoir can now be filled with liquid nitrogen. (If the vacuum is good the external surface of the cryostat will cool only slightly.) After allowing time for the radiation shield to cool fully (the time required is dependent on the design and size of the cryostat), liquid helium can be transferred into the helium can. Liquid helium is never exposed to room temperature. In order to achieve this a vacuum insulated transfer tube is employed which is pre-cooled with cold helium gas. The vacuum insulated dewar in

---

* The theory & practical were done simultaneously. The full results of the work done in chapter 4 were only known after the cryostats had been implemented.

which the helium is stored is normally attached to the helium return line. On transfer the return line is shut and pressure is applied to the liquid helium in order to force it through the transfer tube and into the cryostat. Once the transfer is complete the pressure is removed by reopening the return line. This provides cooling to about four Kelvin.

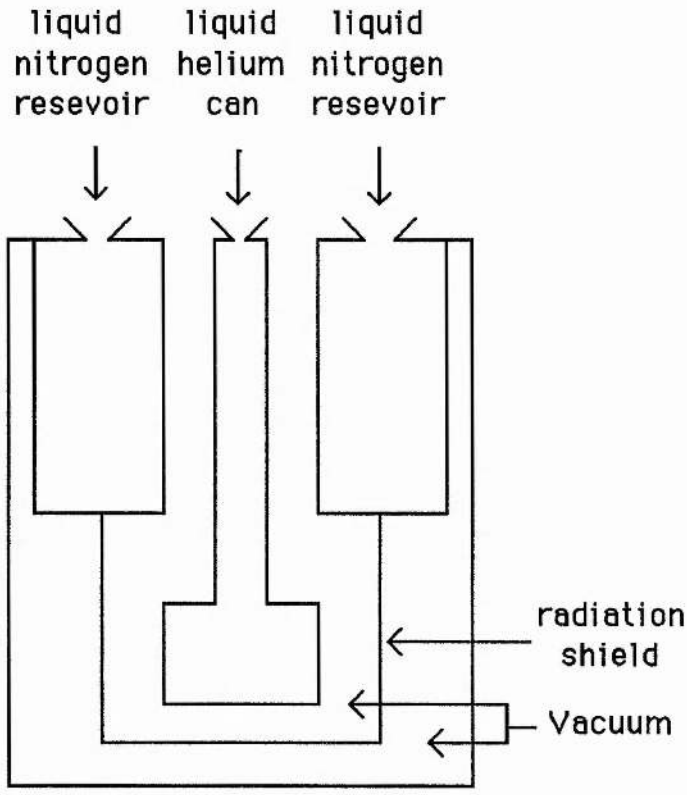

Figure 5.1 : Basic cryostat design

In order to reduce the temperature further the helium can may be connected to a pump line which will reduce the pressure above the liquid helium and so lower the boiling point. This can reduce the temperature to below 1.5 Kelvin.

The differences between the cryostats used were due to the different purposes and requirements of the experiments carried out.

5.2.3 Cyclotron Emission Cryostat

The first experiment was ambitious. It was designed to imitate the conditions involved with the cyclotron resonance emission experiments of Gornik[2] and Kobayashi et.al.[3], but with the crystal exterior to the helium can. This was so that a helium window would not be required. An external magnet was employed as this was available.

A cryostat (courtesy of Prof. J.W.Allen) that had been used for similar purposes was modified for use in the experimentation.

The desired requirements and constraints on the cryostat were as follows :-

1/ The magnet used, a 1Tesla Iron-core Bitter magnet (courtesy of Dr.P.Riedi) with a pole separation of 5cm, restricts the diameter of the tail of the cryostat. The size of the pole plates and their surrounds determined the overall design of the tail in order that the crystal be within a uniform magnetic field.

2/ Due to the helium can not penetrating the uniform magnetic field and a new helium can not being available, a post of high conductivity copper was attached to the end of the helium can. The crystal was then positioned at the end of the post in a Quasi-resonant cavity (see figure 5.2).

3/ As one of the aims of the experiment was to obtain emission and preferably into free space, the system was designed with a window at the end of the tail of the cryostat. Also a feedhorn for guiding the radiation out was included.

---

[2]Gornik, Phys.Rev.Letts. 29 , 595 (1972)

[3]Kobayashi et.al., Phys.Rev.Letts 30 , 702 (1973)

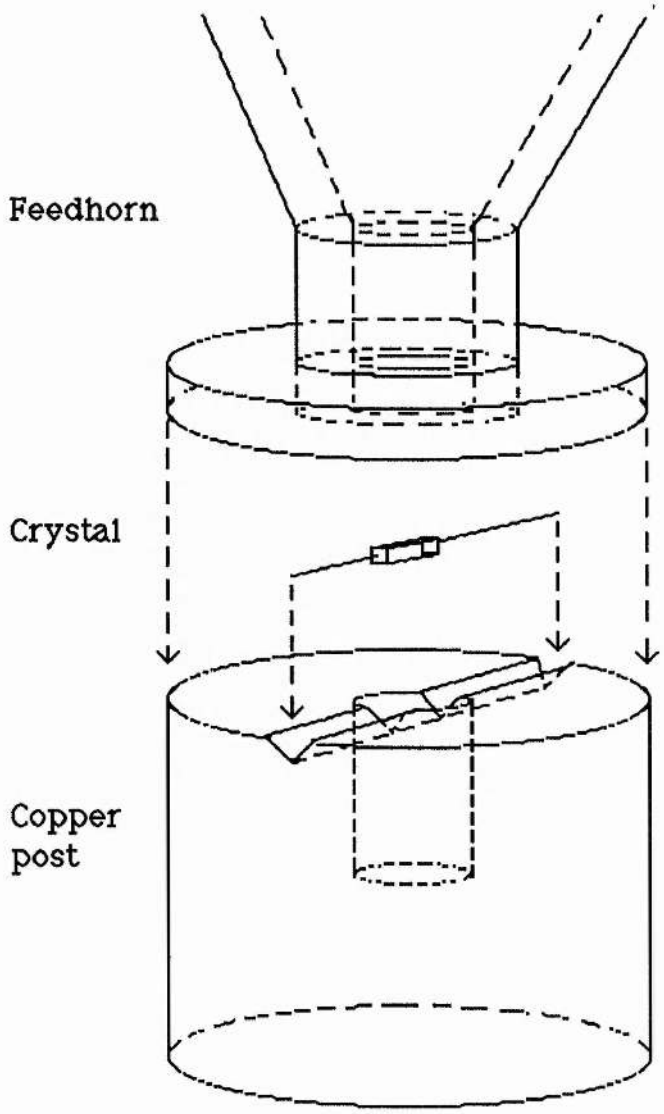

Figure 5.2 : Positioning of the crystal to the post (The post is attached to the bottom of the helium can so that the above situation is inverted)

4/ The wires attached to the crystal were heat-sinked to the copper post, the helium can and the radiation shield (attached to the nitrogen jacket) before passing out of the vacuum by means of a 10 pin connector.

For a diagrammatic representation of the design of the cryostat used in the experiments, see figure 5.3.

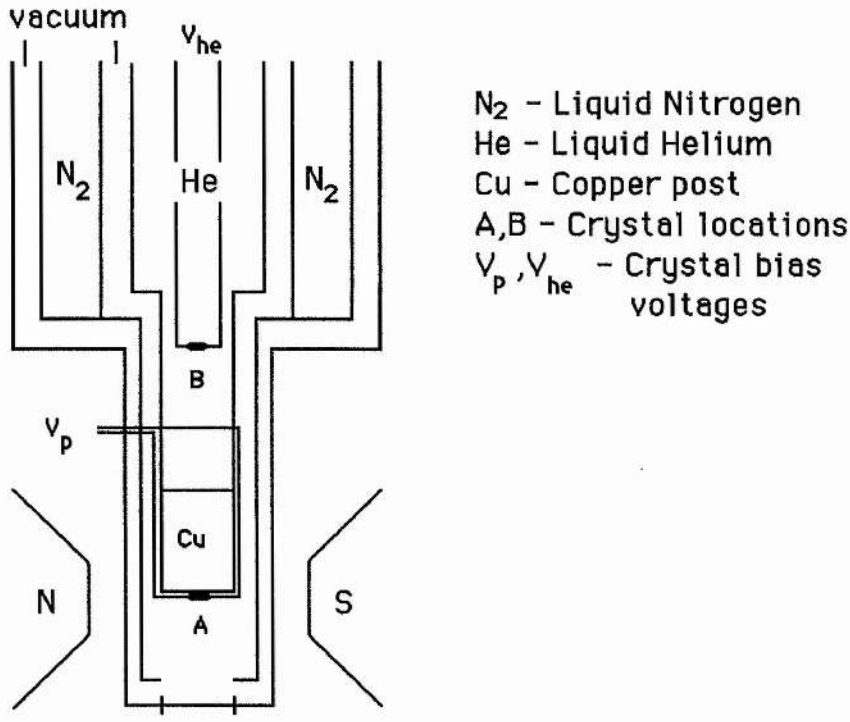

Figure 5.3 : Diagrammatic representation of the cyclotron-resonance cryostat

A new top plate for the cryostat was built with a 10 pin electrical connection so that crystals could be mounted within the helium can for study and comparison purposes.

On obtaining initial results there was some evidence for the belief that the heat transfer from the crystal was not efficient enough to maintain the crystal at a steady temperature. To check this a crystal was mounted inside the helium can so that it would be immersed in liquid helium and similar fields were applied to it.Though as this crystal could not lie within the uniform magnetic field, no magnetic field was applied during the comparison measurements.

The results of this comparison indicated that heating was a problem and so the following experiments were set up with the crystal immersed in liquid helium. The problem of coupling radiation from the crystal out of the cryostat was temporarily neglected.

5.2.4 Cryostat For Electrical Characteristics Comparison

Due to some non-linear and chaotic behaviour obtained, a similar experiment was set up in QM & WC in London. On those experiments yielding interesting non-linear behaviour and hysterisis, it was decided that some experiments should be set up to compare the two different crystals in order to identify the effects that were unique to each crystal and preparation technique.

The crystals from QMWC were mounted on a rod in such a way that it was more convenient to place the rod into a cryostat than remove and remount the crystals. This necessitated the use of another cryostat. A glass cryostat, courtesy of Mr. J.G.M.Armitage, was found to satisfy all requirements, except that it would not be possible to apply a magnetic field. This was not necessary for observing the electrical characteristics of interest.

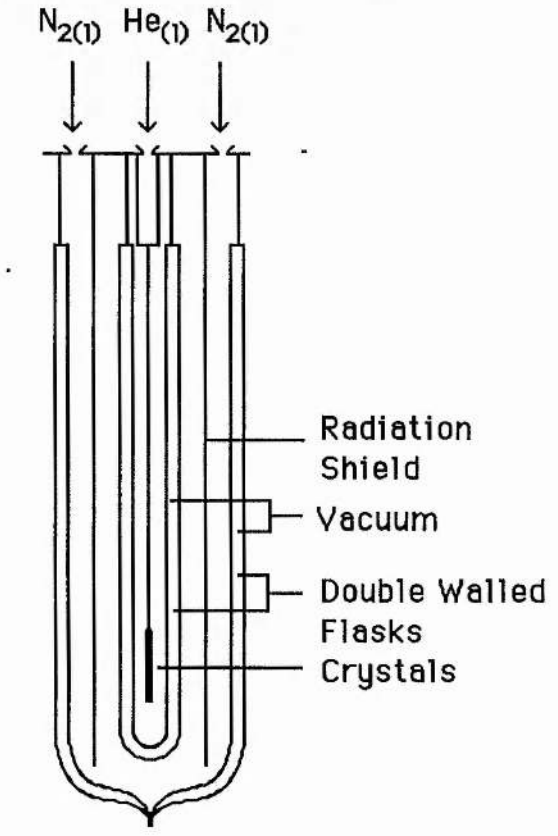

Figure 5.4 : Diagrammatic representation of the glass cryostat used in the comparison and resistance with temperature experiments.

5.2.5 The Hall Effect Cryostat

To confirm the properties of the crystal as quoted by the manufacturer, Hall effect measurements were carried out. A cryostat built for Hall measurements was kindly made available by Dr.D.M.Finlayson. This cryostat was similar to the glass cryostat described above. It differed in that the tail of the cryostat was reduced in diameter so that it could fit between the poles of an iron core magnet.

5.2.6 The Detector Cryostat

In order that an InSb detector might be used (so that the emission and detection might take place within a liquid helium bath), it was necessary to set up an experiment to test the crystal as a detector. As the only sources available (at frequencies close to

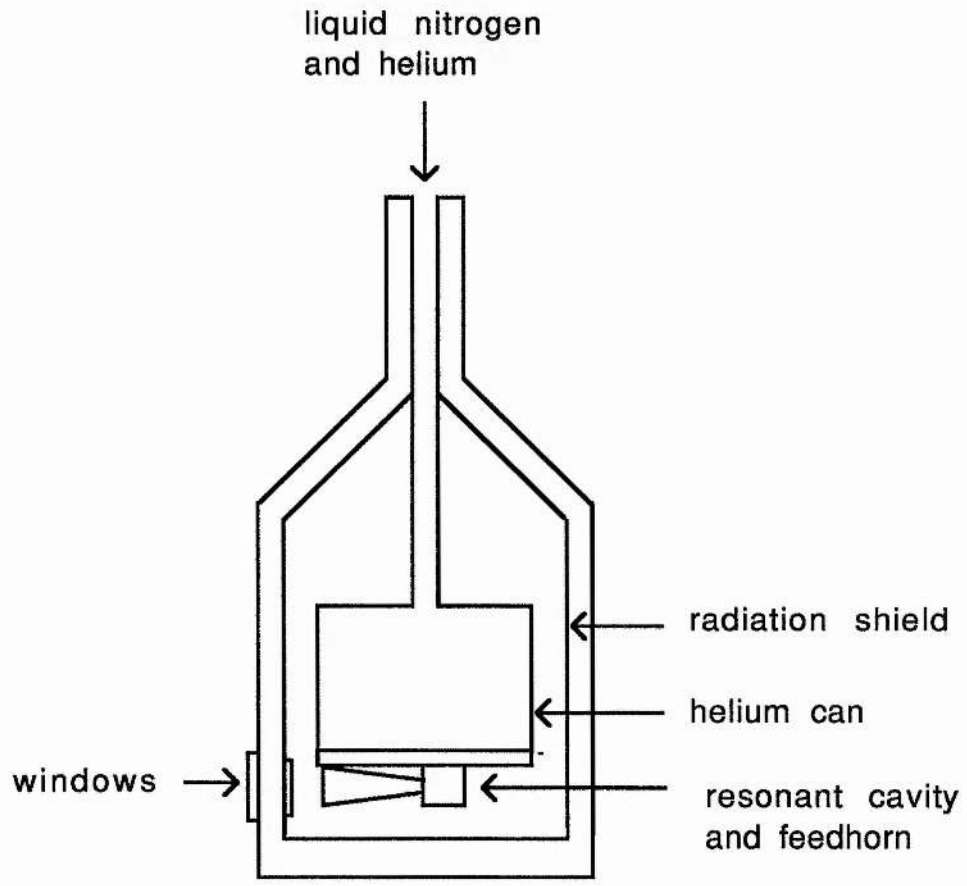

Figure 5.5 : The Detector Cryostat

those required) were GaAs Gunn diodes which operate at room temperature, the problem of coupling radiation between room and helium temperatures was encountered once more. Again the crystal is attached to the external surface of the helium can in a resonant cavity with a feedhorn attached (see figure 5.5). The cryostat used was designed as a detector cryostat. It differs from the other cryostats used in that it has no liquid nitrogen reservoir. The radiation shield is attached at the top of the cryostat to the helium can and is cooled by placing liquid nitrogen into the helium can. Once the radiation shield is cold the liquid nitrogen is removed and liquid helium is transferred into the cryostat.

5.3 **The Magnets Used**

Two Magnets were used. The first (courtesy of Dr.P.C.Riedi) with the CR emission cryostat. This was a 0 to 1.0 Tesla Bitter magnet, with pole faces of 100 mm diameter and 50 mm separation. This magnet was calibrated to at least ten Gauss (10^{-3} T) allowing a variety of fields to be used. The second (courtesy of Dr.D.M.Finlayson) was dedicated for use with the Hall effect cryostat. This was a 0 to 0.7 Tesla iron core magnet, with pole faces of 57mm diameter and 50mm separation. This magnet was not calibrated for any value other than 0.7 T and was therefore only used to obtain that field.

5.4 **Development of Bias Circuitry**

5.4.1 Curve Tracer Circuit

In order to obtain the most accurate data over the largest range possible, two different methods were used in obtaining the E-J (electric field versus current density) characteristics of the crystals. At low field an I-V (current-voltage) curve tracer, courtesy of Mr.M.R.Robertson, was employed (see figure 5.6 for the circuit diagram of the curve tracer). This was to obtain the greatest sensitivity at low fields.

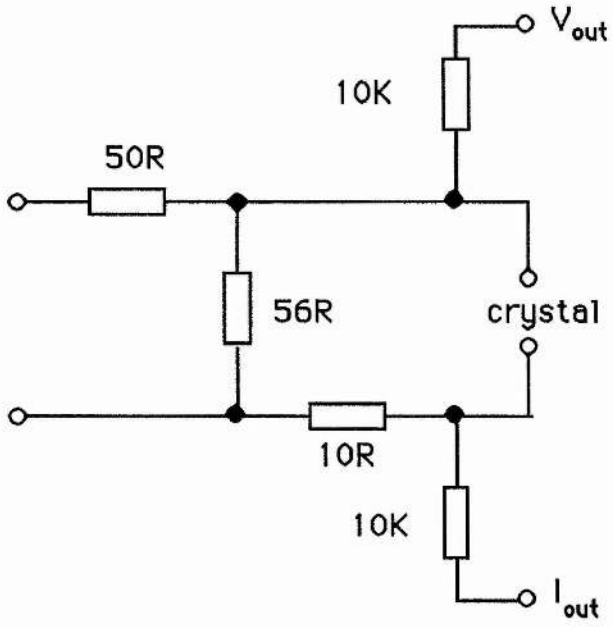

figure 5.6 : Circuit diagram for the curve tracer used to obtain I-V characteristics

5.4.2 High Field Pulsed Bias Circuit

At medium and high fields the curve tracer was used, but due to data handling and heating problems a pulse generator was also used. An operational amplifier (μA759) was used in the voltage follower configuration to boost the current output of the pulse generator to a maximum of 325mA (see figure 5.7). The pulse duration was varied to examine possible heating effects.

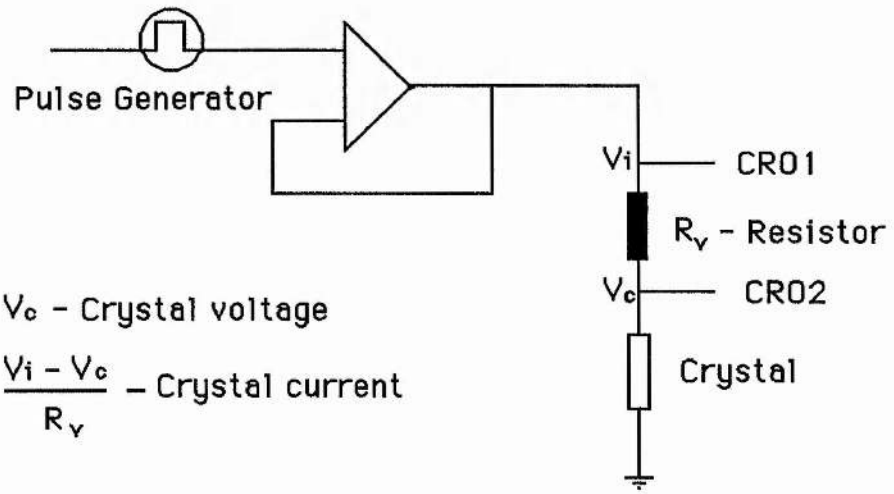

Figure 5.7 : Diagrammatic representation of basic pulsed bias circuit

For the pulsed bias voltage the current was calculated by obtaining the voltage across the crystal and a series resistor and the voltage across the crystal, taking the difference between these and dividing by the resistance of the series resistor.

5.4.3 Complex-Pulse High-Field Bias Circuit

The next development was to produce a bias circuit able to provide high fields in short pulses. This served a dual process : The first to enable I-V characteristics to be determined with a greatly reduced heating effect and the second to provide the facility with which to probe hysteresis loops. The specifications decided upon included the ability to provide pulses of between 0.2 & 2μs at a rate of 100KHz (see figure 5.8). These pulses are to be produced in bursts of 100 every 10ms. A secondary pulse, of width between 0.6 & 6ms, is to be available at a rate of 100Hz (see figure 5.9). The above two pulses could be varied, in amplitude, between 0 & 14 V. They could also be combined to provide a 'porcupine pulse' (see figure 5.10). A block diagram of the circuit constructed is shown in figure 5.11.

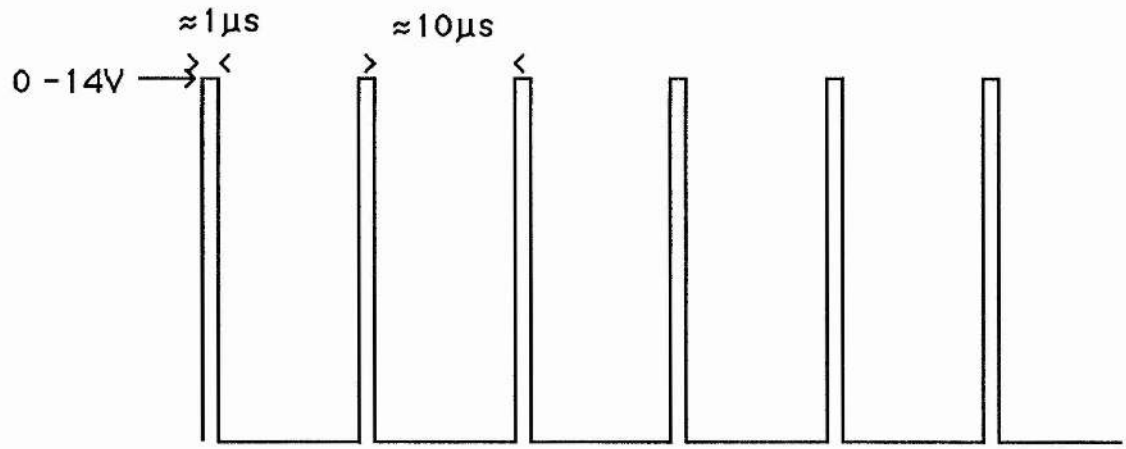

Figure 5.8 : Microsecond Pulse Generator Output

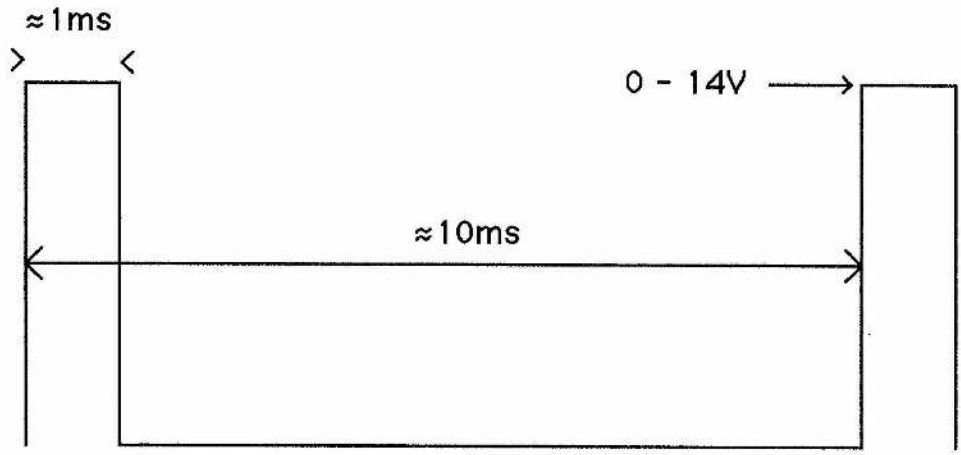

Figure 5.9 : Millisecond Pulse Generator Output

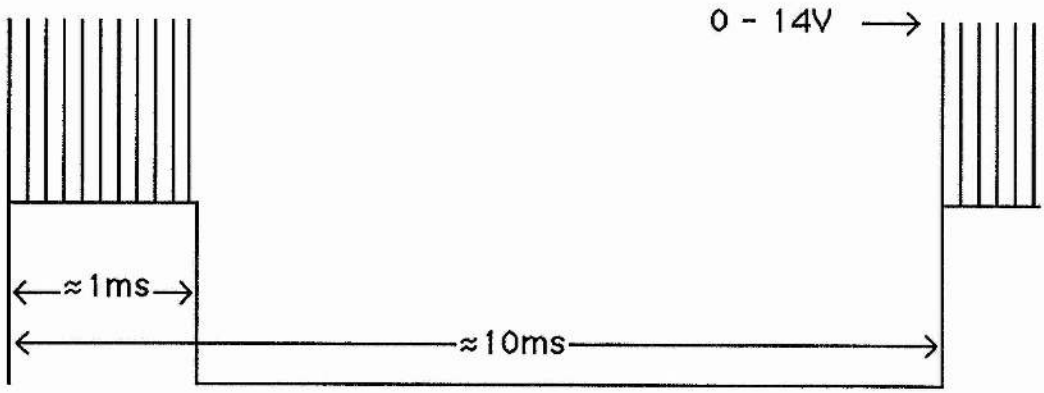

Figure 5.10 : Output When Pulses Are Combined

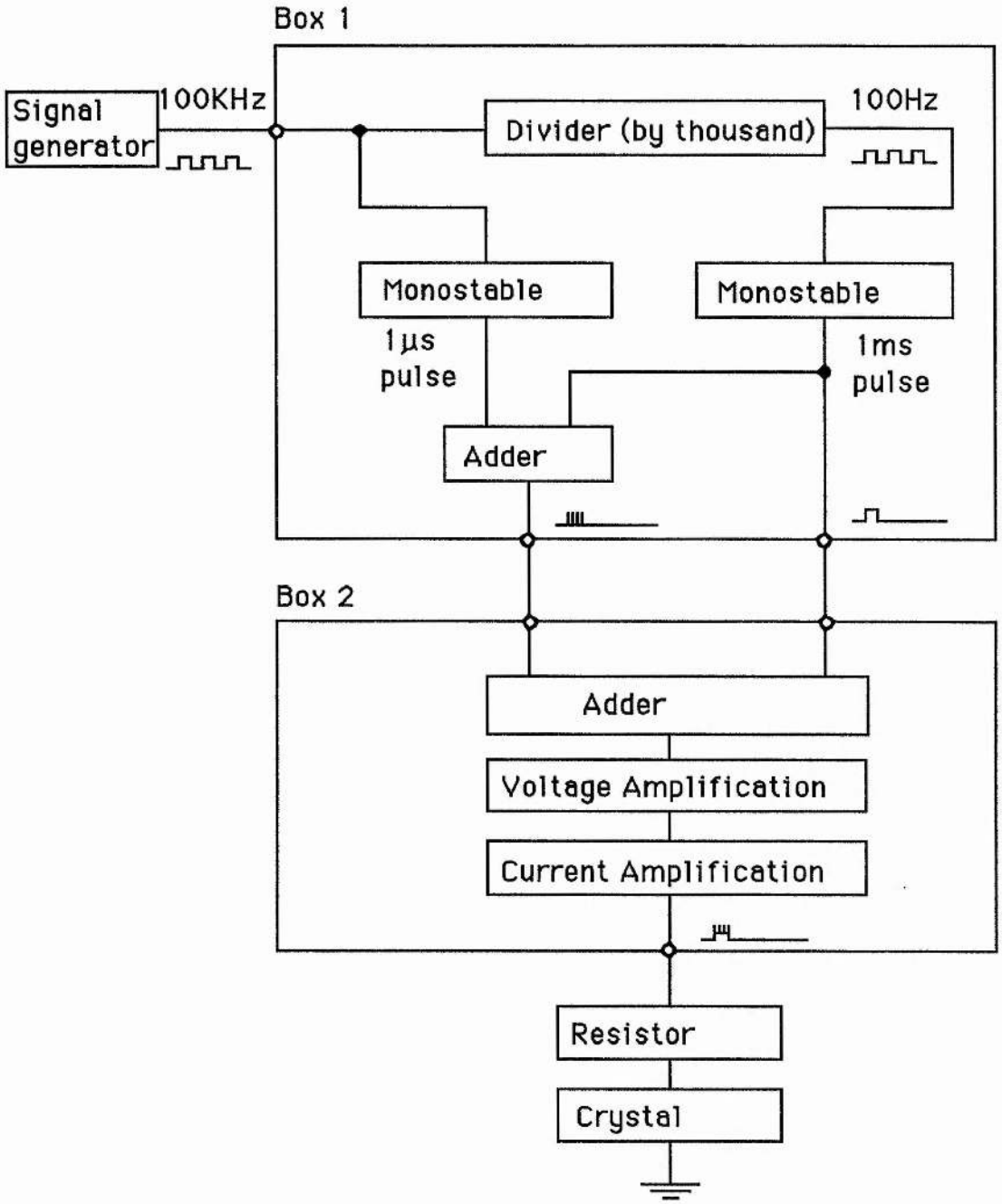

Figure 5.11 : Diagrammatic Representation of the Pulsed Bias Circuit

5.5 Details of the Crystals Used

High purity crystals from three different samples were used. Two crystals one from sample 1 and one from sample 2 were kindly lent by Dr.G.White of Queen Mary & Westfield College. The third sample was acquired from Cominco inc.. More than one crystal was taken from the sample supplied by Cominco inc.. Hall effect measurements, described in section 6.4, confirmed the data quoted for sample three and provided evidence for the assumption that the crystal was evenly doped, as there was little variance in carrier concentration values. The presence of deep donors is discussed in section 6.4.5. The basic properties, as quoted by the manufacturers, for the samples used are given in fig. 5.12.

Characteristics	Size (vol) (mm^3)	carrier conc. $n_e(10^{13} cm^{-3})$	mobility $(10^5 cm^2 V^{-1} s^{-1})$	impurity conc. $n_i(10^{15} cm^{-3}$
sample 1	$1x(0.5)^2\pi$	1.7-3.25	4.25-4.45	1.5
sample 2	7x2.5x0.3	2.4-4.2	2-5.6	1
sample 3	1.5x0.8x0.4	8.5-11	>6	0.8

Figure 5.12 : Table of crystal characteristics.(The sizes given are the crystal sizes. The crystal size for crystals from sample 3 is a typical size. The sizes varied however. The impurity concentrations were estimated from the mobility values.)

5.5.1 The Electrical Contacts for the Crystals

Several different contacting procedures were used. These involved : Alloying indium dots onto the surface of the crystal; Alloying indium onto the ends of the crystal ; A combination of the above two and by placing metal point contacts against the surface. Due to the small crystal sizes, it was not possible to prepare a four wire system and a two wire system was adopted. This made it

impossible to check on the resistance of the contacts and their possible effect on the electrical characteristics. Initial results showed the characteristics to be independent of the contacting method used. So the effect of the contacts is not thought to be large or relevant. Further comment on this problem is given section 7.

6 RESULTS OF PRACTICAL APPROACH

6.1 The Initial Practical Approach Using The Cyclotron-Resonance Emission Cryostat.

6.1.1 Introduction & Experimental Method

The first aim of the practical approach was to duplicate some of the cylotron-resonance (CR) emission results obtained by Gornik[1,2,3]. One modification on Gornik's approach was neccessitated by the equipment available: In order to place the crystal within the magnetic field the crystal was mounted on a copper post attached to the helium can (see figure 5.3), as opposed to being within the helium. To assist the transport of emission from the crystal to outside the cryostat the crystal was placed in a resonant cavity with a feedhorn attached in the direction of the cryostat's window (see figure 5.2 & 5.3).

The initial bias circuit involved merely a battery and a potential divider. Results were to show that this was inadequate and the use of a pulse generator was introduced. This was unable to provide enough current so a buffer op amp was employed on the pulse generators output (see figure 5.7).

The current - voltage characteristics of a high purity (uncompensated donor concentration = $10^{14}cm^{-3}$) n-InSb crystal (from sample 3), of dimensions 2.5 x 1 x 0.45mm^3, were measured at lattice temperatures equal to liquid nitrogen (77K), liquid helium (4.2K) and pumped liquid helium (1.5K) temperatures. That is, the cryostat was filled with these liquids and the crystal temperature was perceived not to deviate greatly from these values. It was impossible to place a thermometer next to the crystal and so determine the exact lattice temperature. The measurements were carried out under constant voltage conditions.

---

[1]Gornik, Phys.Rev.Letts. 29 , 595 (1972)
[2]Gornik, Optics & Laser Tech. 7 , 121 (1975)
[3]Gornik, Conf.,ed.-Ryan, 329 (1978)

6.1.2 Experimental Results

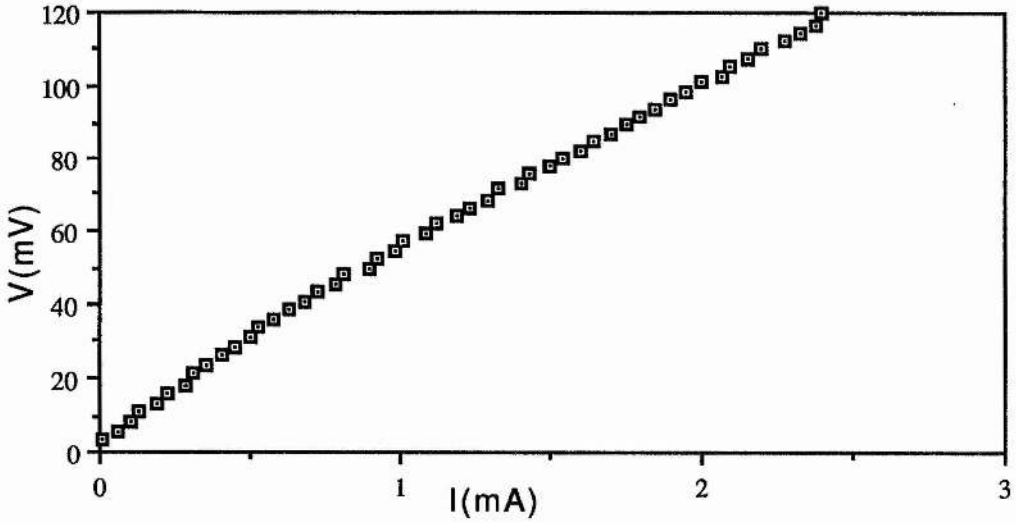

Figure 6.1 : Plot of the electrical characteristics of an n-InSb crystal at nominally 77K.

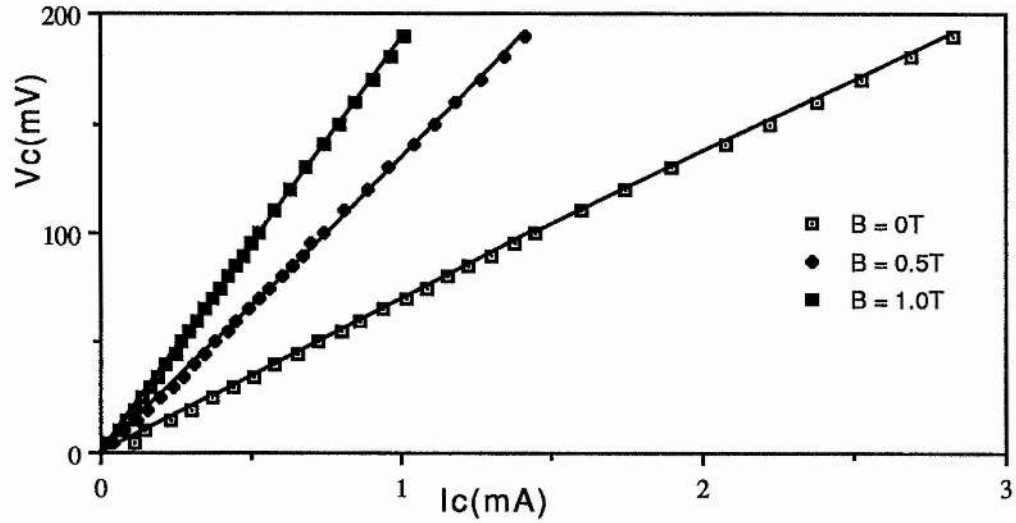

Figure 6.2 : Electrical characteristics of n-InSb at nominally 4.2K with applied magnetic fields of zero to one Tesla.

6.1.3 Conclusions From The Initial Results

The results presented in figures 6.1 and 6.2 led to two simple conclusions. The first is that the electric field applied to the crystal is insufficient for inducing distinct non-linearities in the characteristics. An attempt to rectify this inadequacy led to the results at greater electric fields depicted in figure 6.3. This just further proved the inadequacy of the original bias circuit, as this circuit could also not provide enough power.

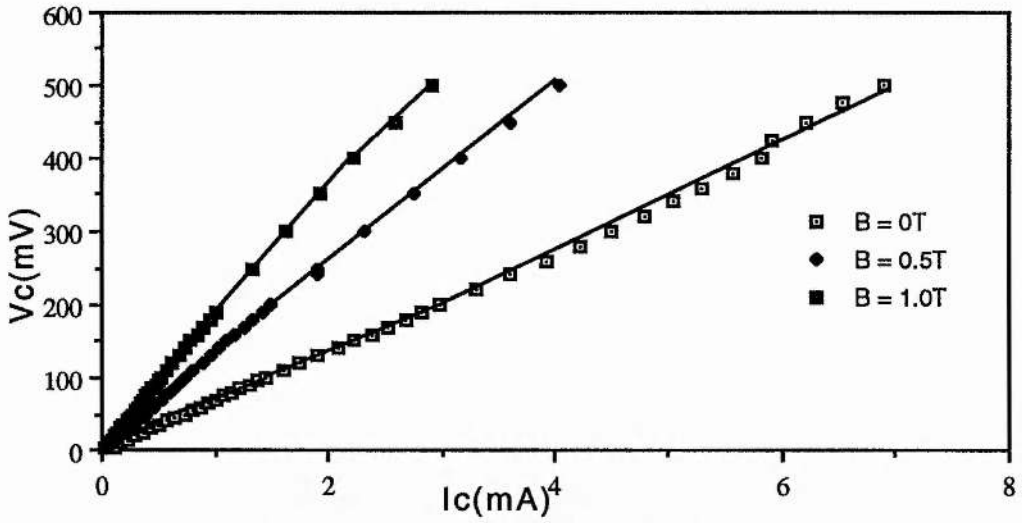

Figure 6.3 : The electrical characteristics for the n-InSb crystal under increased applied electric fields at nominally 4.2K.

The other conclusion, which also has a bearing on the level of electric field required, was that crystal heating was occurring. The crystal was not in good thermal contact with the copper post and so not in good thermal contact with the liquid helium. This would reduce the ability of the cryostat to cool the crystal below the temperature of the radiation shield. This problem was clearly demonstrated when the results, in figures 6.1,6.2,6.3 and several subsequent experiments, were combined as shown in figure 6.4.

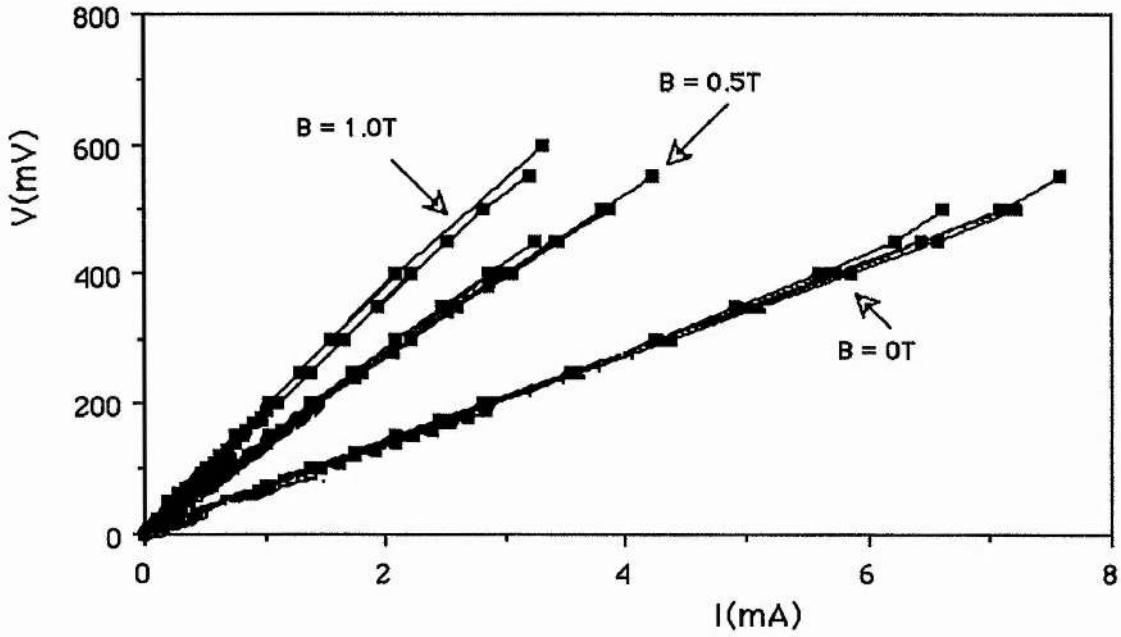

Figure 6.4 : Combined results of data on electrical characteristics of n-InSb crystal obtained between 14.9.90 and 15.3.91 at nominally 4.2K for applied magnetic fields of zero, one-half and one Tesla with the helium can filled with liquid nitrogen, liquid helium and pumped liquid helium.

6.1.4 Results From Placing a Crystal Inside the Helium Can

To obtain results where the crystal temperature would be known, a crystal was placed within the helium can. This unfortunately could not be done with the crystal positioned between the poles of the magnet, so the ability to apply a longitudinal field of known strength was sacrificed. With it went the immediate prospect of CR emission. Also a pulsed bias circuit was introduced to reduce the heating effects. A fairly simplistic pulse generator was employed and it was unable to provide the power required so an operational amplifier was connected to act as a current source.

The results obtained from the crystal within the helium showed non-linearity, negative differential resistivity and chaotic properties. The last two properties were found to be due to the non-linearity of the crystal reacting with a wire wound potentiometer, as replacement of the potentiometer with a metal-film resistor removed the effects. With the potentiometer in the circuit,

oscillations, of about 10MHz, were initiated at two different (but repeatable) voltages. The amplitude and duration of these oscillations varied with the bias voltage. The initial results showed distinct NDR with the bias voltage unable to be more than two volts. Just before the large decrease in bias voltage the pulse shape became increasingly unstable. As these results are largely unintelligible due to the large numbers of unrestricted variables an analysis of them is neglected.

The non-linearity was shown to be an inherent crystal property and the results are shown in figure 6.5

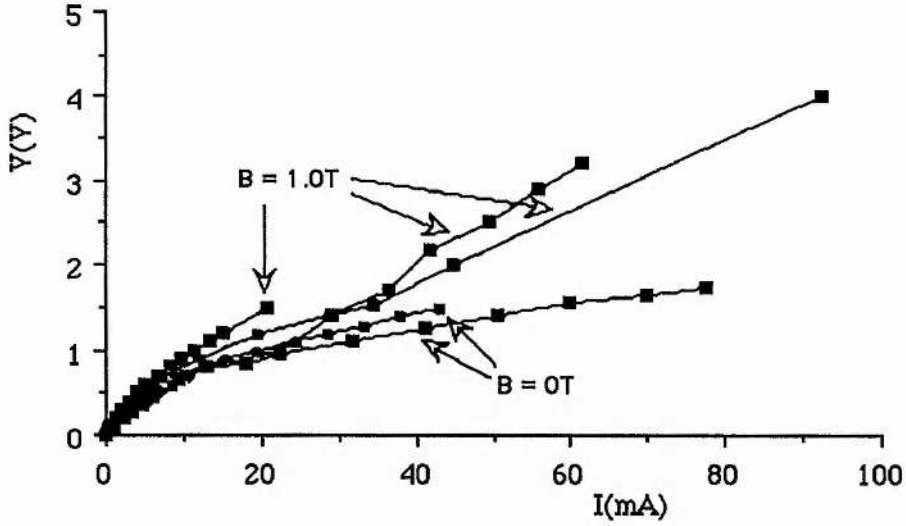

Figure 6.5 : Electrical characteristics of n-InSb at 1.5K, showing distinct non-linearities. The values of magnetic field depicted are values of the magnetic field between the poles, not values of the magnetic field through the crystal and are only given as an indication.

6.1.5 Conclusion

The results presented in figure 6.5 show a high resistance region followed by a transition, at higher electric fields, to a lower resistance region. Though the magnetic field values cannot be taken as accurate they indicate that the transition is not dependent on magnetic field strength. Also that the magneto-resistance effect is only noticeable above the transition. An unsupported suggestion for the cause of the non-linearity is that at low energies the most

efficient energy scattering process for the electrons is that involving piezo-electric acoustic phonons. At higher energies this scattering process is insufficient for removing the energy gained from the electric field. At this point a current 'run-away' will occur unless another scattering process can remove the energy. Potential deformation acoustic phonon scattering is deemed most eligible. The two different scattering processes attain equilibrium at differing rates. This is observed in the different dynamic resistances in the two regions. This NDC mechanism was first suggested by Conwell[4] based on the work of Bok[5] and Kogan[6]

[4]Conwell,Sol.Stat.Phys.,suppl 9 , 81 (1967)

[5]Bok, Ann.Radioelec. 15 , 120 (1960)

[6]Kogan, Sov.Phys.-Sol.State. 4 , 1813 (1963)

6.2 A Comparison Study of the Electrical Characteristics of High Purity n-InSb

6.2.1 Introduction

After the results obtained in attempting to obtain CR emission, a similar experiment was done at Queen Mary & Westfield College (QMW) by White & Puplett. Their results confirmed the existence of the non-linear electrical properties and a joint experiment at QMW resulted in the first observations of a related hysteresis. In order that these properties could be investigated further and a comparison with the crystals used in St Andrews be made, White kindly lent some of the crystals (samples 1 & 2 in figure 5.12) employed at QMW. This comparison would help to remove the possibility that the properties were unique to a particular crystal or contacting procedure. Details of the crystals are given in figure 5.12. Details of the contacting procedures employed are given in section 5.6. To accommodate the rod on which the QMW crystals were mounted a new cryostat had to be acquired. A glass cryostat suitable for the task (described in section 5.2.4) was made available by the kind permission of Mr.Armitage. The same pulsed bias supply as used for the CR emission cryostat was used.

6.2.2 Comparison of Electrical Characteristics of the n-InSb Crystals

The initial results obtained with the new cryostat provided evidence of deformation of the bias pulse across the crystal. Further experimentation and an analysis of the deformation of the pulse, showed the deformation to be equivalent to the hysterisis observed at QMW. Confirmation of non-linearities observed at low electric field by White et.al.[7], were also obtained. The data on the low field electrical characteristics is displayed in figure 6.6.

---

[7]White et.al., Private Communication.

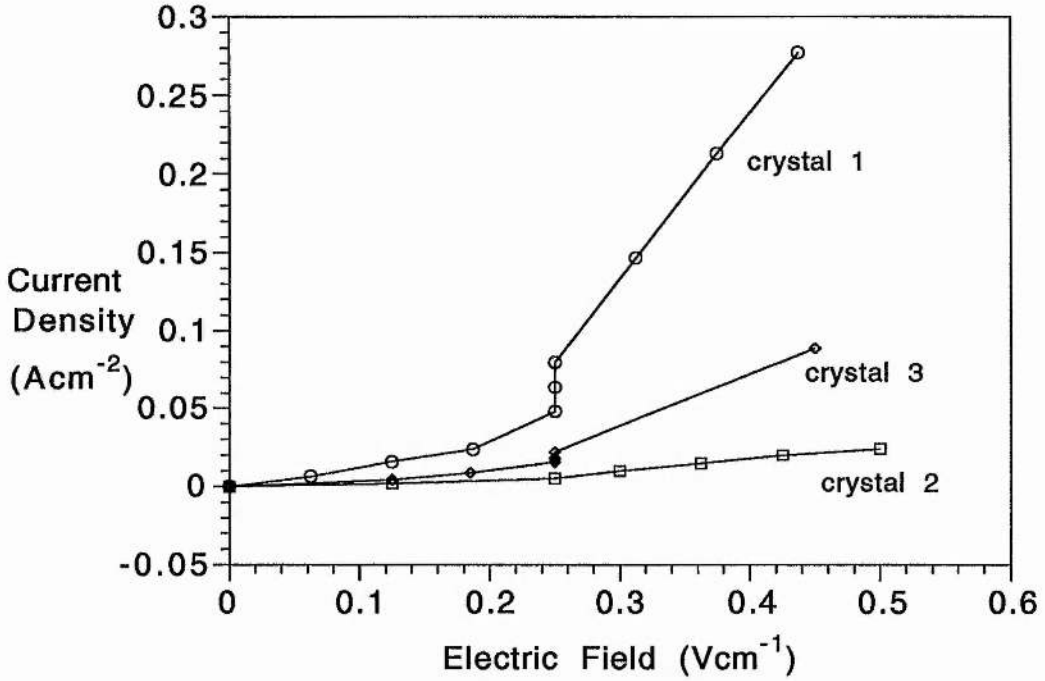

Figure 6.6 : Low field electrical characteristics of the three different high purity n-InSb samples at 4.2K.

6.2.2.1 Analysis Method & Results for High Electric Fields

The method for analysis of the pulse deformation is as follows: A pulse, 1ms in duration, is applied to the crystal. The pulse is monitored across the crystal and across the combination of the crystal and a series resistor. Initially the bias across the crystal is steady and the current is calculated by taking the difference between the two voltages monitored and dividing by the value of the series resistor. (This method is depicted in figure 5.7.) On reaching an onset voltage the pulse across the crystal is deformed as depicted in figure 6.7. The maximum voltage is noted as the rising edge voltage. The minimum voltage is that of the falling edge. This provides the hysteresis curves displayed in figures 6.8 & 6.9. These concur with curves obtained with a curve tracer from which, unfortunately no hard copies could be made. The length of the pulse before the transition between maximum and minimum voltages is taken to be the minimum pulse length required to obtain the transition at that voltage.

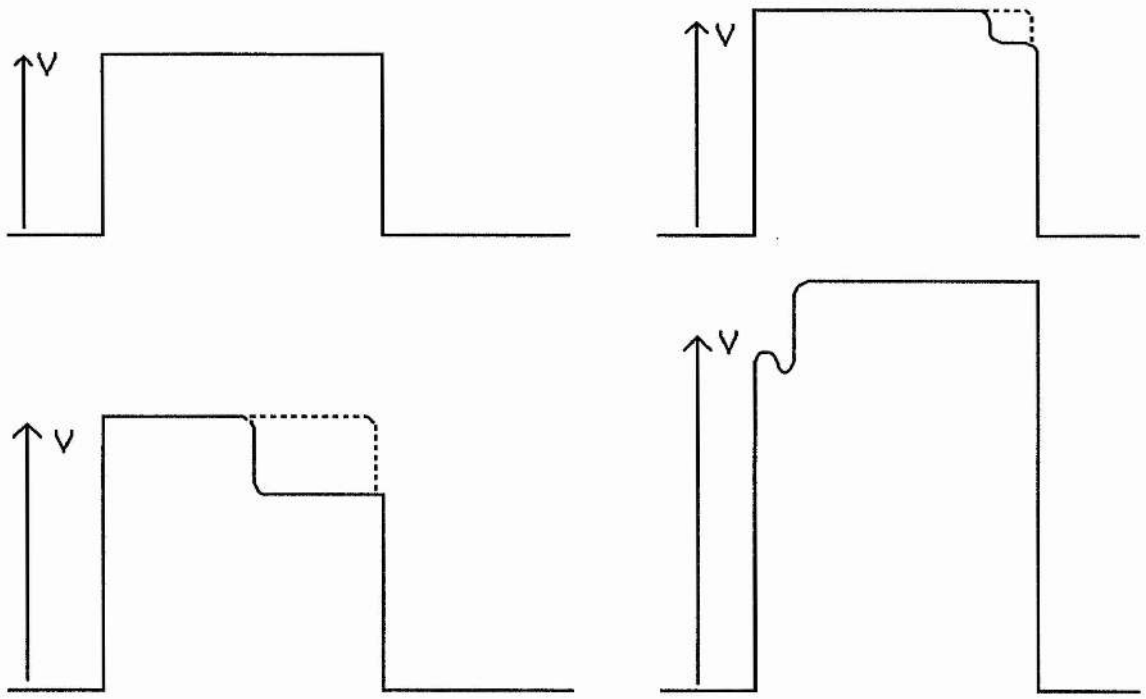

Figure 6.7 : Pulse deformation for increasing bias voltages

This was shown to be reasonable as the same results were obtainable by reducing the pulse length until the transition was removed. On increasing the pulse length, however, it was found that the transition would not be triggered until the pulse length was well in excess of the equilibrium transition point. This is depicted in figure 6.7 by the dotted lines.

The results obtained from the above are given in figures 6.8, 6.9, 6.10 & 6.11.

6.2.2.2 The Electrical Characteristics as Derived From the Pulse Deformation Method

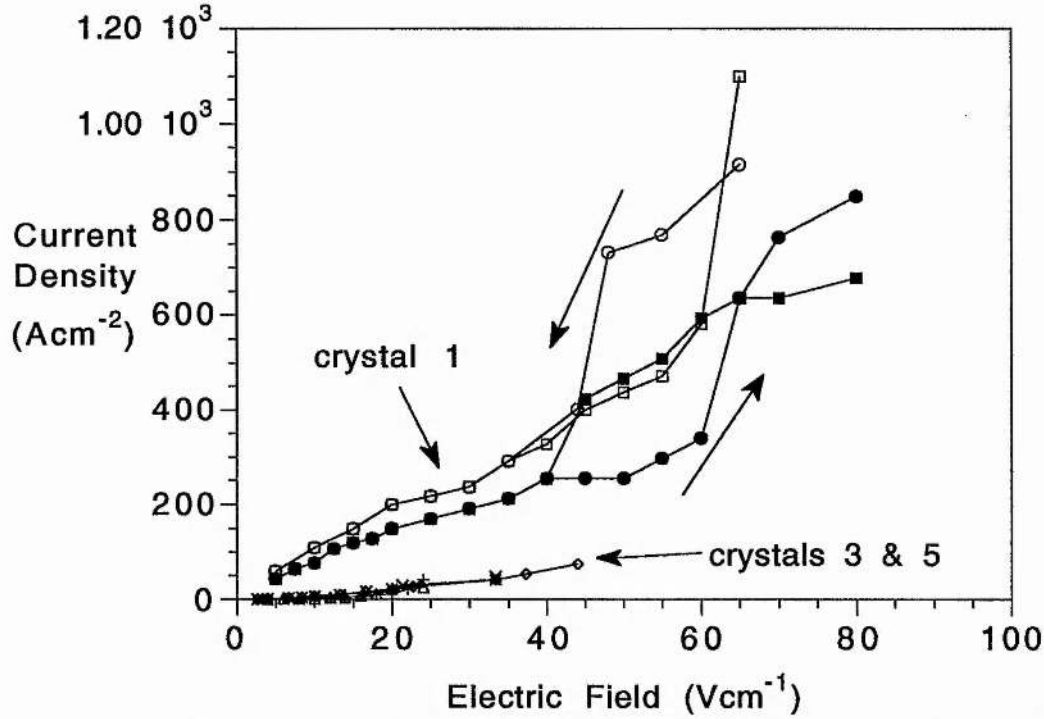

Figure 6.8 : Electrical characteristics, at 4.2K, of crystals of n-InSb from St.Andrews (crystals 3 & 5) and from QMW (crystal 1). crystal 2 was of substantially larger dimensions than the above and so was only useful in confirming low field results.

The above results were repeated at 1.5K. The results of this investigation are given in figures 6.9, 6.10 & 6.11. The upper trace depicted for crystal 1 is for a 200Hz pulse repetition rate (the other results are for a 100Hz pulse repetition rate).

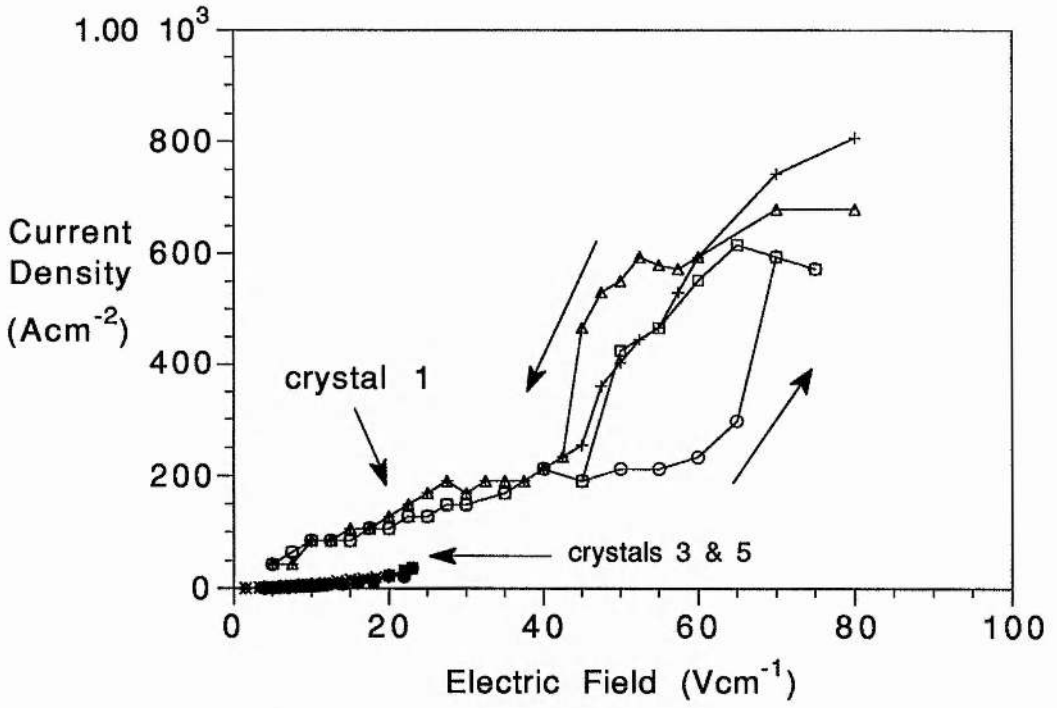

Figure 6.9 : Electrical Characteristics of the St.Andrews and QMW Crystals at 1.5K

A probe into the onset conditions for the pulse deformation was also made and the results from this investigation are shown in figures 6.10 & 6.11.

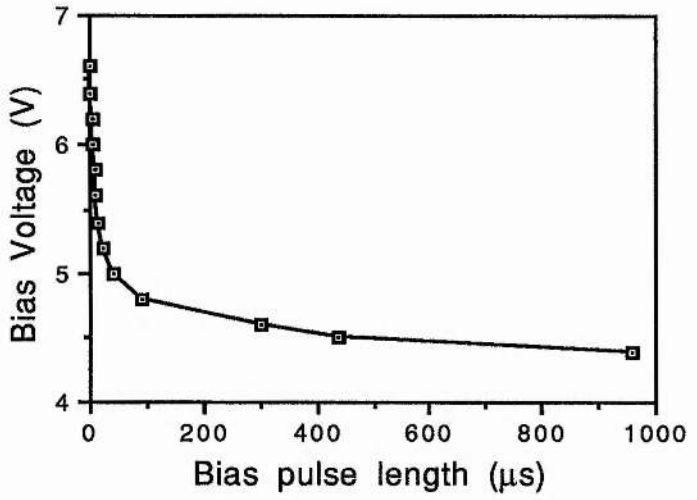

Figure 6.10 : Dependence of the onset bias voltage (for pulse deformation) on the pulse length.

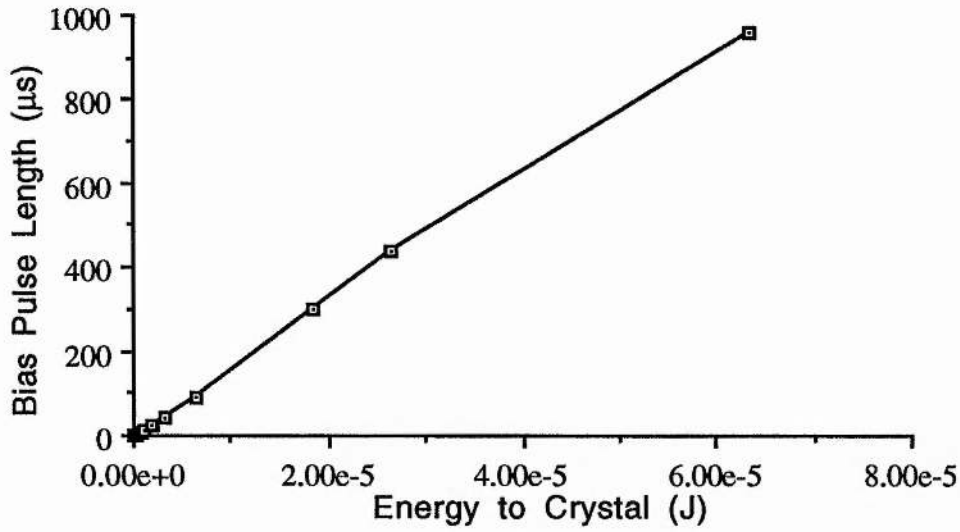

Figure 6.11 : Data showing the relation between the length of bias pulse and the energy delivered to crystal 1 by the electric field before threshold.

Figure 6.11 shows the energy delivered to the crystal before the transition occurs. The energy was calculated as the product of the bias voltage, the bias current and the length of the pulse before the transition (The pulse length is varied by the bias voltage as shown in figure 6.10).

6.2.2.3 Initial Conclusions From the Results

From both figure 6.8 and figure 6.9 it could be seen that the original non-linearity observed in crystal 1 was at low electric fields and that the high field non-linearity and associated hysteresis was a new phenomena. Also apparent was the inability of the bias power supply to produce a sufficiently large electric field across crystals 2 & 3 to observe hysteresis.

Figures 6.10 & 6.11 Indicate that the effect of crystal heating may still be influential. The E-J curve, as seen on an oscilloscope by means of a curve tracer, was observed to drift to higher conductivities. From figure 6.11, it can be seen that the energy delivered is effectively proportional to the length of the pulse employed. A possible explanation for this behaviour is that the crystal is able to dissipate more energy through transport to the liquid helium when the pulse is longer (and the bias voltage smaller)

and so more energy is required to heat the electron distribution to its value at threshold. Also possible is the situation where the scattering process is less effective at higher electron energies In this situation the increased acceleration due to the increased field will reduce the effect of the scattering and the electron distribution will gain threshold more quickly.

6.2.3 Conclusion on the Comparison of the Crystals at Low Electric Fields

The comparison of the three different crystals at low electric field values ($E < 1 Vcm^{-1}$, see figure 6.6), provided further confirmation of low electric field non-linearity. An explanation for this may be found in "High Field Transport in Semiconductors" where Conwell[8] shows how S-type NDR (under constant current conditions) is possible when there is the transition between piezo-electric and potential deformation acoustic phonon scattering as the dominant energy relaxation mechanism. Under the constant voltage conditions in which the above was obtained the non-linearities observed might then be expected.

The conductivity in this region, though, can be seen to vary from crystal to crystal. An explanation for this may be that proposed by Zylbersztejn[9] when he discovered that the conductivity in InSb varied with crystal size. This is due to the effect of size on the phonon distribution. An increased size reduces the energy relaxation rate. This increases the average electron energy which increases the momentum relaxation rate and thus decreases the conductivity. This correlates with the results shown in figures 6.6, 6.8 & 6.9. Another explanation may be found in the differences in electrical properties such as impurity concentration and carrier concentration. This is discussed further in section 6.5.

---

[8]Conwell, Sol.Stat.Phys.,Suppl 9 , 81 (1967)

[9]Zylbersztejn, 'Phys of Semicond.', Proc.7thInt.Conf.,1964(A.P.,New York,1965)

6.2.4 Conclusion From the High Electric Field Measurements

The dominant relaxation mechanism, for crystal 1, at high electric fields ($E > 10\ Vcm^{-1}$) is now probably optical phonon scattering, which due to its high efficiency causes a marked decrease in conductivity until the average energy of the electrons is greater than a threshold value. Work done by Stratton[10] has shown that it is possible to calculate a threshold field beyond which optical phonon scattering is no longer effective. Conwell[11] has discussed the situation : Beyond the threshold field the rate of energy loss due to optical phonon scattering is proportional to $E^{-1/2}$. So also is the rate of energy loss due to inter-electron collisions. The rate of energy from the electric field to the electrons is proportional to $E^{1/2}$. The suggested relaxation mechanism beyond this threshold are electron-hole interaction, spontaneous emission (stimulated emission is balanced by absorption) of photons, accoustic phonon scattering and multiple phonon scattering.

Using values obtained by Ehrenreich[12], Stratton[10] obtained a threshold field of $170Vcm^{-1}$. The values used were for room temperature and their applicability at very low temperatures is not known. Values have been taken that are thought to be more valid at low temperatures. These values give a threshold field of $97Vcm^{-1}$ which is similar to the threshold for the hysteresis in the results shown. Consideration for the size of the crystal should also be taken into account as this may affect the threshold field in the results obtained.

---

[10]Stratton, Proc.Roy.Soc.(London) A246 , 406 (1958)

[11]Conwell, Sol.Stat.Phys.,Suppl 9 , 158 (1967)

[12]Ehrenreich, J.Phys.Chem.Sol. 2 , 131 (1957)

6.3 Measurement of the Temperature Dependence of the Resistance of High Purity n-InSb.

6.3.1 Introduction

On cooling the cryostats a note of the change in the crystals resistance was taken. It was apparent that the change was not linear with temperature. This vague observation was confirmed by work done by Puplett et.al.[13], though this work was also not thorough (the only measured temperature points being room temperature, 300K, and liquid nitrogen temperature, 77K). It is known that at room temperature n-InSb acts as a metal and at liquid nitrogen temperature it acts as an extrinsic semiconductor. In between these two temperature there lies a transition which according to Puplett et.al. is extremely rapid. It was decided that, as the equivalent temperature for the energy of an optical phonon also lies in this region, a more rigorous study should be undertaken in order that the temperature at which the drop in resistance occurs should be located. The resistance with temperature relation could then also be compared with the resistance with bias voltage relation (as calculated from the electrical characteristics measured).

6.3.2 Experimental Approach and Results in the Determination of the Relation Between Resistance and Temperature in n-InSb

To measure the temperature a calibrated diode* was placed in good thermal contact with crystal 1, with crystal 5 in close proximity. (Crystal 3 had undergone a non-reversible physical change and had to be replaced by crystal 5 which was also taken from sample 3.) Liquid nitrogen was then poured into the outer flask of the glass cryostat and the resistance of the crystal and diode were measured. The resistance of the diode could then be converted into the temperature. The results are given in figures 6.12 & 6.13.

---

[13]Puplett & White, Private Communication (see appendix 6.1)

* Calibrated by V.Scott for the temperature range 77 to 300K (see appendix 6.2)

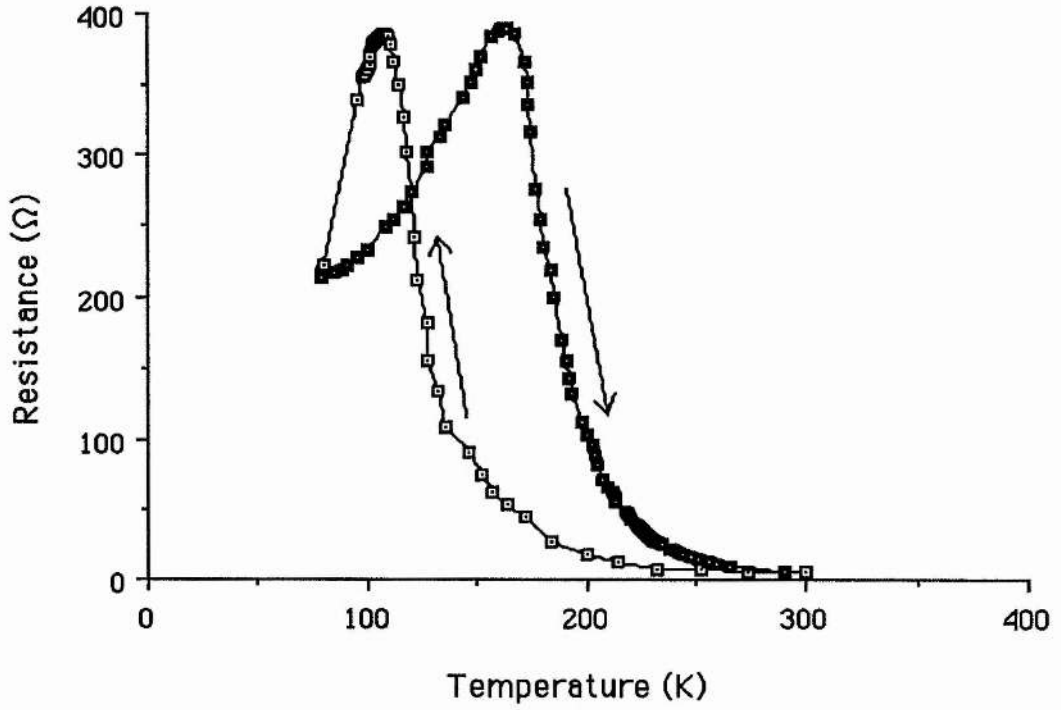

Figure 6.12 : Resistance with temperature relation for crystal 1

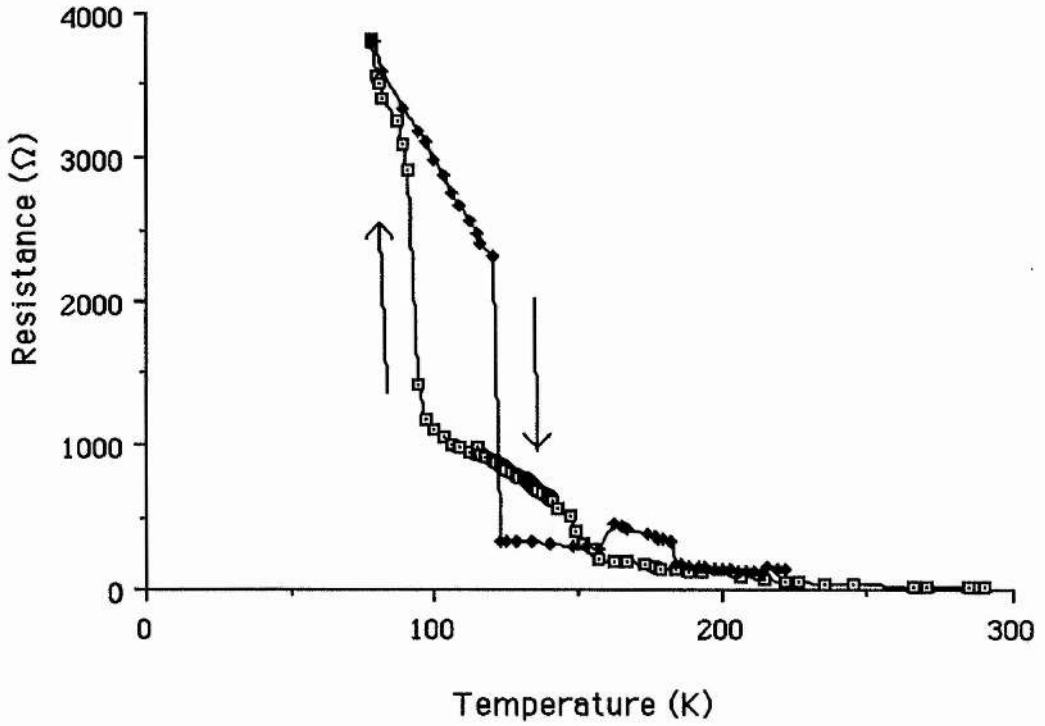

Figure 6.13 : Resistance with temperature relation for crystal 5.

6.3.3 Defintions of Electron Temperatures and Comparison of the Resistance with Electric Field Relation to the Resistance with Temperature Relation

At low electric fields and low temperatures the effect of the potential is to heat up the electron distribution whilst having little effect on the phonon distributions. Thus low electric fields are equivalent to a small temperature increase. Once the electric field is large enough to have a substantial effect on the phonon distributions the temperature equivalence of an electric field no longer holds. It has been shown, though, that whilst acoustic phonon scattering is the dominant relaxation process the electron distribution can still be described by a Maxwell-Boltzmann distribution which has been heated (This is due to inter-electron scattering, whilst not causing relaxation is efficient enough at redistributing energy should an imbalance occur). The temperature required to obtain the distribution, if it were entirely heat induced, is known as the effective electron temperature when the distribution is induced by an electric field. This definition also holds for very low electric field values.

When optical phonon scattering becomes the dominant relaxation process the electron distribution can no longer remain as a Maxwell-Boltzmann distribution because the optical phonon scattering is more efficient at causing a distortion in the electron energy distribution than the inter-electron scattering is at restoring the Maxwell-Boltzmann distribution. At this point the concept of an effective electron temperature becomes meaningless. A somewhat more vague definition of effective electron temperature can still have some meaning, however.

If it is possible to obtain similar electrical characteristics by lattice heating to those obtained by the application of an electric field then an effective lattice temperature may be defined and determined by comparison of the electrical characteristics. This effective temperature assumes that the interaction between the electrons and optical phonons is such that any heating of either distribution does not cause an effectively instantaneous heating of the other distribution. Due to the high efficiency of the optical phonon scattering this is unlikely. To check on the validity of the

above reasoning, the relations of resistance with temperature (figures 6.12 & 6.13) were compared with the relations of resistance with electric field.

6.3.4 Determination of the Relation Between the Electric Field and the Resistance of the InSb Crystals

The electrical characteristics of the above crystals were measured (giving results compatible with those shown in figures 6.8 & 6.9) and the data transformed to show the relation between the static resistance of the crystal and the electric potential across it. These results are given in figures 6.14 & 6.15.

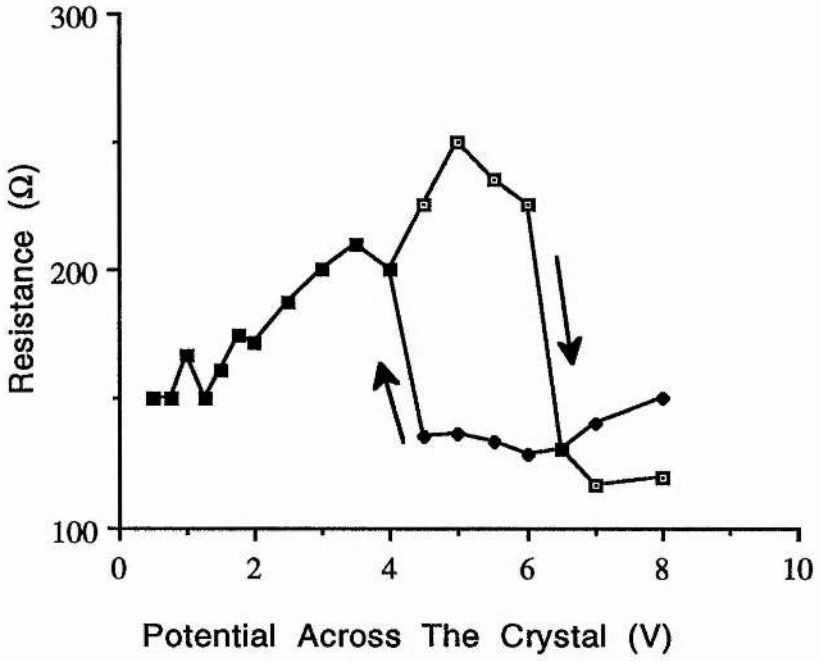

Figure 6.14 : Change in Resistance with Temperature for Crystal 1 (Compare with figure 6.12)

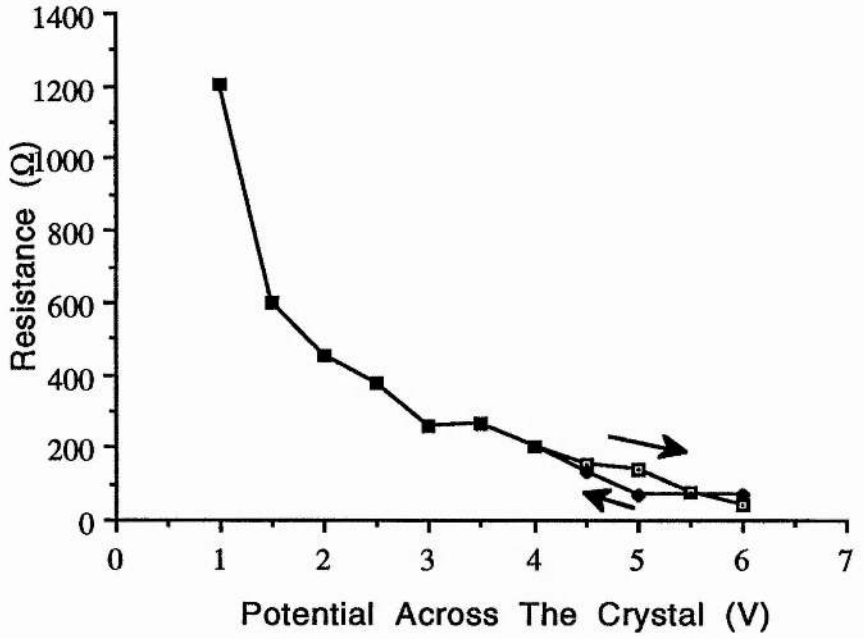

Figure 6.15 : Change in Resistance with Temperature for Crystal 5 (compare with figure 6.13)

6.3.5 Conclusions on Comparing the Change in Resistance With Either Temperature or Electric Field.

From figures 6.12, 6.13, 6.14 & 6.15. It is apparent that although the basic relations are similar, the hysteresis occurs in different places and the values of resistance are substantially higher in the temperature experiments. Also apparent is the high resistance of crystal 5 in comparison with crystal 1 at low electric fields. This could be due to the greater concentration of impurities and current carriers in crystal 5. An increase in impurities will cause greater ionised impurity scattering. An increase in current carriers will increase the number of electrons in the high energy end of the electron distribution causing phonon interaction to be greater and occur at lower fields and temperatures. Evidence for this would appear to be seen in figure 6.13 where the transition from high resistance to low resistance occurs at a lower temperature than the transition for crystal 1, shown in figure 6.12. Another possible cause for the differences may be due to the difference in size of the two crystals. This as mentioned in section 6.2.3 can cause a difference in conductivity and hence in the resistance of the

crystals. The results here add further evidence to the importance of size as an influence on the electrical characteristics. The transition to low resistance in crystal 5 being at a lower temperature than the transition in crystal 1 is a result that could have been predicted (and can be explained) by this size effect.

A question was raised as to whether the temperature hysteresis was purely a time delay problem caused by the differing response times of the diode and the crystal to temperature. This was seen not to be possible as the data suggests that the crystal has the longer response time, whereas observations, made during the measurements, indicated that the crystal had the shorter response time.

The differences between figures 6.12 & 6.14 and 6.13 & 6.15 are expected as one is heating the phonon distribution rather than the electron distribution. The resistance of crystal 1, in figure 6.14, after transition is the major discrepancy and as yet no satisfactory explanation for this has been found. This result does, however, agree with the results by Puplett et.al.[1]. The differences between the electric field induced resistance and the temperature induced resistance, indicate that the transfer of energy from phonons to electrons is less efficient than the reverse process. This could provide an explanation for the hysteresis. The differences between the two crystals imply that different scattering processes are involved during the large decreases in resistance.

6.4 Measurement of the Carrier Concentration

6.4.1 Introduction

The results so far still leave questions unanswered. In an attempt to increase comprehension and enable mobilities to be deduced from the measurements, a measurement of the carrier concentration over the range of electric fields involved was undertaken. If the hysteresis is involved with the transition between semiconductor (extrinsic conduction) and metal characteristics (intrinsic conduction) then the measurement of the carrier concentration will indicate the introduction of the intrinsic concentration. If it is not involved with the transition, but only with the saturation of optical phonon scattering then the carrier concentration should remain effectively constant.

6.4.2 Practical Considerations

Another cryostat was employed for the measurement of the carrier concentration. This was designed specifically for use in the Hall method of determining carrier concentration. The details of the cryostat and the magnet are dealt with in section 5.2.5. The initial results indicated that the constant current source was not sufficiently powerful. On replacing it, temporarily, with a bench power supply, the problems of a continuous bias were made apparent. The crystal on reaching the transition pulled enough current to blow the power supply's fuse. This led to the design of a new complex pulse power supply capable of producing 0.5 to 5 μs and 0.5 to 5 ms pulses and a combination of both for potentials up to 15 Volts. This was designed so as to enable further probing of the hysteresis without excessive heating problems. The details of the circuit are presented in section 5.4.3.

The results were only obtainable for crystals taken from sample 3. This obviously reduces the measurements' importance with respect to the hysteresis. The assumption that the electrical charateristics are uniform throughout sample 3 has been made. As more than one sample was used in the measurements, the validity of that assumption was checked. It would also be possible to

confirm the values for the crystals given by the manufacturers (see figure 5.12)

6.4.3 Current Carrier Concentration Results

The first results (see figure 6.16) were obtained whilst the bias circuitry was unable to reach the transition region. The results were, however, able to confirm the carrier concentration values quoted for the crystal by the manufacturers.

The next results were obtained using a bench power supply as constant current source and do not have a high degree of accuracy. These are displayed in figure 6.17 where the equivalent electrical characteristics are also given.

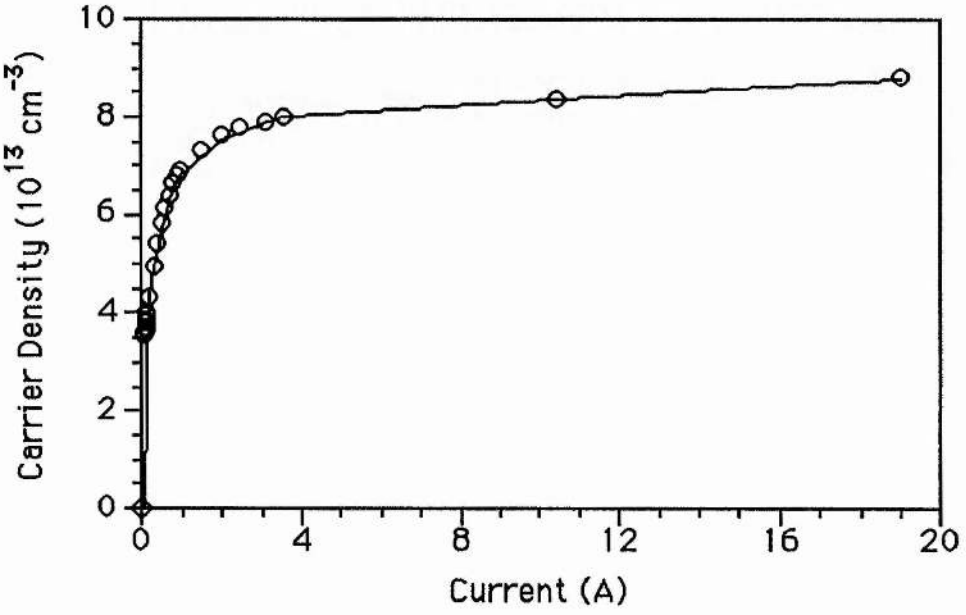

Figure 6.16 Carrier concentration in crystral 6 as measured by the Hall effect at low electric field values. (The lattice temperature = 4.2K)

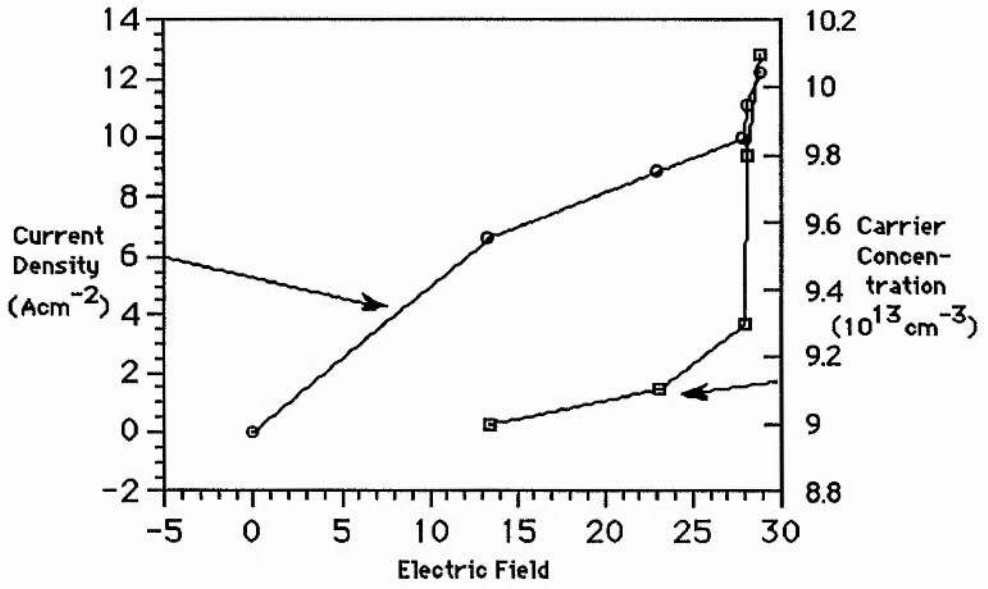

Figure 6.17 : Carrier concentration and electrical characteristics of crystal 6 at high electric field values. (The lattice temperature = 4.2K)

6.4.4 Conclusions and Further Results

The results displayed in figure 6.17 show charateristics similar to those obtained by Glicksmann & Steele[14] at 77K, though the threshold field is considerably lower. In order to obtain results from which substantial conclusions could be made, the bias source was replaced by that used for the measurement of the electrical characteristics (the circuit is described in section 5.4.3 and is depicted in figure 5.11). The carrier concentration was then measured in two more crystals and the results compared (see figure 6.18). The results show that at an electric field of just greater than

[14]Glicksmann & Steele, Phys.Rev.Letts. 2 , 461 (1959)

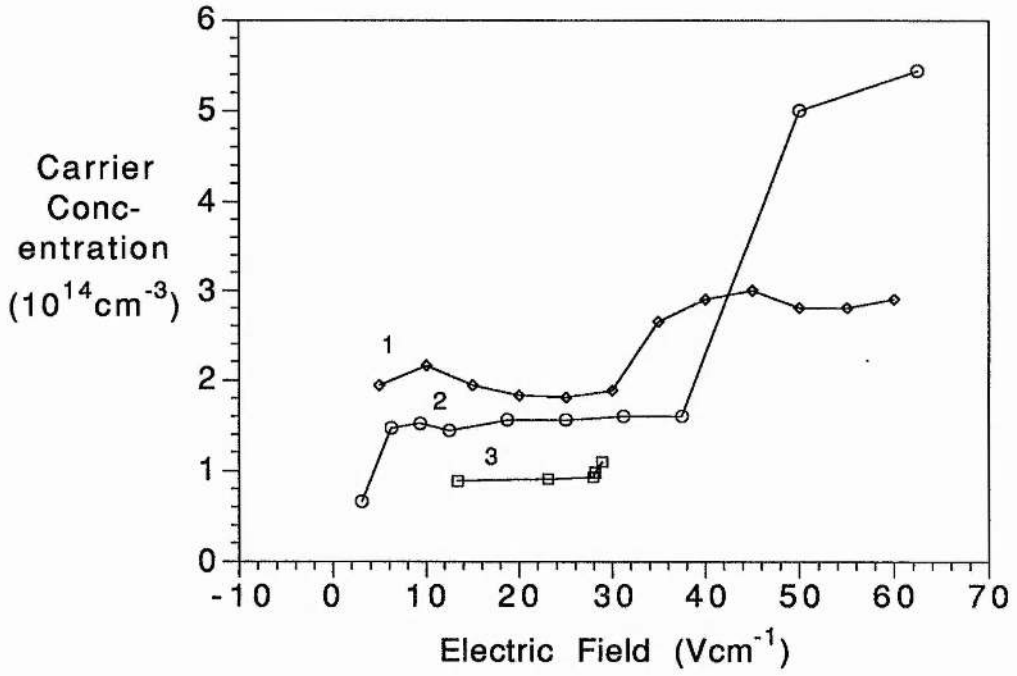

Figure 6.18 : Variation in carrier concentration with electric field for three crystals (all taken from the sample 3). Crystal 3 in this figure is crystal 6 in figure 6.17. (The lattice temperature = 4.2K)

$30Vcm^{1}$(in the presence of a magnetic field of 0.7 Tesla) there is an increase in carrier concentration. Beyond this increase, the carrier concentration becomes effectively constant (within measurement error).

This implies the existence of deep donor levels. The existence of deep donor levels in high-purity crystals has been noted before[15] with a corresponding effect on the electron mobility. The effect of deep donors could further explain the difference in electrical characteristics between crystal 1 and crystals 3 & 5. The electrical characteristics were measured simultaneously with the carrier concentration and the results of that measurement are presented in figure 6.19.

---

[15]Tifonov & Yaremenko, Sov.Phys.Semicon. 5 , 839 (1971)

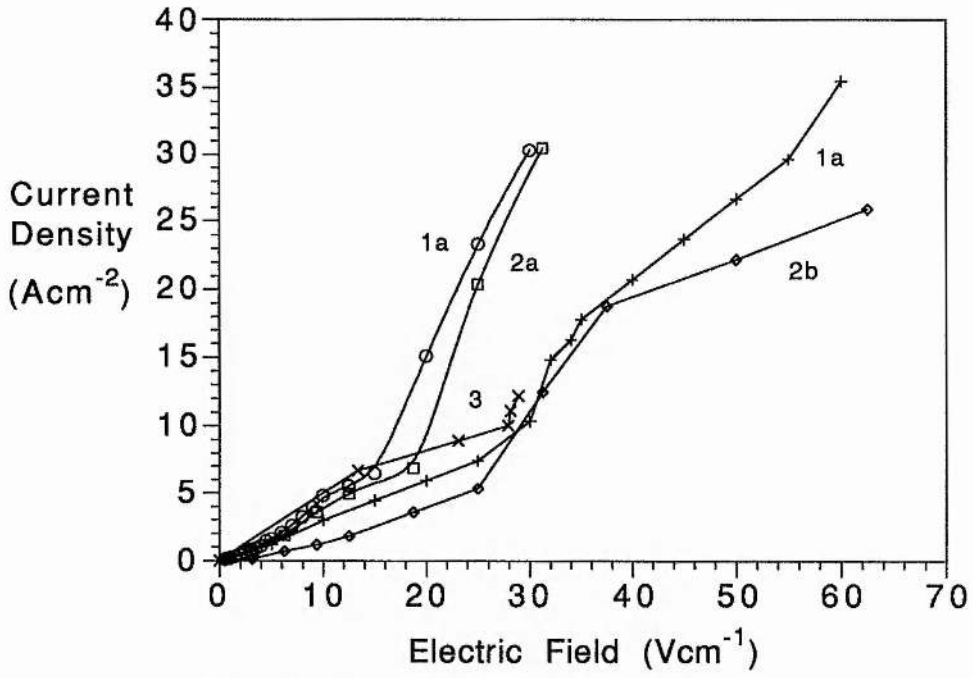

Figure 6.19 : Electrical charateristics of the crystals used to obtain the results shown in figure 6.18. (The numbering of the crystals is the same. 2a : B = 0T, 1,2b &3 : B = 0.7T)

The resistive effect of the magnetic field can be seen. The ionisation of the deep donors can be seen to cause a step in the electrical characteristics.

6.4.5 Conclusion

The measurement of the carrier concentration, in crystals similar to crystals 3 & 5, has shown the existence of deep donors. This provides a further reason and explanation for the difference in electrical characteristics between crystal 1 and crystals 3 & 5. The presence of the deep donors leads to an overall decrease in the mobility as their presence indicates an increase in the impurity concentration. This will cause an increase in the ionised impurity scattering. At ionisation there may be an increase in conductivity, however, as there is an increase in carrier concentration. The above effects have been noted by Tifonov & Yaremenko[16] for high purity n-InSb crystals.

---

[16]Tifonov & Yaremenko, Sov.Phys.Semicon. 5 , 839 (1971)

This provides further evidence for the suggestion, made in section 6.3.5, that different processes are involved with the large decreases in resistance. It would now appear that the decrease in resistance in crystal 5 with electric field is due to the impact ionisation of deep impurities. This could also be the cause of the hysterisis in that crystal.

6.5 Calculation Of Electron Mobility From The Data

6.5.1 Introduction

Now that the carrier concentration and current density versus the electric field have been measured, the electron mobility can be calculated using the expression,

$$\sigma = \frac{J}{E_F} = ne\mu$$

where, σ = electron conductivity
J = current density
E_F = electric field
n = carrier concentration
e = electron charge
μ = electron mobility

6.5.2 Variation of Conductivity with Electric Field

The conductivities of crystals 1, 3 & 5 were calculated and the results of this calculation are given in figures 6.20 and 6.21. The variations of conductivity with electric field are included here as, when the carrier concentration is constant, they are proportional to the variations of mobility with electric field. They also provide information for the region above which the carrier concentration has been measured.

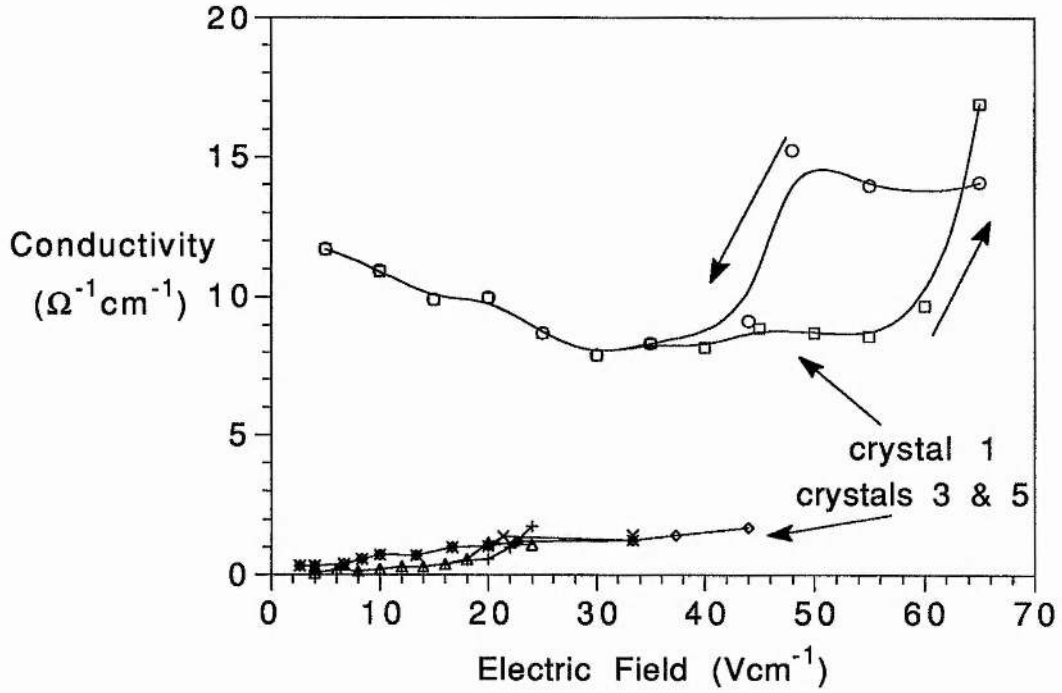

Figure 6.20 Variation of conductivity with electric field at a lattice temperature of 4.2 K.

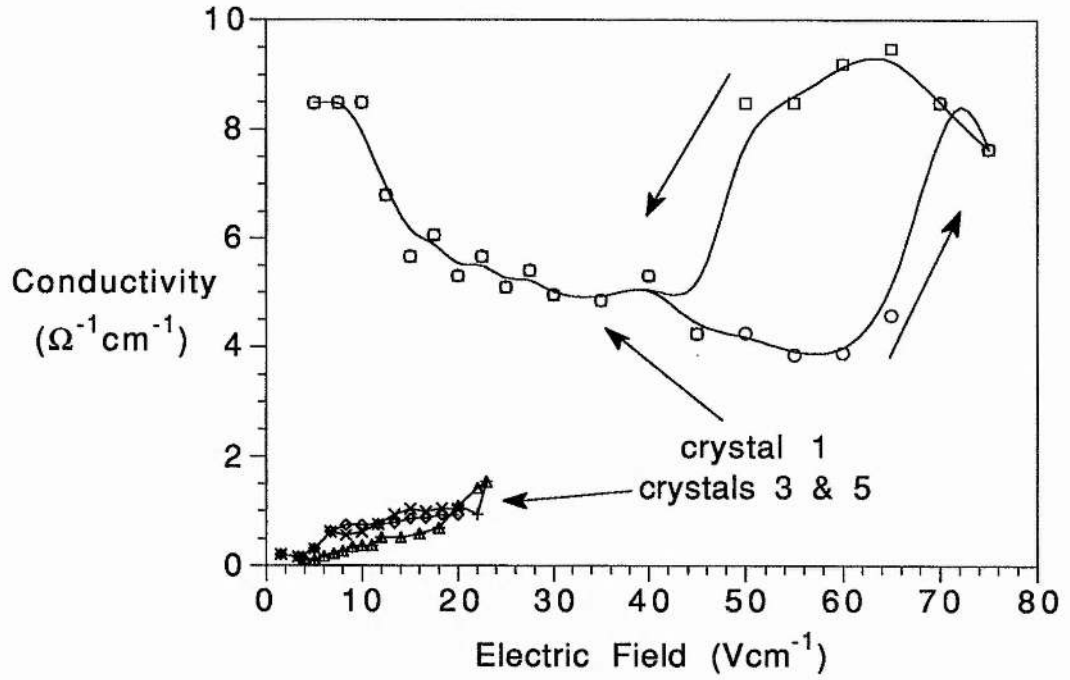

Figure 6.21 : Variation of conductivity with electric field at a lattice temperature of 1.5 K.

6.5.2.1 Conclusions From the Conductivity Variations

The results shown in figures 6.20 & 6.21 show the differences in the electrical characteristics between crystal 1 and crystals 3 and 5. Crystal 1 shows a decrease in conductivity (caused by an approximately constant carrier concentration and a decrease in mobility with electric field due to acoustic and optical phonon scattering) followed at high field by a sharp increase in conductivity (with an accompanying hysterisis). Crystals 3 and 5 show an increase in conductivity followed by a greater increase in conductivity. The surmise is that due to the deep donors, the electron concentration is not constant with electric field (as shown in section 6.4.4). The increase in ionised impurity concentration will cause a decrease in conductivity at low fields, but as the elecron concentration increases the conductivity will increase and when the deep donor level is impact-ionised the sharp increase in carrier concentration will be reflected in the conductivity as a greater rate of increase.

The sharp increase in conductivity at high field in crystal 1 is possibly due to the increase in carrier concentration due to the introduction of the intrinsic concentration. Otherwise it could be due to the saturation of optical scattering causing an increase in mobility. Both processes could be involved. Also a possibility is the involvement of electron hole scattering about which, as a scattering process, little is known. Further study is needed to divine the true nature of the electric charateristics in this region. This, unfortunately, is beyond the scope of this thesis. The problem is discussed further in section 7.

6.5.3 Variation of Mobility With Electric Field

Accepting that the range of electric field values at which the carrier concentrations have been determined are limited, the following is of limited value. Unfortunately the carrier concentration for crystal 1 at the fields involved with the hysterisis could not be obtained. The main object of the calculation of the mobility variations presented here are, therefore, to obtain

confirmation of the crystals electrical properties as given in section 5.5. These properties can determine some of the high

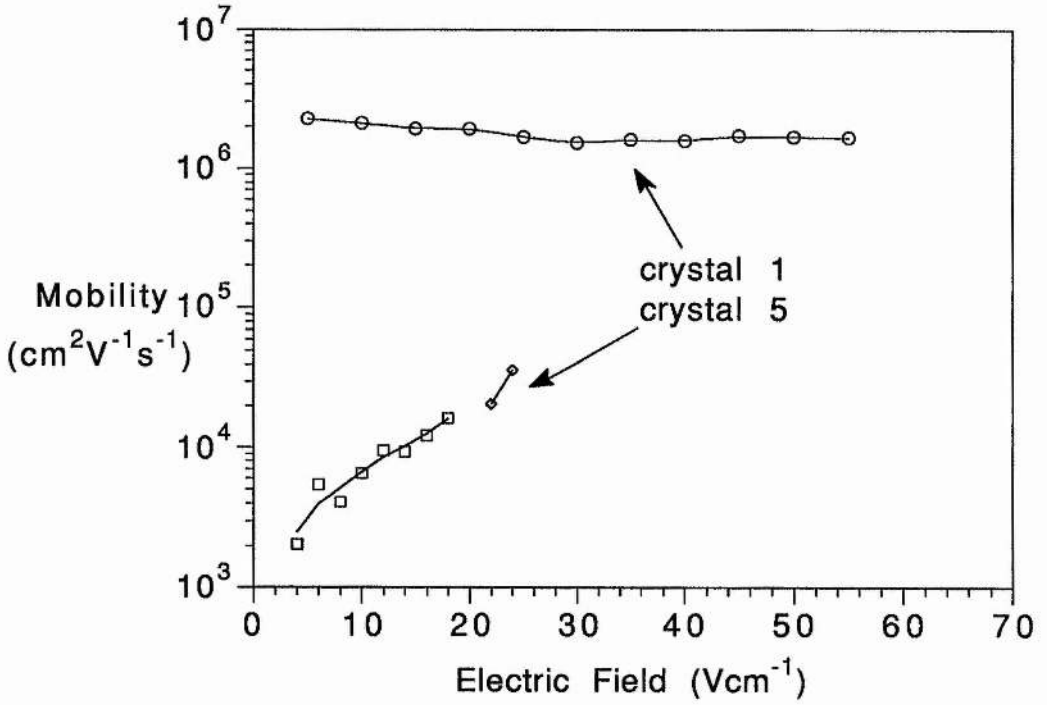

Figure 6.22 : Variation of mobility with electric field for crystals with a lattice temperature of 4.2K

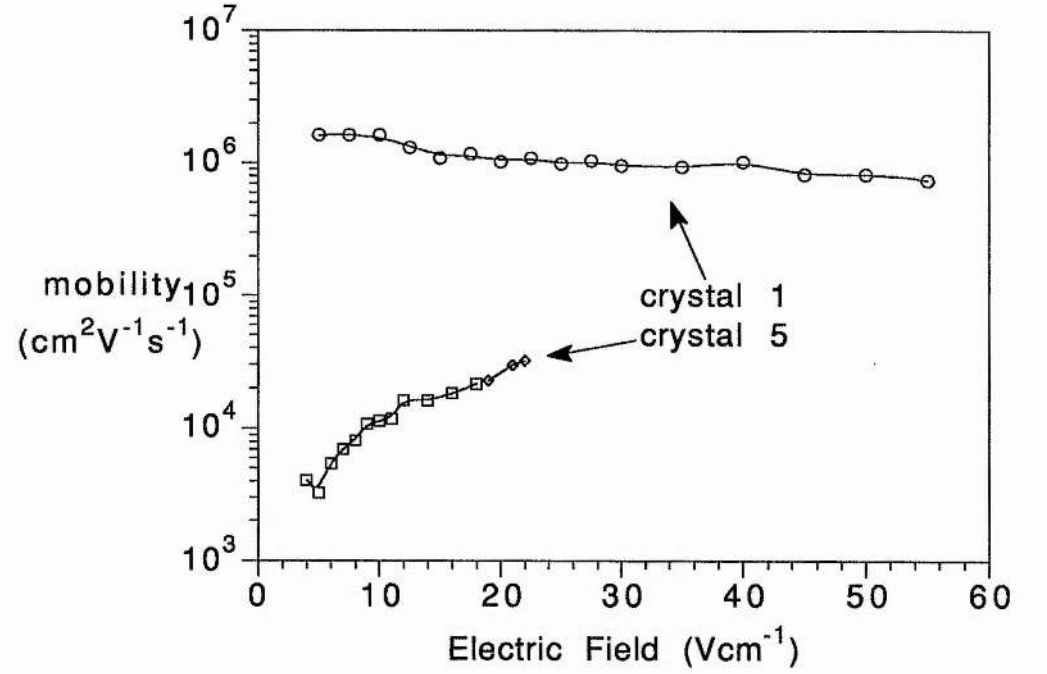

Figure 6.23 : Variation of mobility with electric field for crystals with a lattice temperature of 1.5K.

field properties. The variations of mobility with electric field are given in figures 6.22 & 6.23.

6.5.4 Conclusion

Figures 6.22 & 6.23 further show the differences between crystal 1 and crystals like crystal 5. It would appear that, due to the increased effect of the ionised impurity scattering and possibly the effect of the increased size on the phonon distribution, the conductivity has been affected such that the applied electric field is insufficient to excite the electrons into the optical phonon scattering region. That the scattering has had a large effect on the mobility can be seen by the size of the reduction in mobility from that expected if no deep donors were present (see manufacturers data in section 5.5). The contamination of the samples must have occured after the manufacturers measurements, as they measured an uncompensated donor concentration of $\approx 10^{14}$ cm^{-3} which correlates with the concentration measured before the deep donors are ionised (see section 6.4.4).

The mobility variation of crystal 1 is typical for a high purity crystal. The value of its maximum mobility is somewhat higher than that quoted by the manufacturers at 77 K. This implies that either the maximum mobility occurs at a temperature other than 77K, or the lattice temperatures of 1.5 and 4.2 K have a noticeable effect. Both of these are possible. A high purity sample (impurity concentration $\approx 10^{14}$ cm^{-3}) would expect to have a maximum mobility value at a temperature of $\approx$ 50 K, so values taken at 77 K are expected to be below maximum. This can not provide the whole difference between the quoted values and the measured values so it is suggested that remaining difference is due to the low lattice temperatures.

6.6 **InSb as a Detector**

6.6.1 Introduction

The following work was done to provide a helium temperature detector for emission experiments. It is included here as the results give information on the optical properties and an indication of the scattering regime in which emission (and detection) occurs.

6.6.2 Experimental Proceedure

The cryostat used is described in section 5.2.6. The bias circuitry was purposefully kept as simple as possible and consisted of a battery connected to the crystal by means of a potential divider. Also connected across the crystal is an amplifier with a gain of 1000. The circuit is shown in figure 6.24.

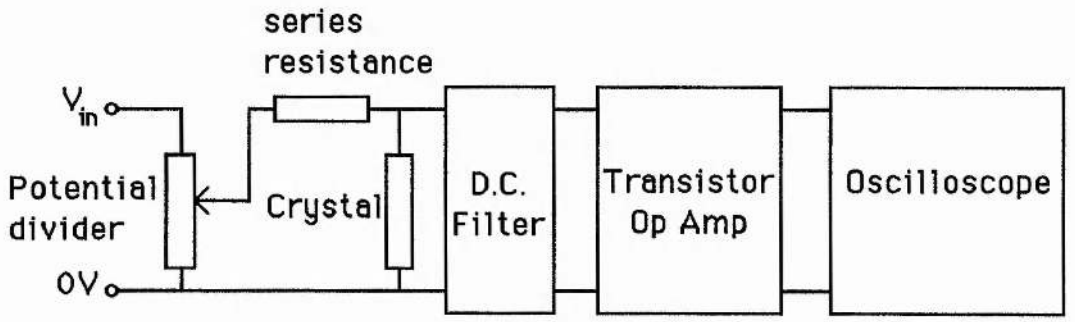

Figure 6.24 : Detector Bias and Amplification Circuit

Since InSb detects as a bolometer, it detects variations in power. So on cooling the cryostat and applying a bias voltage a known variation in incoming radiation must be applied in order to obtain values for the responsivity. Two features are essential as the responsivity is expected to be high ($\approx$ 1 KVW^{-1}). The variance in input power must be small and the total input power must be low, so as to prevent the crystal response from saturating. A GaAs Gunn diode oscillator which provided $\approx$ 100μW at 144 GHz was used. The radiation from the Gunn diode was shone into the cryostat and simultaneously measured using a TK free space power meter. As 100μW was seen to cause saturation (as expected, since 100μW of

power will generate a signal of 100mV in a detector of responsivity equal to ≈ 1 KVW^{-1} and the bias voltage is typically ≈ 40mV) attenuation was required.

In order to decrease the input power a quasi-optical circuit, using polarisers as attenuators, was implemented. The circuit is shown in figure 6.24. The viability of the circuit was tested by measuring the output power of the Gunn diode, by means of the TK free space power meter*, with and without the polarisers between the two. The two powers measured were 103μW and 51μW.

The circuit shown in figure 6.25 also provided the opportunity to test the detectors sensitivity to the polarisation of incoming radiation. Horizontal, 45° and vertically polarised radiation was shone into the detector. The same result was recorded for each so the crystal would appear insensitive to polarisation. This is to be expected since photon absorption is an energy gain process with no preferential direction.

6.6.3 Experimental Results

On illuminating the external window of the cryostat with ≈ 5 μW at a frequency of 20 Hz, the crystal, with a bias voltage of 40mV, was seen to have an A.C. variation of frequency equal to 20 Hz and amplitude equal to 1.2 mV. This implies a Detectivity of 240 VW^{-1}. This is somewhat low for an InSb detector, but since many components have not been optimised it is acceptable.

Of more importance is the noise figure. To obtain this all radiation was prevented from entering the cryostat. The voltage attributable to noise in the detector circuit was equal to ≈ 20 μV. This is equivalent to a power of 100 nW. This was measured across a 40 KHz bandwidth. So the Noise Equivalent Power (N.E.P.), which is defined as over a 1 Hz bandwidth is equal to 1.56 $nW(Hz)^{-1/2}$. This is rather large for an optimised InSb detector, but for the situation considered is reasonable.

It was found that the detectivity of the crystal was a maximum when the radiation was chopped at a frequency of 5 Hz and

---

* My thanks to D.A.Robertson for setting up and operating the TK power meter

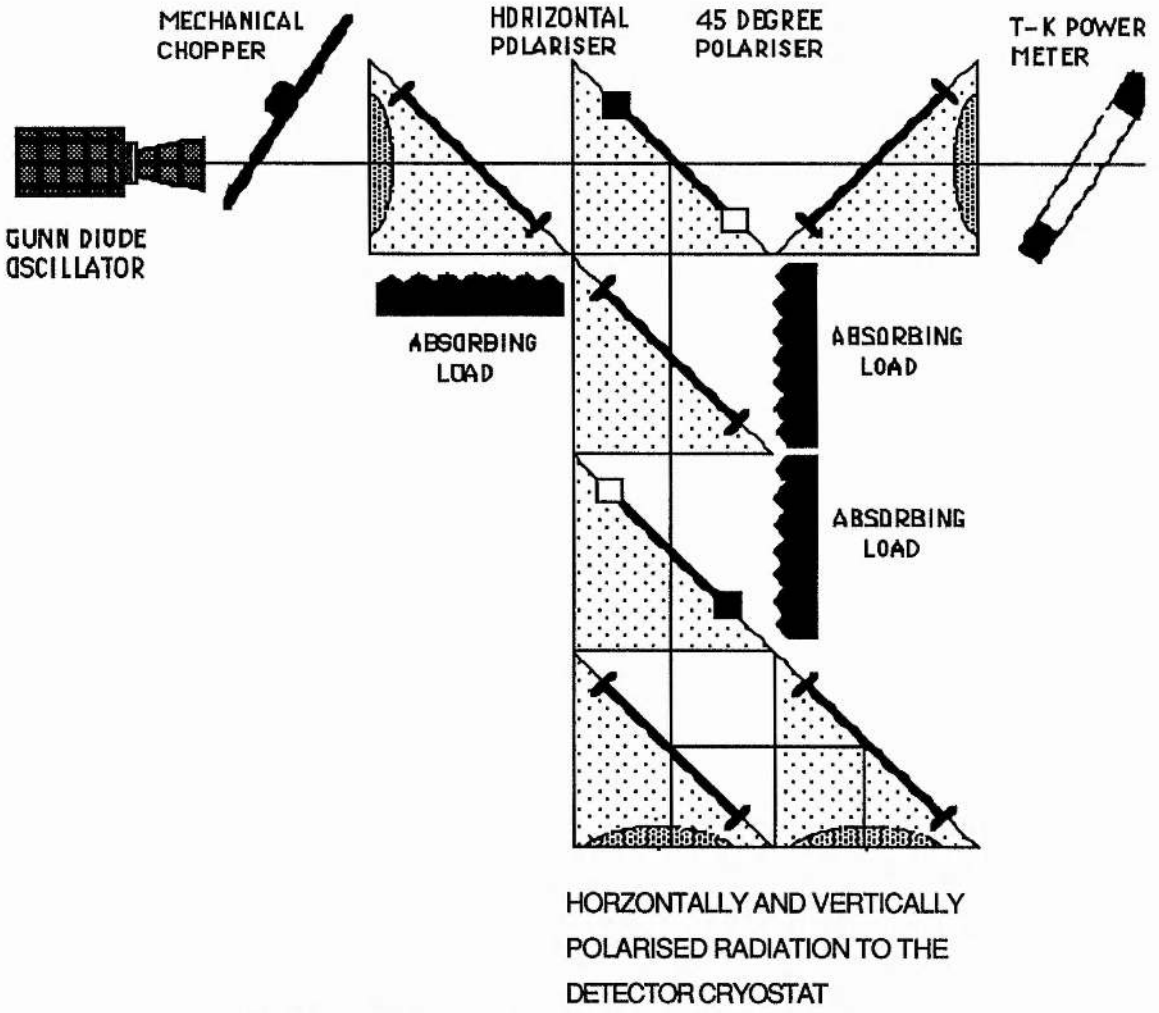

Figure 6.25 : Quasi-optical attenuation circuit for the characterisation of the detector.

the bias voltage was equal to ≈ 40 mV. The electrical charateristics of the crystal used, which was from sample 3, were identical to the other crystals and showed the transition from high resistivity to lower resistivity at low electric fields. The transition occured at a bias voltage of ≈ 30 mV which indicates that the greatest detectivity is to be found just above the transition.

6.6.4 Conclusion

If the transition is, as believed, between two acoustic phonon energy relaxation process then one might expect the effect of photon absorption to be greatest just above transition since this is when the rate of energy relaxation due to phonon scattering is at a minimum.

The problem of saturation occurs at high radiation powers and greater bias voltages as the hot-electron effect becomes important. In this region an increase in electron energy will decrease the electron conductivity countering any increase at lower electron energies. The above mentioned effect of radiation on the electrical charateristics was observed on an oscilloscope displaying the current voltage characteristics. A diagrammatic representation of this is given in figure 6.26.

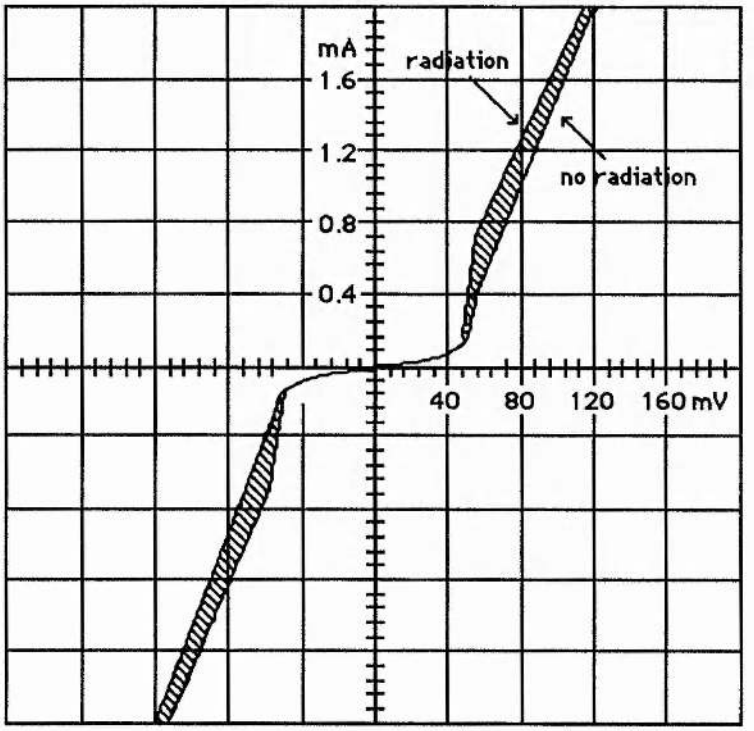

Figure 6.26 : Representation of the observed effect of radiation on the electrical characteristics of the detector crystal (c.f. figure 6.6)

7 CONCLUSION

The primary inspiration for the work on which this thesis is based, was the development of a tuneable far infra-red source based on Landau level transitions, as initially developed by Gornik[1], into a quasi-optical coherent source in the sub-millimetre region which would be tuneable over the majority of the region. The linewidth (and possibly the efficiency) would be enhanced by the placement of the n-InSb crystal in a quasi-optical resonant cavity. This was, sadly, not achieved.

In the attempt, a series of measurements and calculations on the electrical characteristics of n-InSb were made and it is these that form the basis of this thesis. These results have added to the understanding of the electrical characteristics of n-InSb and have added further evidence of, as yet, unexplained phenomena.

This chapter will try to summarise, briefly, all the results and conclusions obtained and point out where further study would be useful. Also included is a brief discussion of the future of n-InSb as a sub-millimetre wave source, taking into account the results and conclusions of this thesis.

The numerical evaluations of Zawadski's equations[2] and their combination for momentum scattering have been obtained. The numerical evaluation of Conwell's energy loss/gain rate equations[3] have also been obtained. These calculations of the variations of energy and momentum with (effective/average) electron energy/temperature, have shown that for low fields (where the electron energy distribution can be described by the Maxwell-Boltzmann distribution) the electrical characteristics can be determined with some accuracy. At high fields (where the electron energy distribution can no longer be described by the Maxwell-Boltzmann distribution) the lack of accurate knowledge of the electron energy distribution limits the scope of the theory.

The results confirm the results of earlier investigations which show that whilst ionised impurity scattering is the dominant

---

[1]Gornik et.al., Optics & Laser Tech 7 , 121 (1975); I.R. Phys., 16 , 109 (1976) & I.R.Phys. 18 , 691 (1978)

[2]Zawadski, Hbk.Semicon., 1 , 750 (1982)

[3]Conwell, Sol.Stat.Phys.,Suppl. 9 (1967)

momentum scattering process and potential deformation acoustic phonon scattering is the dominant energy scattering process, the mobility increases with electron energy/temperature. A maximum value for the mobility occurs for an electron temperature of between 50 and 100 K (dependent on the impurity and carrier concentrations). This maximum is caused by the acoustic and/or optical phonon scattering processes becoming the dominant momentum scattering process. For electron temperatures below 50 K, the inter-electron interaction affects both momentum and energy scattering processes and maintains the electron energy distribution as a Maxwell-Boltzmann distribution. For electron temperatures abov 50 K, the energy scattering is mainly by optical phonon emission and for electron temperatures above 100 K the momentum scattering is also mainly by optical phonon emission.

At low electric fields ($\approx$ 0.25 Vcm-1) a non-linear effect has been noted. The two most likely explanations for this are the impact ionisation of donors and the transition of the main energy scattering process from a saturated energy scattering process to another scattering process which requires higher electron energies to obtain balance. The results obtained show no sharp increase in electron concentration at the electric fields involved. Indeed, the carrier concentration shows a steady increase through the region concerned, before reaching the expected value equal to the uncompensated donor concentration (measured at 77 K). The conclusion might appear to contradict earlier investigations, but those were carried out at lower temperatures and under the effect of a magnetic field. Under those conditions the effect of impact ionisation of 'frozen out' impurities on the electrical characteristics is expected to be several orders of magnitude larger than the energy scattering process transition. With low magnetic fields and low temperatures a combination of the two effects may be seen.

At medium electric fields ($\approx$ 20 Vcm^{-1} when B = 0 T; $\approx$ 30 Vcm^{-1} when B = 0.7 T), a non-linearity was observed in crystals 3, 5 and all other crystals taken from sample 3. The measurement of the electron concentration before, during and after this region showed a sharp rise in the carrier concentration linked to this non-linearity. The conclusion is that the wafer has been contaminated and a deep donor has been introduced. The concentration of the uncompensated

deep donors varied between crystals from 1 x 10^{14} to 3 x 10^{14} cm^{-3}. The effect on the electron conductivity and mobility was large. The mobility quoted by the manufacturers was not achievable. In fact, a mobility a tenth of that quoted (for a lattice temperature of 77K) was the maximum obtained (though this was not thought to be the absolute maximum). This result provides confirmation of a similar result obtained by Trifonov & Yaremenko. The proposal is that the decrease in conductivity is due to the increase in ionised impurity scattering. The validity of this proposal for the results of Trifonov & Yaremenko[4] is unknown as the total impurity concentration is not divulged. The above proposal is also dependent on the compensation of the deep donors being large (> 0.99). Another possible cause of the low mobility is resistive contacts. The resistive effect could not be directly evaluated as a two wire system was used throughout. The observation that three separate contacting arrangements provided the identical electrical characteristics, leads to the conclusion that either the different contacts have exactly the same resistive effect (which is possible but unlikely) or the contacts have no noticeable effect.

At high electric fields (≈ 80 Vcm^{-1}) a non-linearity with an accompanying hysteresis was observed. This confirmed results obtained by Puplett et.al.[5]. The non linearity may also be connected with spontaneous sub-millimetre wave oscillations under impact ionisation conditions as considered (theoretically) by Vladimirov et.al.[6]. Emission from this region was first observed by Larrabee & Hicinbothem[7]. They recorded microwave emission for electric fields of 250 Vcm^{-1} at a lattice temperature of 77 K. This coincides with the large increase in the current density and the onset of a large hysteresis as observed by Puplett et.al.. If the hysteresis is linked with the impact ionisation of the valence band then the reduction of the lattice temperature is seen to reduce the critical field to ≈ 70 Vcm^{-1} though the current density remains at about 250 Acm^{-2}.

Under the assumption that impact ionisation of the valence band occurs, most of the electrical characteristics observed can be

---

[4]Trifonov & Yaremenko, Sov.Phys.Semicond. 5 , 839 (1971)

[5]Puplett & White, Private Communication (see appendix 6.1)

[6]Vladimirov et.al., Sov.Phys.Semicond. 14 , 247 (1980) & 15 , 23 (1981)

[7]Larrabee & Hicinbothem, Proc.7th.Int.Conf.on Phys.of Semicon., 2 , 181 (Paris,1964)

qualitatively explained. The hysteresis is due to the large increase in carriers and an apparent reluctance for the electrons to relax back to the valence band. The relaxation time is extremely long and approximated from Puplett et.al.'s results to be ≈ 1ms. This agrees well with the observations made here. The non-linearities beyond the critical field, as observed by Puplett et.al. are, as yet, unexplained, though the theory of Vladimirov et.al. does predict the appearance of a dynamic negative differential conductance connected with sub-millimetre wave emission in this region.

The conclusion is that, whilst impact ionisation of the valence band is likely to be the most influential process in the region, further study should be done to obtain information on the electron energy distribution, the intrinsic concentration, the effect of polar optical scattering, the effect of electron hole scattering and the possibility of optical phonon saturation in this region. This ought to be done to obtain the full picture.

Finally, the conclusions on the sub-millimetre wave emission, including the above results, are as follows. For sources which utilise the transitions between Landau levels, the condition for an optimised linewidth is a low field, where electron-phonon interaction is small compared with inter-electron interaction. This condition is a maximum in the absence of a magnetic field at an electric field just above the energy scattering process transition (as noted from the detector characterisation). For maximum power one requires a high field to obtain as many electrons with high energy as possible. Exciting electrons to energies greater than the optical phonon energy is detrimental though, as the electrons will be rapidly relaxed and cannot take part in emission. The interaction with the optical phonons will also cause lattice heating which will broaden the landau levels and hence the linewidth. Under the presence of a magnetic field (necessary for the presence of Landau levels) the electric field levels required are greater, though the field for optimum linewidth is still just above the low field non-linearity. Typical output powers from an n-InSb crystal placed in a light pipe, 40 cm from an n-InSb detector, are 0.12 μW at 1.4 THz and 0.07 μW at 700 GHz. The minimum linewidth obtained is 2.5cm^{-1} which is equivalent to 12 GHz. The placement of the crystal in a resonant cavity could greatly decrease the linewidth, but may also

have an adverse effect on the output power. The situation has not been studied closely, but could be important as it is possible that the resonant cavity could increase the efficiency of the emission process at the signal frequency. This would then improve both the linewidth and the output power. The effect of the cavity on the output power is unknown, but with quasi-optical resonant cavities, with Q - factors of several million, readily available the linewidth could be reduced to ≈ 500 KHz. This compares well with far infra-red lasers in the region.

There are two alternatives to the Landau emission source. The first is that involving the emission related to the impact ionisation of electrons in the valence band. Emission has been observed at low frequencies, but the theoretical appreciation predicts the presence of emission at frequencies into the sub-millimetre wave region. The emission is likely to be similar to that of a noise source as there is nothing to make any one frequency preferential. The effective temperature of the electrons involved is high and the effective temperature of the 'noise source' is expected to be high (10^4 to 10^5 K[8]). Again, the application of a resonant cavity to the situation would have an unknown effect. The second alternative is that of a spin-flip laser. Dimitriev et.al. have demonstrated that a population inversion between the spin-down and spin-up levels of the zeroth Landau levels is possible. The conditions required include, a magnetic field such that the second Landau level has an energy greater than the optical phonon energy (B = 3 T), and an incident intensity of greater than 0.5 Wcm^{-2} and less than 50 Wcm^{-2} or greater than 100 Wcm^{-2}. The population inversion was observed by transmission measurements. The emission properties for a magnetically tuneable spin-flip laser (if the population inversion can be converted into lasing) are unknown, except that the frequency of emission will be equal to a third of the cyclotron emission frequency. So a magnetic field of 2.5 T will cause the frequency to be 1.7 THZ. For frequencies in the range 300 GHz to 1 THz, the magnetic field will be such that the third Landau level will have an energy less than the optical phonon energy and the excitation to the zeroth level will be through the fourth Landau level. Whether a

---

[8]Toshimitsu et.al. Appl.Phys.Letts. 8 , 157 (1966) & Bekefi et.al., Phys.Rev.Letts. 19 , 24 (1967)

population inversion is achievable under these conditions has not been investigated, but would be of interest.

APPENDICES

Appendix 4.1 : Numerical Values for the Variation of the Fermi Level with Temperature and Carrier Concentration

Temp-erature (K)	b	$^{o}L_{o}^{3/2}$	n(a)	$^{o}L_{o}^{3/2}$	n(b)	$^{o}L_{o}^{3/2}$	n(c)	$^{o}L_{o}^{3/2}$	n(d)
1.5	5.5 e4	1.013	0.00	5.0670	2.7	10.13	4.5	50.66	13.7
4.2	1.54 e3	0.216	-1.80	1.08	0.1	2.16	1.1	10.8	4.5
50	0.018	5.3 e3	-5.50	0.026	-4.0	0.053	-3.2	0.26	-1.5
77	0.028	2.8 e3	-6.00	0.01378	-4.7	0.028	-3.9	0.1378	-2.4
100	0.037	1.97 e3	-6.50	9.4 e3	-5.0	0.019	-4.4	0.093	-2.7
150	0.055	0.0109	-5.00	0.015	-4.6	0.02	-4.4	0.061	-3.2
200	0.073	0.097	-2.80	0.099	-2.75	0.103	-2.7	0.129	-2.65
250	0.092	0.376	-1.70	0.378	-1.70	0.38	-1.6	0.399	-1.5
300	0.11	0.932	-0.65	0.934	-0.65	0.935	-0.6	0.95	-0.55
350	0.13	1.785	0.20	1.786	0.20	1.788	0.2	1.799	0.25

$b = \frac{k_B T_L}{E_G}$, $^{o}L_{o}^{3/2}$ = generalised Fermi integral = fraction of electron concentration over the density of states and n(a,b,c,d) are the values of the Fermi levels (in eV above the C.B. minimum) for crystals of carrier concentrations 10^{13}, 5×10^{13}, 10^{14} & 5×10^{14} cm^{-3}.

Appendix 4.2 : Numerical Values for the Variation of the Screening Wavelength with Temperature and Carrier Concentration

Temp-erature (K)	$^{o}L_{1}^{1/2}$	λ	$^{o}L_{1}^{1/2}$	λ
2	5.40e-01	1.20e+02	1.50e+00	7.40e+01
4	1.20e-01	2.00e+02	5.50e-01	9.45e+01
50	4.00e-03	6.00e+02	1.60e-02	2.98e+02
77	3.50e-03	6.20e+02	9.00e-03	3.57e+02
100	3.00e-03	5.80e+02	7.00e-03	3.79e+02
150	7.10e-03	3.40e+02	1.00e-02	2.67e+02
200	7.00e-02	1.00e+02	7.30e-02	9.88e+01
250	2.00e-01	5.60e+01	2.10e-01	5.51e+01
300	4.00e-01	3.80e+01	4.80e-01	3.48e+01
350	9.50e-01	2.40e+01	9.50e-01	2.38e+01

Temp-erature (K)	$\sigma_L^{1/2}$ 1	λ	$\sigma_L^{1/2}$ 1	λ
2	2.07e+00	6.30e+01	3.69e+00	4.70e+01
4	9.50e-01	7.20e+01	2.07e+00	4.87e+01
50	4.00e-01	1.88e+02	1.80e-01	8.89e+01
77	1.85e-02	2.49e+02	7.60e-02	1.23e+02
100	1.00e-02	2.90e+02	6.10e-02	1.28e+02
150	1.25e-02	2.56e+02	4.40e-02	1.37e+02
200	7.50e-02	9.74e+01	8.75e-02	9.02e+01
250	2.26e-01	5.30e+01	2.46e-01	5.09e+01
300	5.00e-01	3.41e+01	5.50e-01	3.25e+01
350	9.50e-01	2.38e+01	9.50e-01	2.38e+01

The screening wavelength is given in nanometers and the carrier concentrations are as given in appendix 4.1

Appendix 4.3 : Numerical Values for the Variation of Electron Lifetime and Mobility with Electron Temperature Under Ionised Impurity Scattering for Different Carrier Concentrations and an Impurity Concentration of $10^{15}cm^{-3}$.

Temp-erature (K)	$1/F_{ii}(a)$	$\tau_{ii}(a)$	$\mu_{ii}(b)$	$1/F_{ii}(b)$	$\tau_{ii}(b)$	$\mu_{ii}(b)$
1.5	1.83e+00	4.87e-13	6.80e+04	3.42e+00	1.50e-12	2.00e+05
4.2	4.80e-01	6.03e-13	8.30e+04	1.16e+00	1.46e-12	1.97e+05
50	1.50e-01	7.69e-12	1.04e+06	1.90e-01	9.70e-12	1.30e+06
75	1.44e-01	1.35e-11	1.80e+06	1.70e-01	1.60e-11	2.16e+06
100	1.37e-01	1.98e-11	2.70e+06	1.55e-01	2.25e-11	3.04e+06

Temp-erature (K)	$1/F_{ii}(c)$	$\tau_{ii}(c)$	$\mu_{ii}(c)$
1.5	8.40e+00	2.45e-12	3.30e+05
4.2	1.82e+00	2.40e-12	3.25e+05
50	2.30e-01	1.18e-11	1.60e+06
75	1.90e-01	1.78e-11	2.40e+06
100	1.60e-01	2.32e-11	3.14e+06

The lifetime is given in seconds and the mobility in $cm^2V^{-1}s^{-1}$. The concentrations are as in appendix 4.1

Appendix 4.4 : Numerical Values of the Variation of the Electron Lifetimes and Mobilities, Under Piezo-Electric Acoustic Phonon Scattering, with Electron Temperature at Various Lattice Temperatures.

Temp-erature (K)	$\tau_{pe}(T_e=T_L)$	$\mu_{pe}(T_e=T_L)$	τ_{pe}(1.5K)	μ_{pe}(1.5K)
5.0000	1.27e-08	1.70e+09	4.23e-08	5.73e+09
10.000	8.98e-09	1.20e+09		
20.000	6.35e-09	8.59e+08	8.47e-08	1.15e+10
40.000	4.49e-09	6.07e+08		
60.000	3.66e-09	4.96e+08	1.47e-07	1.98e+10
80.000	3.18e-09	4.30e+08		
100.00	2.84e-09	3.84e+08	1.89e-07	2.56e+10
120.00	2.59e-09	3.51e+08		
140.00	2.40e-09	3.25e+08	2.24e-07	3.03e+10
160.00	2.25e-09	3.04e+08		
180.00	2.12e-09	2.86e+08		
200.00	2.00e-09	2.72e+08	2.68e-07	3.62e+10

Temp-erature (K)	τ_{pe}(4.2K)	μ_{pe}(4.2K)	τ_{pe}(77K)	μ_{pe}(77K)
5.0000	1.52e-08	2.06e+09		
10.000				
20.000	3.04e-08	4.11e+09		
40.000				
60.000	5.27e-08	7.13e+09		
80.000			3.30e-09	4.50e+08
100.00	6.80e-08	9.20e+09	3.69e-09	4.99e+08
120.00				
140.00	8.05e-08	1.09e+10	4.37e-09	5.90e+08
160.00				
180.00				
200.00	9.62e-08	1.30e+10	5.22e-09	7.06e+08

The lifetime is given in seconds the mobility is given in $cm^2V^{-1}s^{-1}$. The lattice temperatures are given in the brackets.

Appendix 4.5 : Numerical Values of the Variation of the Electron Lifetime and Mobility, Under Potential Deformation Acoustic Phonon Scattering, with Electron Temperature at Various Lattice Temperatures.

Temp-erature (K)	$\tau_{pd}(T_e=T_L)$	$\mu_{pd}(T_e=T_L)$	$\tau_{pd}(1.5K)$	$\mu_{pd}(1.5K)$
10.000	2.77e-10	3.75e+07	1.85e-09	2.50e+08
20.000	9.80e-11	1.33e+07		
40.000	3.47e-11	4.69e+06		
60.000	1.89e-11	2.55e+06		
80.000	1.23e-11	1.66e+06		
100.00	8.77e-12	1.18e+06	5.25e-10	7.90e+07
120.00	6.67e-12	9.00e+05		
140.00	5.29e-12	7.16e+05		
160.00	4.33e-12	5.86e+05		
180.00	3.63e-12	4.90e+05		
200.00	3.10e-12	4.19e+05	4.10e-10	5.59e+07
220.00	2.70e-12	3.64e+05		
240.00	2.36e-12	3.16e+05		
260.00	2.10e-12	2.83e+05		
280.00	1.87e-12	2.53e+05		
300.00	1.69e-12	2.28e+05	3.38e-10	4.57e+07
320.00	1.53e-12	2.07e+05		
340.00	1.40e-12	1.89e+05		
360.00	1.28e-12	1.74e+05		
380.00	1.18e-12	1.60e+05		
400.00	1.10e-12	1.48e+05	2.90e-10	3.95e+07

Temp-erature (K)	τ_{pd}(4.2K)	μ_{pd}(4.2K)	τ_{pd}(77K)	μ_{pd}(77K)
10.000	6.60e-10	8.90e+07		
20.000				
40.000				
60.000				
80.000			1.27e-11	1.72e+06
100.00	2.09e-10	2.82e+07	1.14e-11	1.54e+06
120.00				
140.00				
160.00				
180.00				
200.00	1.48e-10	2.00e+07	8.05e-12	1.09e+06
220.00				
240.00				
260.00				
280.00				
300.00	1.20e-10	1.63e+07	6.58e-12	8.89e+05
320.00				
340.00				
360.00				
380.00				
400.00	1.04e-10	1.41e+07	5.70e-12	7.70e+05

The lifetime is given in seconds the mobility is given in $cm^2V^{-1}s^{-1}$. The lattice temperatures are given in the brackets.

Appendix 4.6 : Numerical Values of the Variation of the Electron Lifetime and Mobility, Under Polar Optical Phonon Scattering, with Electron Temperature at Various Lattice Temperatures.

Temperature (K)	$\mu(<\Theta)$	$\mu(>\Theta)$	F_{op}	τ(Zaw)	μ(Zaw)
80	4.20e+06		9.33e-01	1.50e-12	2.06e+05
100	2.20e+06		9.21e-01	1.38e-12	1.87e+05
120	1.40e+06				
140	1.00e+06		8.93e-01	1.20e-11	1.63e+05
160	7.70e+05		8.73e-01	1.15e-12	1.56e+05
180	6.18e+05				
200	5.13e+05		8.18e-01	1.10e-12	1.49e+05
240			7.73e-01	1.06e-12	1.44e+05
250		2.88e+05			
260		2.82e+05	7.19e-01	1.10e-12	1.49e+05
270		2.77e+05			
280		2.72e+05			
290		2.68e+05			
300		2.63e+05	6.59e-01	1.12e-12	1.51e+05
320		2.55e+05			
340		2.47e+05	5.95e-01	1.16e-12	1.57e+05
360		2.40e+05	5.26e-01	1.28e-12	1.73e+05
380		2.33e+05			
400		2.28e+05			

Lifetimes are in seconds and mobilities are in $cm^2V^{-1}s^{-1}$. The first two columns are from using Blatt's equations and are for electron temperatures below and above the Einstein temperature. The last three columns are from using Zawadski's equations with the Screening function and the lifetime and mobility.

Temperature (K)	$\mu(T_L)$	μ(1.5K)	μ(4.2K)	μ(77K)
80	3.00e+06	1.60e+08	5.70e+07	3.10e+06
100	8.00e+05	5.30e+07	1.90e+07	1.00e+06
200	2.50e+05	3.30e+07	1.20e+07	6.50e+05
300	1.00e+05	2.00e+07	7.14e+06	3.90e+05
400	7.00e+04	1.86e+07	6.66e+06	3.34e+05

The above is calculated from data obtained by Trifonov & Yaremenko. Again the lifetimes are in seconds and mobilities are in $cm^2V^{-1}s^{-1}$. The lattice temperatures are given in the brackets.

Appendix 4.7 : Numerical Values of the Variation of the Electron Lifetime and Mobility, Under Non-Polar Optical Phonon Scattering, with Electron Temperature at Various Lattice Temperatures.

Temp-erature (K)	$\tau(T_L)$	$\mu(T_L)$	τ(1.5K)	μ(1.5)
80	5.26e-08	6.71e+09	2.80e-06	3.57e+11
140	1.20e-08	1.45e+09	1.12e-06	1.36e+11
190	3.62e-09	4.20e+08	4.59e-07	5.30e+10
250	1.57e-09	1.70e+08	2.60e-07	2.86e+10
300	8.64e-10	9.06e+07	1.73e-07	1.81e+10
350	5.18e-10	5.14e+07	1.21e-08	1.20e+10
400	3.32e-10	3.10e+07	8.85e-08	8.31e+09
Temp-erature (K)	τ(4.2)	μ(4.2)	τ(77K)	μ(77)
80	1.00e-06	1.30e+11	5.26e-08	6.71e+09
140	4.00e-07	4.87e+10	2.40e-08	2.90e+09
190	1.65e-07	1.90e+10	8.60e-09	9.98e+08
250	9.34e-08	1.03e+10	4.90e-09	5.40e+08
300	6.17e-08	6.47e+09	3.24e-09	3.40e+08
350	4.32e-08	4.28e+09	2.27e-09	2.25e+08
400	3.16e-08	2.97e+09	1.66e-09	1.56e+08

The lifetime is given in seconds the mobility is given in $cm^2V^{-1}s^{-1}$. The lattice temperatures are given in the brackets.

Appendix 4.8 : Numerical Values of the Variation in the Rate of Energy Loss from the Electrons Through Acoustic Phonon Scattering for lattice temperatures of 1.5, 4.2 & 77 K.

Temperature (K)	dE/dt (1.5K) (W)	dE/dt (4.2K) (W)	dE/dt (77K) (W)
5	1.59e-15	3.63e-16	
10	5.46e-15	3.72e-15	
20	1.68e-14	1.43e-14	
30	3.17e-14		
40	4.14e-14		
50	6.96e-14	6.57e-14	
60	9.20e-14		
70	1.16e-13		
80			5.45e-15
100	2.00e-13	1.94e-13	4.67e-14
200	5.70e-13	5.62e-13	3.53e-13
300	1.05e-12	1.04e-12	7.84e-13
400	1.62e-12	1.61e-12	1.31e-12

Appendix 4.9 : Numerical Values of the Variation of the Rate of Energy Loss form the Electrons Through Optical Phonon Scattering at lattice temperatures of 4.2 and 77 K.

Temperature (K)	(X)	dE/dt (4.2) (W)	(X)	dE/dt (77K) (W)
20	7.16e-7	3.45e-15		
50	3.7e-3	1.73e-11		
80	2.9e-2	1.32e-10		
90	4.3e-2	1.97e-10		
100	5.9e-2	2.69e-10	3.5e-2	1.58e-10
120	9.44e-2	4.14e-10		
140	1.33e-1	5.98e-10		
160	1.7e-1	7.36e-10		
180	2.1e-1	9.09e-10		
200	2.4e-1	1.04e-09	2.22e-1	9.61e-10
220	2.75e-1	1.18e-09		
240	3.07e-1	1.30e-09		
260	3.36e-1	1.41e-09		
280	.64e-1	1.53e-09		
300	3.91e-1	1.65e-09	3.75e-1	1.58e-09
320	4.1e-1	1.74e-09	3.95e-1	1.68e-09
340	4.36e-1	1.82e-09	4.21e-1	1.75e-09
360	4.54e-1	1.85e-09	4.4e-1	1.80e-09
380	4.77e-1	1.92e-09	4.64e-1	1.87e-09
400	4.92e-1	1.94e-09	4.78e-1	1.89e-09

The value denoted by (X) is equal to the bracketted term in equation 4.48.

Appendix 5.1 : Data on sample 3 as given by the manufacturer.

Cominco Ltd. / P.O. Box 3000, Trail, British Columbia, Canada V1R 4S8
Tel. (604) 364-4772 / Telex 041-4426.

Cominco Electronic Materials

tronic Materials

INDIUM ANTIMONIDE

Test Report
Certificate of Compliance

Date: November 2, 1988
Customer: University of St. Andrews
Purchase Order Number:
Contract Number: C 61744-A
Item Number:

NADA AWARDS FOR EXCELLENCE 1985

Electronic Grade: 6/9 Carrier Type: N Dopant: Nil

Lot Number(s): W-4105-H Slice No. 69
No. of Slices: 1

Lot Weight(s) (g): 2.0
Dimensions: Thick: 0.4 +/- 0.025 mm Lateral Dia: 31 X 34 mm

Face Orientation: (111) Nominal Edge Flat: (N/A) +/-
Etch Pit Density: <10 (average pits/cm²)

ELLENCE IN INNOVATION

Surface Finish

A Surface: Both Faces Lapped.
B Surface:

Electrical Parameters at 77K

Lot W-4105-H

Resistivity (ohm-cm)	0.005 - 0.11	
Mobility (cm²/V-S)	>6.0	E5
Carriers (cm⁻³)	0.05 - 1.1	E14

Comments: This slice is packaged with a label adjacent to the A face.

Slice handling instructions are enclosed.

This is to certify that all work done, materials and/or processes furnished or performed are in accordance with our normal process controls and meet all requirements of the specifications called for on this purchase order and referenced documents.

Certified by: D.A. Vanness Title: Foreman, Semiconductor Plant 1

S.O. #4454

Appendix 5.2 : Crystal Preparation and Contacting Procedures

Preparation of Crystals from sample 3

1/ Remove crystal from Iso-Propanol
2/ Wash with Toluene, Acetate & Acetone (in that order)
3/ Cleave with scalpel blade

Contacting Procedure for crystals from sample 3

1/ 'Dots' of Indium were cut;
2/ The Dots were placed at the ends of the crystals, they were pressed on firmly but gently so as to affix them;
3/ The crystal was then placed onto a hot-plate in a gas chamber;
4/ An inert gas mixture was passed through the chamber and over the crystal;
5/ The crystal was then heated to 160°C (Indium melting point),
6/ Flushed with acid,
7/ Heated to 350°C (the alloying temperature),
8/ Flush with acid,
9/ And left for five minutes;
10/ The crystal was then allowed to cool;
11/ Once the crystal had been cool for several minutes it was removed from the hot-plate;
12/ A dot of nail varnish was placed on the crystal so as to stick it to a piece of filter paper;
13/ The filter paper was then securely attached below a microscope;
14/ The top half of the indium dots were then melted and wires inserted into the dots;
15 The nail varnish was then removed by Acetone.

The crystal from sample 1 was contacted in a similar way, though the whole process was done inside a gas chamber. Also the indium dots surrounded the entire ends of the crystal whereas in the above method they were place on the ends. The detector crystal was contacted at one end as described above and was placed in a bath of indium at the other.

Appendix 6.1 : Report by Puplett & White which gives confirmation of results obtained here and gives other data of relevance and interest.

Electrical Characteristics of Indium Antimonide Detector F18.

Introduction.

The voltage-current characteristic of the Indium Antimonide detector F18 has been coarsely measured throughout the range of 0 to 16 volts, between 0 and 2 Amps and temperatures between 4.2K and 290K. The measurements were made using a triangular shaped pulse with a rise time of approximately 2ms. It is found that the detector shows marked negative slope resistance at three different voltages depending upon the temperature.

Measurement System.

A schematic diagram of the measurement system is shown in Fig. 1.

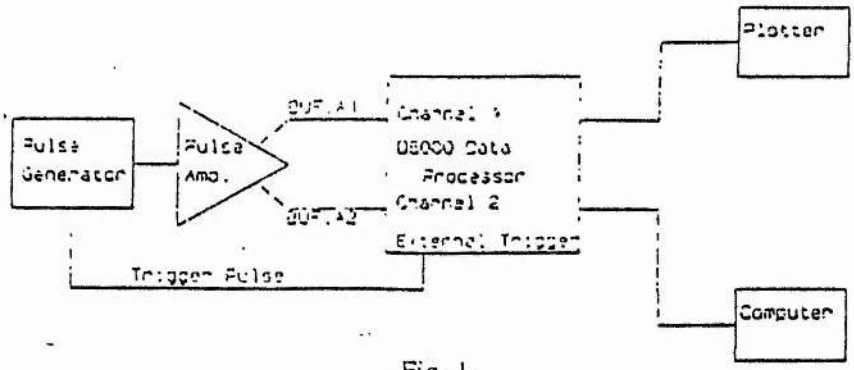

Fig. 1.

The circuit diagram of the pulse amplifier is shown in Fig. 2.

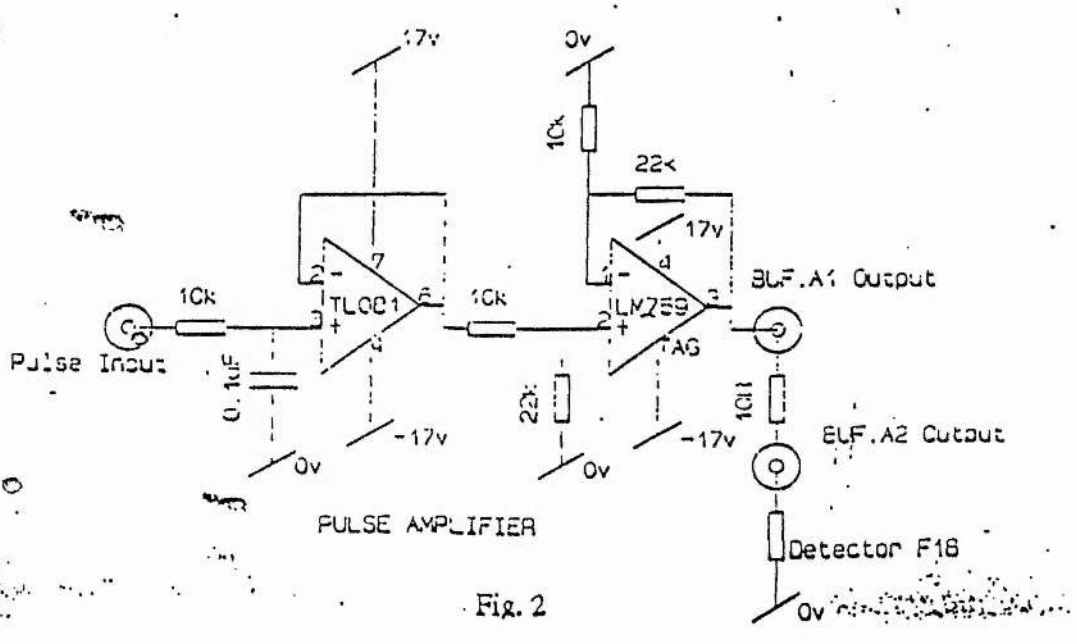

Fig. 2

A positive going pulse of variable amplitude, approximately 2ms wide and with a period of 1 second was integrated using a simple RC circuit having a time constant of 10ms to give an approximate triangular waveform. This signal was buffered with an unity gain amplifier and was further amplified by a factor of two in a power amplifier. The signal was then applied to the detector through a load resistor of 10 Ohms. This resistor was on one occasion changed to an Ohm to obtain a higher electrical field across the detector. Likewise the width of the pulse was varied for the same reason. This was usually to initiate the negative slope resistance characteristic.

The voltage across the load resistance and the detector, that is the voltage at the BUF.A1 output and the corresponding voltage across the detector at the BUF.A2 output was sampled at 20us intervals using a Analogic D6000 Data Processor. Normally 256 samples were taken. Using these values the D6000 can be programmed to calculate the current through the detector and its resistance as follows:-

```
10 SUB.A1 = BUF.A1 - BUF.A2
20 DIV.A1 = SUB.A1 / A          /* DIV.A1 is the current . A = 10. */
30 DIV.A2 = BUF.A2 / DIV.A2     /* DIV.A2 is the resistance. */
```

Where 'A' has previously been assigned the value of the load resistance.

Plots of resistance v. voltage or current v. voltage can then be made.

It has been useful to store the values in BUF.A1 and BUF.A2 on a PC type computer. Further reduction of the data is then easily done using a spreadsheet.

A trace of BUF.A1 and BUF.A2 is shown in Fig. 3 below.

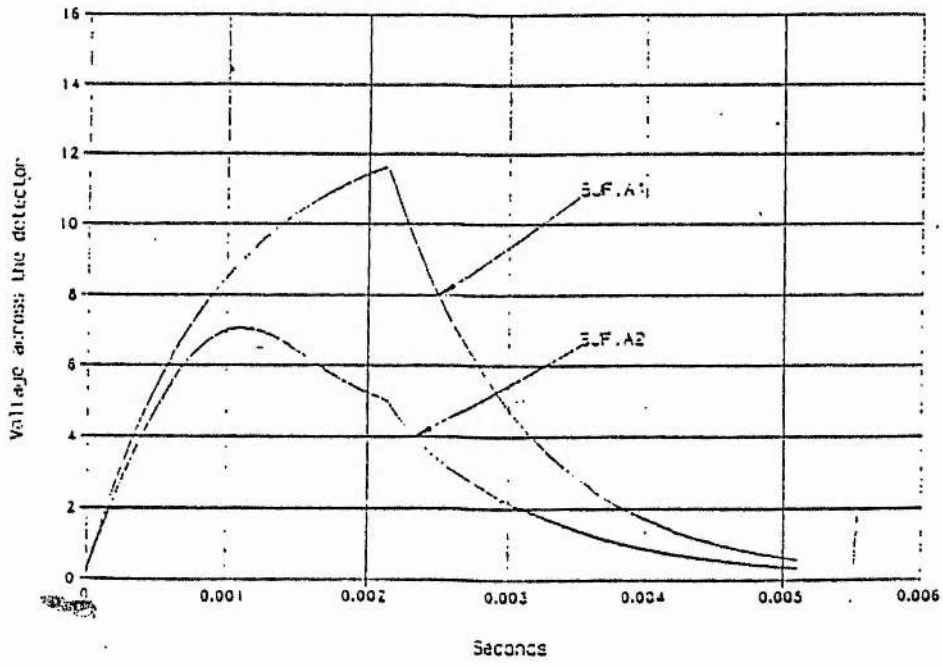

Fig. 3

Test Results.

Figs. 4 and 5 shows the i-v characteristics of a 47 Ohm resistance and a diode.

Figs. 6 and 7 show the i-v characteristic of the detector for low voltage and current at 4.2K. Normally the detector would be biased somewhere on the i-v curve of Fig. 6. The noise on the trace in fig. 6 is the digitization noise of the D6000.

Since these characteristics are those expected, it is assumed that the measurement system performs correctly.

Low Temperature Results.

The detector element and its mount was mounted on a length of 3mm diameter stainless steel tubing to form a dipstick. A calibrated germanium resistance thermometer was placed near to the detector and the resistance measured with the 4-wire method using a resistance bridge. The calibration of the thermometer has been proved to be wrong by later measurements. However the it is felt that the calibration is good at 4.2K and progressively getting worse as the temperature rises, such that at 77K the thermometer is indicating 90K. Therefore the values that appear beside the various curves in the following figures should be taken to indicate trends in the temperature.

The range of temperature was obtained by dipping the detector into boiling liquid Helium or boiling liquid Nitrogen to give the 4.2K and the 77K fixed points and intermediate temperatures up to room temperature (290K) by withdrawing the dipstick from the liquid.

4.2K to 80K Results.

The resistance - voltage characteristics are shown in Figs. 8a and 8b. The Fig. 8a shows the characteristic for the voltage increasing across the detector element and Fig 8b the rest of the measurement. These measurements have been split in this way to show the effect of temperature rather than the hysteresis. The letters labelling the curves refer to the data file in which the data is stored and can be used to cross reference between Figs. 8a and 8b. The temperature is an estimate, bearing in mind the comments above.

For the 4.2K measurements the temperature is well defined since the detector and thermometer were both in the liquid helium. This means that the difference in the voltage across the detector element at 4 to 5 volts, where the resistance changes so abruptly for curves T,V,and W, cannot be explained simply by temperature effects, unless these changes occur for temperature differences of about 5mK. The temperature of 5mK is the temperature corresponding to the differences in the thermometer resistance if our calibration is good at 4.2K. This effect may well explain the observation that Jim and Dayrl make, when they say that the falling edge of the pulse in their pulse measurements jumps about. Or, which is more possible, the measurements are at fault.

The data in Fig. 8b shows only a little sign of any abrupt changes in resistance in curves CC and DD at 4 Volts. A possible explanation for this is that the carriers are loosing their energy through interaction with the lattice of the crystal.

The data shown in Fig. 9 illustrates the warming of the detector element. For this graph the detector was slowly withdrawn from the liquid Helium until an estimated temperature 80K was reached. A constant pulse width and amplitude was kept throughout.

77K to 290K Results.

The data in Figs. 10a and 10b were obtained by slowly inserting the detector into the cold gas above liquid Helium. Considering the uncertainties in the temperature measurements in this range of temperatures the values given are really guesses. For example later measurements indicate that the curve 'Q' was taken at about 77K. This data of this curve shows that there is a large negative slope resistance at 12 to 13 volts.

After the measurement above the detector went open circuit. Reconnecting it the following three measurements were made before it again failed.

Quite large amounts of power are dissipated in the detector element, for example for curve 'Q' in Fig. 10b the power at 10 volts is about 5 Watts. Given this large dissipated power there was the possibility that the detector element was being heated to quite high temperatures, say just below room temperature. The resistance verses time curve of Fig. 15 taken as the element warmed to room temperature shows that the peak resistance is about the same as it is on curve 'Q' in Fig. 10a.

To test this theory a magnetic field of about 0.2 Tessla was placed such that the lines of flux cut the detector perpendicular to electric field. The Figs. 11 and 12 show the result obtained with the field and without the field. It is obvious from these figures that the negative slope resistance of the detector element is not the consequence of a physical increase in temperature.

For Figs 11 and 12 the load resistance was decreased to 1 Ohm to obtain a higher voltage across the detector to get it to "strike". Although this was successful the consequence was that the results are more noisy due to current being proportional to the difference between two near equal voltages. The traces for 0.2T have both been smoothed with the digital filter:- $R_n = (R_{n-2} + R_{n-1} + R_n + R_{n+1} + R_{n+2}) / 5$. Where R_n is the resistance of the n^{th} data point.

Fig. 13 shows the element characteristic at an ambient temperature of 290K with the same conditions as above.

Fig. 14 is somewhat of a mess! It shows how the resistance is changing as the detector element is allowed to warm from 77K. The various bands of traces are due to the graph plotting routine of the D6000 auto-scaling. It is better to ignore the bands 'B' to 'F'. Band 'A' however does show that time rate of change of the negative slope resistance is very high. Although it is not obvious from the graph the time of transition is about the same as the sampling time of the D6000.

Two other observations:-

a).The small increase in the resistance after the transition is notable. This can also be seen in Fig. 11.

b).The minimum resistance is about the same as the resistance at 290K. This also applies to Figs 11 and 12.

Observations that were made but not PROVEN.

I did feel that for the measurements at 77K the negative slope resistance did not immediately "strike", particularly when first cooled. I had to increase the pulse width until it did so.

Illuminating the detector element with a torch, made the negative slope resistance occur at a lower voltage. This effect was not observed with a red or yellow light emitting diode close to the element. An infra-red diode has not yet been tried. The effect could have been due to the intensity of the radiation and not to the wavelength or intensity and wavelength.

Comment.

If the i-v characteristic of Fig. 6 and 7 is reformed as a resistance-voltage characteristic then it shows the same type of negative slope resistance found at higher temperature. Therefore the mechanism that accounts for Figs. 6 and 7 could account for the others.

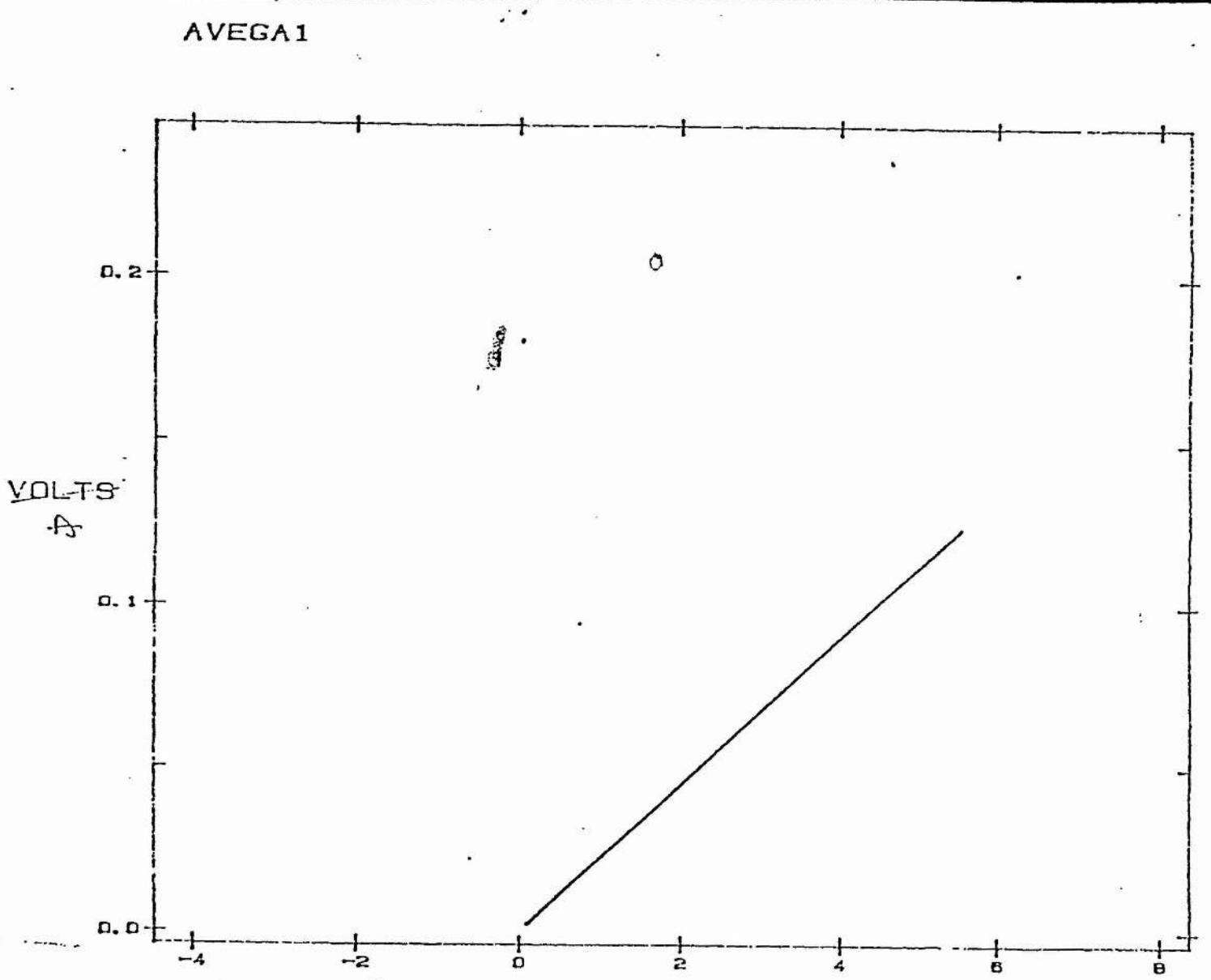

FIG 4

UNITA1

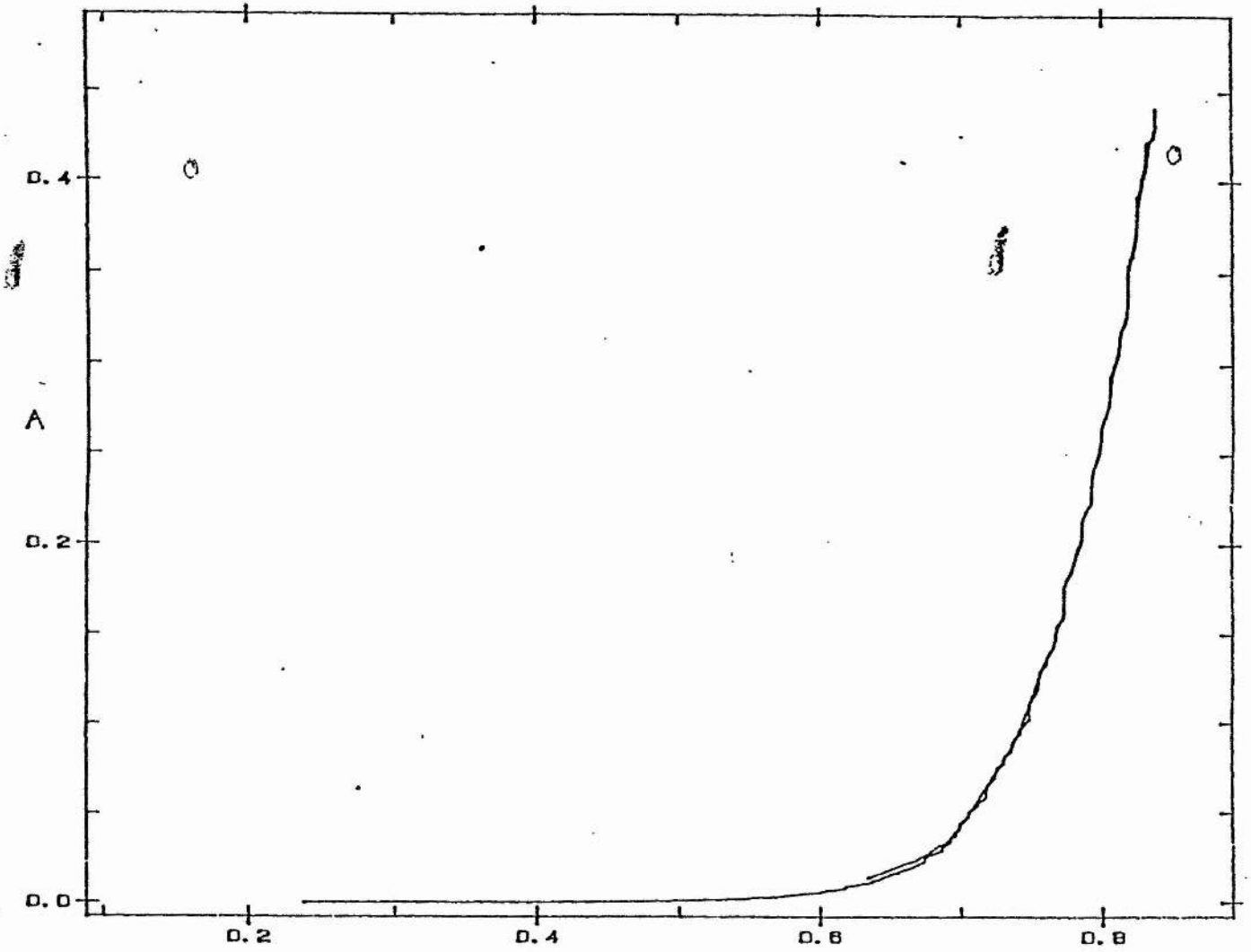

Fig 5

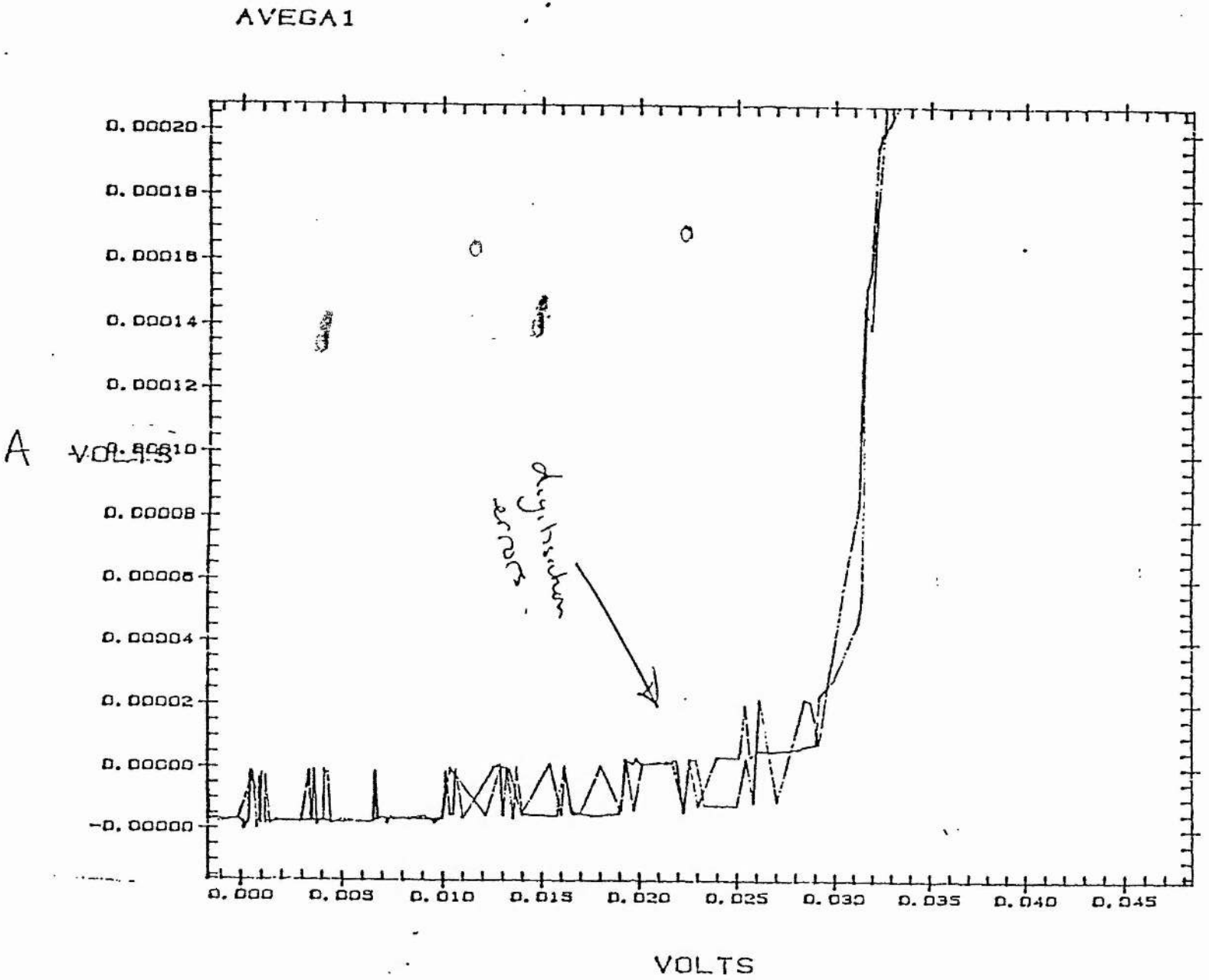
AVEGA1
0.00020
0.00018
0.00016
0.00014
0.00012
0.00010
0.00008
0.00006
0.00004
0.00002
0.00000
-0.00000
A
VOLTS
0.000
0.005
0.010
0.015
0.020
0.025
0.030
0.035
0.040
0.045
VOLTS

Fig. 6.

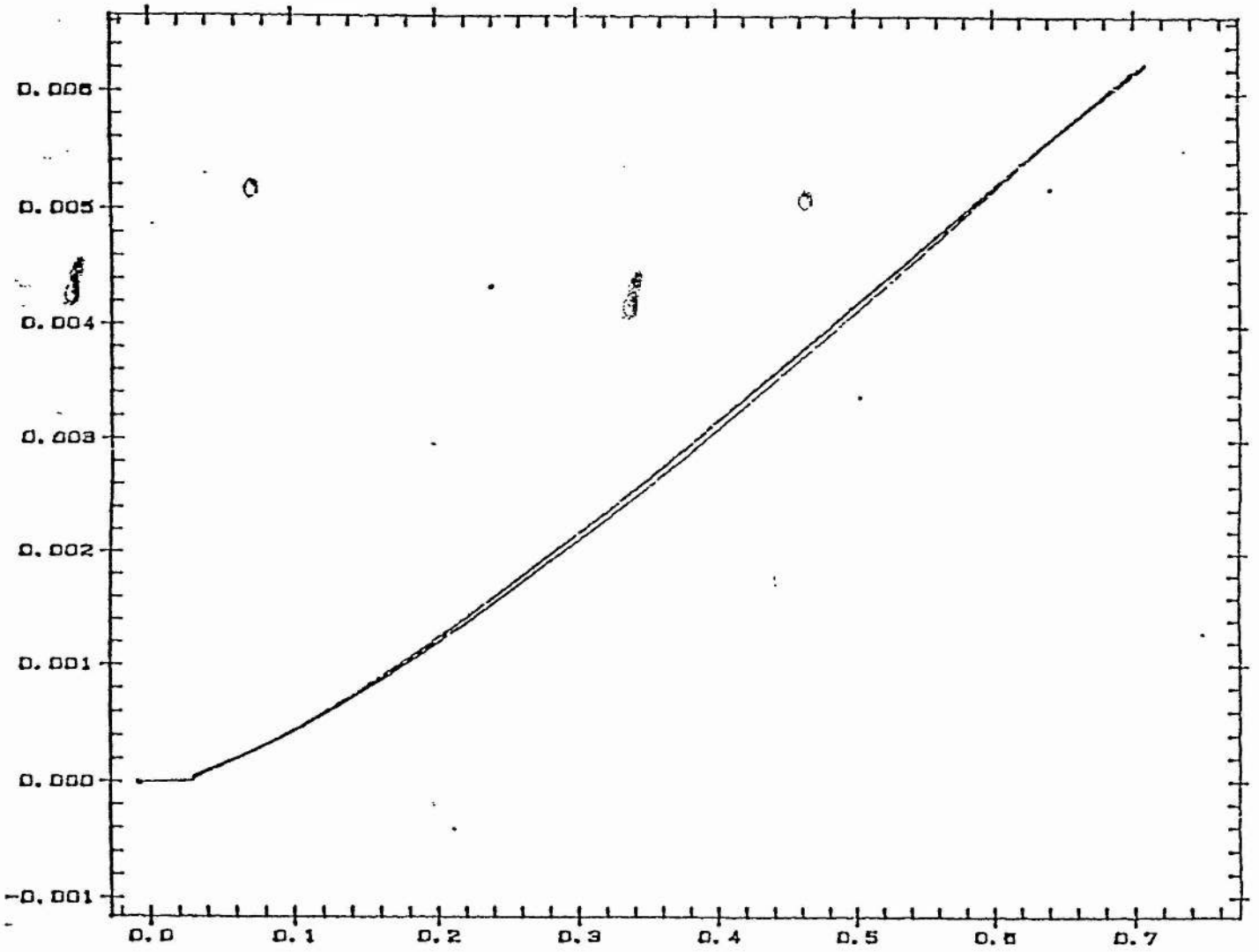
0.006
0.005
0.004
0.003
0.002
0.001
0.000
-0.001
0.0
0.1
0.2
0.3
0.4
0.5
0.6
0.7
AMPS
VOLTS

Fig 7

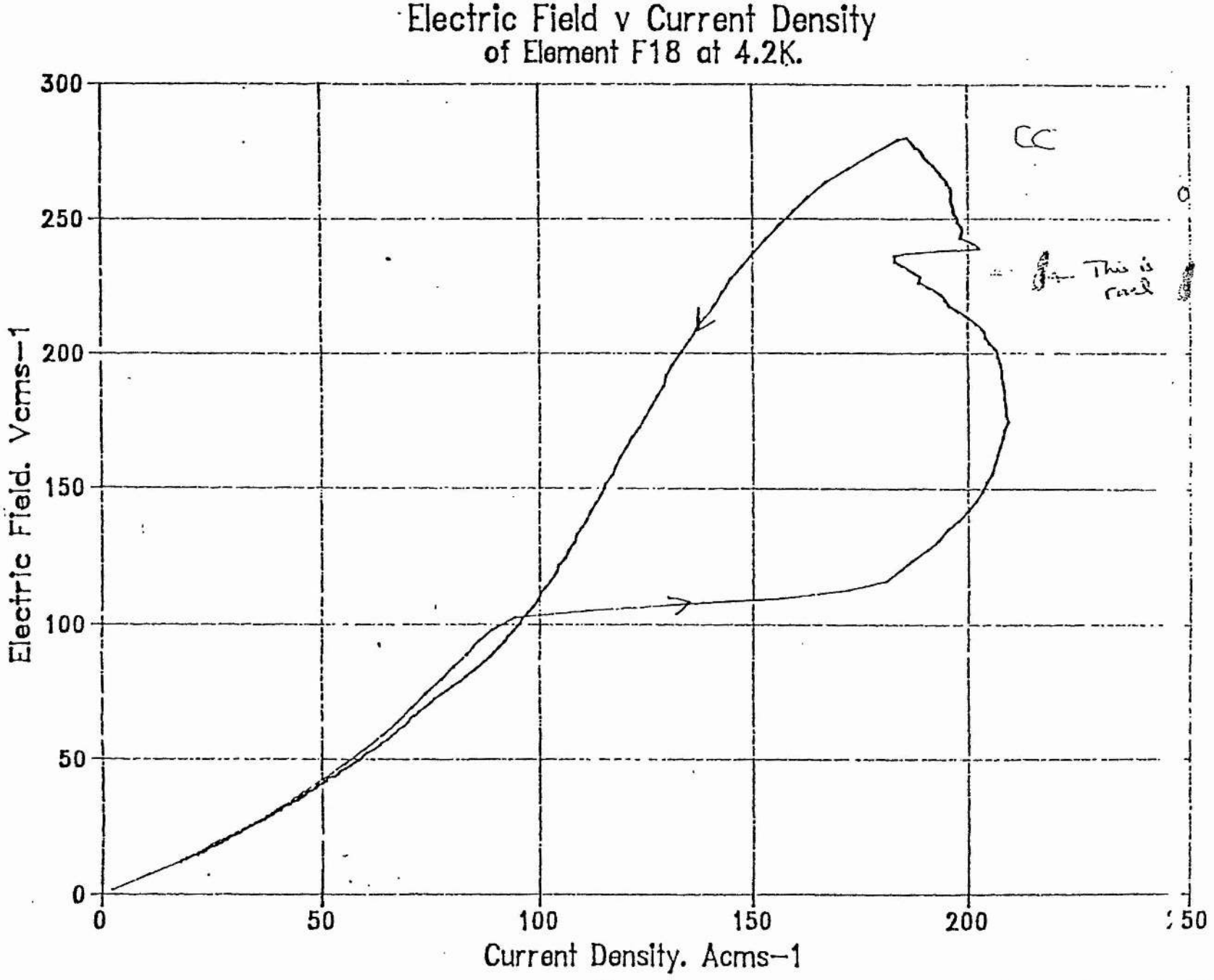
Electric Field v Current Density
of Element F18 at 4.2K.
300
250
200
150
100
50
0
Electric Field. Vcms-1
0
50
100
150
200
250
Current Density. Acms-1
CC
This is
real

Temperature – Resistance – Voltage
of Element F18.

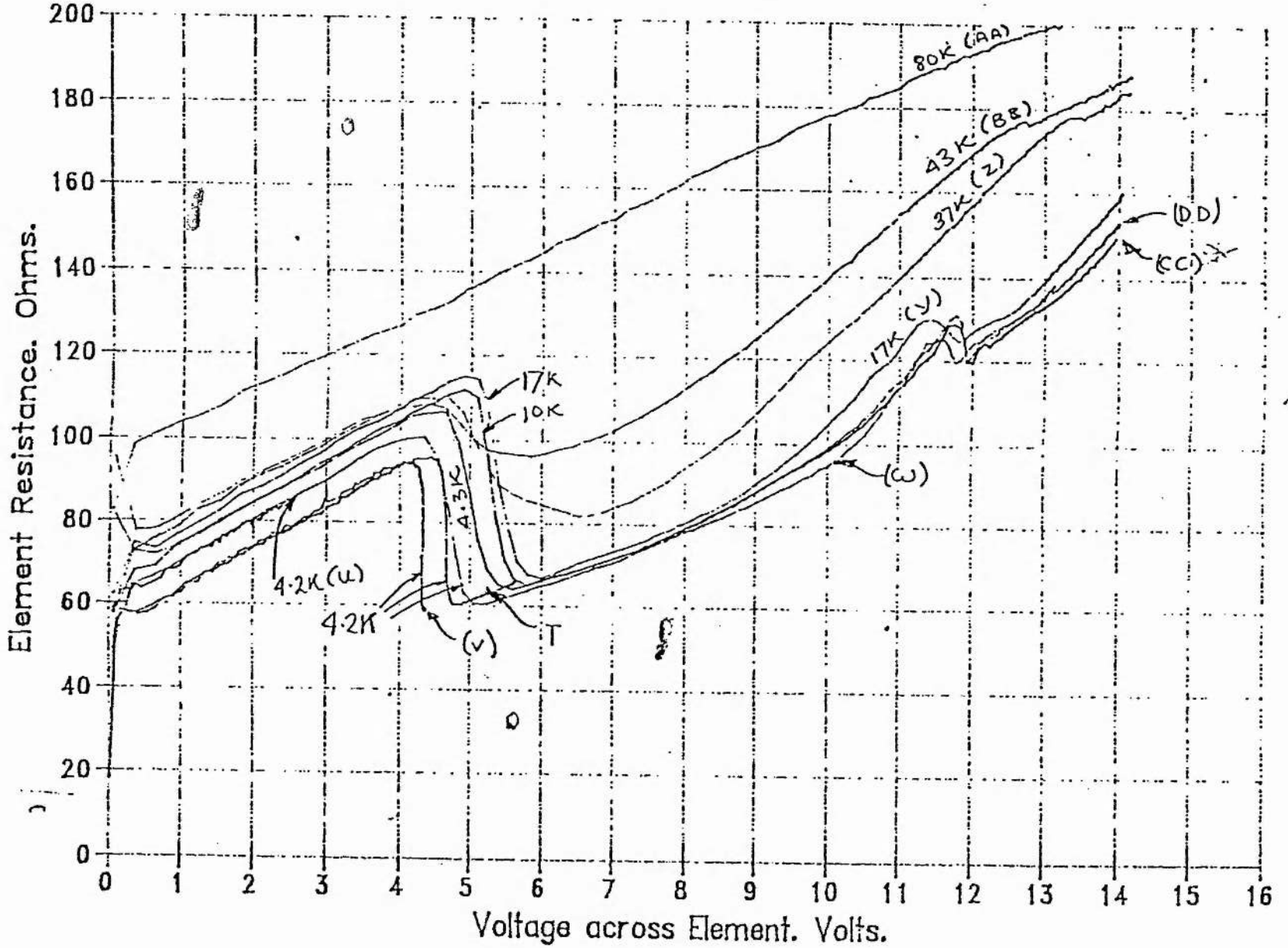

Temperature – Resistance – Voltage of Element F18.

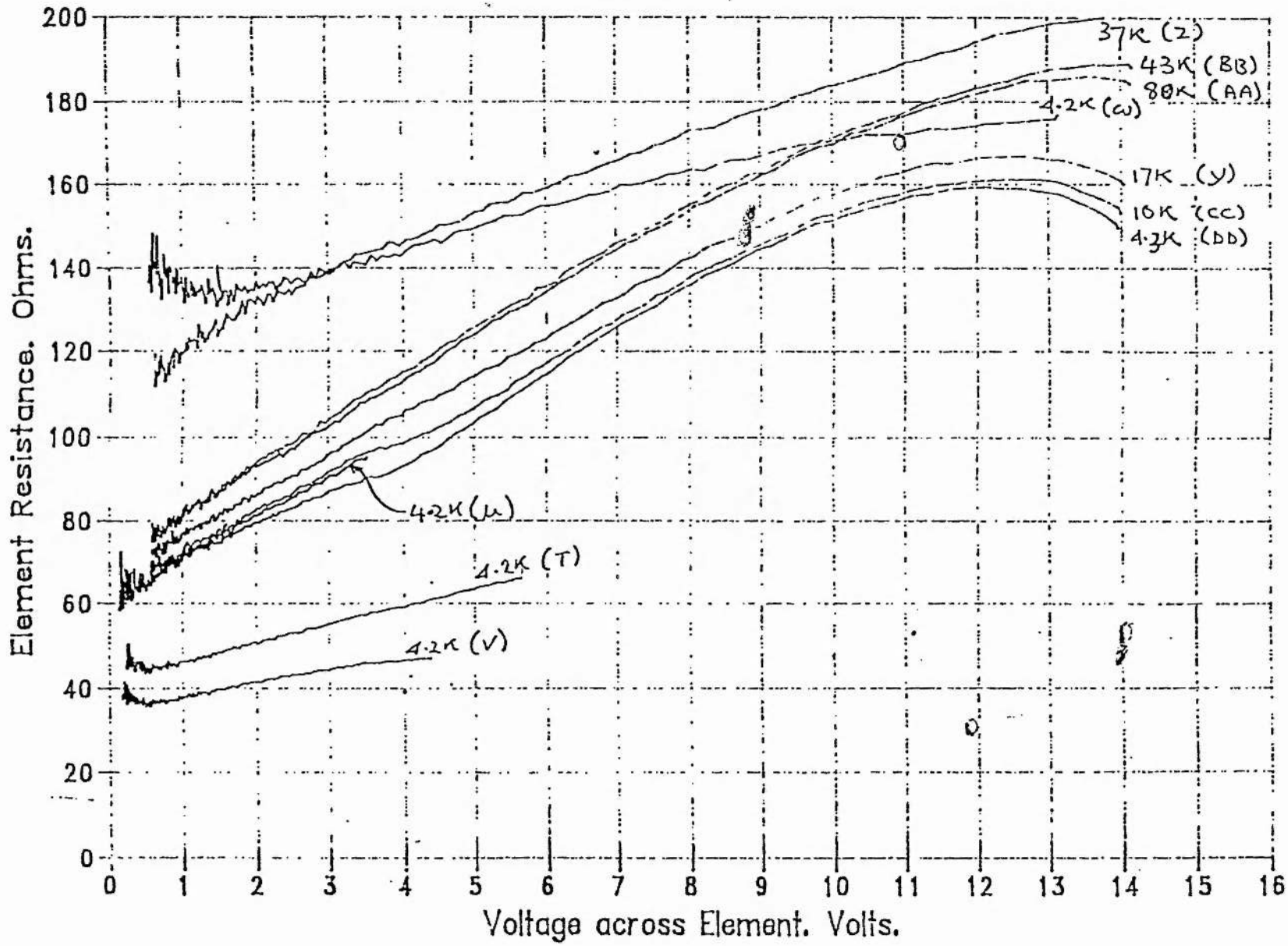

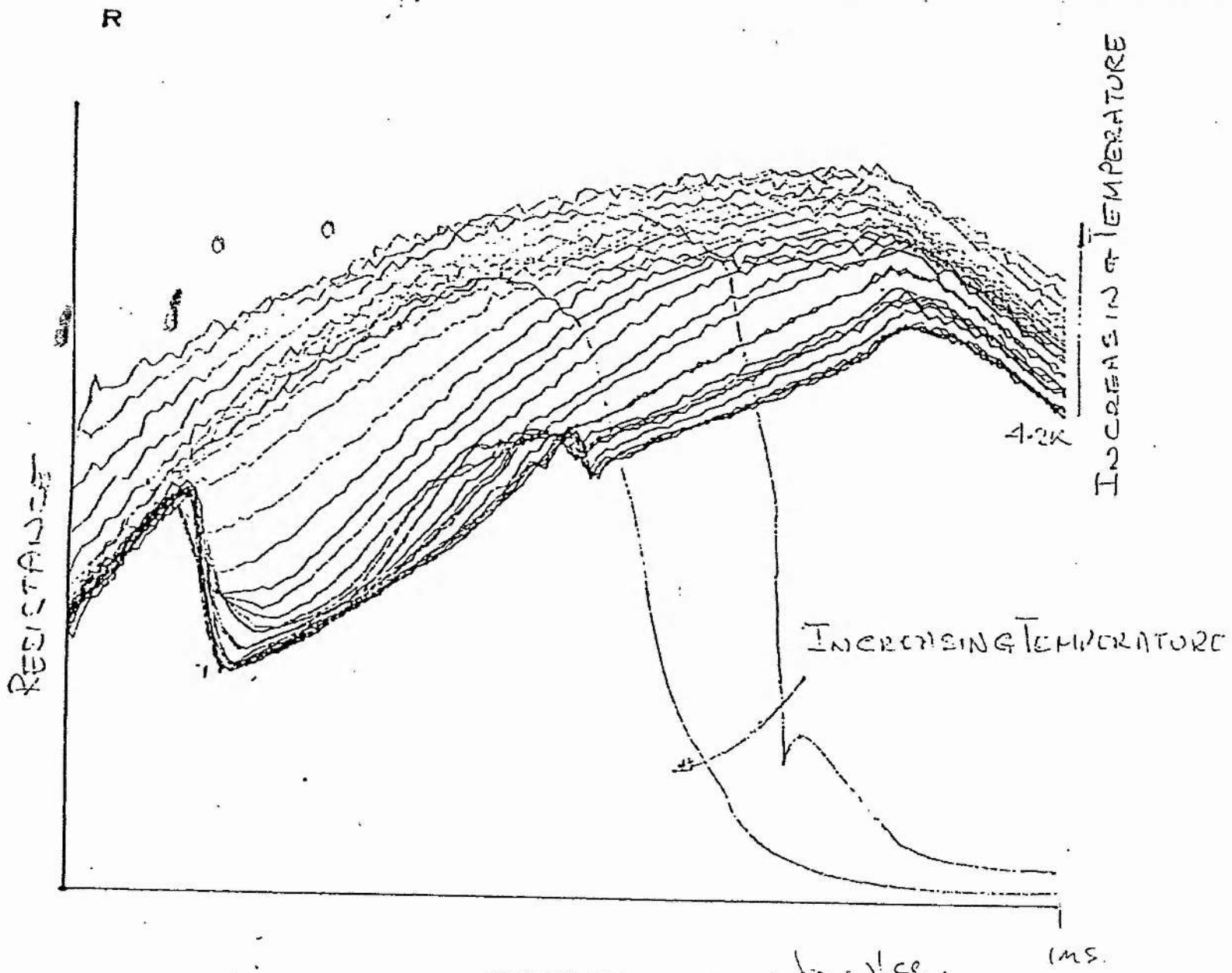
R
RESISTANCE
4·2K
INCREASING TEMPERATURE
INCREASING TEMPERATURE
1MS.
SECONDS

Fig 4.

Temperature – Resistance – Voltage
of Element F18.

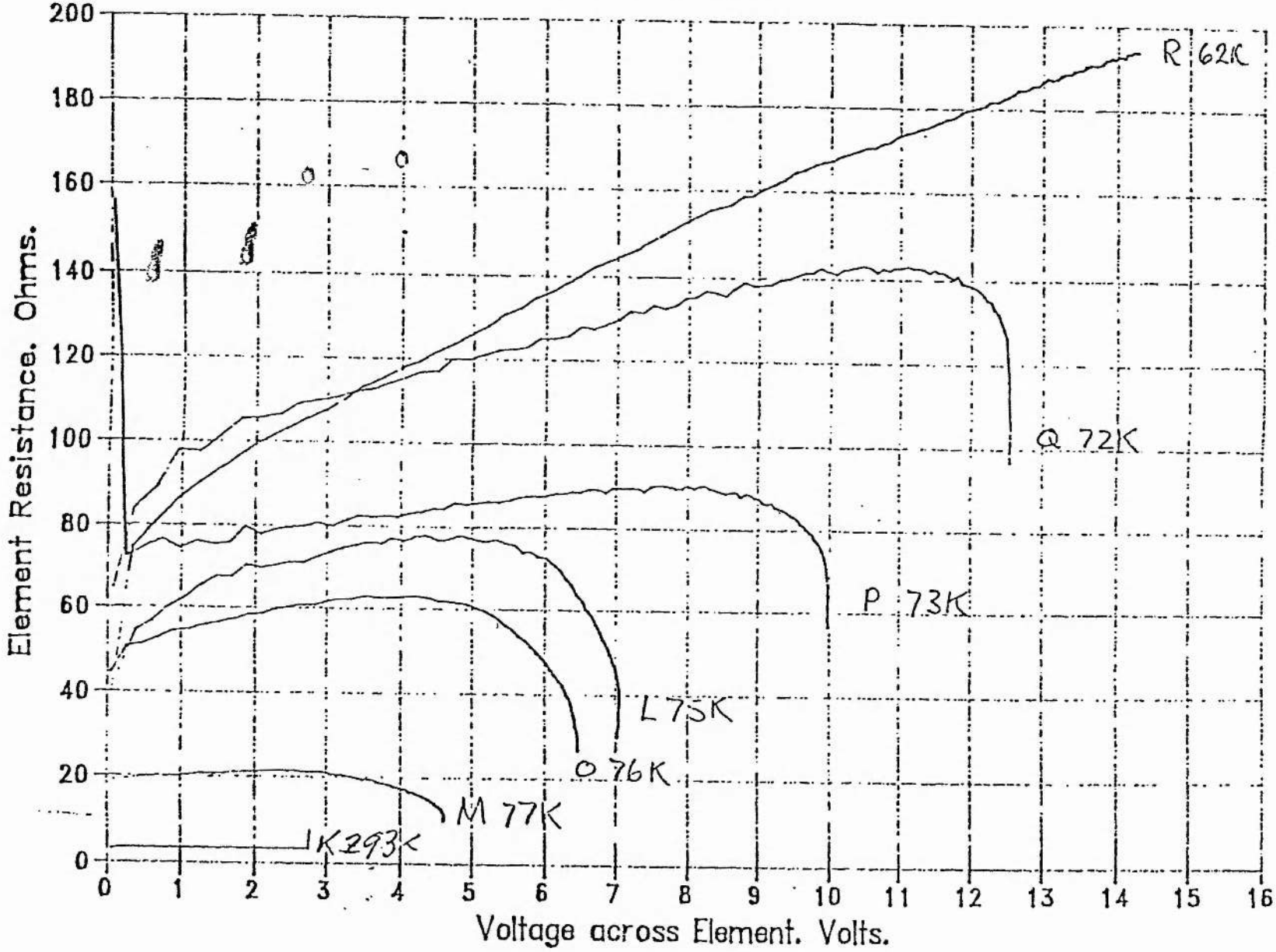

Temperature – Resistance – Voltage of Element F18.

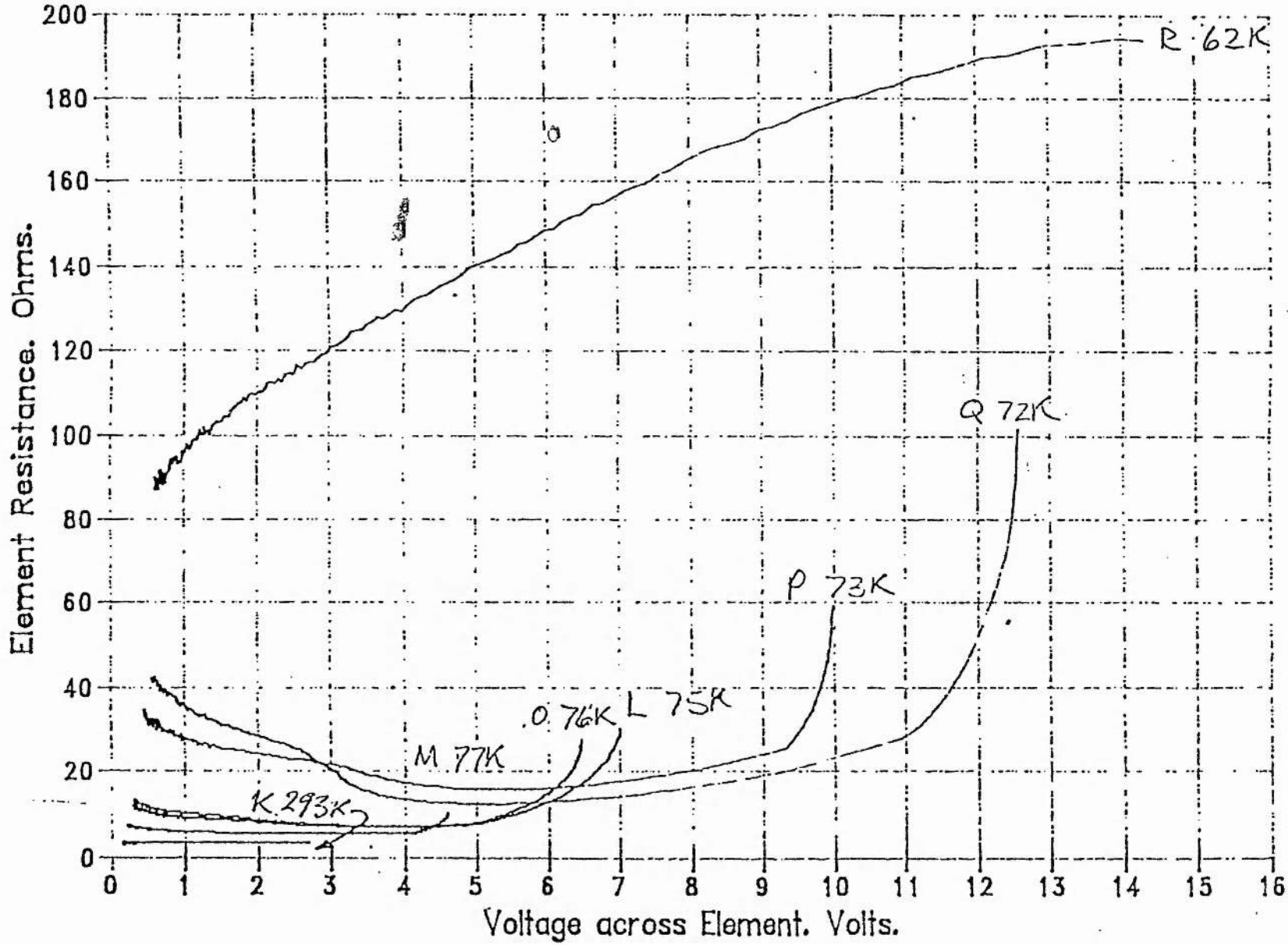

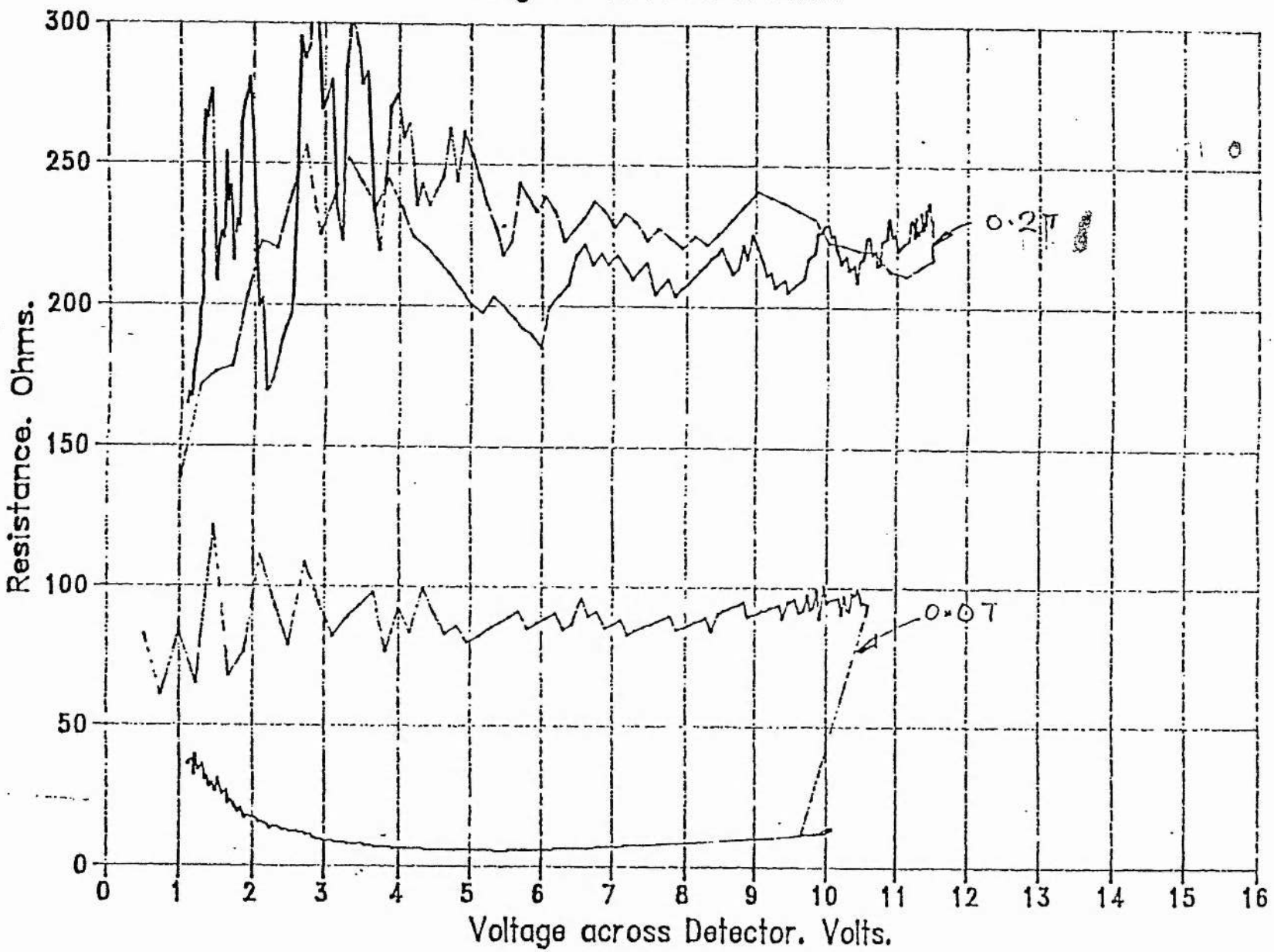
Resistance v Voltage at 77K.
Magnetic Field 0T & 0.2T.
Resistance. Ohms.
300
250
200
150
100
50
0
0 1 2 3 4 5 6 7 8 9 10 11 12 13 14 15 16
Voltage across Detector. Volts.
0·2T
0·0T

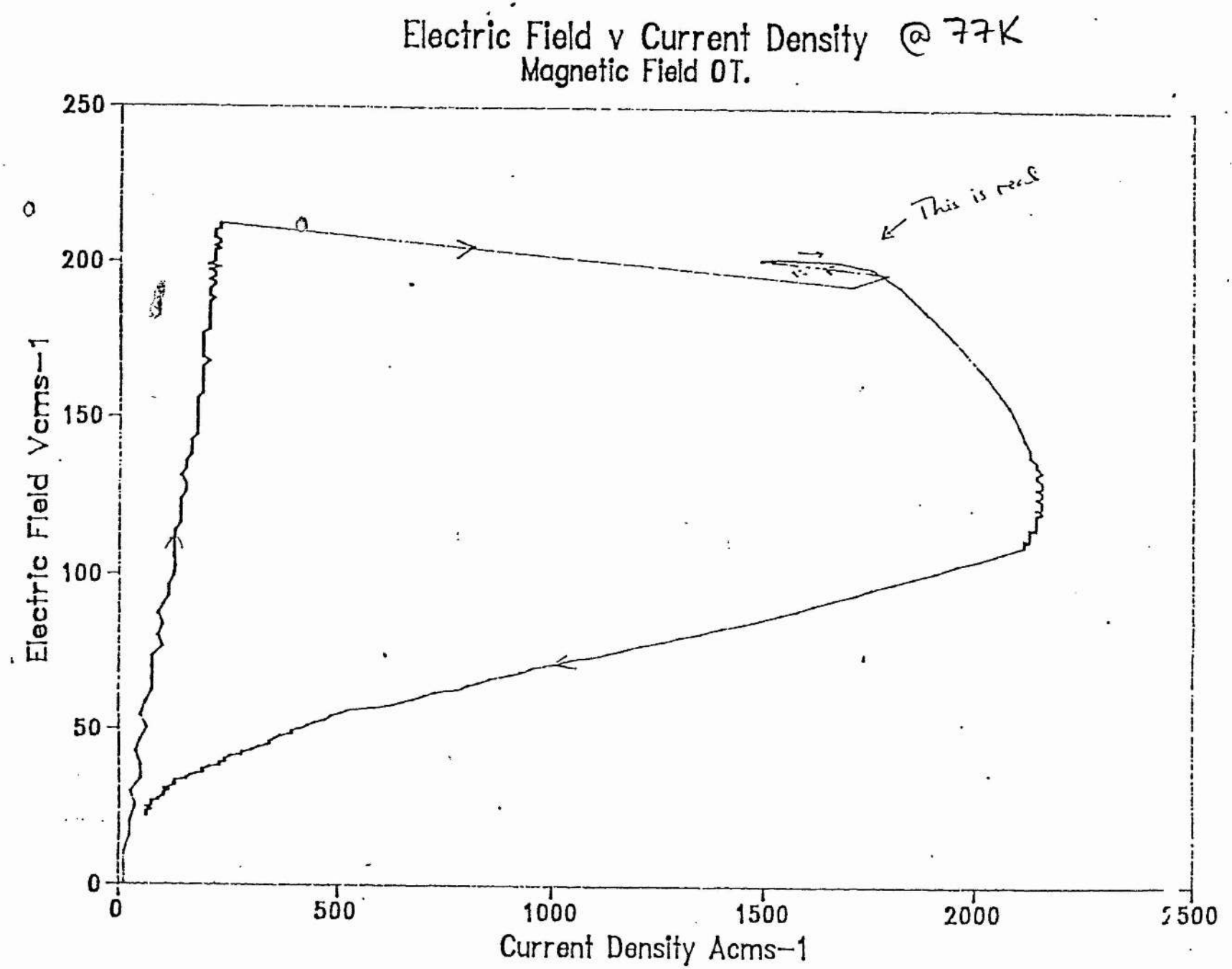
Electric Field v Current Density @ 77K
Magnetic Field 0T.
This is real
Electric Field Vcms−1
Current Density Acms−1
0
50
100
150
200
250
0
500
1000
1500
2000
2500

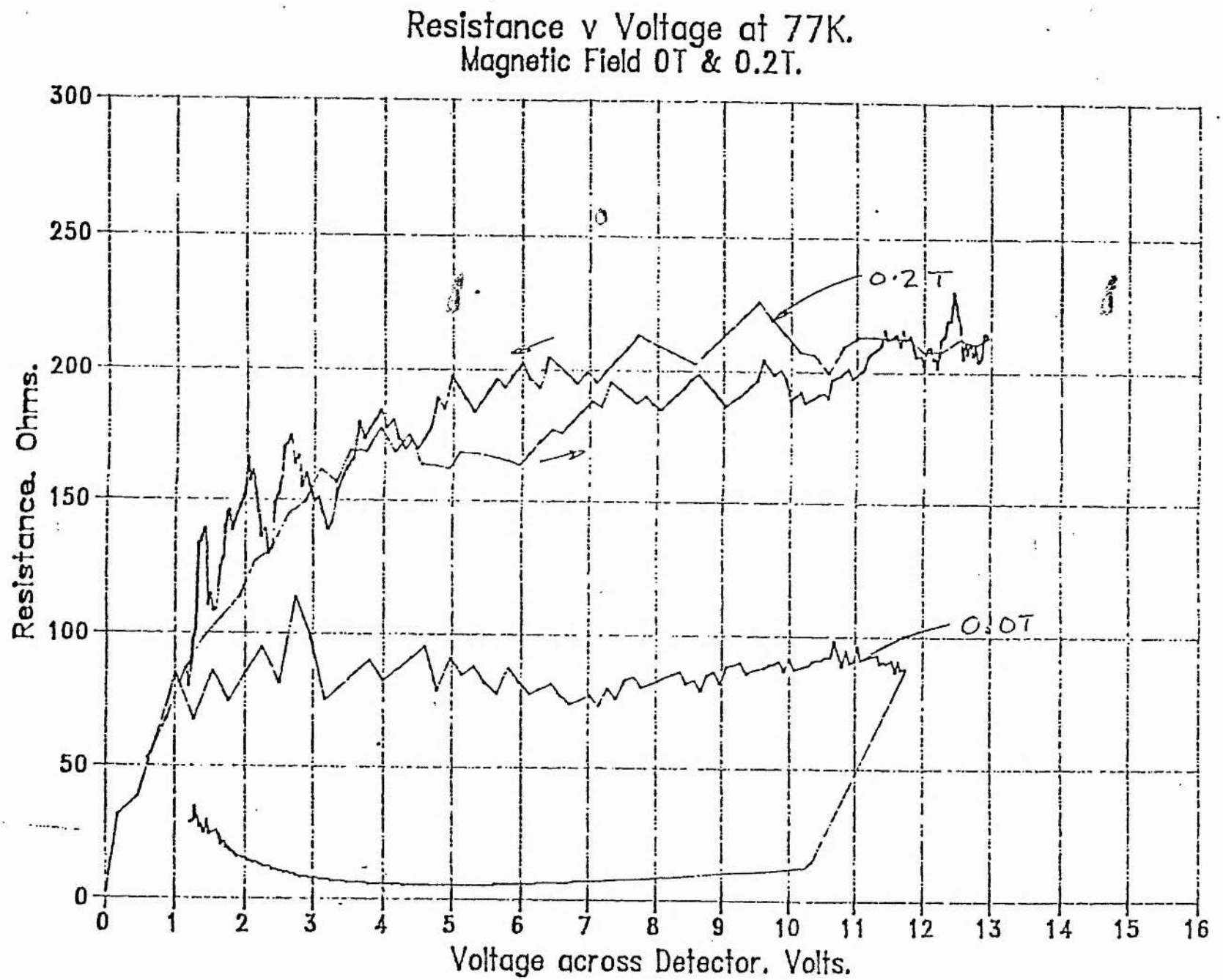
Resistance v Voltage at 77K.
Magnetic Field 0T & 0.2T.
Resistance. Ohms.
300
250
200
150
100
50
0
0.2T
0.0T
0
1
2
3
4
5
6
7
8
9
10
11
12
13
14
15
16
Voltage across Detector. Volts.

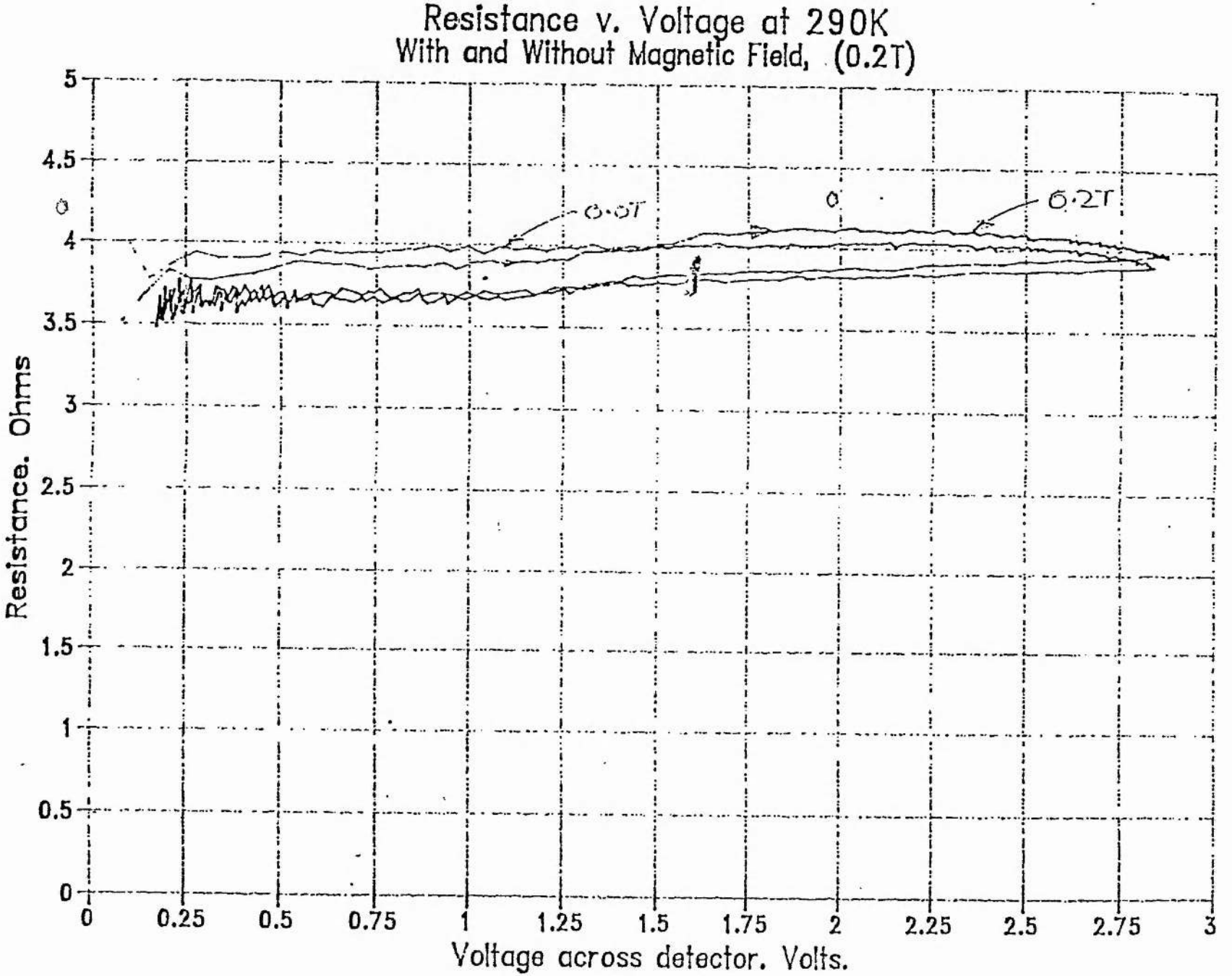
Resistance v. Voltage at 290K
With and Without Magnetic Field, (0.2T)
0·0T
0·2T
Resistance. Ohms
Voltage across detector. Volts.
0
0.5
1
1.5
2
2.5
3
3.5
4
4.5
5
0.25
0.75
1.25
1.75
2.25
2.75

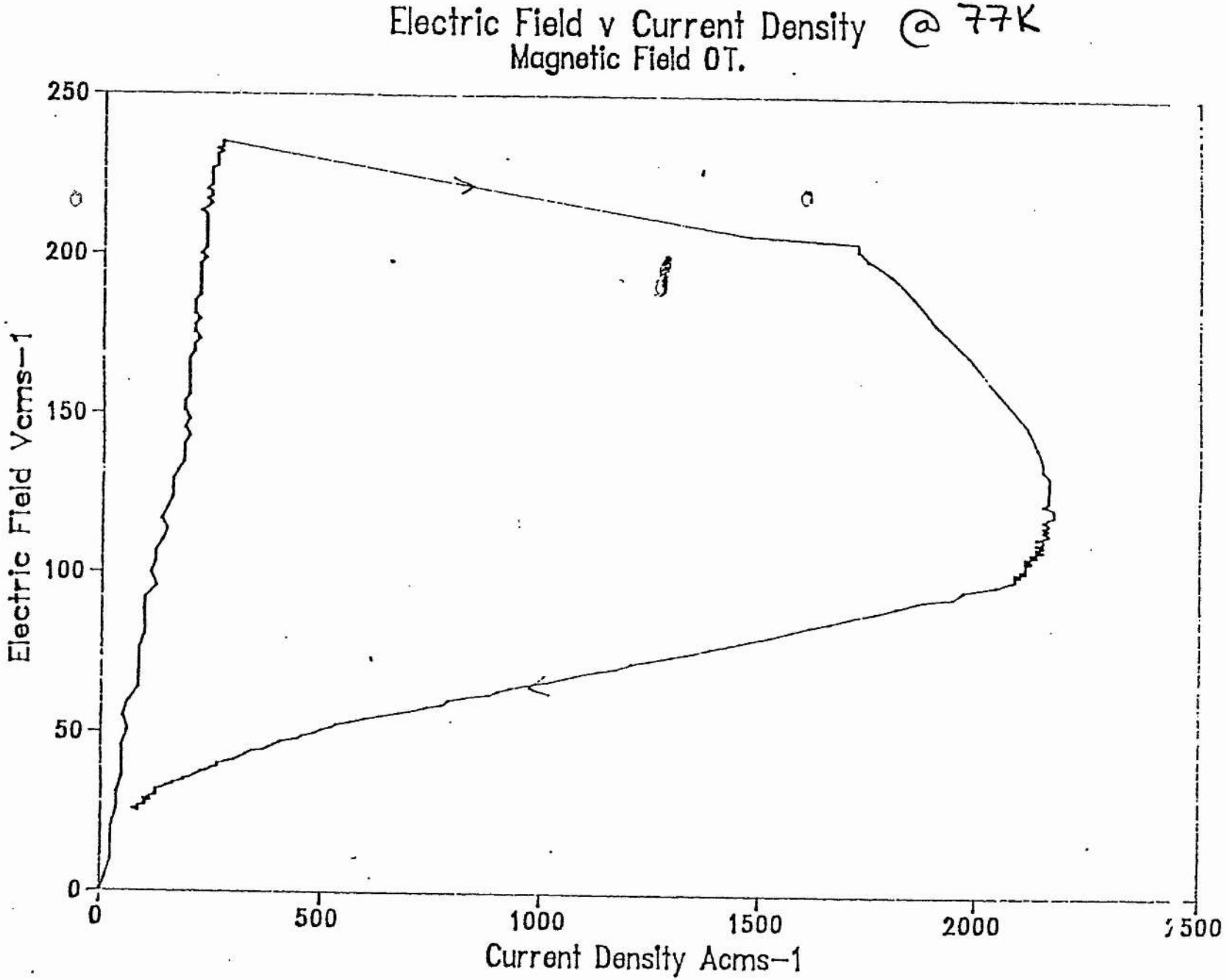
Electric Field v Current Density @ 77K
Magnetic Field 0T.
250
200
150
100
50
0
Electric Field Vcms−1
0
500
1000
1500
2000
2500
Current Density Acms−1

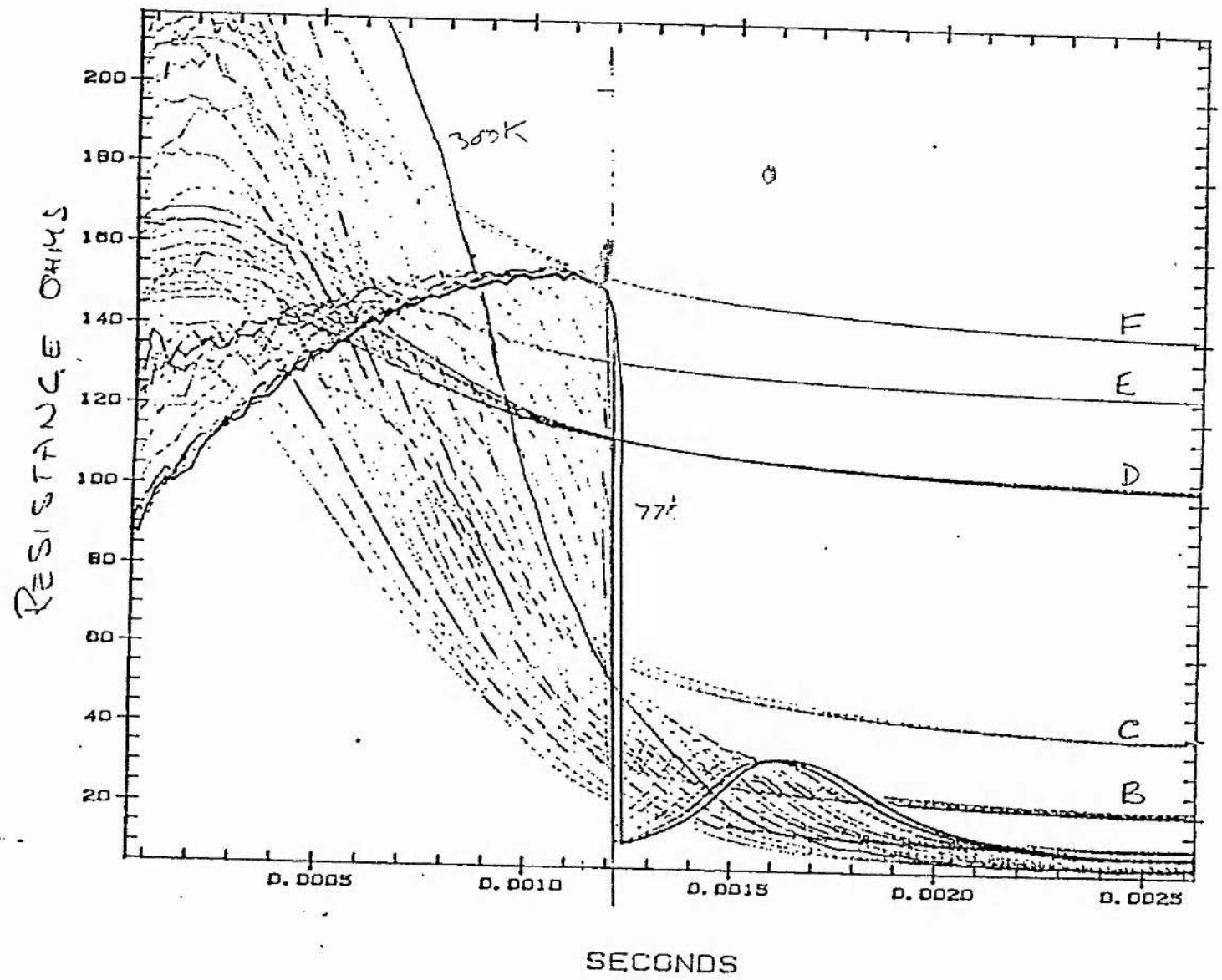
RESISTANCE OHMS
200
180
160
140
120
100
80
60
40
20
300K
77K
F
E
D
C
B
0.0005
0.0010
0.0015
0.0020
0.0025
SECONDS

Fig 14.

TRMEAN

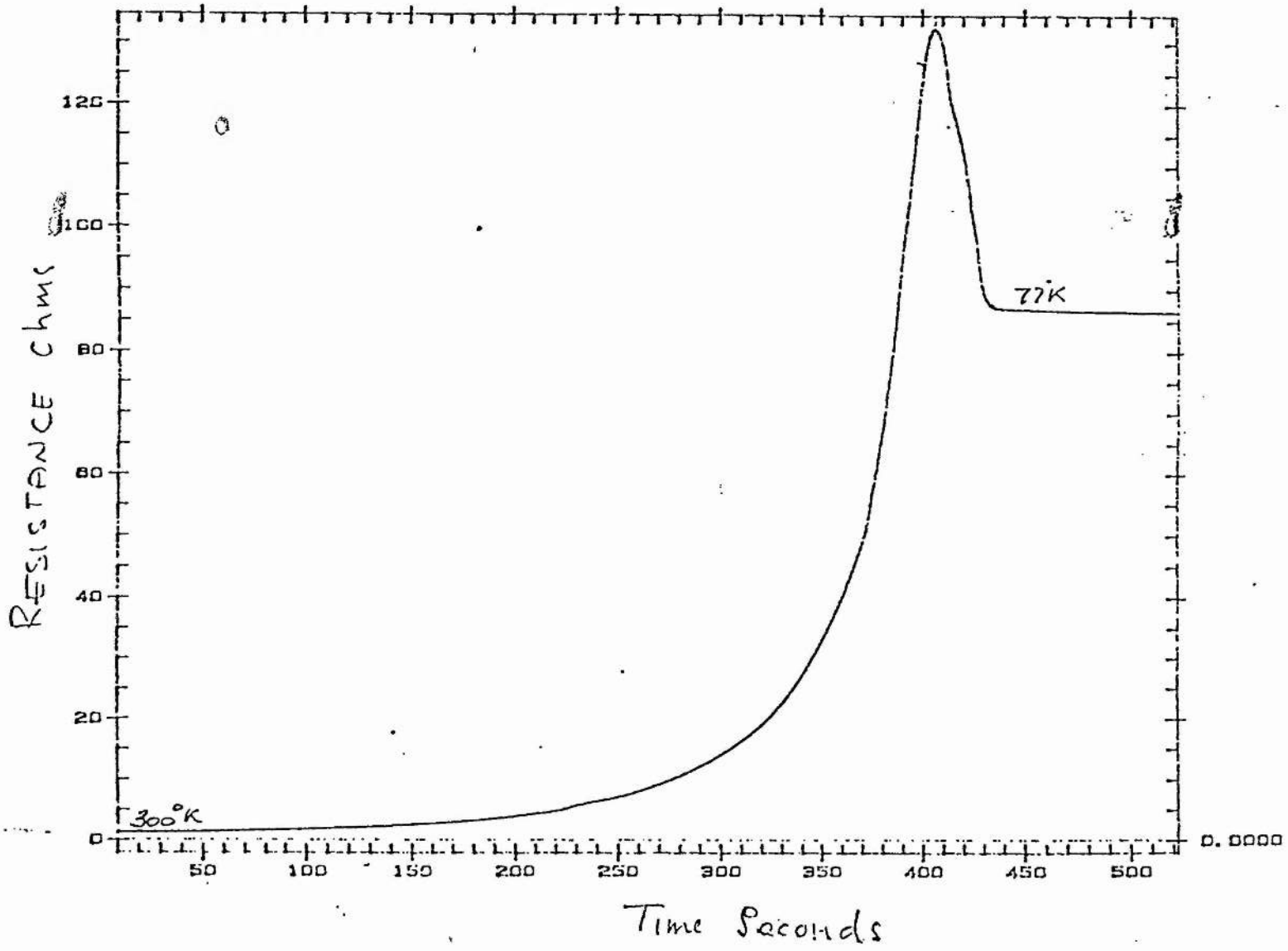

Fig. 15

Appendix 6.2 : Calibration Data for Diode used as a thermometer in the Resistance versus temperature measurements. The data was obtained by V.Scott, who kindly made the diode available for use here.